Carbon Nanotubes Composites: Engineering, Properties and Applications

A thesis submitted in fulfilment of the requirement for the degree of

Doctor of Philosophy

Engineering (Nanotechnology)

By Mohammed Obid Alsawat

November 2016

THE UNIVERSITY of ADELAIDE

School of Chemical Engineering

Faculty of Engineering, Computer, and Mathematical Sciences

The University of Adelaide

CONTENTS

ABSTRACT iv

PREFACE vii

LIST OF PUBLICATIONS viii

Published Articles viii

Submitted Articles ix

Conference Presentations ix

DECLARATION xi

ACKNOWLEDGEMENTS xii

CHAPTER 1: Introduction 1

1.1 Discovery, Structure and Properties of Carbon Nanotubes 2

1.2 Fabrication of Carbon Nanotubes 4

1.2.1 Arc Discharge Methods 5

1.2.2 Laser Ablation Methods 5

1.2.3 Chemical Vapour Deposition (CVD) Methods 6

1.3 Template-Assisted Approach 9

1.3.1 Nanoporous Anodic Alumina Template 9

1.3.2 Titania Nanotubes Template 14

1.4 Modification of Carbon Nanotubes 18

1.5 Carbon Nanotubes Composite Membranes 23

1.5.1 Membrane Definition 23

1.5.2 Fabrication of Vertically Aligned Carbon Nanotubes Membranes 23

1.6 Carbon Nanotubes as Molecular Transport Channels 27

1.7 Carbon Nanotubes as Coupling Material for Photocatalysis Applications 30

1.7.1 Introductory Background 30

1.7.2 Carbon Nanotubes and Titania Composite 32

1.8 Challenges for CNTs-Based Composites for Molecular Transport and Photocatalysis Applications 33

1.9 Objectives 34

1.10 Thesis Structure 36

1.11 References 38

CHAPTER 2: Experimental Methods 57

2.1 Introduction and Objectives 58
2.2 Materials and Chemicals 58
2.3 Synthesis of Nanoporous Anodic Alumina Membranes (NAAMs) Templates 58
2.4 Synthesis of Titania Nanotubes (TNTs) Templates 61
2.5 Synthesis of CNTs-NAAMs and CNTs-TNTs Composites 61
2.6 Transport Studies of CNTs-NAAMs Composite Membranes 65
2.7 Photodegradation Study of CNTs-TNTs Composite 68
2.8 Structural and Chemical Characterizations 69
2.8.1 Scanning Electron Microscopy (SEM) 69
2.8.2 Energy Dispersive X-ray Spectroscopy (EDX) 70
2.8.3 Transmission Electron Microscopy (TEM) 70
2.8.4 X-ray Photoelectron Spectroscopy (XPS) 71
2.8.5 Raman Spectroscopy 71
2.8.6 X-ray Diffraction Spectroscopy (XRD) 72
2.8.7 UV-Visible Spectroscopy 72
2.9 References 73

CHAPTER 3: Carbon Nanotube-Nanoporous Anodic Alumina Composite Membranes with Controllable Inner Diameters and Surface Chemistry: Influence on Molecular Transport and Chemical Selectivity 75

CHAPTER 4: Carbon Nanotubes-Nanoporous Anodic Alumina Composite Membranes: Influence of Template on Structural, Chemical and Transport Properties 94

CHAPTER 5: Influence of Surface Chemistry on the Ionic Conductivity of Vertically Aligned Carbon Nanotube Composite Membranes 131

CHAPTER 6: Facile and Controllable Route for Nitrogen Doping of Carbon Nanotubes Composite Membranes by Catalyst-Free Chemical Vapour Deposition 143

CHAPTER 7: Synthesis of Carbon Nanotubes-Nanotubular Titania Composites by Catalyst-Free CVD Process: Insights into the Formation Mechanism and Photocatalytic Properties 163

CHAPTER 8: Conclusions and Future Work 174

8.1 Conclusions 175
8.1.1 Carbon Nanotube-Nanoporous Anodic Alumina Composite Membranes with Controllable Inner Diameters and Surface Chemistry: Influence on Molecular Transport and Chemical Selectivity 175
8.1.2 Carbon Nanotubes-Nanoporous Anodic Alumina Composite Membranes: Influence of Template on Structural, Chemical and Transport Properties 177
8.1.3 Influence of Surface Chemistry on the Ionic Conductivity of Vertically Aligned Carbon Nanotube Composite Membranes 178
8.1.4 Facile and Controllable Route for Nitrogen Doping of Carbon Nanotubes Composite Membranes by Catalyst-Free Chemical Vapour Deposition 179
8.1.5 Synthesis of Carbon Nanotubes-Nanotubular Titania Composites by Catalyst-Free CVD Process: Insights into the Formation Mechanism and Photocatalytic Properties 180
8.2 Future work 181

ABSTRACT

Carbon nanotubes (CNTs) an unique 1-dimensional sp^2 carbon structure have attracted significant scientific interest in the last decades due to their outstanding and unique transport, electrical, mechanical and thermal properties. These nanostructures have been envisaged for a broad range of applications. Nevertheless, their applicability for potential applications are strongly dependent on their physical and chemical properties. Therefore, new nanofabrication approaches that allow the production of CNTs with precisely engineered properties (i.e. dimension, surface chemistry, chemical composition, etc.) could enable and spread the applicability of these carbon-based nanostructures across more relevant applications. In this context, this thesis aims at developing advanced fabrication methodologies to produce CNTs-based composites with precisely engineered dimensions and properties for addressing gap in knowledge about molecular transport inside CNTs structures and specific problems related to molecular separation and advanced photocatalysts for environmental and energy applications. CNTs composites were produced by growing vertically aligned multi-walled carbon nanotubes (MWCNTs) inside nanoporous anodic alumina membranes (NAAMs) and titania nanotubes (TNTs), produced by anodisation of aluminium and titanium substrates, respectively, through a catalyst-free chemical vapour deposition (CVD) approach.

It was demonstrated that the dimensional features of CNTs-NAAMs composite membranes can be precisely engineered by the anodisation conditions and electrolyte used to produce the host templates and the deposition time during the CVD process. Thermal annealing and wet and dry oxidation processes were explored as means of controlling the surface chemistry of the inner walls of CNTs. Both dimensional features and surface chemistry were observed to have significant impacts on the molecular transport and selectivity properties of CNTs-NAAMs

composite membranes assessed by analysing the transport of two models molecules with different hydrophilic-hydrophobic and charge properties.

Electrochemical impedance spectroscopy (EIS) investigations on CNTs-NAAMs composite membranes featuring different chemistry (i.e. as-produced and modified with charged oxygen species) revealed that their electrochemical properties can be readily tuned by controlling their surface chemistry, which is critical to understand the properties of these composite membranes for desalination applications.

Furthermore, a new strategy aiming to modify the inner wall surfaces of CNTs-NAAMs composite membranes by doping their structure with nitrogen was developed. The crucial role of the precursor source C/N ratio in the formation of N-doped CNTs has been revealed. Characterisations of the structure of N-doped CNTs composite membranes and liberated tubes indicate that this nanofabrication method enables the chemical modification of CNTs without obstruction or morphological changes. The chemical composition analysis showed a dependency of nitrogen doping levels on the precursor source. The tunability and enhancement in the transport performance and chemical selectivity properties of CNTs-NAAMs after nitrogen doping have been established for the first time.

Finally, a composite platform for photocatalytic applications based on CNTs-TNTs has been developed. Investigations on their photocatalytic properties evaluated *via* the degradation of an organic model molecule revealed that CNTs induces a synergistic effect on the photocatalytic activity of TNTs, enhancing it up to one order of magnitude as compared to bare TNTs.

The results and investigations presented in this thesis advance the knowledge in designing CNTs and CNTs-based composite membranes with different physical and chemical properties in a precise manner for transport and photocatalysis applications. These results are envisaged valuable contribution towards advancing the existing knowledge in the field of CNTs composite

membranes and carbon materials in general and boosting the applicability of these systems across multiple disciplines and industrial applications.

PREFACE

This thesis is submitted as a 'thesis by publication' in accordance with "Specifications for Thesis 2013" of The University of Adelaide. The outcomes of 3.5 years PhD research are 9 peer-reviewed journal articles [8 published and 1 submitted]. Furthermore the PhD research was also presented at 3 national conferences. Five research chapters included in this thesis were published (4) and submitted (1) as research articles in highly ranked journals in the field. A complete list of publications is provided in the following pages.

LIST OF PUBLICATIONS

Peer-reviewed Journal Articles

Published Articles

1. **Alsawat, M.** Altalhi, T. Kumeria, T. Santos, A. and Losic, D. Carbon nanotube-nanoporous anodic alumina composite membranes with controllable inner diameters and surface chemistry: Influence on molecular transport and chemical selectivity. *Carbon,* 93 (2015): 681-692. (IF= 6.16)
2. **Alsawat, M.** Altalhi, T. Gulati, K. Santos, A. and Losic, D. Synthesis of carbon nanotubes-nanotubular titania composites by catalyst-free CVD process: Insights into the formation mechanism and photocatalytic properties. *ACS Applied Materials & Interfaces,*7.51 (2015): 28361-28368. (IF= 6.72)
3. **Alsawat, M.** Kant, K. Altalhi, T. Santos, A. and Losic, D. Influence of surface chemistry on the ionic conductivity of vertically aligned carbon nanotube composite membranes. *RSC Advances*, 6.50 (2016): 44288-44296. (IF= 3.84)
4. **Alsawat, M.** Altalhi, T. Santos, A. and Losic, D. Facile and controllable route for nitrogen doping of carbon nanotubes composite membranes by catalyst-free chemical vapour deposition. *Carbon*, 106 (2016): 295-305. (IF= 6.16)
5. **Alsawat, M.** Altalhi, T. Shapter, J. G. and Losic, D. Influence of dimensions, inter-distance and crystallinity of titania nanotubes (TNTs) on their photocatalytic activity. *Catalysis Science & Technology*, 4.7 (2014): 2091-2098. (IF= 5.42)
6. Maher, S. **Alsawat, M.** Kumeria, T. Fathalla, D. Fetih, G. Santos, A. and Losic, D. Luminescent silicon diatom replicas: self-reporting and degradable drug carriers with

biologically derived shape for sustained delivery of therapeutics. *Advanced Functional Materials*, 25.32 (2015): 5107-5116. **(Featured as Journal Cover)** (IF=11.8)

7. Kumeria, T. Yu, J. **Alsawat, M.** Kurkuri, M. D. Santos, A. Abell, A. D. and Losic, D. Photo-switchable membranes based on peptide-modified nanoporous anodic alumina: Toward smart membranes for on-demand molecular transport. *Advanced Materials*, 27.19 (2015): 3019-3024. **(Featured as Journal Cover)** (IF=17.49)
8. Viswanathan, S. S. Kumeria, T. Gulati, K. Prideaux, M. Rahman, S. **Alsawat, M.** Santos, A. Atkins, G. J. and Losic, D. Localized drug delivery of selenium (Se) using nanoporous anodic aluminium oxide for bone implants. *Journal of Materials Chemistry B*, 3.35 (2015): 7090-7098. (IF= 4.72)

Submitted Article

9. **Alsawat, M.** Altalhi, T. Santos, A. and Losic, D. Carbon nanotubes-nanoporous anodic alumina composite membranes: influence of template on structural, chemical and transport properties. *ACS Applied Materials & Interfaces*, 2016. **(Submitted)**

Conference Presentations:

1. **Alsawat, M.** Kant, K. Altalhi, T. and Losic, D. Tuning of electrochemical properties of carbon nanotube membranes by chemical modification. International Conference on Nanoscience and Nanotechnology 2014, Adelaide, Australia, Feb 2014. **(Poster Presentation)**
2. **Alsawat, M.** Altalhi, T. Santos, A. and Losic, D. On the optimisation of the chemical selectivity of carbon nanotube membranes via doping with nitrogen: Enhancing transport properties by chemistry, The Royal Australian Chemical Institute Conference 2014, Adelaide, Australia, Dec 2014. **(Poster Presentation)**

3. **Alsawat, M.** Altalhi, T. Shapter, J. G. and Losic, D. Synthesis, Characterization and Photocatalytic Activity of Titania Nanotubes. CHEMECA 2013, Brisbane, Australia, Oct 2013. **(Poster Presentation)**

DECLARATION

I certify that this work contains no material which has been accepted for the award of any other degree or diploma in my name, in any university or other tertiary institution and, to the best of my knowledge and belief, contains no material previously published or written by another person, except where due reference has been made in the text. In addition, I certify that no part of this work will, in the future, be used in a submission in my name for any other degree or diploma in any university or other tertiary institution without the prior approval of the University of Adelaide and where applicable, any partner institution responsible for the joint-award of this degree.

I give consent to this copy of my thesis when deposited in the University Library, being made available for loan and photocopying, subject to the provisions of the Copyright Act 1968.

The author acknowledges that copyright of published works contained within this thesis resides with the copyright holder(s) of those works.

I also give permission for the digital version of my thesis to be made available on the web, via the University's digital research repository, the Library Search and also through web search engines, unless permission has been granted by the University to restrict access for a period of time.

MOHAMMED OBID ALSAWAT

ACKNOWLEDGEMENTS

First and foremost, praises and thanks to the God, the Almighty, for all of the graces and blessings he has given over the years and for granting me the capability to complete this PhD thesis. The completion of this PhD thesis could not have been possible without the advice, support and contribution, throughout this 3.5 years long amazing journey (PhD degree), of many people, who are sincerely appreciated and gratefully acknowledged.

I would like to express my special thanks to my supervisors Prof. Dusan Losic and Dr. Abel Santos for introducing me to the nanotechnology field (in particular, the field of CNTs composite membrane and materials). I particularly appreciate Prof. Losic who has been a constant source of support and inspiration over the years. He believed in me and gave me his priceless trust and the total freedom to explore ideas and to be an independent young researcher. I cannot express my gratitude towards Dr. Santos in words for all of the support he gave me through up and down times during this PhD study, and for treating me like a younger brother. He is one of the best people I have known in both personal and scientific values. I consider myself to be very lucky to have had mentors like Prof. Losic and Dr. Santos.

I am highly grateful to Dr. Tariq Altalhi who has helped me in times when I had nowhere to go. Without his support and brotherhood I will never ever be able to succeed.

I would like to give special thanks to Dr. Tushar Kumeria who is a great man and has always supported me during the hard times of this PhD study.

I thank current and former Losic group's members, in particular Dr. Karan Gulati, Dr. Krishna Kant, Dr. Mahaveer Kurkuri, and Shervin Kabiri for their collaboration.

I would also like to thank the Chemical Engineering workshop staff, particularly Jason Peak, Michael Jung, and Jeffrey Hiorns, for assistance with the fabrication of the permeation cell.

The support and technical assistance from Dr. Animesh Basak and Mr Ken Neubauer at the Electron Microscope Unit, The University of Adelaide are highly appreciated.

I would like to acknowledge Taif University (Ministry of Education, Saudi Arabia) for funding my scholarship.

I will be forever indebted to my mother, my father, my brothers (Hatem, Khaled, Ahmad, Abdullah and Nawaf) and my sisters for believing in me and my dreams and for their love, prayers and blessings throughout my life. My wife's family including her mother, her father, her brothers (Hany, Abdullah, Abdulrahman, Abdulaziz, Omar, Muhammed and Rayan) and her sisters is another pillar and their support are extremely grateful.

Finally, I deserve the biggest acknowledgment for my family. Asma Alsuwat, my wife, who has always been by my side through thick and thin. Nothing would have been possible without her support and endless love "Your sheer love is unparalleled". Rose, my daughter, who has been the best stress buster through her songs and funny talks. Raseel, a sweet girl who has joined our family six months ago.

I dedicate this PhD thesis to the special people in my life:

My parents

My wife

My daughters

My brothers and sisters

CHAPTER 1

INTRODUCTION

Mohammed Obid Alsawat

School of Chemical Engineering, The University of Adelaide, South Australia 5005, Australia

CHAPTER 1: Introduction

1.1. Discovery, Structure and Properties of Carbon Nanotubes

Carbon nanotubes (CNTs) are a 1-D structure with tubular morphology and an allotrope of carbon composed of sp^2 covalently bonded carbon atoms arranged in hexagonal patterned sheet. The CNT sheet, or graphene sheet, is seamlessly rolled up to provide a hollow cylindrical structure, which can be microns in length and nanometres in diameter. This feature distinguishes CNTs from other carbon-based nanostructures, such as fullerenes and graphene. Based on the number of graphene sheets, CNTs can be classified into two different categories; i) single-walled carbon nanotubes (SWCNTs) consisting of one layer of graphene with typical diameters ranging from 1 – 2 nm, and ii) multi-walled carbon nanotubes (MWCNTs) consisting of two or more layers of graphene grown concentrically to the centre of the nanotubes with typical diameters ranging from 3 – 30 nm (**Figure 1.1**) [1-4]. The differing dimensions of these two types of CNTs result in significantly different properties.

The earliest studies that report on the tubular nature of some nano-sized carbon filaments were reported as early as 1952 by Radushkevich and Lukyanovich [5, 6]. However, the scientific community has credited Sumio Iijima with the discovery of MWCNTs, reported in his paper in Nature in 1991 [7]. In this study, Iijima described the structure of CNTs and provided empirical evidence of their existence to bring CNTs to the awareness of the scientific community. The technique used by Iijima was essentially based on the arc discharge method to produce fullerenes. However, Iijima found a by-product at the cathode, which on subsequent transmission electron microscopy (TEM) analysis, was found to be multi-walled carbon nanotubes (MWCNTs) with a diameter ranging from 4 - 30 nm and up to 1 μm in length. This work became a base for subsequent studies in the field of CNT technology. It is worthwhile to note that early reports on SWCNTs

were published in 1993 in two papers published independently in Nature, one by Iijima and Ichihashi [8] and the other by Bethune *et al.* [9].

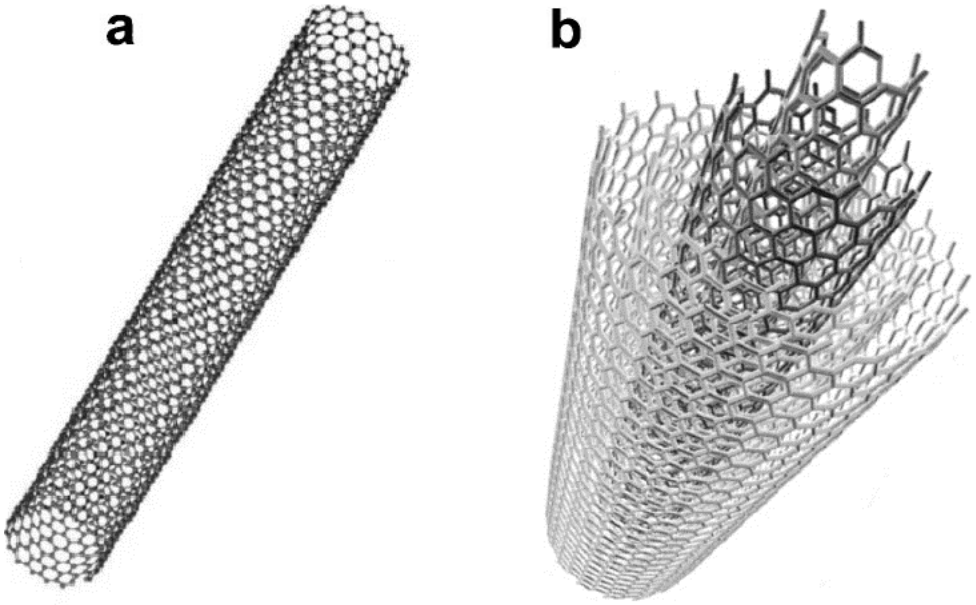

Figure 1.1. Schematic diagrams of single and multi-walled carbon nanotubes. (a) Single-walled carbon nanotube (SWCNT); and (b) multi-walled carbon nanotubes (MWCNTs). (Source [4]).

Structurally, CNTs can be classified into three different types as a function of conformational arrangement of hexagonal units to the tube axis, where rolled graphene sheet is defined by the so-called chiral vector of CNTs: $C_h = na_1 + ma_2$ (**Figure 1.2**), where the integers (n, m) are the number of steps along the unit vectors (a_1 and a_2) of the hexagonal lattice. The three types of CNTs structures can be identified using the indices n and m [10, 11]:

i) If n = m, the nanotubes are termed Armchair

ii) If m = 0, the nanotubes are termed Zigzag

iii) Otherwise, the nanotubes are termed Chiral

Schematic representations of these three identified chiralities of CNTs are presented in **Figure 1.2**.

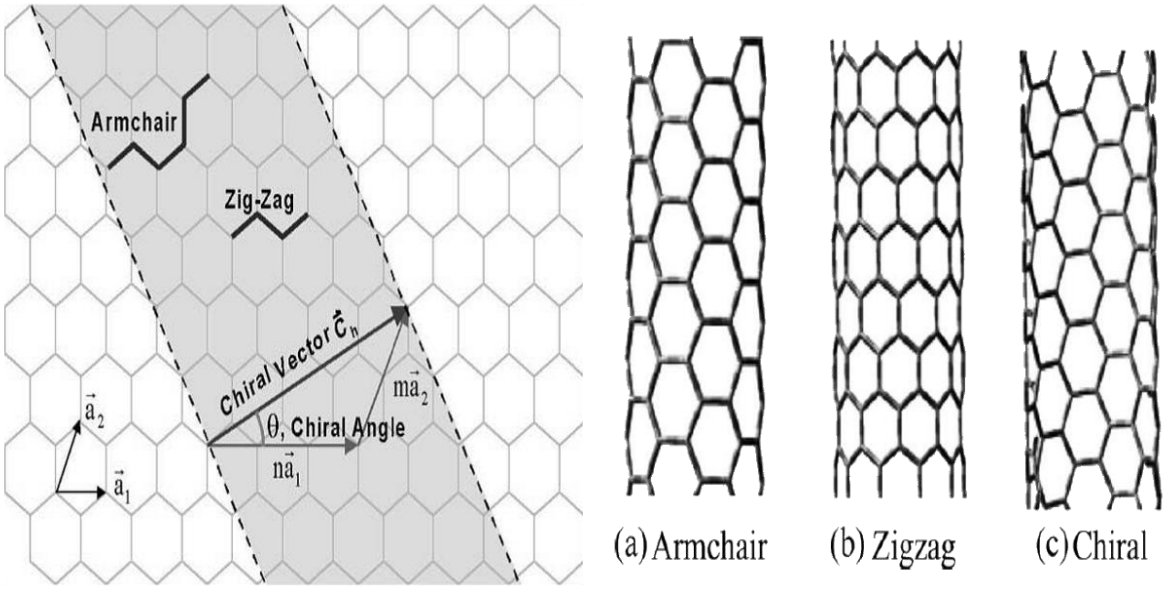

Figure 1.2. Schematic diagram showing how a hexagonal sheet of graphite is 'rolled' to form a carbon nanotube (left) and the three different chiralities of CNTs (right) (Source [10, 11]).

The outstanding and unique properties of CNTs, including transport, electrical, mechanical and thermal properties, offer enormous potential for practical applications [12]. Examples include, but are not limited to, field emission, anode for lithium ion batteries, capacitor and chemical sensors, electrodes, tips for scanning probe microscopies, water desalination, gas pervaporation, nanofiltration of biological mixtures, transdermal drug delivery and energy storage applications [13-20]. The geometric features (i.e. diameter and length) of CNTs are considered as determining parameters of their chemical and physical properties. Therefore, control of these CNTs features is of critical importance for advancing CNTs performance and properties in the above-mentioned applications.

1.2. Fabrication of Carbon Nanotubes

Several techniques are used to produce CNTs [21]. Arc discharge, laser ablation and chemical vapour deposition are the most common techniques used to produce a broad variety of CNTs. These methods use different energy sources (electric field, heat and high intensity light) to decompose carbon sources and form CNTs. These methods are described in the following sections.

1.2.1. Arc Discharge Methods

CNTs have been produced in different ways to achieve high yields and a high degree of purity. Iijima pioneered a fabrication method for MWCNTs via arc discharge method using graphite electrode carbon sources [7]. The process involves running an electric arc between two graphite electrodes in inert atmosphere to generate high temperature (> 3000°C) and vapourise carbonaceous material. The resultant soot on the cathode was shown to be a low yield of MWCNTs accompanied with a high yield of fullerenes. To control yield and purity of MWCNTs, experimental conditions, such as current density, inert gas pressure and stability of the plasma formed between electrodes, need to be optimised [22, 23]. To produce SWCNTs a metal catalyst, such as cobalt, must be involved in the process [8]. However, CNTs produced by this method are accompanied with amorphous carbon and small defect concentrations. Therefore, a post-purification step is mandatory to obtain pure CNTs. Moreover, this technique is relatively expensive and its ability to produce CNTs is limited to gram-scale quantities. A schematic diagram of the process and SEM of CNTs produced using this method are shown in **Figure 1.3a and b**.

1.2.2. Laser Ablation Methods

Laser ablation uses high intensity light (i.e. laser) as an energy source to decompose a carbon source to form CNTs. Smalley's group reported, for the first time, production of CNTs using this method [24]. These researchers produced SWCNTs using a laser beam to vapourise a mixture of graphite rod (carbon source) and transition metal catalysts in inert atmosphere at 1200°C. The vapourised carbon atoms condense as SWCNTs and are collected at the end of process. This method can produce MWCNTs in the absence of a catalyst and presence of pure graphite. The ultimate product of the laser ablation method is tangled CNTs with a considerable amount of by-products, similar to the arc discharge method. Therefore, time-consuming purification procedures

are required. A schematic diagram of the process and SEM of CNTs produced using this method are shown in **Figure 1.3c and d**.

It is important to point out that the aforementioned techniques have inherent drawbacks to produce pure CNTs with hollow, uniform and controlled geometric features (i.e. dimension and shape). Such features are required for CNTs to mimic natural protein channels and to pass into membrane systems for mass transport [25].

1.2.3. Chemical Vapour Deposition Methods

Currently, chemical vapour deposition (CVD) is the most commonly utilised CNT production method. This process involves passing a flow of carbon precursor over a metal catalyst to provide nucleation sites for CNT growth at temperatures typically ranging from 500 – 900°C in inert atmosphere at controlled pressure (**Figure 1.3e**). Catalyst materials, Fe, Ni or Co, are deposited on a substrate of silica, alumina or copper. Different parameters, such as catalyst, carbon source, inert gas flow rate, temperature and time, play a key role in determining the properties of the resulting product. Production of MWCNTs and SWCNTs using CVD methods were first reported by Endo *et al.* and Dai *et al.* in 1993 and 1996, respectively [26, 27]. In contrast to the two aforementioned methods (i.e. arc discharge and laser ablation), CVD processes are flexible, cost-competitive and industrially scalable. Moreover, this fabrication method allows control of CNT geometric features, although this can be significantly affected by small differences in catalyst particle size.

Despite the advantages of CVD methods for the production of CNTs as compared to other methods, CNTs structures obtained by these methods have characteristics that are unsuitable for some applications, such as transport, filtration and separation processes. Examples of these characteristics are internal closures (**Figure 1.3f**) and residues of metal catalyst particles (**Figure 1.3f**) which exist even after post-purification treatments. While these chemical contaminations make the resulting CNTs potentially toxic for humans and the environment [28], geometric defects

present in the structure of resulting CNTs can obstruct or completely block the flow inside CNTs, preventing their application in the above-mentioned applications.

Other CVD-based nanofabrication approaches make it possible to avoid the intrinsic limitations discussed above, enabling production of CNTs with optimal chemical and geometric features for flowing-based applications (i.e. controlled geometries, uniform, straight and hollow cylindrical geometric features). These techniques are based on the use of nanoporous templates, such as nanoporous anodic alumina (NAA) and titania nanotubes (TNTs), taking advantage of their catalytic role for deposition of carbon from different carbon sources [29, 30].

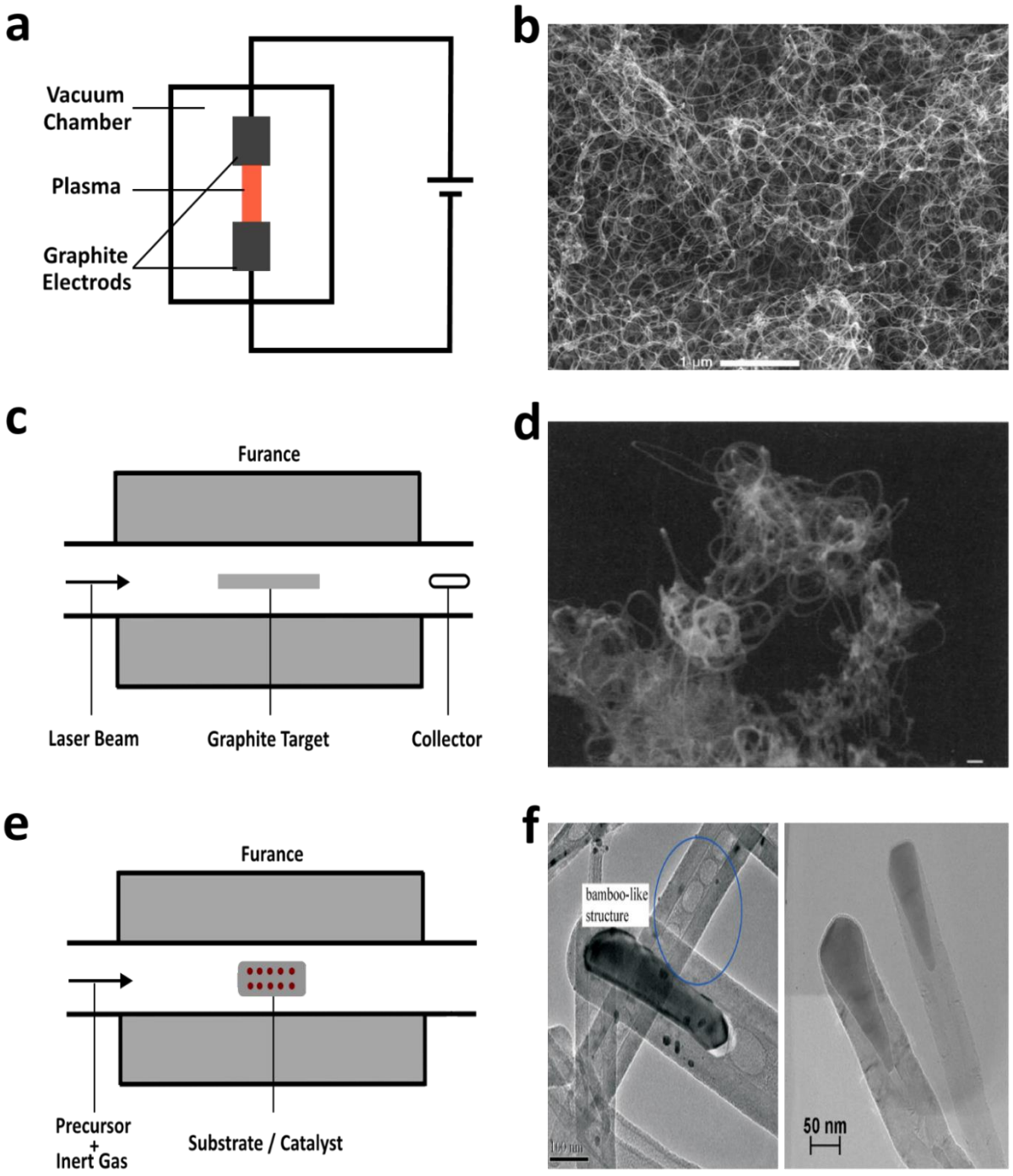

Figure 1.3. Schematic diagram of different methods of CNTs fabrication. (a) Arc discharge; (c) laser ablation; and (e) chemical vapour deposition. (b, d and f). Corresponding SEM and TEM images showing the morphology of CNTs produced using these methods (Source [31-34]).

1.3. Template-Assisted Approach

Template synthesis is a technology widely used to synthesise nanostructures due to its ability to control morphology of these structures. In this approach, nanoporous or macroporous membranes or films are produced first by different approaches to serve as templates for synthesising nanostructures with controlled dimensions through deposition of different materials inside the templates [35-37]. Once the nanostructure material is synthesised, the template can remain to produce composite nanostructures or selectively removed to produce free-standing nanostructures. Electrochemical anodic oxidation (or anodisation) is a simple and self-driven process for modifying surfaces by creating nanoporous oxide films over the surface of some valve metals to obtain either porous or tubular structures, depending on the type of the metal, electrolyte and applied potential [38-41]. The formation of self-organised nanostructures by the electrochemical anodisation process has been reported for various materials including Al and Ti [29, 30, 38, 42, 43]. Among available template materials, nanoporous anodic alumina (NAA) and titania nanotubes (TNTs) prepared by the self-ordering electrochemical anodisation process are considered outstanding host templates for production of nanostructures used for broad applications [44-48]. This is due to the uniform, well-defined and ordered nanoporous/nanotubular structures that these templates provide and the capability of engineering their geometric features with precision by an industrially scalable and cost-competitive process.

1.3.1. Nanoporous Anodic Alumina Template

Electrochemical anodisation of aluminium is a century old, industrially scalable and cost-competitive process used in the metal finishing industry to create an oxide film over an aluminium surface (i.e. alumina) that was initially developed by Bengough and Stuart to protect aluminium from corrosion [49]. With the help of electron microscopy in the 1950s, the nanoporous structure of the alumina layer produced by this electrochemical anodisation process was revealed. Since

then, research has explored the different parameters involved in the anodisation process of aluminium (i.e. applied potential, time, temperature, electrolyte, etc.) to obtain a uniform and well-ordered structure of NAA and understand the physical and chemical properties of NAA. Among these research efforts, introduction of the two-step anodisation approach, reported in 1995 by Masuda and Fukuda, is considered the most important breakthrough in electrochemical anodisation of aluminium technology. This two-step approach results in controlling the dimensional features of NAA by means of anodisation parameters [29]. The first anodisation step forms a thick oxide layer on the aluminium surface with irregular size distribution of nanopores due to repulsive forces and resulting mechanical stress between neighbouring pores. This layer is selectively removed to obtain hexagonally organised pits on the aluminium surface. The second anodisation step typically results in formation of an oxide layer with a uniform hexagonal close-packed cell arrangement with central cylindrical nanopores from top to bottom featuring a regular size distribution (**Figures 1.4b**). Furthermore, pore bottoms can be opened by removing the oxide barrier layer [50, 51]. This fabrication process is facile, relatively cost effective and can be scalable industrially. The geometric features of NAA, including pore diameter (d_p), pore length (L_p) and interpore distance (d_{int}), can be finely controlled by anodisation conditions. NAA with various pore diameters ranging from 15 to 250 nm can be obtained by controlling anodisation potential and the electrolyte used. Pore length can be controlled by anodisation time and interpore distance can be controlled using different electrolytes and anodisation voltages. These geometric features of NAAs are schematically described in **Figure 1.4a** [52-54].

In a typical anodisation process, aluminium foil is connected to the anode and platinum, or another conducting material, is connected to the cathode of a direct current (DC) power supply and both are immersed in an aqueous acid electrolyte solution (**Figures 1.4c**) [55]. The most commonly used acid electrolyte solutions utilised to grow NAA are sulphuric acid (H_2SO_4), oxalic acid ($H_2C_2O_4$) and phosphoric acid (H_3PO_4) [29, 42, 43].

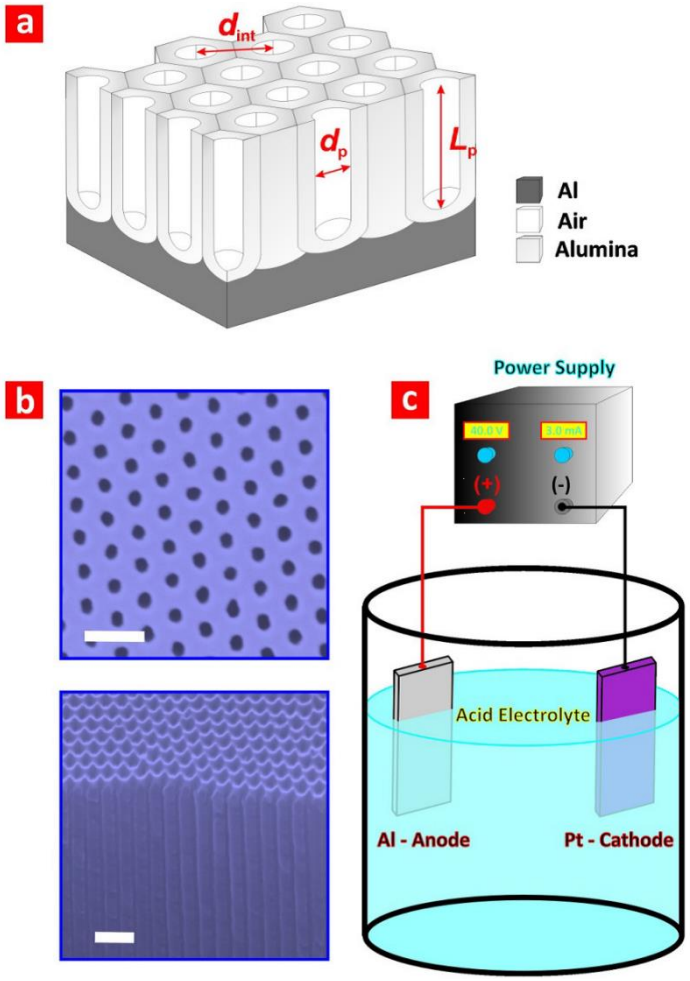

Figure 1.4. Schematic illustration showing (a) the geometric features of NAA (i.e. pore diameter, pore length and interpore distance), (b) top and cross sectional view SEM images of a typical NAA structure produced by electrochemical anodisation of Al in acid-based electrolyte (scales bar = 400 nm and 250 nm, respectively), and (c) schematic illustration of the basic electrochemical anodisation setup used to produce NAA. (Source [52]).

The formation mechanism of NAA is based on two competing and continuous processes: the oxidation of metal at the metal/oxide interface and oxide dissolution at the oxide/electrolyte interface [39]. These processes can be expressed by the following redox equations:

i) Formation of alumina (aluminium/alumina interface – anode)

$$2Al(s) + 3H_2O(l) \leftrightarrow Al_2O_3(s) + 6H^+(aq) + 6e^- \quad (1.1)$$

ii) Dissolution of alumina (alumina/electrolyte interface – anode)

$$Al_2O_3(s) + 6H^+(aq) \rightarrow 2Al^{3+}(aq) + 3H_2O(l) \quad (1.2)$$

iii) Diffusion of aluminium cations (within oxide barrier layer – anode)

$$2Al(s) \rightarrow 2Al^{3+}(aq) + 6e^- \quad (1.3)$$

iv) Hydrogen evolution (electrolyte/cathode interface – cathode)

$$6H^+(aq) + 6e^- \rightarrow 3H_2(g) \quad (1.4)$$

Due to unique physical, mechanical and chemical properties, NAAs have been used for production of one and two dimensional nanostructure materials (i.e. nanowires, nanorods, and nanotubes) using different approaches [44-48]. In addition to uniform, well-ordered structure and controllable dimensional features, the NAA surface can be easily functionalised using different approaches. Hydroxyl groups present at the NAA surface can be easily functionalised either by physical/gas-phase techniques or chemical methods [40, 56] to obtain NAAs with selective surface chemistry for specific applications.

The fabrication of nanomaterials using NAA as a template, reported for the first time by Martin *et al.*, allowed synthesis of various nanomaterials including polymers, metals and semiconductors [35, 36, 57-59]. This development facilitated the formation of nanomaterials using a template-direct approach which has attracted considerable interest from several research groups.

Many research groups have made extraordinary contributions to the synthesis of CNTs using nanoporous anodic alumina as templates. The earliest report was that of Kyotani *et al.* in 1995 [37, 60]. This group pioneered preparation of CNTs with different dimensions (i.e. pore diameters and

lengths) by carbonisation of propylene (as a gaseous carbon source) at 800°C using two different types of NAA template (i.e. commercial and home-made) (**Figure 1.5**). This study demonstrated the capability of template-assisted catalyst-free CVD to produce highly ordered arrays of CNTs structures with controllable dimensional features by replicating template dimensions. Subsequently, other groups synthesised such aligned CNTs structures using NAA as a template [34, 61-68].

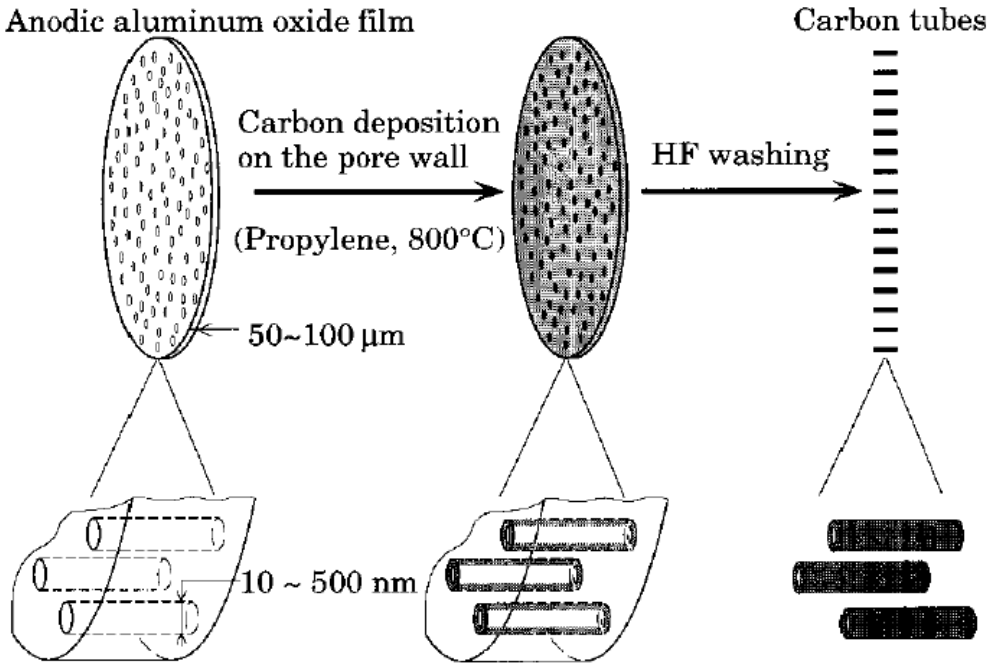

Figure 1.5. Schematic of the CNTs fabrication process by template-assisted free-catalyst CVD process using NAA as a template. (Source [60]).

In most reported studies, CNTs growth was promoted by use of a metal catalyst, in which the metal catalyst nanoparticle (commonly Co, Ni or Fe) is first electrochemically deposited at the bottom of alumina pores (**Figure 1.6**) [34, 62-68]. Then, the catalyst undergoes the activation process by exposure to a hydrogen stream at elevated temperature. The growth of CNTs is significantly affected by small differences in catalyst particle size. Moreover, impurities in resulting CNTs negatively impact CNTs performance for some applications. Some examples are blocked nanotubes, which hinder transport (i.e. flow) inside CNTs, while catalytic contaminations are

potentially toxic for humans and the environment, preventing the use of these nanostructures for drug delivery and biomedical applications [28].

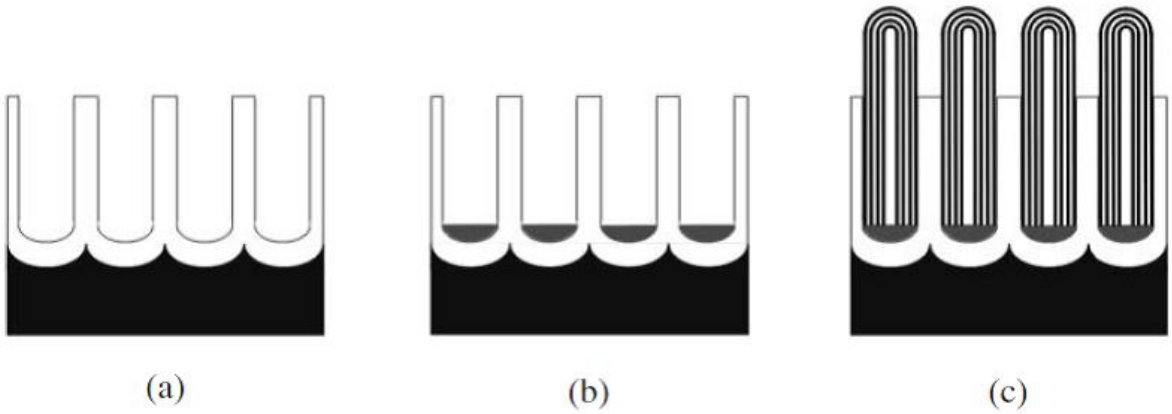

Figure 1.6. Schematic of the CNTs fabrication process by template-assisted catalyst CVD process using NAA as a template (Source [66]). (a) NAA template, (b) catalyst (Ni) is electrochemically deposited at the bottom of pores and (c) CNTs grown along the inner wall of NAA template.

Generally, aligned arrays of CNTs structures prepared using a NAA template have gained interest as a promising nanomaterial in different applications. For example, controllable dimension features and uniformity of these structures make it possible to develop field emitter devices [69, 70]. In electronic applications, arrays of CNTs-NAAs have been used as nanocapacitors [71] and for electrochemical energy storage and production [72]. They have also been used for developing sensors due to their unique electromechanical properties [73].

1.3.2. Titania Nanotubes Template

Fabrication of anodic titanium oxide structures was reported for the first time in 1999 by Zwilling *et al.* [74, 75]. In their study, chromic acid and a small amount of hydrofluoric acid were used to form titania nanotubes (TNTs) with limited tube length and a low degree of ordering. The observation of this structure was limited to the presence of hydrofluoric acid in the electrolyte mixture. After that report, formation of nanotubular structures in titania has attracted considerable

interest from several research groups. Similar to anodisation of aluminium, significant research effort has focused on the anodisation process of titanium to understand the role of different anodisation parameters (i.e. applied potential, time, electrolyte composition, pH, etc.) and their influence on resulting structures [38, 76-78]. Typically, TNTs are produced by anodisation of titanium in fluoride-based electrolytes. This is a simple, straightforward, inexpensive, self-driven and scalable process. The basic set-up for the self-ordering process, based on electrochemical anodisation of titanium, is shown in **Figure 1.7a**. In a typical anodisation process using titanium metal, titanium foil is connected to the anode and platinum, or another conducting material, is connected to the cathode of a direct current (DC) power supply and both are immersed in an aqueous electrolyte.

The formation mechanism of anodic titanium oxide is the same as that of anodic aluminium oxide, which is based on two competing and continuous processes: oxidation of metal at the oxide/metal interface and oxide dissolution at the oxide/electrolyte interface. The growth of oxide takes place at the titanium surface as a result of the interaction of titanium with O_2^- or OH^- anions. At the anode, titanium (Ti) is oxidised to Ti^{4+} cations under high voltage. Ti^{4+} cations migrate from the oxide/metal interface to the electrolyte/oxide interface and then into the solution by an electric field [79, 80]. This field assists dissolution of the oxide at the electrolyte/oxide interface and migration towards the metal oxide interface [81]. These processes can be expressed by the following redox equations:

$$Ti + 2H_2O \rightarrow TiO_2 + 4H^+ + 4e^- \quad (1.5)$$

$$Ti^{4+} + solv \rightarrow Ti^{4+}_{solv} \quad (1.6)$$

$$4H^+ + 4e^- \rightarrow 2H_2 \quad (1.7)$$

$$TiO_2 + 6F^- + 4H^+ \rightarrow [TiF_6]^{2-} + 2H_2O \quad (1.8)$$

$$Ti^{4+} + 6F^- \rightarrow [TiF_6]^{2-} \quad (1.9)$$

The typical morphology of TNT layers formed by the self-organised anodisation process in fluorine containing electrolytes (i.e. vertical arrays of cylindrical nanopores open at top and closed at the bottom) are shown in **Figure 1.7b and c** [82]. Structural features of TNTs, including tube diameter, length and inter-tube distance, can be precisely controlled through anodisation conditions (i.e. applied potential, anodisation time and electrolyte water content, respectively) [83]. These controllable structural features are key advantages of TNTs for use as a template for production of tubular nanostructures, including CNTs, with precisely engineered dimensional features by deposition of the desired material within TNT pores.

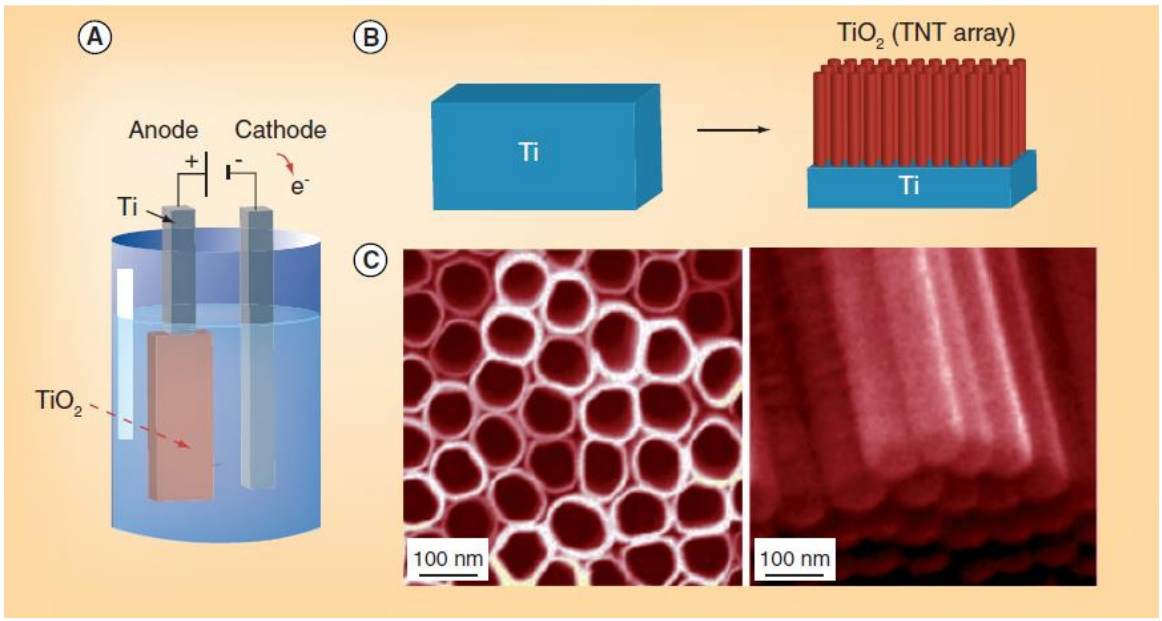

Figure 1.7. (a) Schematic illustration of the basic electrochemical anodisation setup used to produce TNTs; (b) fabrication process of vertically aligned arrays of TNTs on Ti substrate; and (c) top and cross sectional view SEM images of typical TNT structure produced by electrochemical anodisation of Ti in fluoride-based electrolyte (Source [82]).

A literature survey revealed limited reports on CNTs synthesis using TNTs as templates via the CVD process [84-87]. Eswaramoorthi and Hwang reported on the fabrication of CNTs using a catalyst-free CVD process with anodic titanium oxide as a template [84, 85]. The template was obtained by anodisation of pure titanium in a mixture of 1M H_2SO_4 and 0.5% HF used as

electrolyte at a constant potential of 40 V for 72 h. CNTs were formed by the CVD process using acetylene as carbon source. However, CNTs overgrew the template surface, therefore an appropriate purification process was needed to obtain CNTs-based composite material with accessible tube surfaces suitable for many applications. A particular application is to increase photocatalytic activity where reactants (i.e. light and targeted molecules) diffuse inside the tubular structure of CNTs-TNTs composite material.

Hesabi *et al.* and Mishre *et al.* reported on fabrication of CNTs-TNTs composites using a catalyst-based CVD process with ferrocene and cobalt as catalysts, respectively [86, 87]. These metal catalyst nanoparticles are first electrochemically deposited at the bottom of TNTs, then CNTs are formed during the CVD process through diffusion of C species along the catalyst particle (**Figure 1.8**). The main obstacle of using catalyst-based CVD methods for production of CNTs structures, besides several other disadvantages of catalyst-based CVD previously mentioned, is that residues of metal catalyst particles exist after post-purification treatments making the resulting CNTs potentially toxic to humans and the environment [28]. Therefore, this disadvantage could prevent the use of these CNTs-TNTs composites in environmental applications, such as photocatalysis.

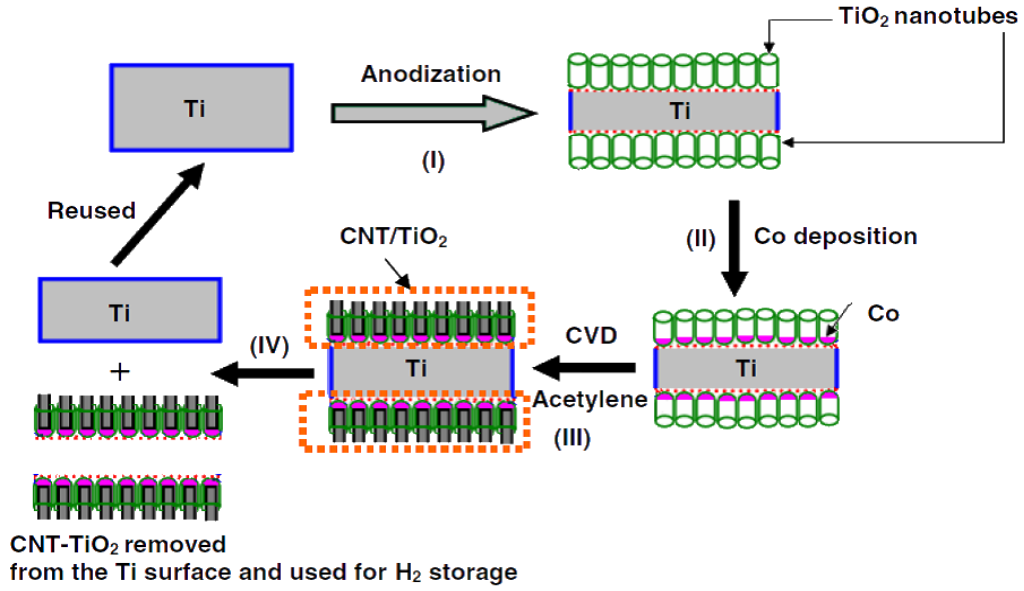

Figure 1.8. Schematic of CNTs fabrication by template-assisted catalyst CVD process using TNTs as a template (Source [86]).

The formation mechanism of CNTs produced by template-directed methods using a catalyst-free CVD process is not yet completely understood. Some research effort has been directed to addressing this knowledge gap since the first reports about fabrication of this type of CNTs structures in 1995. These efforts take into account the catalytic role of template material and subsequent thermal decomposition [88, 89]. However, more investigations are needed considering other possible aspects, including template nature and structural features, carbon source and so on.

1.4. Modification of Carbon Nanotubes

Pure CNTs are hydrophobic and chemically inert by nature as they are based on sp^2 carbon bonding. The nature of C – C bonds in CNT structure is responsible for these properties. Modification of CNT properties is a key factor to advancing performance for a wide range of applications [90]. Generally, two main routes are identified for surface functionalisation of CNTs: covalent and non-covalent functionalisation. Each route has advantages and disadvantages. Covalent functionalisation can be divided into two strategies, namely, direct covalent sidewall functionalisation and defect functionalisation. The former involves change in hybridisation of carbon in CNTs from sp^2 to sp^3 resulting in disruption of the π electron system in CNTs, while the latter takes advantage of chemical transformation of defect sites present in the structure of CNTs. **Figure 1.9** summarises these two strategies of covalent surface functionalisation of CNTs [91] which is recognised as an effective method for solubilisation or stable dispersion of CNTs, even though it often generates defects on CNT structure. Moreover, the ability to control the location of functionalisation is advantageous over non-covalent functionalisation.

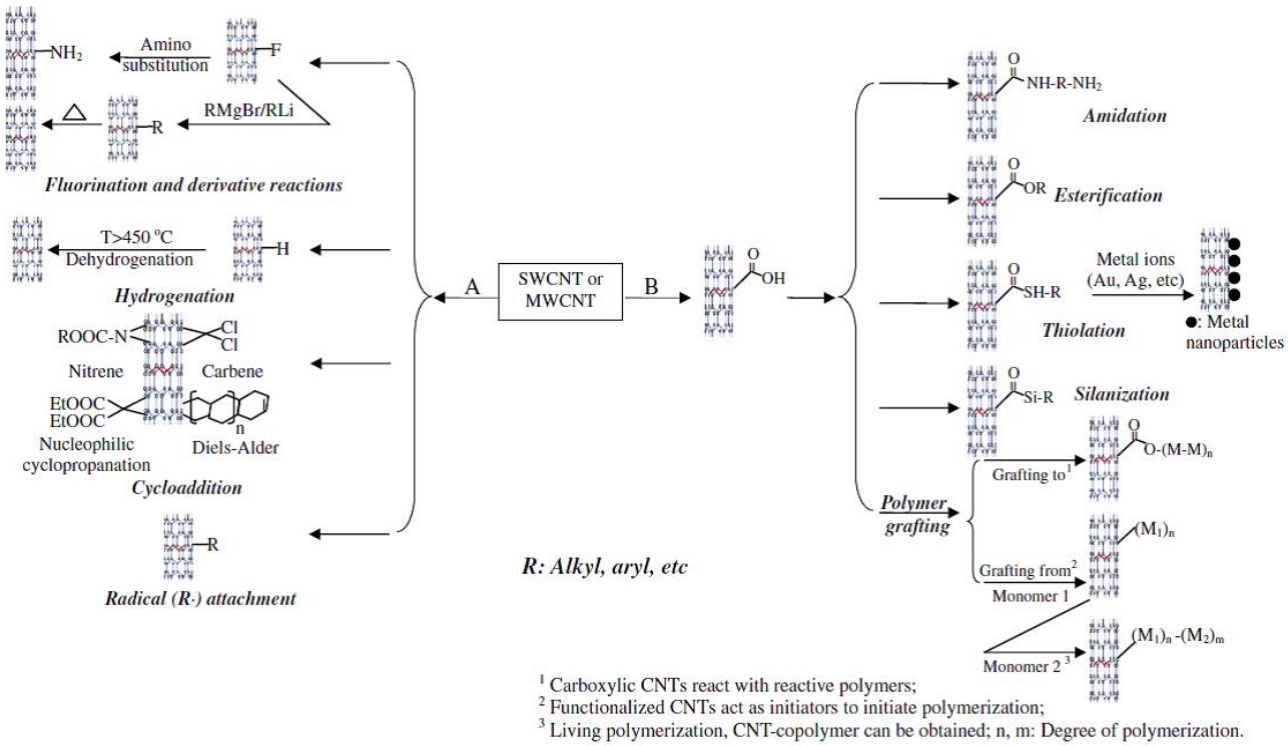

Figure 1.9. Summary of two strategies for covalent surface functionalisation of CNTs. (a) Direct functionalisation; and (b) defect functionalisation (Source [91]).

The non-covalent functionalisation strategy involves simple procedures to modify CNTs while retaining their structural properties. The CNTs can be non-covalently functionalised using various approaches including absorption of small aromatic molecules, surfactants and polymer grafting methods [92-94].

Oxidation is a common surface modification technique. Initially, oxidising acid, such as concentrated nitric acid or a mixture of nitric and sulphuric acid, was used for end-cap opening, filling and shortening CNTs [95, 96]. The oxidation process results in imparting oxygen-containing functional groups (e.g. -COOH, -OH, -C=O) into the CNT surface using strong oxidising agents including nitric acid (HNO_3) [97, 98], sulphuric acid (H_2SO_4) [99], sulphuric acid/hydrogen peroxide (piranha) [100, 101], ozone (O_3) [102] and perchloric acid ($HClO_4$) [103]. These oxidising agents have also been used to remove amorphous carbon and residual catalyst particles from CNTs structures. It is important to note that processes using harsh acids generally

alter surface features by generating defects on the graphitic structure of CNTs and result in destruction of CNTs sidewalls and breaking of CNTs [100, 101] leading to significant changes in CNTs performance for different applications. Note that these processes take place in the outer wall surfaces of CNTs. Modification of CNTs inner wall surfaces is discussed less in the literature because to modify CNTs inner surfaces the tubes tips need to be open and outer surfaces need to be protected. These requirements are not attainable by conventional methods used to prepare CNTs, however, templated-assisted methods make it possible to enable selective modification of CNTs inner surfaces while keeping outer surfaces intact [104]. For aligned CNTs structures, where alignment is a favourable configuration for CNTs to advance performance in many applications, care should be taken to not affect structural integrity during oxidation treatment. Oxidation can be further used to covalently attach molecules (e.g. alkyl groups, polymers, etc.) to CNTs [105-107].

Doping with foreign atoms (heteroatoms) is another avenue that aims to modify CNTs chemical structure, thus altering CNTs properties, and different experimental protocols have been examined including endohedral, intercalation and substitutional doping (**Figure 1.10**) [108]. In endohedral doping, the atoms or molecules are encapsulated in the CNTs hollow core, while in intercalation doping they are intercalated between the CNTs outer shells. Substitutional doping differs from the previous two approaches in that dopant atoms substitute C atoms in the graphitic lattice commonly resulting in generation of defects in CNTs structure as a result of the difference in atomic sizes. This process leads to rearrangement of C atoms in the graphitic network.

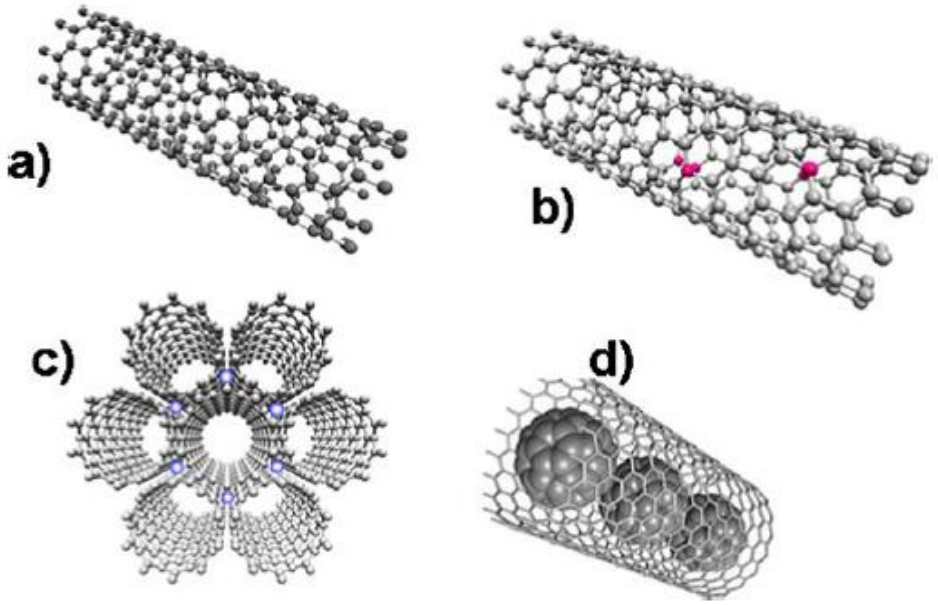

Figure 1.10. Schematic of the different protocols for modifying CNTs structure. (a) Pristine SWCNT; (b) substitutional; (c) intercalation; and (d) endohedral doping (Source [108]).

Among the different dopants including phosphorus (P), boron (B) and sulphur S, nitrogen (N) doping of CNTs has attracted much attention especially in electronic applications. As nitrogen has close atomic size to that of carbon (i.e. nitrogen contains one additional electron compared to carbon), nitrogen-doped CNTs structures may exhibit novel electronic and catalytic properties [109]. Nitrogen doping of CNTs has been explored for tuning and enhancing a set of CNTs properties, such as physical, chemical and catalytic activity properties [110-112].

Many studies have reported on CNTs doping with nitrogen [113-119], with most studies examining catalyst-based CVD processes using ferrocene as a metal catalyst. Besides the inherent drawbacks of catalyst-based CVD mentioned earlier, using metal catalysts to produce nitrogen doped CNTs structures always result in CNTs with periodic interlinked structures inside the nanotubes (i.e. a bamboo-like structure) (**Figure 1.11**) due to interaction between catalyst metal particles and CN species (i.e. difference in diffusion of CN species along the catalyst particle between bulk and surface) [120-122]. Moreover, significant changes in CNTs dimensions as a

result of incorporation of nitrogen atoms have been observed [113, 114]. These drawbacks have diminished the use of nitrogen doped CNTs structures in many applications, particularly molecular transport through their hollow tubular structures.

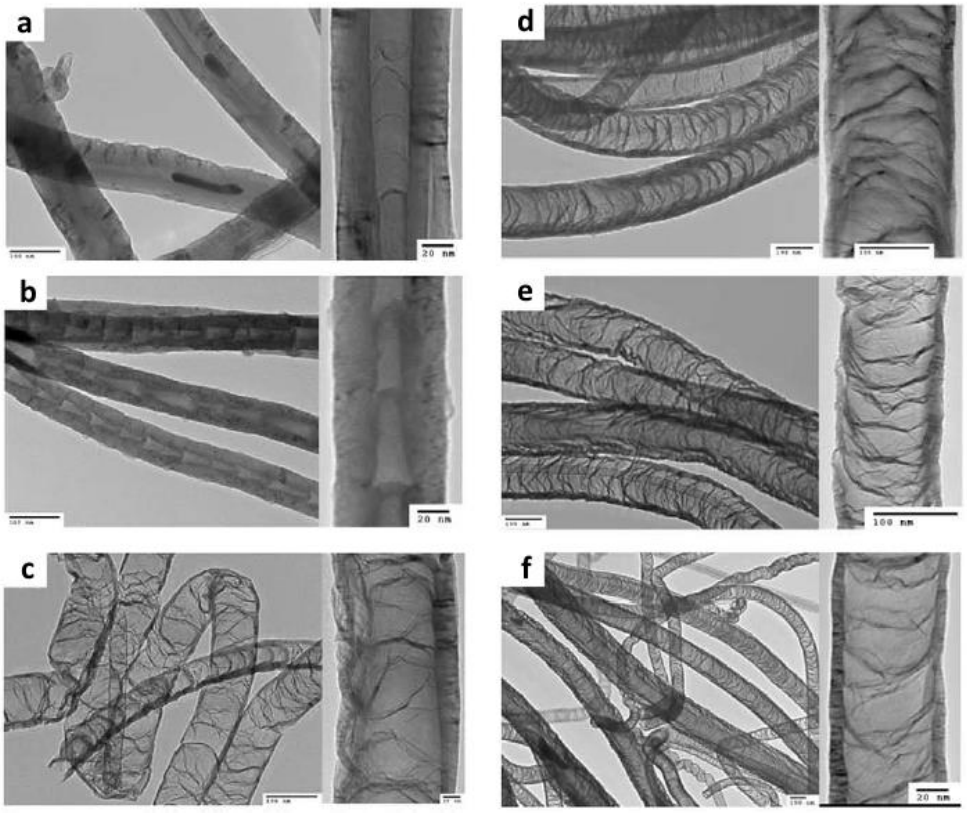

Figure 1.11. TEM images of CNTs structures produced by the catalyst-based CVD process using melamine as a precursor showing the characteristic bamboo-like structure with different nitrogen content of (a) 0%; (b) 1.5%; (c) 3.1%; (d) 5.4%; (e) 8% and (f) 8.4% (Source [115]).

A facile route to dope CNTs structure remains challenging, particularly for CNTs membranes with selective dopant atoms that do not affect geometric features.

1.5. Carbon Nanotubes Composite Membranes

1.5.1. Membrane Definition

Membrane can generally be defined as a semi-permeable barrier that prevents contact between two phases which can selectively control transport of chemical species through the membrane [123]. Based on structure, membranes can be classified as either porous or dense. Porous membranes can have a symmetric structure where pores are the same size, or asymmetric structure where pores are of different sizes [124]. Pore size is the distance between opposite walls of the pore. According to the International Union of Pure and Applied Chemistry (IUPAC), porous materials can be divided into three different ranges based on pore size, microporous < 2 nm, mesoporous 2-50 nm and macroporous > 50 nm [125]. For membrane-based separation technology, utilising dense membranes is limited due to low permeability in comparison to porous membranes [126]. Based on membrane pore size and separated species size, membrane systems can be classified into four types: microfiltration (MF), ultrafiltration (UF), nanofiltration (NF) and reverse osmosis (RO) [127].

1.5.2. Fabrication of Vertically Aligned Carbon Nanotubes Membranes

Two structural configurations have been identified for CNTs-based composite membranes:

i) Membranes with randomly distributed bundles of CNTs.

ii) Membranes with vertically aligned arrays of CNTs.

The formation of vertically aligned carbon nanotube membranes is of particular interest as this configuration endows the resulting membrane systems with better performance over membranes composed of randomly distributed bundles of CNTs [128, 129]. Alignment of CNTs can be obtained prior to, during or after composite fabrication. Hinds' group at the University of Kentucky [130] reported on fabrication of CNTs membranes with vertically aligned arrays of CNTs. Their

approach involved the catalyst-based CVD process using ferrocene to prepare CNTs. To maintain alignment, the space between CNTs was filled using a polymer (50 weight-percent solution of polystyrene and toluene) (**Figure 1.12**). The plasma oxidation process was used to remove excess polymer from the top surface and to open CNTs tips forming CNTs membranes. However, this approach is complex and the ultimate membrane structure is obtained after several days.

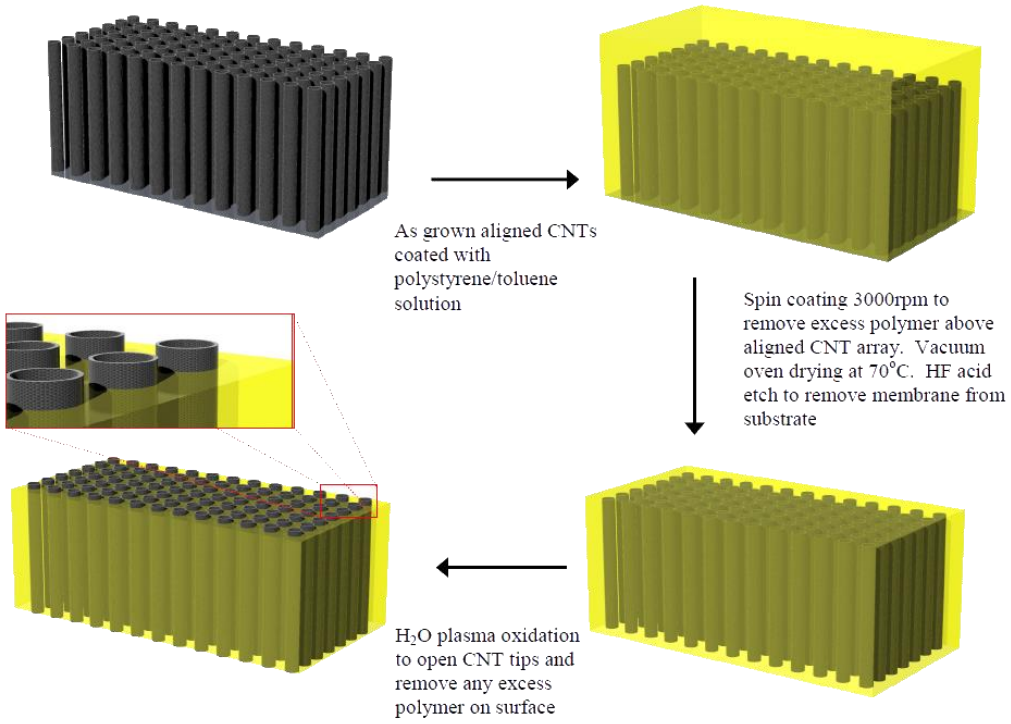

Figure 1.12. Schematic of the fabrication process of aligned CNTs membranes by embedding CNTs in a polymer matrix (Source [130]).

Another approach proposed by Holt and co-workers [131], was also based on the catalyst-based CVD process. The process starts with selective deposition of a thin layer of iron catalyst (~ 5-10 nm) by electron beam evaporation on Si substrate. This step is followed by many steps to prepare CNTs embedded in a silicon nitride matrix (**Figure 1.13**). The ultimate membrane structure is again obtained after several days.

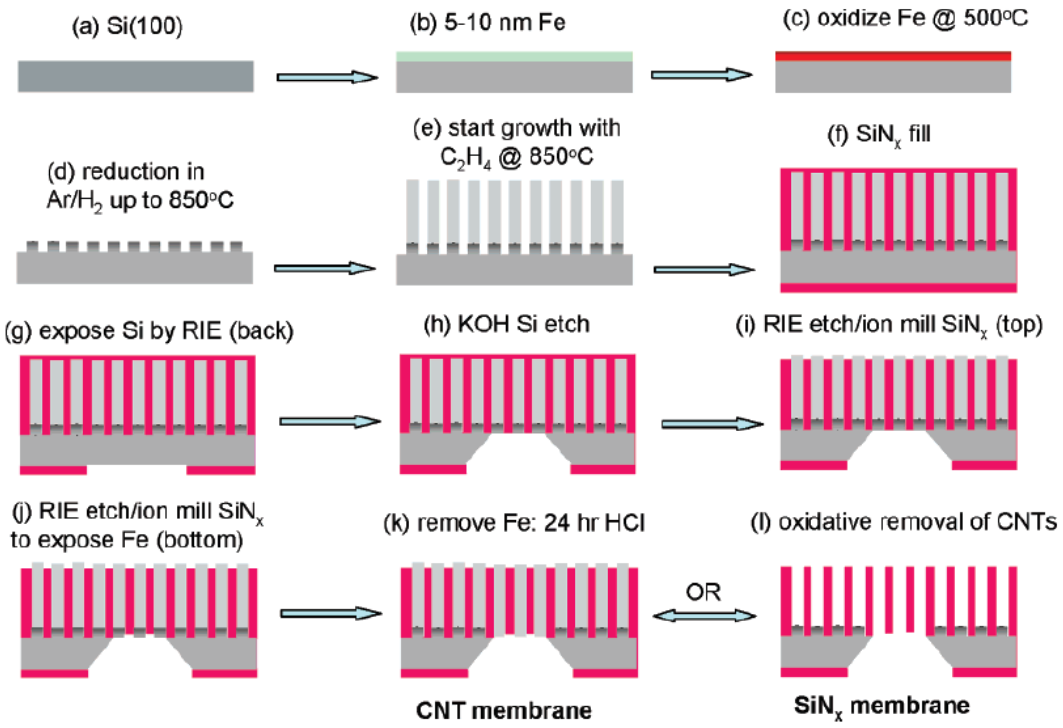

Figure 1.13. Schematic of the multi-step fabrication process of aligned CNTs membrane by embedding CNTs in silicon nitride matrix (Source [131]).

Along with the complex and time consuming processes of the abovementioned techniques to prepare aligned CNTs membranes, other inherent drawbacks should be pointed out. For example, these techniques are dependent on using a metal catalyst and, as previously mentioned, catalyst CVD processes have several disadvantages. Moreover, these methods require the use of expensive laboratory facilities that limit production of these membranes to the laboratory scale.

These drawbacks can be addressed by using a catalyst-free CVD process utilising nanoporous anodic alumina membranes (NAAMs) and titania nanotubes (TNTs) as templates to prepare CNTs membranes with vertically aligned arrays of CNTs. Schneider *et al.* reported on the formation of composite structures consisting of CNTs grown inside commercial NAAMs by a catalyst-free CVD process using propylene as a gaseous carbon source [88]. However, a by-product was found at the composite top surface recognised by SEM to be ca. 20 µm amorphous carbon layer (**Figure 1.14**). This layer blocks the pore entrance of the composite resulting in inaccessible CNTs

channels. Therefore, an appropriate purification process to remove this layer must be applied to obtain CNTs-based composite membranes with desirable features for many applications (e.g. transport, catalyst and separation, etc.).

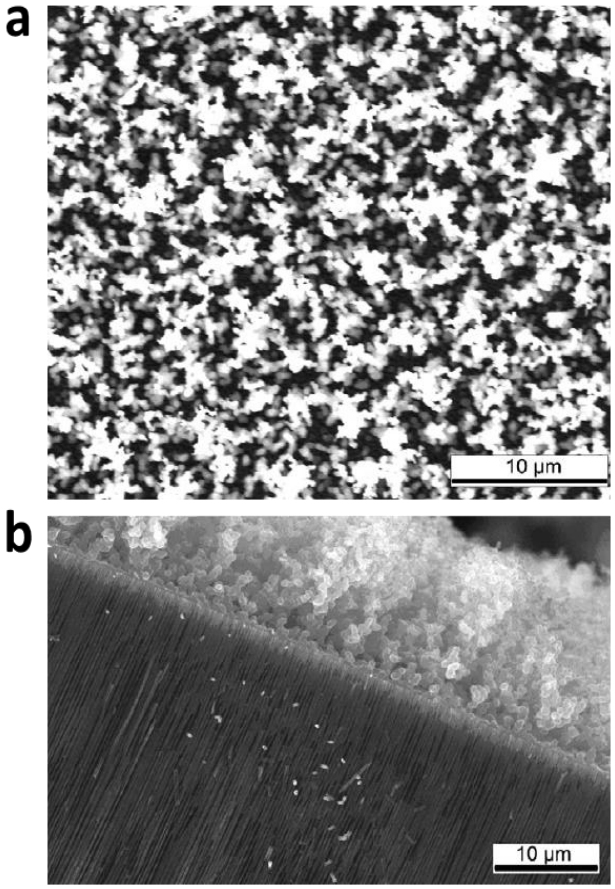

Figure 1.14. SEM images of CNTs-based composite membrane. (a) Top view and (b) side view showing coverage of the membrane surface with a thick amorphous carbon layer (Source [88]).

Recently, Sarno *et al.* fabricated CNTs inside commercial NAAMs by a catalyst-free CVD process using different hydrocarbons (acetylene, propylene, ethylene and methane) as gaseous carbon sources [132]. Despite the use of different gaseous carbon sources, including propylene as used in the Schneider *et al*. study, the disinclining of the SEM analysis of the composite membrane top surface did not allow to determine whether the carbon by-product was formed or not. Note that branching cylindrical pores is a characteristic feature of commercial NAAMs, therefore using them as a template results in branched CNTs structures.

A significant challenge remains to develop and characterise CNTs membranes with favourable characteristics for transport investigations, namely uniform and vertically aligned arrays of CNTs, controlled geometric and surface chemistry features, accessible tubes with no catalyst particles or internal closures.

1.6. Carbon Nanotubes as Molecular Transport Channels

The earliest study reporting on the capability of CNTs inner core use as nanochannel containers, demonstrated by Ajayan and Ijima in 1993 [133], focused on the influence of annealing in liquid lead on structural features of CNTs and subsequent filling with molten material through capillary action (i.e. a one-step process). In the same year, their group reported on opening of CNTs using gas oxidation reaction and its impact on filling (a two-step process) [134]. These researchers concluded that filling open CNTs with inorganic materials is more difficult than the one-step filling process.

Dujardin *et al.* studied wetting and capillarity of MWCNTs (2-20 nm) and SWCNTs (1.4 - 2.4 nm) in two separate publications. These authors found that liquids with a surface tension of less than 180 mN/m (e.g. water and organic solvents) in the range of 130-190 mN/m can wet MWCNTs and SWCNTs, respectively [135, 136].

Several molecular dynamic simulations and experimental studies have successfully demonstrated the outstanding transport properties and chemical selectivity of CNTs for a broad range of gases and molecules [128, 137-141]. Hummer *et al.* reported on water transport through CNTs based on molecular dynamic simulations [142] and suggested that the process of flowing water molecules through hydrophobic CNTs channels leads to H-bond formation between water molecules along the nanotube axis. These bonds, and weak interaction between water molecules and the smooth hydrophobic graphitic walls, facilitate extraordinary flow of water molecules. Sholl and Johnson [138, 143] reported on transport of light gases (e.g. H_2 and CH_4) through CNTs based on molecular

dynamic simulations. They found that transport rates in CNTs are orders of magnitude faster than in crystalline microporous zeolites and ascribed this finding to the smooth graphitic walls of CNTs and lack of friction at the interface between the hydrophobic graphitic walls of CNTs and gas molecules. However, note that these authors only considered defect-free nanotubes in their calculations.

Experimentally, Majumder *et al*. reported on the liquid (e.g. water, ethanol, hexane, etc.) flow through CNTs membranes prepared, using the method proposed by Hinds' group as previously mentioned, with 7 nm pore diameter [137]. These researchers found that liquid flow through CNTs membranes is four to five orders of magnitude faster than predicted by conventional fluid flow theory (**Table 1.1**). Holt *et al*. [128] compared the transport properties of DWCNTs membranes, prepared using the previously mentioned method, to commercial polycarbonate membranes and found that permeability of gas and water in DWCNTs membranes is higher than that of polycarbonate membranes and comparable to flow rates obtained through calculations of molecular dynamic simulations (**Table 1.2**).

Table 1.1. Flow of different solvents through CNTs membranes with 7 nm pore diameter (Source [137]).

Liquid	Initial permeability*	Observed flow velocity†	Expected flow velocity†	Slip length (mm)
Water	0.58	25	0.00057	54
	1.01	43.9	0.00057	68
	0.72	9.5	0.00015	39
Ethanol	0.35	4.5	0.00014	28
iso-Propanol	0.088	1.12	0.00077	13
Hexane	0.44	5.6	0.00052	9.5
Decane	0.053	0.67	0.00017	3.4

Table 1.2. Comparisons of experimental air flow rates observed for several CNTs membranes with Knudsen model predictions, and of experimental water flow rates with continuum flow model predictions (Source [128]).

Membrane	Pore diameter (nm)	Pore density (cm^{-2})	Thickness (μm)	Enhancement over Knudsen model* (minimum)	Enhancement over no-slip, hydrodynamic flow† (minimum)	Calculated minimum slip length‡ (nm)
DWNT 1	1.3 to 2.0	$\leq 0.25 \times 10^{12}$	2.0	40 to 120	1500 to 8400	380 to 1400
DWNT 2	1.3 to 2.0	$\leq 0.25 \times 10^{12}$	3.0	20 to 80	680 to 3800	170 to 600
DWNT 3	1.3 to 2.0	$\leq 0.25 \times 10^{12}$	2.8	16 to 60	560 to 3100	140 to 500
Polycarbonate	15	6×10^{8}	6.0	2.1	3.7	5.1

The aforementioned findings of fast liquid transport through CNTs raises a question regarding the interaction between the CNTs inner wall surface and transported molecules. Therefore, understanding transport properties at the nanoscale is a significant challenge. In this thesis, particular attention is paid to understanding the transport properties of CNTs with diameters in the range of 15-150 nm where a knowledge gap remains. Furthermore, as interfacial properties regulate transport through CNTs membranes, one of the concepts on which this thesis is based, changes in regard to charge of transported molecules, CNTs dimensional features and inner surface chemistry in a controlled manner will have important implications for selectivity properties and transport performance.

1.7. Carbon Nanotubes as Coupling Material for Photocatalysis Applications

This part of the thesis presents the second application of CNTs as a coupling material for photocatalysis applications.

I.7.1. Introductory Background

The advanced oxidation process (AOP) is a promising method to reduce water pollution and address water shortage problems [144, 145]. The photochemical advanced oxidation process for water treatment has been successfully commercialised in recent years. In 1972, Fujishima and Honda reported on photocatalytic decomposition of water on titanium dioxide electrodes for the first time, and since then photocatalysis has been successfully used for degradation of a broad variety of contaminants [146]. Photocatalysis is a simple process in which light of appropriate energy is used to activate a catalyst, usually a semiconductor, to generate an electron-hole pair and allowing redox reactions to take place. Photocatalysis based on nano-catalysts has been successfully demonstrated for degradation of multiple contaminants based on the fact that specific surface area plays a key role in the photocatalysis process. Consequently, using a nano-catalyst with high specific surface area leads to more adsorption sites for photocatalytic reactions making the process more efficient and effective [147].

Among various semiconductors, nanosized titanium dioxides (TiO_2) have attracted considerable attention as an effective photocatalyst due to unique properties, including large specific surface area, chemical stability, non-toxicity, high photocatalytic activity and low cost. TiO_2 has different crystalline structures and the most common polymorphs are rutile, anatase and brookite. Rutile is the most stable form of TiO_2, while anatase is the most active form that can be transformed into rutile by heating in the range of 400 to 1200 °C. The anatase TiO_2 structure provides high photocatalytic activity due to higher surface area and higher degree of hydroxylation of anatase in

comparison to other crystallographic phases. It has a large band gap (about 3.2 eV) which can be excited by UV light with wavelengths less than 388 nm [148].

Photocatalysis processes mainly rely on formation of reactive species, such as hydroxyl radicals (•OH). The hydroxyl radical is a powerful oxidant with the highest thermodynamic oxidation potential of common chemical species (~ 2.8 V) [149]. The photocatalysis process begins with absorption of a photon with energy equal or higher than the band gap energy (Eg) of TiO_2 [3.2 eV (anatase) or 3.0 eV (rutile)]. This leads to transition of the electron from the valance band (VB) to the conduction band (CB) creating a hole with a positive charge in the valance band (Eq. 1.10). This step is followed by many steps (Eq. 1.11-1.14) to form hydroxyl radicals that can decompose organic pollutants to carbon dioxide (CO_2) and water (H_2O) (Eq. 1.15) [149] (**Figure 1.15)**.

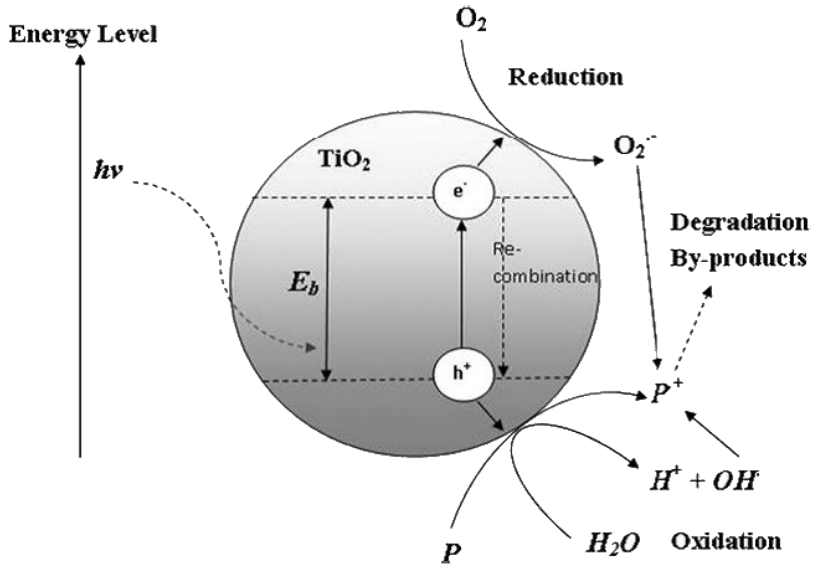

Figure 1.15. TiO_2 photocatalysis process in the presence of a water pollutant (P) [150].

Electron-hole pairs can rapidly recombine on the TiO_2 surface before redox reactions take place, thus decreasing efficiency of the TiO_2 catalyst.

$$TiO_2 + h\nu \rightarrow h^+_{vb} + e^-_{cb} \quad (1.10)$$

$$h^+_{vb} + H_2O_{ads} \rightarrow H^+ + \bullet OH \quad (1.11)$$

$$h^{+}_{vb} + 2OH^{-}_{ads} \rightarrow OH^{-} + \bullet OH \quad (1.12)$$

$$e^{-}_{cb} + O_{2\,ads} \rightarrow O_2^{\bullet -} \quad (1.13)$$

$$2O_2^{\bullet -} + 2H_2 \rightarrow 2 \bullet OH + 2OH^{-} + O_2 \quad (1.14)$$

$$\bullet OH + Organics \rightarrow H_2O + CO_2 \quad (1.15)$$

Different approaches have been used in attempts to increase the efficiency of a TiO_2 photocatalyst by absorbing solar energy and minimising or eliminating rapid recombination of the electron-hole pair, including doping TiO_2 with non-metal elements (nitrogen, sulphur and carbon) [151-154] and chemically modified n-TiO_2 [155, 156]. Another approach explored enhancement of TiO_2 photocatalytic efficiency by fabricating nanocomposites that combine TiO_2 with other materials, such as Ag [157], Pt [158], SiO_2, ZrO_2 [159] and Cu_2O [160]. Among the aforementioned composites, coupling TiO_2 with CNTs has recently attracted much attention due to the potential to overcome the intrinsic limitations of TiO_2. Therefore, this type of composite material is discussed in more detail below.

1.7.2. Carbon Nanotubes and Titania Composite

Due to the exceptional properties of CNTs, including electrical properties, high aspect ratio, high adsorption capacity, and chemical and thermal stability, they have been demonstrated as outstanding coupling materials to overcome the limitations of TiO_2 catalysts [161, 162]. The CNTs/TiO_2 composite has been used in different applications, such as solar cells, photo-catalysis and lithium storage [163-165].

To date, several studies have demonstrated that CNTs-TiO_2 composites prepared via a sol–gel approach can be a means of enhancing photocatalytic efficiency of TiO_2 [166-169]. However, this approach has intrinsic limitations, such as the difficulty of preparing uniform composites, which limit the positive impact of coupling these two materials. Another limitation is that most of TiO_2-

based composites explored were powder forms of TiO_2 which have less photocatalytic activity than nanotubular TiO_2 structures [170, 171]. Therefore, development of CNTs-TNTs composite materials with precisely designed and engineered physical and chemical features is of critical importance for improving the photocatalytic properties of TiO_2. Recently, Qu X *et al*. reported on a preparation method to produce a uniform composite structure of CNTs-TNTs using anodic aluminium oxide (AAO) membranes as templates to grow TNTs [172]. Although this method results in arrays of CNTs-TNTs with controlled geometry, the preparation of highly ordered AAO templates by a two-step anodisation process is time-consuming. In that respect, the direct utilisation of TNTs grown by anodising titanium substrates, as mentioned earlier, is considered a more facile approach to synthesise CNTs-TNTs composite structures with controlled geometry, taking advantage of a catalyst-free CVD approach. The nanotubular geometry of such photocatalyst is desired for providing a short carrier diffusion path in the nanotube wall and straight diffusion path for reactants [83, 170].

1.8. Challenges for CNTs-Based Composites for Molecular Transport and Photocatalysis Applications

The use of CNTs-based composite systems as conduits for molecular transport and catalysts, in combination with TiO_2 for photocatalysis applications, require CNTs to have precisely controlled physical and chemical properties to address the problems and intrinsic limitations of existing materials and achieve optimal performance for specific applications. Examples of the problems that need to be addressed are difficulty in controlling geometric features, contamination and incorporation of impurities into CNTs structure from catalyst particles and carbon precursors, presence of amorphous carbon structure on the membrane surface after deposition, internal closures, and selective modification of CNTs structures. Consequently, more extensive research is required to identify nanofabrication methods for advanced CNTs membranes with precisely controlled transport and chemical selectivity for electrophoretic and potential-based separation of

molecules, and to enhance the photocatalytic properties of TNTs for engineering advanced CNTs-TNTs electrodes for photocatalytic applications. Some of key challenges are:

1. Fabrication of CNTs composite membranes with controllable dimensional features and surface chemistry.
2. Selective modification of CNTs inner wall surface of composite membranes to achieve optimal performance in transport applications.
3. Understanding the transport of ions/molecules through CNTs membranes under different driving forces, such as concentration gradient and electrical field.
4. Fabrication of a uniform composite material of CNTs inside nanotubular structure of TNTs to obtain full advantages of using nanotubular geometry for photocatalysis.

1.9. Objectives

The broad objective of this thesis was to develop a CNT composite membrane/material with favourable characteristics for molecular transport and photocatalysis applications based on the catalyst-free CVD process using NAAMs and TNTs as templates. The specific objectives/aims of this thesis are:

1. To demonstrate fabrication of CNTs composite membranes with controllable dimensions (i.e. pore diameter and length) and surface chemistry by:
   - Fabricating CNTs composite membranes by growing vertically aligned MWCNTs inside NAAMs through a catalyst-free CVD approach.
   - Controlling CNTs dimensions *via* deposition time during the CVD process and length of NAAMs.
   - Controlling surface chemistry of CNTs inner walls *via* thermal annealing and wet and dry oxidation processes.

- Exploring the influence of CNTs dimensions and surface chemistry on transport and selectivity properties.

2. To demonstrate fabrication of CNTs composite membranes with controllable dimensions using different types of NAAMs templates by:

   - Fabricating CNTs composite membranes by growing vertically aligned MWCNTs inside different types of NAAMs through a catalyst-free CVD approach.
   - Exploring the influence of NAAM template types on structural and chemical properties of the resulting CNTs.
   - Explaining the formation mechanism of CNTs inside NAAMs of distinct chemical composition.
   - Analysing the effect of the NAAM template on transport properties of the resulting composite membranes.

3. To explore the effect of selective chemical modification of the inner surface of CNTs composite membranes on electrochemical properties by:

   - Modifying the inner wall surface of CNTs membranes through a wet oxidation process using hydrogen peroxide.
   - Demonstrating how surface chemistry inside CNTs can influence ionic conductivity and electrochemical properties of CNTs-NAAMs composite membranes using different electrolyte concentrations.
   - Understanding transport mechanisms of ions and molecules inside CNTs under an electrical field.

4. To selectively dope the structure of CNTs composite membranes with nitrogen atoms by:

- Fabricating N-doped CNTs composite membranes by growing vertically aligned N-doped MWCNTs inside NAAMs through a catalyst-free CVD approach.
- Determining the role of C/N ratio of carbon and nitrogen precursors in the formation and nitrogen content of N-doped CNTs-NAAMs using different precursor mixtures containing carbon and nitrogen at different ratios.
- Assessing transport performance and chemical selectivity of the resulting composite membranes (i.e. undoped and N-doped CNTs-NAAMs composite membranes).

5. To demonstrate the catalyst-free synthetic process of CNTs-TNTs composites by:
    - Fabricating CNTs composite material by growing vertically aligned MWCNTs inside TNTs through a catalyst-free CVD approach.
    - Explaining the formation mechanism of CNTs inside arrays of TNTs.
    - Evaluating photocatalytic properties of prepared CNTs-TNTs composites.

1.10. Thesis Structure

Chapter 1 provides a description of the thesis topic and its significance. Emphasis is placed on providing background information regarding fabrication and modification techniques of CNTs structures and other advances in the field of CNTs composite membranes and materials.

Chapter 2 provides details on materials and methods including NAAMs, TNTs and CNTs fabrication, and various investigations to evaluate applicability of CNTs composites for transport and photocatalytic applications. This chapter also briefly defines structural and chemical characterisation techniques used throughout this thesis.

Chapter 3 describes the fabrication of CNTs composite membranes with controllable nanotube dimensions (inner diameter and length) and surface chemistry produced by a template-assisted catalyst-free CVD process using NAAMs as a template and explores their influence on the transport properties and chemical based transport selectivity.

Chapter 4 discusses fabrication of CNTs composite membranes with controllable dimensions using different types of NAAM templates with a specific focus on exploring the influence of NAAM template type on structural and chemical properties of resulting CNTs composite membranes. The formation mechanism of CNTs inside NAAMs of distinct chemical composition is also explored and explained. Additionally, the effect of the NAAM template on transport properties of the resulting composite membranes is analysed.

Chapter 5 explores how surface conduction and electrochemical properties of CNTs composite membranes produced by a template-assisted catalyst-free CVD process using NAAMs as a template can be readily tuned by chemical modification of the inner surface using a simple oxidation process.

Chapter 6 reports on finely and selectively doping the structure of CNTs composite membranes with nitrogen. This chapter also describes the role of C/N ratio of carbon and nitrogen precursors in the formation and nitrogen content of N-doped CNTs-NAAMs which was determined using different mixtures of precursors. Furthermore, molecular transport and chemical selectivity properties of N-doped CNTs-NAAMs with different doping levels are assessed.

Chapter 7 presents the fabrication of CNTs inside TNTs templates by a catalyst-free CVD approach as composite platforms for photocatalytic applications. Furthermore, the formation mechanism of CNTs inside TNTs without using metal catalysts is explored and explained.

Chapter 8 summarises results of the investigations conducted in this thesis and provides a perspective for future research directions.

1.11. References

[1] Dai H. Carbon Nanotubes: Synthesis, Integration, and Properties. *Accounts of Chemical Research*. 2002;35(12):1035-44.

[2] Iijima S. Carbon nanotubes: past, present, and future. *Physica B: Condensed Matter*. 2002;323(1-4):1-5.

[3] Paradise M, Goswami T. Carbon nanotubes - Production and industrial applications. *Materials & Design*. 2007;28(5):1477-89.

[4] Terranova ML, Sessa V, Rossi M. The world of carbon nanotubes: an overview of CVD growth methodologies. *Chemical Vapor Deposition*. 2006;12(6):315-25.

[5] Radushkevich L, Lukyanovich V. O strukture ugleroda, obrazujucegosja pri termiceskom razlozenii okisi ugleroda na zeleznom kontakte. *Zurn Fisic Chim*. 1952;26(1):88-95.

[6] Monthioux M, Kuznetsov VL. Who should be given the credit for the discovery of carbon nanotubes? *Carbon*. 2006;44(9):1621-3.

[7] Iijima S. Helical microtubules of graphitic carbon. *Nature*. 1991;354(6348):56-8.

[8] Iijima S, Ichihashi T. Single-shell carbon nanotubes of 1-nm diameter. 1993.

[9] Bethune D, Klang C, De Vries M, Gorman G, Savoy R, Vazquez J, et al. Cobalt-catalysed growth of carbon nanotubes with single-atomic-layer walls. 1993.

[10] Thostenson ET, Ren Z, Chou T-W. Advances in the science and technology of carbon nanotubes and their composites: a review. *Composites Science and Technology*. 2001;61(13):1899-912.

[11] Dervishi E, Li Z, Xu Y, Saini V, Biris AR, Lupu D, et al. Carbon nanotubes: synthesis, properties, and applications. *Particulate Science and Technology*. 2009;27(2):107-25.

[12] Popov VN. Carbon nanotubes: properties and application. *Materials Science and Engineering: R: Reports*. 2004;43(3):61-102.

[13] Lee CJ, Park J, Kang SY, Lee JH. Growth and field electron emission of vertically aligned multiwalled carbon nanotubes. *Chemical Physics Letters*. 2000;326(1):175-80.

[14] Landi BJ, Ganter MJ, Cress CD, DiLeo RA, Raffaelle RP. Carbon nanotubes for lithium ion batteries. *Energy & Environmental Science*. 2009;2(6):638-54.

[15] Kong J, Franklin NR, Zhou C, Chapline MG, Peng S, Cho K, et al. Nanotube molecular wires as chemical sensors. *Science*. 2000;287(5453):622-5.

[16] Li J, Stevens R, Delzeit L, Ng HT, Cassell A, Han J, et al. Electronic properties of multiwalled carbon nanotubes in an embedded vertical array. *Applied Physics Letters*. 2002;81(5):910-2.

[17] Corry B. Designing carbon nanotube membranes for efficient water desalination. *The Journal of Physical Chemistry B*. 2008;112(5):1427-34.

[18] Noy A, Park HG, Fornasiero F, Holt JK, Grigoropoulos CP, Bakajin O. Nanofluidics in carbon nanotubes. *Nano Today*. 2007;2(6):22-9.

[19] Majumder M, Stinchcomb A, Hinds BJ. Towards mimicking natural protein channels with aligned carbon nanotube membranes for active drug delivery. *Life Sciences*. 2010;86(15):563-8.

[20] Reddy ALM, Gowda SR, Shaijumon MM, Ajayan PM. Hybrid nanostructures for energy storage applications. *Advanced Materials*. 2012;24(37):5045-64.

[21] Szabó A, Perri C, Csató A, Giordano G, Vuono D, Nagy JB. Synthesis methods of carbon nanotubes and related materials. *Materials*. 2010;3(5):3092-140.

[22] Ebbesen T, Ajayan P. Large-scale synthesis of carbon nanotubes. *Nature*. 1992;358(6383):220-2.

[23] Seraphin S, Zhou D, Jiao J, Withers JC, Loutfy R. Effect of processing conditions on the morphology and yield of carbon nanotubes. *Carbon*. 1993;31(5):685-9.

[24] Guo T, Nikolaev P, Rinzler A, Tomanek D. D. T. Colbert and RE Smalley. *Nature*. 1995.

[25] Ismail A, Goh PS, Sanip S, Aziz M. Transport and separation properties of carbon nanotube-mixed matrix membrane. *Separation and Purification Technology*. 2009;70(1):12-26.

[26] Endo M, Takeuchi K, Igarashi S, Kobori K, Shiraishi M, Kroto HW. The production and structure of pyrolytic carbon nanotubes (PCNTs). *Journal of Physics and Chemistry of Solids*. 1993;54(12):1841-8.

[27] Dai H, Rinzler AG, Nikolaev P, Thess A, Colbert DT, Smalley RE. Single-wall nanotubes produced by metal-catalyzed disproportionation of carbon monoxide. *Chemical Physics Letters*. 1996;260(3):471-5.

[28] Gracial Tejral NRP, Havel J. Carbon nanotubes: toxicological impact on human health and environment. *Carbon*. 2009;7(1):1-13.

[29] Masuda H, Fukuda K. Ordered metal nanohole arrays made by a two-step replication of honeycomb structures of anodic alumina. *Science*. 1995;268(5216):1466-8.

[30] Roy P, Berger S, Schmuki P. TiO2 nanotubes: synthesis and applications. *Angewandte Chemie International Edition*. 2011;50(13):2904-39.

[31] Journet C, Maser W, Bernier P, Loiseau A, De La Chapelle ML, Lefrant dlS, et al. Large-scale production of single-walled carbon nanotubes by the electric-arc technique. *Nature*. 1997;388(6644):756-8.

[32] Thess A, Lee R, Nikolaev P, Dai H. Crystalline ropes of metallic carbon nanotubes. *Science*. 1996;273(5274):483.

[33] Lin J-Y, Cheng P-J. CVD of Carbon Nanotubes with Catalytic Nanoparticles. *淡江理工學刊*. 2007;10(2):103-6.

[34] Yap H, Ramaker B, Sumant A, Carpick R. Growth of mechanically fixed and isolated vertically aligned carbon nanotubes and nanofibers by DC plasma-enhanced hot filament chemical vapor deposition. *Diamond and Related Materials*. 2006;15(10):1622-8.

[35] Martin CR. Membrane-based synthesis of nanomaterials. *Chemistry of Materials*. 1996;8(8):1739-46.

[36] Martin CR. Nanomaterials--a membrane-based synthetic approach: *DTIC Document*; 1994.

[37] Kyotani T, Tsai L-f, Tomita A. Formation of ultrafine carbon tubes by using an anodic aluminum oxide film as a template. *Chemistry of Materials*. 1995;7(8):1427-8.

[38] Ghicov A, Schmuki P. Self-ordering electrochemistry: a review on growth and functionality of TiO 2 nanotubes and other self-aligned MO x structures. *Chemical Communications*. 2009(20):2791-808.

[39] Lee W, Park S-J. Porous anodic aluminum oxide: anodization and templated synthesis of functional nanostructures. *Chemical Reviews*. 2014;114(15):7487-556.

[40] Jani AMM, Losic D, Voelcker NH. Nanoporous anodic aluminium oxide: Advances in surface engineering and emerging applications. *Progress in Materials Science*. 2013;58(5):636-704.

[41] Lee W, Ji R, Gösele U, Nielsch K. Fast fabrication of long-range ordered porous alumina membranes by hard anodization. *Nature Materials*. 2006;5(9):741-7.

[42] Masuda H, Hasegwa F, Ono S. Self-Ordering of Cell Arrangement of Anodic Porous Alumina Formed in Sulfuric Acid Solution. *Journal of the Electrochemical Society*. 1997;144(5):L127-L30.

[43] Masuda H, Yada K, Osaka A. Self-ordering of cell configuration of anodic porous alumina with large-size pores in phosphoric acid solution. *Japanese Journal of Applied Physics*. 1998;37(11A):L1340.

[44] Kant K, Losic D, Sabzi RE. Template synthesis of nickel, cobalt, and nickel hexacyanoferrate nanodot, nanorod, and nanotube arrays. *International Journal of Nanoscience*. 2011;10(01n02):1-6.

[45] Masuda H, Ohya M, Asoh H, Nakao M, Nohtomi M, Tamamura T. Photonic crystal using anodic porous alumina. *Japanese Journal of Applied Physics*. 1999;38(12A):L1403.

[46] Martin CR. Nanomaterials: A Membrane-Based Synthetic Approach. *Science*. 1994;266(5193):1961-6.

[47] Hoyer P. Formation of a titanium dioxide nanotube array. *Langmuir*. 1996;12(6):1411-3.

[48] Routkevitch D, Bigioni T, Moskovits M, Xu JM. Electrochemical fabrication of CdS nanowire arrays in porous anodic aluminum oxide templates. *The Journal of Physical Chemistry*. 1996;100(33):14037-47.

[49] Bengough G, Stuart J. The anodic oxidation of aluminium and its alloys as a protection against corrosion. *British Patent*. 1923;223.

[50] Lillo M, Losic D. Pore opening detection for controlled dissolution of barrier oxide layer and fabrication of nanoporous alumina with through-hole morphology. *Journal of Membrane Science*. 2009;327(1–2):11-7.

[51] Losic D, Losic Jr D. Preparation of porous anodic alumina with periodically perforated pores. *Langmuir*. 2009;25(10):5426-31.

[52] Santos A, Kumeria T, Losic D. Nanoporous anodic alumina: a versatile platform for optical biosensors. *Materials*. 2014;7(6):4297-320.

[53] Santos A, Kumeria T, Losic D. Nanoporous anodic aluminum oxide for chemical sensing and biosensors. *TrAC Trends in Analytical Chemistry*. 2013;44:25-38.

[54] Li A, Müller F, Birner A, Nielsch K, Gösele U. Hexagonal pore arrays with a 50–420 nm interpore distance formed by self-organization in anodic alumina. *Journal of Applied Physics*. 1998;84(11):6023-6.

[55] Ghicov A, Schmuki P. Self-ordering electrochemistry: a review on growth and functionality of TiO2 nanotubes and other self-aligned MOx structures. *Chemical Communications*. 2009(20):2791-808.

[56] Kumeria T, Santos A, Losic D. Nanoporous anodic alumina platforms: engineered surface chemistry and structure for optical sensing applications. *Sensors*. 2014;14(7):11878-918.

[57] Liang W, Martin CR. Template-synthesized polyacetylene fibrils show enhanced supermolecular order. *Journal of the American Chemical Society*. 1990;112(26):9666-8.

[58] Brumlik CJ, Martin CR. Template synthesis of metal microtubules. *Journal of the American Chemical Society*. 1991;113(8):3174-5.

[59] Klein JD, Herrick RD, Palmer D, Sailor MJ, Brumlik CJ, Martin CR. Electrochemical fabrication of cadmium chalcogenide microdiode arrays. *Chemistry of Materials*. 1993;5(7):902-4.

[60] Kyotani T, Tsai L-f, Tomita A. Preparation of ultrafine carbon tubes in nanochannels of an anodic aluminum oxide film. *Chemistry of Materials*. 1996;8(8):2109-13.

[61] Zhi L, Wu J, Li J, Kolb U, Müllen K. Carbonization of Disclike Molecules in Porous Alumina Membranes: Toward Carbon Nanotubes with Controlled Graphene-Layer Orientation. *Angewandte Chemie International Edition*. 2005;44(14):2120-3.

[62] Che G, Lakshmi B, Martin C, Fisher E, Ruoff RS. Chemical vapor deposition based synthesis of carbon nanotubes and nanofibers using a template method. *Chemistry of Materials*. 1998;10(1):260-7.

[63] Li J, Papadopoulos C, Xu J, Moskovits M. Highly-ordered carbon nanotube arrays for electronics applications. *Applied Physics Letters*. 1999;75(3):367-9.

[64] Iwasaki T, Motoi T, Den T. Multiwalled carbon nanotubes growth in anodic alumina nanoholes. *Applied Physics Letters*. 1999;75(14):2044-6.

[65] Jeong S-H, Hwang H-Y, Hwang S-K, Lee K-H. Carbon nanotubes based on anodic aluminum oxide nano-template. *Carbon*. 2004;42(10):2073-80.

[66] Hashishin T, Tono Y, Tamaki J. Guide growth of carbon nanotube arrays using anodic porous alumina with ni catalyst. *Japanese Journal of Applied Physics*. 2006;45(1R):333.

[67] Yuan Z-h, Huang H, Liu L, Fan S-s. Controlled growth of carbon nanotubes in diameter and shape using template-synthesis method. *Chemical Physics Letters*. 2001;345(1):39-43.

[68] Suh JS, Lee JS. Highly ordered two-dimensional carbon nanotube arrays. *Applied physics letters*. 1999;75(14):2047-9.

[69] Yu WJ, Cho YS, Choi GS, Kim D. Patterned carbon nanotube field emitter using the regular array of an anodic aluminium oxide template. *Nanotechnology*. 2005;16(5):S291.

[70] Gao H, Mu C, Wang F, Xu D, Wu K, Xie Y, et al. Field emission of large-area and graphitized carbon nanotube array on anodic aluminum oxide template. *Journal of Applied Physics*. 2003;93(9):5602-5.

[71] Sohn JI, Kim Y-S, Nam C, Cho B, Seong T-Y, Lee S. Fabrication of high-density arrays of individually isolated nanocapacitors using anodic aluminum oxide templates and carbon nanotubes. *Applied Physics Letters*. 2005;87(12):123115.

[72] Che G, Lakshmi BB, Fisher ER, Martin CR. Carbon nanotubule membranes for electrochemical energy storage and production. *Nature*. 1998;393(6683):346-9.

[73] Rashidi A, Omidi M, Choolaei M, Nazarzadeh M, Yadegari A, Haghierosadat F, et al. Electromechanical properties of vertically aligned carbon nanotube. *Advanced Materials Research: Trans Tech Publ*; p. 332-6.

[74] Zwilling V, Aucouturier M, Darque-Ceretti E. Anodic oxidation of titanium and TA6V alloy in chromic media. An electrochemical approach. *Electrochimica Acta*. 1999;45(6):921-9.

[75] Zwilling V, Darque-Ceretti E, Boutry-Forveille A, David D, Perrin M-Y, Aucouturier M. Structure and physicochemistry of anodic oxide films on titanium and TA6V alloy. *Surface and Interface Analysis*. 1999;27(7):629-37.

[76] Macak JM, Tsuchiya H, Schmuki P. High-aspect-ratio TiO2 nanotubes by anodization of titanium. *Angewandte Chemie International Edition*. 2005;44(14):2100-2.

[77] Macak JM, Tsuchiya H, Taveira L, Aldabergerova S, Schmuki P. Smooth anodic TiO2 nanotubes. *Angewandte Chemie International Edition*. 2005;44(45):7463-5.

[78] Macak JM, Sirotna K, Schmuki P. Self-organized porous titanium oxide prepared in Na 2 SO 4/NaF electrolytes. *Electrochimica Acta*. 2005;50(18):3679-84.

[79] Mor GK, Varghese OK, Paulose M, Shankar K, Grimes CA. A review on highly ordered, vertically oriented TiO 2 nanotube arrays: fabrication, material properties, and solar energy applications. *Solar Energy Materials and Solar Cells*. 2006;90(14):2011-75.

[80] Su Z, Zhou W. Formation mechanism of porous anodic aluminium and titanium oxides. *Advanced Materials*. 2008;20(19):3663-7.

[81] O'sullivan J, Wood G. The morphology and mechanism of formation of porous anodic films on aluminium. Proceedings of the Royal Society of London A: Mathematical, Physical and Engineering Sciences: *The Royal Society*; p. 511-43.

[82] Gulati K, Aw MS, Findlay D, Losic D. Local drug delivery to the bone by drug-releasing implants: perspectives of nano-engineered titania nanotube arrays. *Therapeutic Delivery*. 2012;3(7):857-73.

[83] Alsawat M, Altalhi T, Shapter JG, Losic D. Influence of dimensions, inter-distance and crystallinity of titania nanotubes (TNTs) on their photocatalytic activity. *Catalysis Science & Technology*. 2014;4(7):2091-8.

[84] Eswaramoorthi I, Hwang L-P. Synthesis and characterisation of larger diameter multi-walled carbon nanotubes over anodic titanium oxide template. *Carbon*. 2006;44(11):2341-4.

[85] Eswaramoorthi I, Hwang L-P. Anodic titanium oxide: a new template for the synthesis of larger diameter multi-walled carbon nanotubes. *Diamond and Related Mmaterials*. 2007;16(8):1571-8.

[86] Mishra A, Banerjee S, Mohapatra SK, Graeve OA, Misra M. Synthesis of carbon nanotube–TiO2 nanotubular material for reversible hydrogen storage. *Nanotechnology*. 2008;19(44):445607.

[87] Hesabi ZR, Allam NK, Dahmen K, Garmestani H, A. El-Sayed M. Self-standing crystalline TiO2 nanotubes/CNTs heterojunction membrane: Synthesis and characterization. *ACS Applied Materials & Interfaces*. 2011;3(4):952-5.

[88] Schneider JJ, Maksimova NI, Engstler J, Joshi R, Schierholz R, Feile R. Catalyst free growth of a carbon nanotube–alumina composite structure. *Inorganica Chimica Acta*. 2008;361(6):1770-8.

[89] Sarno M, Tamburrano A, Arurault L, Fontorbes S, Pantani R, Datas L, et al. Electrical conductivity of carbon nanotubes grown inside a mesoporous anodic aluminium oxide membrane. *Carbon*. 2013;55:10-22.

[90] Gao C, Guo Z, Liu J-H, Huang X-J. The new age of carbon nanotubes: an updated review of functionalized carbon nanotubes in electrochemical sensors. *Nanoscale*. 2012;4(6):1948-63.

[91] Ma P-C, Siddiqui NA, Marom G, Kim J-K. Dispersion and functionalization of carbon nanotubes for polymer-based nanocomposites: a review. Composites Part A: *Applied Science and Manufacturing*. 2010;41(10):1345-67.

[92] Coleman JN, Dalton A, Curran S, Rubio A, Davey A, Drury A, et al. Phase separation of carbon nanotubes and turbostratic graphite using a functional organic polymer. *Advanced Materials*. 2000;12(3):213-6.

[93] Moore VC, Strano MS, Haroz EH, Hauge RH, Smalley RE, Schmidt J, et al. Individually suspended single-walled carbon nanotubes in various surfactants. *Nano Letters*. 2003;3(10):1379-82.

[94] Matarredona O, Rhoads H, Li Z, Harwell JH, Balzano L, Resasco DE. Dispersion of single-walled carbon nanotubes in aqueous solutions of the anionic surfactant NaDDBS. *The Journal of Physical Chemistry B*. 2003;107(48):13357-67.

[95] Tsang S, Chen Y, Harris P, Green M. A simple chemical method of opening and filling carbon nanotubes. *Nature*. 1994;372(6502):159-62.

[96] Liu J, Rinzler AG, Dai H, Hafner JH, Bradley RK, Boul PJ, et al. Fullerene pipes. *Science*. 1998;280(5367):1253-6.

[97] Dettlaff-Weglikowska U, Benoit J-M, Chiu P-W, Graupner R, Lebedkin S, Roth S. Chemical functionalization of single walled carbon nanotubes. *Current Applied Physics*. 2002;2(6):497-501.

[98] Goyanes S, Rubiolo G, Salazar A, Jimeno A, Corcuera M, Mondragon I. Carboxylation treatment of multiwalled carbon nanotubes monitored by infrared and ultraviolet spectroscopies and scanning probe microscopy. *Diamond and Related Materials*. 2007;16(2):412-7.

[99] Zhang J, Zou H, Qing Q, Yang Y, Li Q, Liu Z, et al. Effect of chemical oxidation on the structure of single-walled carbon nanotubes. *The Journal of Physical Chemistry B*. 2003;107(16):3712-8.

[100] Rosca ID, Watari F, Uo M, Akasaka T. Oxidation of multiwalled carbon nanotubes by nitric acid. *Carbon*. 2005;43(15):3124-31.

[101] Datsyuk V, Kalyva M, Papagelis K, Parthenios J, Tasis D, Siokou A, et al. Chemical oxidation of multiwalled carbon nanotubes. *Carbon*. 2008;46(6):833-40.

[102] Li M, Boggs M, Beebe TP, Huang C. Oxidation of single-walled carbon nanotubes in dilute aqueous solutions by ozone as affected by ultrasound. *Carbon*. 2008;46(3):466-75.

[103] Lu C, Chiu H. Adsorption of zinc (II) from water with purified carbon nanotubes. *Chemical Engineering Science*. 2006;61(4):1138-45.

[104] Kyotani T, Nakazaki S, Xu W-H, Tomita A. Chemical modification of the inner walls of carbon nanotubes by HNO 3 oxidation. *Carbon*. 2001;39(5):782-5.

[105] Hamon MA, Chen J, Hu H, Chen Y, Itkis ME, Rao AM, et al. Dissolution of single-walled carbon nanotubes. *Advanced Materials*. 1999;11(10):834-40.

[106] Chen J, Rao AM, Lyuksyutov S, Itkis ME, Hamon MA, Hu H, et al. Dissolution of full-length single-walled carbon nanotubes. *The Journal of Physical Chemistry B*. 2001;105(13):2525-8.

[107] Riggs JE, Guo Z, Carroll DL, Sun Y-P. Strong luminescence of solubilized carbon nanotubes. *Journal of the American Chemical Society*. 2000;122(24):5879-80.

[108] Ayala P, Arenal R, Loiseau A, Rubio A, Pichler T. The physical and chemical properties of heteronanotubes. *Reviews of Modern Physics*. 2010;82(2):1843.

[109] Terrones M, Jorio A, Endo M, Rao A, Kim Y, Hayashi T, et al. New direction in nanotube science. *Materials Today*. 2004;7(10):30-45.

[110] Chun K-Y, Lee HS, Lee CJ. Nitrogen doping effects on the structure behavior and the field emission performance of double-walled carbon nanotubes. *Carbon*. 2009;47(1):169-77.

[111] Bian S-W, Ma Z, Song W-G. Preparation and characterization of carbon nitride nanotubes and their applications as catalyst supporter. *The Journal of Physical Chemistry C*. 2009;113(20):8668-72.

[112] Gong K, Du F, Xia Z, Durstock M, Dai L. Nitrogen-doped carbon nanotube arrays with high electrocatalytic activity for oxygen reduction. *Science*. 2009;323(5915):760-4.

[113] Bulusheva L, Okotrub A, Kurenya A, Zhang H, Zhang H, Chen X, et al. Electrochemical properties of nitrogen-doped carbon nanotube anode in Li-ion batteries. *Carbon*. 2011;49(12):4013-23.

[114] Koós AA, Dowling M, Jurkschat K, Crossley A, Grobert N. Effect of the experimental parameters on the structure of nitrogen-doped carbon nanotubes produced by aerosol chemical vapour deposition. *Carbon*. 2009;47(1):30-7.

[115] Liu H, Zhang Y, Li R, Sun X, Désilets S, Abou-Rachid H, et al. Structural and morphological control of aligned nitrogen-doped carbon nanotubes. *Carbon*. 2010;48(5):1498-507.

[116] Sharifi T, Nitze F, Barzegar HR, Tai C-W, Mazurkiewicz M, Malolepszy A, et al. Nitrogen doped multi walled carbon nanotubes produced by CVD-correlating XPS and Raman spectroscopy for the study of nitrogen inclusion. *Carbon*. 2012;50(10):3535-41.

[117] Maldonado S, Morin S, Stevenson KJ. Structure, composition, and chemical reactivity of carbon nanotubes by selective nitrogen doping. *Carbon*. 2006;44(8):1429-37.

[118] Xu W, Kyotani T, Pradhan BK, Nakajima T, Tomita A. Synthesis of Aligned Carbon Nanotubes with Double Coaxial Structure of Nitrogen-Doped and Undoped Multiwalls. *Advanced Materials*. 2003;15(13):1087-90.

[119] Yang Q, Xu W, Tomita A, Kyotani T. Double coaxial structure and dual physicochemical properties of carbon nanotubes composed of stacked nitrogen-doped and undoped multiwalls. *Chemistry of Materials*. 2005;17(11):2940-5.

[120] Reyes-Reyes M, Grobert N, Kamalakaran R, Seeger T, Golberg D, Rühle M, et al. Efficient encapsulation of gaseous nitrogen inside carbon nanotubes with bamboo-like structure using aerosol thermolysis. *Chemical Physics Letters*. 2004;396(1):167-73.

[121] Sumpter BG, Meunier V, Romo-Herrera JM, Cruz-Silva E, Cullen DA, Terrones H, et al. Nitrogen-mediated carbon nanotube growth: diameter reduction, metallicity, bundle dispersability, and bamboo-like structure formation. *ACS Nano*. 2007;1(4):369-75.

[122] Wang Y, Tang G, Koeck F, Brown B, Garguilo J, Nemanich R. Experimental studies of the formation process and morphologies of carbon nanotubes with bamboo mode structures. *Diamond and Related Materials*. 2004;13(4):1287-91.

[123] Boissière C, Martines MU, Larbot A, Prouzet E. On the specific filtration mechanism of a mesoporous silica membrane, prepared with non-connecting parallel pores. *Journal of Membrane Science*. 2005;251(1):17-28.

[124] Burggraaf AJ. Important characteristics of inorganic membranes. *Membrane Science and Technology*. 1996;4:21-34.

[125] Antonietti M, Ozin GA. Promises and problems of mesoscale materials chemistry or why meso? *Chemistry-A European Journal*. 2004;10(1):28-41.

[126] Hsieh H, Bhave R, Fleming H. Microporous alumina membranes. *Journal of Membrane Science*. 1988;39(3):221-41.

[127] Sagle A, Freeman B. Fundamentals of membranes for water treatment. *The Future of Desalination in Texas*. 2004;2:137-54.

[128] Holt JK, Park HG, Wang Y, Stadermann M, Artyukhin AB, Grigoropoulos CP, et al. Fast mass transport through sub-2-nanometer carbon nanotubes. *Science*. 2006;312(5776):1034-7.

[129] Endo M, Muramatsu H, Hayashi T, Kim Y, Terrones M, Dresselhaus M. Nanotechnology:'Buckypaper'from coaxial nanotubes. *Nature*. 2005;433(7025):476-.

[130] Hinds BJ, Chopra N, Rantell T, Andrews R, Gavalas V, Bachas LG. Aligned multiwalled carbon nanotube membranes. *Science*. 2004;303(5654):62-5.

[131] Holt JK, Noy A, Huser T, Eaglesham D, Bakajin O. Fabrication of a carbon nanotube-embedded silicon nitride membrane for studies of nanometer-scale mass transport. *Nano letters*. 2004;4(11):2245-50.

[132] Sarno M, Sannino D, Leone C, Ciambelli P. CNTs tuning and vertical alignment in anodic aluminium oxide membrane. *Journal of Natural Gas Chemistry*. 2012;21(6):639-46.

[133] Ajayan PM. Capillarity-induced filling of carbon nanotubes. *Nature*. 1993;361(6410):333-4.

[134] Ajayan P, Ebbesen T, Ichihashi T, Iijima S, Tanigaki K, Hiura H. Opening carbon nanotubes with oxygen and implications for filling. *Nature*. 1993;362(6420):522-5.

[135] Dujardin E, Ebbesen T, Hiura H, Tanigaki K. Capillarity and wetting of carbon nanotubes. *Science*. 1994;265(5180):1850-2.

[136] Dujardin E, Ebbesen TW, Krishnan A, Treacy MM. Wetting of single shell carbon nanotubes. *Advanced Materials*. 1998;10(17):1472-5.

[137] Majumder M, Chopra N, Andrews R, Hinds BJ. Nanoscale hydrodynamics: enhanced flow in carbon nanotubes. *Nature*. 2005;438(7064):44-.

[138] Skoulidas AI, Ackerman DM, Johnson JK, Sholl DS. Rapid transport of gases in carbon nanotubes. *Physical Review Letters*. 2002;89(18):185901.

[139] Sokhan VP, Nicholson D, Quirke N. Fluid flow in nanopores: Accurate boundary conditions for carbon nanotubes. *The Journal of Chemical Physics*. 2002;117(18):8531-9.

[140] Mao Z, Sinnott SB. Separation of organic molecular mixtures in carbon nanotubes and bundles: molecular dynamics simulations. *The Journal of Physical Chemistry B*. 2001;105(29):6916-24.

[141] Mao Z, Sinnott SB. A computational study of molecular diffusion and dynamic flow through carbon nanotubes. *The Journal of Physical Chemistry B*. 2000;104(19):4618-24.

[142] Hummer G, Rasaiah JC, Noworyta JP. Water conduction through the hydrophobic channel of a carbon nanotube. *Nature*. 2001;414(6860):188-90.

[143] Chen H, Johnson JK, Sholl DS. Transport diffusion of gases is rapid in flexible carbon nanotubes. *The Journal of Physical Chemistry B*. 2006;110(5):1971-5.

[144] De Lasa HI, Serrano B, Salaices M. Photocatalytic reaction engineering: *Springer*; 2005.

[145] Kaneko M, Okura I. Photocatalysis science and technology. *Kodansha Springer*. 2002.

[146] Fujishima A. Electrochemical photolysis of water at a semiconductor electrode. *Nature*. 1972;238:37-8.

[147] Zlámal M, Krýsa J, Jirkovský J. Photocatalytic degradation of acid orange 7 on TiO2 films prepared from various powder catalysts. *Catalysis letters*. 2009;133(1-2):160-6.

[148] Banerjee AN. The design, fabrication, and photocatalytic utility of nanostructured semiconductors: focus on TiO. *Nanotechnology, Science and Applications*. 2011;4:35-65.

[149] Zhou H, Smith DW. Advanced technologies in water and wastewater treatment. *Journal of Environmental Engineering and Science*. 2002;1(4):247-64.

[150] Chong MN, Jin B, Chow CW, Saint C. Recent developments in photocatalytic water treatment technology: a review. *Water Research*. 2010;44(10):2997-3027.

[151] Asahi R, Morikawa T, Ohwaki T, Aoki K, Taga Y. Visible-light photocatalysis in nitrogen-doped titanium oxides. *Science*. 2001;293(5528):269-71.

[152] Ohno T, Akiyoshi M, Umebayashi T, Asai K, Mitsui T, Matsumura M. Preparation of S-doped TiO 2 photocatalysts and their photocatalytic activities under visible light. *Applied Catalysis A: General*. 2004;265(1):115-21.

[153] Ren W, Ai Z, Jia F, Zhang L, Fan X, Zou Z. Low temperature preparation and visible light photocatalytic activity of mesoporous carbon-doped crystalline TiO 2. *Applied Catalysis B: Environmental*. 2007;69(3):138-44.

[154] Hamal DB, Klabunde KJ. Synthesis, characterization, and visible light activity of new nanoparticle photocatalysts based on silver, carbon, and sulfur-doped TiO 2. *Journal of Colloid and Interface Science*. 2007;311(2):514-22.

[155] Nagaveni K, Hegde M, Ravishankar N, Subbanna G, Madras G. Synthesis and structure of nanocrystalline TiO2 with lower band gap showing high photocatalytic activity. *Langmuir*. 2004;20(7):2900-7.

[156] Khan SU, Al-Shahry M, Ingler WB. Efficient photochemical water splitting by a chemically modified n-TiO2. *Science*. 2002;297(5590):2243-5.

[157] Akhavan O. Lasting antibacterial activities of Ag–TiO 2/Ag/a-TiO 2 nanocomposite thin film photocatalysts under solar light irradiation. *Journal of Colloid and Interface Science*. 2009;336(1):117-24.

[158] Chen Y, Crittenden JC, Hackney S, Sutter L, Hand DW. Preparation of a novel TiO2-based pn junction nanotube photocatalyst. *Environmental Science & Technology*. 2005;39(5):1201-8.

[159] Fu X, Clark LA, Yang Q, Anderson MA. Enhanced photocatalytic performance of titania-based binary metal oxides: TiO2/SiO2 and TiO2/ZrO2. *Environmental Science & Technology*. 1996;30(2):647-53.

[160] Siripala W, Ivanovskaya A, Jaramillo TF, Baeck S-H, McFarland EW. A Cu 2 O/TiO 2 heterojunction thin film cathode for photoelectrocatalysis. *Solar Energy Materials and Solar Cells*. 2003;77(3):229-37.

[161] Liu H, Zuo K, Vecitis CD. Titanium Dioxide-Coated Carbon Nanotube Network Filter for Rapid and Effective Arsenic Sorption. *Environmental Science & Technology*. 2014;48(23):13871-9.

[162] Majumder M, Clayton V, Ajayan AP. 1.14 Carbon Nanotube Membranes: A New Frontier in Membrane Science. *Comprehensive Membrane Science and Engineering*. 2010;1:291-310.

[163] Chen W, Fan Z, Zhang B, Ma G, Takanabe K, Zhang X, et al. Enhanced visible-light activity of titania via confinement inside carbon nanotubes. *Journal of the American Chemical Society*. 2011;133(38):14896-9.

[164] Zhang S, Ji C, Bian Z, Liu R, Xia X, Yun D, et al. Single-wire dye-sensitized solar cells wrapped by carbon nanotube film electrodes. *Nano letters*. 2011;11(8):3383-7.

[165] Cao F-F, Guo Y-G, Zheng S-F, Wu X-L, Jiang L-Y, Bi R-R, et al. Symbiotic coaxial nanocables: Facile synthesis and an efficient and elegant morphological solution to the lithium storage problem. *Chemistry of Materials*. 2010;22(5):1908-14.

[166] Wang W, Serp P, Kalck P, Faria JL. Photocatalytic degradation of phenol on MWNT and titania composite catalysts prepared by a modified sol–gel method. *Applied Catalysis B: Environmental*. 2005;56(4):305-12.

[167] Yu Y, Jimmy CY, Chan C-Y, Che Y-K, Zhao J-C, Ding L, et al. Enhancement of adsorption and photocatalytic activity of TiO 2 by using carbon nanotubes for the treatment of azo dye. *Applied Catalysis B: Environmental*. 2005;61(1):1-11.

[168] Xia X-H, Jia Z-J, Yu Y, Liang Y, Wang Z, Ma L-L. Preparation of multi-walled carbon nanotube supported TiO 2 and its photocatalytic activity in the reduction of CO 2 with H 2 O. *Carbon*. 2007;45(4):717-21.

[169] Gao B, Chen GZ, Puma GL. Carbon nanotubes/titanium dioxide (CNTs/TiO 2) nanocomposites prepared by conventional and novel surfactant wrapping sol–gel methods exhibiting enhanced photocatalytic activity. *Applied Catalysis B: Environmental*. 2009;89(3):503-9.

[170] Macak JM, Zlamal M, Krysa J, Schmuki P. Self-Organized TiO2 Nanotube Layers as Highly Efficient Photocatalysts. *Small*. 2007;3(2):300-4.

[171] Jennings JR, Ghicov A, Peter LM, Schmuki P, Walker AB. Dye-sensitized solar cells based on oriented TiO2 nanotube arrays: transport, trapping, and transfer of electrons. *Journal of the American Chemical Society*. 2008;130(40):13364-72.

[172] Qu X, Cao L, Du F. Fabrication of ordered arrays of CNT/TiO 2 nanotubes and their photocatalytic properties. *RSC Advances*. 2015;5(27):20976-80.

CHAPTER 2

EXPERIMENTAL METHODS

Mohammed Obid Alsawat

School of Chemical Engineering, The University of Adelaide, South Australia 5005, Australia

CHAPTER 2: Experimental Methods

2.1. Introduction and Objectives

A primary requirement for CNTs-based composite for advanced transport and photocatalytic activity properties is to develop and optimise scalable fabrication approach in a cost-competitive and time-effective manner to prepare reproducible vertically aligned arrays of CNTs with desired structural and chemical characteristics. Key platforms for this fabrication are NAAMs and TNTs templates prepared by electrochemical anodisation followed by catalyst-free CVD process to grow CNTs and making CNTs composites for molecular transport and photocatalysis applications. Therefore, this chapter emphasises on basic experimental aspects of this thesis to define the fabrication approaches and structural designing of NAAMs and TNTs template and optimising procedures for catalyst-free CVD growth of CNTs composites, followed by development of required characterisation set-ups for testing transport and catalytic properties. It also briefly defines the structural and chemical characterisation techniques used throughout this thesis.

2.2. Materials and Chemicals

All materials and chemicals, unless otherwise stated, used in the course of all experiments were purchased from Sigma-Aldrich (Australia) and used as received. High purity deionised (DI) water (resistivity 18.2 M Ω cm) from a Milli-Q water purification system was used to prepare all the solutions used in this PhD study.

2.3. Synthesis of Nanoporous Anodic Alumina Membranes (NAAMs) Templates

Although alumina membranes are commercially available, designing and engineering NAAMs have been demonstrated to overcome the defects of commercial NAAMs, including irregular

distribution of pores as a result their branching at membrane's surface or along the pores. Tow-step electrochemical anodisation is the most common methodology utilised to synthesis self-ordered and vertically aligned nanopores structure of NAAMs with different dimensions [1-3].

The electrochemical anodisation setup for NAAMs fabrication consists of 4 main components: aluminium (Al) foil (serves as anode), platinum (Pt) wire (serves as cathode), appropriate electrolyte (acid aqueous solution serves as transporting medium) and power supply (Agilent N5724) (serves as a provider of driving force required to grow pores on Al substrate) (**Figure 2.1**). In the course of the anodisation process, high purity aluminium (Al) foils (thickness 0.32 mm, purity 99.999 %, Goodfellow Cambridge Ltd, UK) are cut to circular chips with a diameter of 1.5 cm and cleaned under sonication in ethanol and water for 10 min, separately. Then, they are brought into contact with a copper (Cu) back-plate in a custom made anodisation holder that permits only a circular area of the Al metal with diameter of 1 cm to be exposed to the electrolyte solution. For electrical connection, the Cu plate was connected to the power supply by an insulating-covered copper wire. The anodisation holder and the Pt wire are partially immersed in a magnetically stirred electrolyte solution in a double jacket beaker cooled to the wanted temperature using a cooling path.

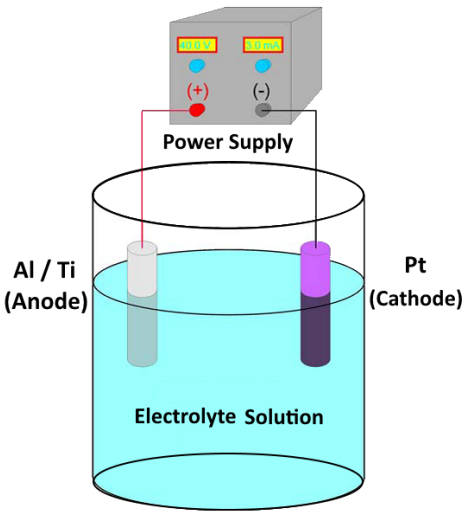

Figure 2.1. Schematic diagram of a basic electrochemical cell for anodising aluminium and titanium substrates.

NAAMs were prepared by a two-step electrochemical anodisation process. Prior to the first anodisation step, the Al chips were electro-polished in a mixture of $HClO_4$ and C_2H_6O 1:4 (*v:v*) at 20 V and 5 °C for 3 min and then dried under nitrogen stream. The electro-polished Al substrates were anodised in different acid electrolytes of H_2SO_4, $H_2C_2O_4$ and H_3PO_4. The first anodisation step was performed for 20 h and the resulting oxide layer was selectively removed in a mixture of H_3PO_4 (0.4 M) and H_2CrO_7 (0.2 M) at 70 °C for 3 h in order to patter the surface of aluminium with hexagonally organised pits. The second anodisation step was carried out for different times, to obtain NAAMs with desired pore lengths, and different applied potential to obtain different pore diameters. The anodisation conditions (anodisation voltages, acid electrolyte concentrations and temperatures) used to produce the different types of NAAMs for this PhD study and the structural characteristics of the resulting NAAMs are summarised in **Table 2.1** (**Chapter 3, 4, 5 and 6**).

After anodisation process, the remaining aluminium substrate was removed in a saturated solution of HCl and $CuCl_2$ followed by chemical opening of the oxide barrier layer at the bottom tips of nanopores in 5 *wt* % H_3PO_4 at 35 °C under current control to have a precise control over the pore opening and avoid undesired pore widening [4, 5].

Table 2.1. Anodisation conditions for fabricating the different types of NAAMs and the structural characteristics of the resulting NAAMs.

Acid Type	**Concentration (M)**	**Voltage (V)**	**Temperature (°C)**	**Pore Diameter (nm)**	**Pore Length (µm)**
H_2SO_4	0.3	25	5 ± 1	25 ± 5	(30,60, 90) ± 2
$H_2C_2O_4$	0.3	40	5 ± 1	40 ± 5	60 ± 2
H_3PO_4	0.1	195	2 ± 1	150 ± 5	60 ± 2

2.4. Synthesis of Titania Nanotubes (TNTs) Templates

Electrochemical anodisation is the most common methodology utilised to synthesis self-ordered TNTs with different dimensions suitable for many applications, and represents a straightforward, inexpensive, self-driven and scalable technology [6]. To synthesis TNTs, electrochemical anodisation setup similar to that of NAAMs fabrication is used with the exception of the use of titanium (Ti) foils (thickness 0.25 mm, purity 99.7 %) which serves as anode here to grow TNTs (**Figure 2.1**) and the use of ethylene glycol with 0.3% (w/v) NH_4F and 3% (v/v) water as anodisation electrolyte. Two-step electrochemical anodisation process was performed to synthesis TNTs. Prior to the first anodisation step, the Ti foils are cut into small pieces of 1.5 × 1.5 cm and polished mechanically using abrasive paper and cleaned under sonication in acetone and ethanol for 10 min, separately. The first anodisation step was performed at 80 V for 2 h at 25 °C and the resulting oxide layer was removed mechanically by sonicating in methanol. The second anodisation step was performed at 80 V for 1 h using the above-mentioned electrolyte to obtain nanotube with diameters and lengths of 100 ± 10 nm and 50 ± 2 μm, respectively (used in **Chapter 7**).

2.5. Synthesis of CNTs-NAAMs and CNTs-TNTs Composites

CNTs were fabricated using a catalyst-free CVD approach previously described [7]. Briefly, vertically aligned multiwalled CNTs (MWCNTs) were grown inside the pores of the two different templates of NAAMs and TNTs by a catalyst-free CVD process. A schematic illustrations of the fabrication process of CNTs-NAAMs and CNTs-TNTs composite used in this PhD study are shown in **Figures 2.2 and 2.3**, respectively.

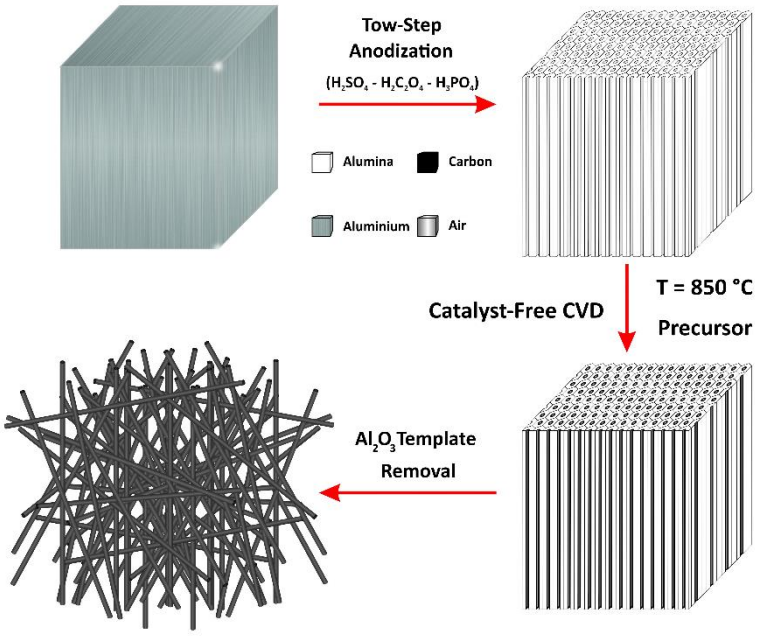

Figure 2.2. Schematic representation of the fabrication process of NAAMs and CNTs-NAAMs composite membrane.

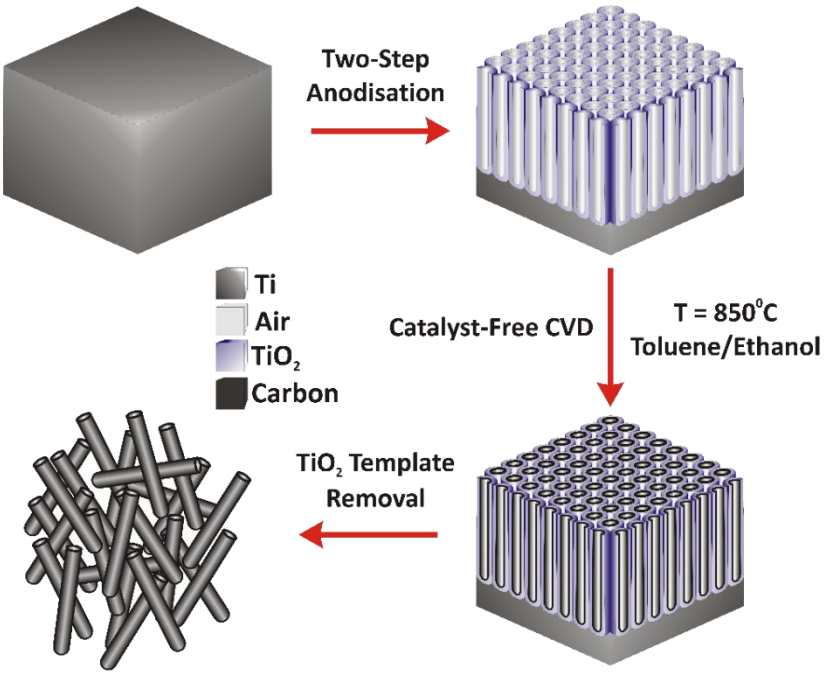

Figure 2.3. Schematic representation of the fabrication process of TNTs and CNTs-TNTs composite.

The CVD process was carried out in a CVD system consisting of a two-stage furnace (1 in **Figure 2.4**) equipped with a cylindrical quartz tube (2 in **Figure 2.4**) (Brother Furnace Co., LTD, China), in which the electrochemically prepared NAAMs and TNTs were placed. The cylindrical quartz tube is connected from the CVD input side to the particle generator (i.e. nebuliser) (Sonaer® Ultrasonic 241PG and 241PGT Particle Generator, USA) (3 in **Figure 2.4**) using custom gas outlets fittings (4 in **Figure 2.4**). The gas inlet of the particle generator is connected to the argon cylinder (5 in **Figure 2.4**) through gas flow controller (6 in **Figure 2.4**). On the CVD output side, the cylindrical quartz tube is connected to the cold trap (7 in **Figure 2.4**) through Purosil hose (8 in **Figure 2.4**) for transferring exhaust gases produced during the CVD process. To efficiently and safely seal the system, stainless steel male and female flanges supported by metallic and non-metallic viton O-rings (9 in **Figure 2.4**) are used to both sides (i.e. CVD inlet and outlet).

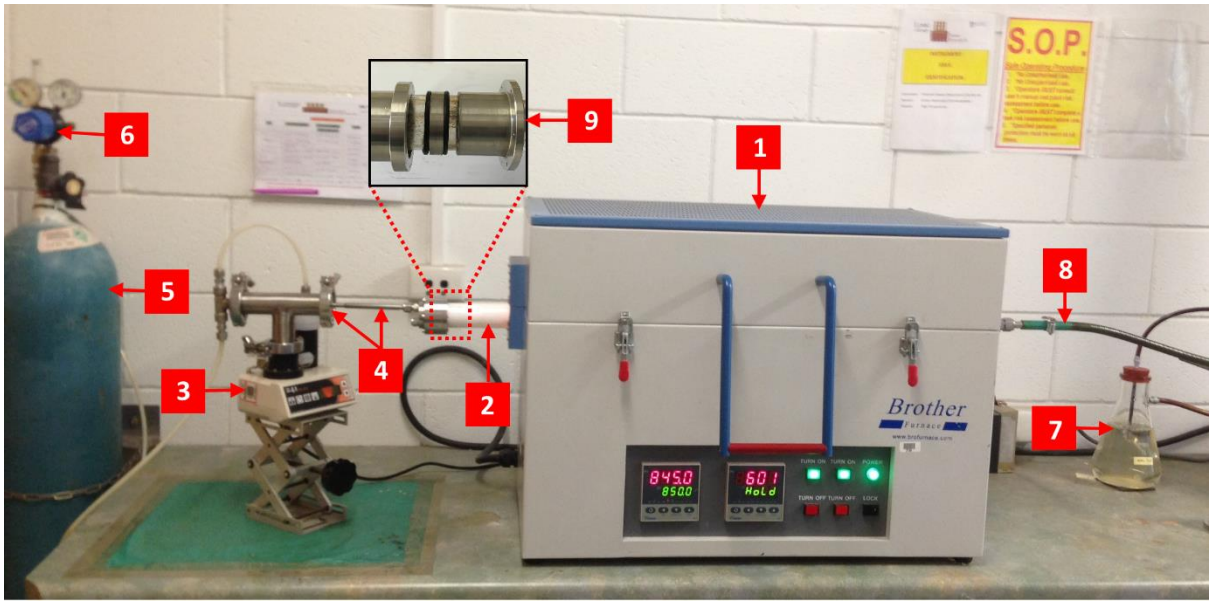

Figure 2.4. Detailed photograph of the complete functioning CVD setup used to fabricate CNTs-NAAMs and CNTs-TNTs composites. (1) Two-stage furnace; (2) cylindrical quartz tube; (3) nebuliser; (4) gas outlets fittings; (5) argon cylinder; (6) gas flow controller; (7) cold trap; (8) Purosil hose and (9) stainless steel male and female flanges supported by metallic and non-metallic viton O-rings.

In the course of the CVD process, the CVD reactor temperature was increased up to 850 °C under argon (Ar) flow, which was used as a carrier gas at flow rate of 1 dm^3 min^{-1}. Once the deposition temperature was reached, the carbon precursor was introduced in the CVD reactor as ultrafine particle aerosols by a particle generator. Different precursors were explored in order to fabricate CNTs composites with different chemistries: namely, (i) a mixture of toluene and ethanol (1:1) (*v:v*) (used in **Chapter 3, 4, 5, 6 and 7**), (ii) N,N-dimethylformamide (DMF), (iii) a mixture of toluene, ethanol and DMF (1:1:1) (*v:v:v*), (iv) pyridine, and (v) a mixture of toluene, ethanol and pyridine (1:1:1) (*v:v:v*) (used in **Chapter 6**). Different deposition times were performed in order to investigate the influence of deposition time on the wall thickness of the resulting CNTs exploring and explaining their formation mechanism inside the pores of NAAMs (described in **Chapter 3 and 4**) and TNTs (described in **Chapter 7**) without of using metal catalysts. After CVD process, the furnace was turned off and Ar was continuously flowed to cool the CVD reactor down to room temperature.

Initial CVD processes, performed by placing NAAMs on ceramic crucible boat used as a sample holder and increasing the reactor temperature rapidly up to 850 °C, resulted in bending and cracking CNTs-NAAMs composites (**Figures 2.5a and 2.5b,** respectively). This was avoided by placing NAAMs in a custom quartz boat and increasing the temperature from 25 °C to 850 °C at a rate of 4 °C min^{-1} (**Figure 2.5c**).

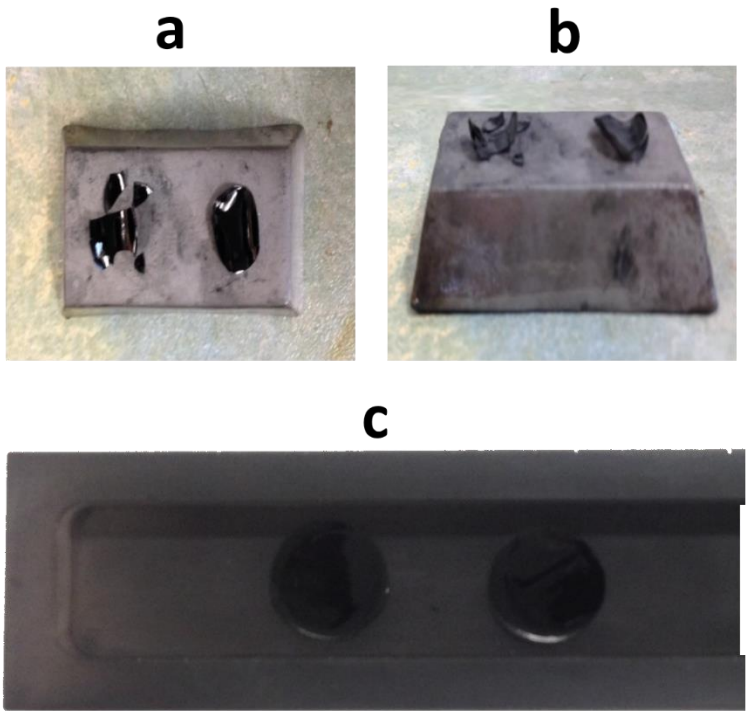

Figure 2.5. Digital photographs of bent (a); cracked (b); and (c) flat CNTs-NAAMs.

2.6. Transport Studies of CNTs-NAAMs Composite Membranes

Concentration-driven transport through the CNTs-NAAMs composite membrane was measured in an experimental set-up detailed in **Figure 2.6**. Briefly, the membrane was assembled in a H-tube permeation cell consists of two half of cells (i.e. feed and permeate cells). The feed cell was filled with a 3 mL of 10 mM of dye solution and the permeate cell was filled with the same level of water to avoid a pressure driven transportation. The CNTs-NAAMs composite membrane was placed between these two halves, which sealed by two polydimethylsiloxane (PDMS) slides to prevent leakage, with an exposed area of 0.0314 cm^2. Two models molecules with different hydrophilic-hydrophobic and charge properties (Rose Bengal $(RosB)^{2-}$ and Tris (2,20-bipyridyl) dichlororuthenium (II) hexahydrate $(Ru(BPY)_3)^{2+}$, respectively were used for transport studies. Their diffusion through the membrane was continuously monitored in real-time by measuring the absorbance in the permeate cell using a UV–Visible fibre optic spectrophotometer (USB4000 Ocean Optics, USA). A software package from Ocean Optics (SpectraSuit) is used for acquiring

data from the spectrometer in wavelength range of 400 - 1000 nm. In all transport experiments performed throughout this thesis, dye's initial concentration in the feed cell was kept constant. Concentrations of $(RosB)^{2-}$ and $(Ru(BPY)_3)^{2+}$ were detected at their maximum absorbance of 552 and 452 nm, respectively, and then fitted to a calibration curve obtained by measuring absorbance of known concentrations of each dye (**Figure 2.7**). A linear plot of the concentration vs time was obtained, and the slope of the plot per unit area of the membrane described the diffusional flux of a particular dye through the membrane. All transport experiments were repeated at least three times and statistically treated. To investigate the effect of the adsorption of transported dye molecules onto the CNTs membrane surface upon the overall transport rates, different control experiments were conducted. This includes: determining the transport rate of a particular dye molecule through a specific CNTs membrane with the use of dry membrane, membrane soaked in the solvent (deionised water) for 1-2 hour, and the use of the same membrane many times while performing washing treatment (rinse with ethanol and deionised water and dry in air for 24 hours) after each time. The effect of the adsorption of dye molecules onto the surface of CNTs membranes on the flow rate of dye through these membranes was found to be negligible in all cases, indicating the very low amount of adsorbed dye molecules onto the membrane surface, which is not influencing its transport rate.

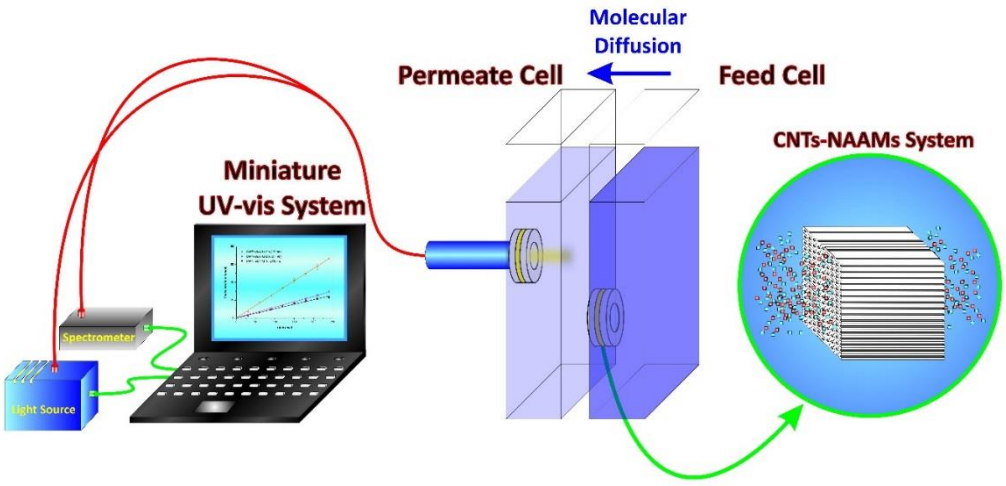

Figure 2.6. Schematic illustration of the permeation cell used for transport measurements of CNTs-NAAMs composite membranes.

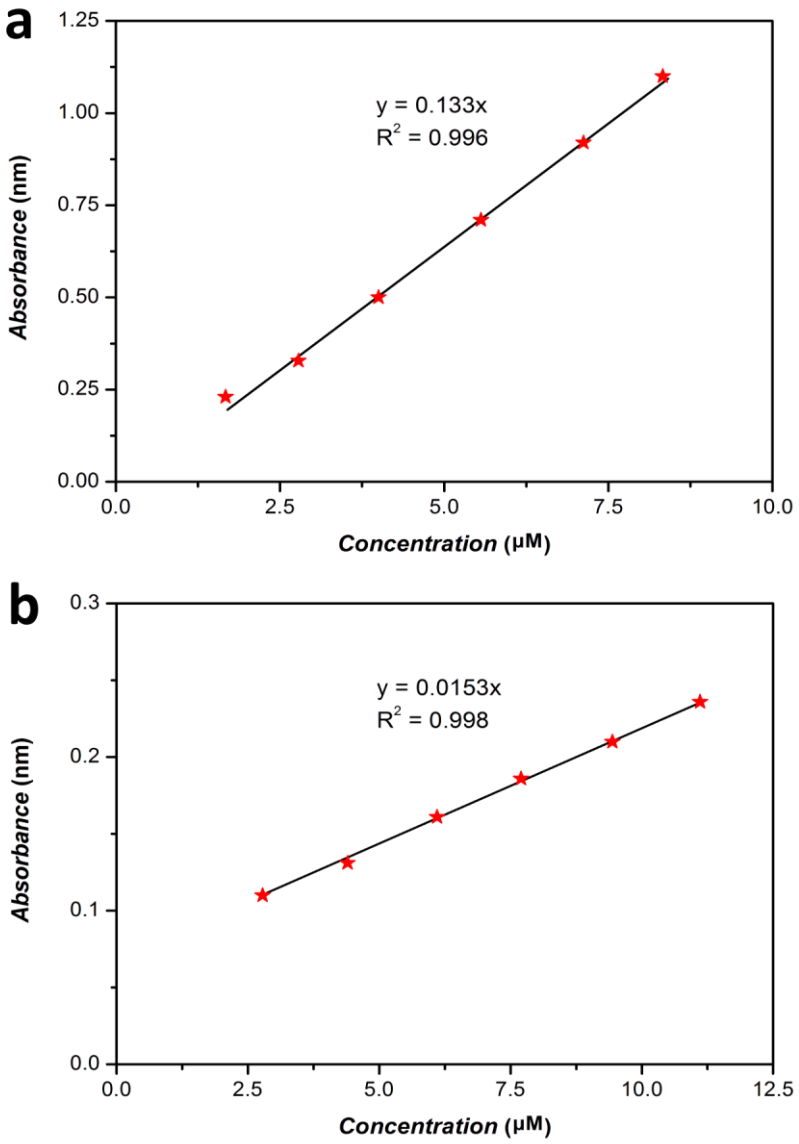

Figure 2.7. Calibration curve of (a) $(RosB)^{2-}$ absorbance (at 552 nm) and (b) $(Ru(BPY)_3)^{2+}$ absorbance (at 452 nm).

Electrically-driven transport through the CNTs-NAAMs composite membrane was measured using the same experimental set-up shown in **Figure 2.6**. However, the two half of cells were filled with 3 mL of NaCl aqueous electrolyte solution and two gold electrodes electrochemical impedance spectroscopy (EIS) were used here, in which one electrode was immersed in one half cell, serving as working and counter electrode. Impedance data were obtained over a frequency

range from 1 Hz to 1 MHz using various concentrations of NaCl electrolyte (i.e. 1, 2, 5, 10, 50 and 100 μM). The modelling of the experimental system was done using EvolCRT software (developed by Department of Chemistry, Wuhan University, China).

2.7. Photodegradation Study of CNTs-TNTs Composite

The photocatalytic activity of TNTs and CNTs-TNTs composites were assessed via the photodegradation of rhodamine B molecules in aqueous solution in a photoreactor using a 1000 W mercury-xenon Hg (Xe) lamp. Briefly, the sample of TNTs or CNTs-TNTs with a diameter of 1 cm (8-10 mg) was placed in a low form beaker, which has a magnetic stirrer at the bottom, of 10 ml of rhodamine B aqueous solution with an initial concentration (C_0) of 1.6 mg/L and irradiated vertically from the top using the Hg (Xe) lamp with a distance of 6 cm. This type of lamp has spectral distribution that includes a continuous spectrum from the ultraviolet to infrared spectrum. Prior to the irradiation process, the reaction solution was continuously stirred in dark for 1 h in order to reach adsorption/desorption equilibrium. At predetermined time intervals, the absorbance of the solution at its maximum (i.e. λ_{abs} = 554 nm) was measured using UV–vis spectroscopy (Cary 60) to analyse the concentration of rhodamine B (C_t) and thus calculate the degradation efficiency through the equation:

$$\text{Degradation efficiency (\%)} = [(C_0 - C_t) / C_0] \times 100 \quad (2.1)$$

where C_0 is the initial concentration of rhodamine B and C_t is the rhodamine B concentration at time t (min).

As a control, the degradation of rhodamine B solution in the absence of either the catalyst (TNTs or CNTs-TNTs) or the Hg (Xe) light was assessed. For this, two control measurements were performed and monitored by UV–vis spectroscopy, first rhodamine B solution was irradiated in the absence of the catalyst and second, the catalyst's sample was immersed in the rhodamine B

aqueous solution in the absence of the light. In both cases, no significant decreases in the rhodamine B concentration was observed confirming the importance of both reactants (i.e. catalyst and light) to catalyses the degradation of rhodamine B.

2.8. Structural and Chemical Characterisations

During the course of this PhD study, different characterisation techniques were used for the structural and chemical characterisations of the different prepared nanostructures and these techniques are briefly discussed in the following subsections.

2.8.1. Scanning Electron Microscopy (SEM)

Scanning electron microscope (SEM) is a type of electron microscope that uses a beam of electrons to image the sample surface. It operates on the same principle as the optical microscopes, however; it uses electrons instead of light because of their short wavelength to improve the image resolution. In principle, the electron gun (source of electrons) generates electron beam that passes through condenser lenses to shrink the beam diameter which then focused by the objective lens into a spot. The final focused spot with a few nanometre diameters is scanned across the sample surface with the resulting signals providing information about the sample's surface morphology. SEM requires conducting samples since it uses electrons for imaging [8-10].

The structural characterisation of the prepared NAAMs, TNTs, CNTs-NAAMs composite membranes, CNTs-TNTs composites and liberated CNTs was performed using a field emission gun scanning electron microscope (FEG-SEM, Quanta 450). For SEM imaging, samples were coated with 5 nm thick platinum layer.

2.8.2. Energy Dispersive X-ray Spectroscopy (EDX)

Energy dispersive X-ray spectroscopy (EDX) uses a beam of electrons to produce elements distribution spectra. It operates on the same principle as the SEM microscopy, however; it uses X-ray electrons to determine the elemental composition of the sample. In principle, high energy X-ray beam interacts with electrons in discrete energy levels. Outer shell electron (high-energy) fills the resultant hole from the exciting inner shell electron (low-energy) and thus characteristic X-rays are produced based on the difference in energy levels of the electrons between inner and outer shells. These produced X-rays are used to determine the elemental composition of the sample [11].

The elemental composition of the as-produced and oxidised CNTs-NAAMs composite membranes was determined using EDAX TEAM EDS with SDD Detector.

2.8.3. Transmission Electron Microscopy (TEM)

Transmission electron microscopy (TEM) is another type of electron microscope that images the sample based on the interaction between electrons and the sample. The difference between the SEM and TEM is that, in the case of SEM, electrons can be reflected from the sample (backscattered) or released as secondary electrons that can be collected to form the image. In contrast, electrons in the TEM penetrate a thin sample and then focused by objective lenses in order to form the image. Therefore, the TEM requires a thin sample (less than 200 nm) to ensure that a reasonable proportion of the incident electrons will contribute to the formation of the final image [10].

The internal structure of CNTs and their wall thicknesses were assessed using a transmission electron microscopy (Philips CM 200 TEM). The templates (NAAMs or TNTs) were selectively dissolved in a 5 wt % HF solution to obtain liberated CNTs, which were washed with deionised water and ethanol. One drop of the solution was placed on a TEM copper grid and dried before characterisation.

2.8.4. X-ray Photoelectron Spectroscopy (XPS)

X-ray photoelectron spectroscopy (XPS), also called electron spectroscopy for chemical analysis (ESCA), is one of the surface analytical techniques that attack the sample with photons, electrons or ions in order to excite the emission of photons, electrons or ions. XPS uses X-ray (photon) to emit electrons from inner-shell orbitals and get information by measuring the energy spectrum of photo-emitted electrons. XPS has been used for the characterisation of CNTs membranes giving valuable information about their elemental composition [12] and chemical bonds [13].

The quantitative and qualitative information about the chemical composition of different CNTs-NAAMs composite membranes, CNTs-TNTs composites and liberated CNTs was obtained by X-ray photoelectron spectroscopy (XPS Kratos Axis Ultra) using the Al Kα (1486.7 eV) monochromatic line.

2.8.5. Raman Spectroscopy

Raman spectroscopy is another surface analytical technique that widely used for the identification of vibrational modes in a system. This is attained by exposing the sample's surface to a monochromatic light, usually intense laser light, and measuring the intensity of the scattered light as a function of frequency. For CNTs, typical Raman profile consists of a G-band peak at 1582 cm^{-1}, attributed to graphitic or highly ordered CNTs sidewalls and a D-band peak at 1350 cm^{-1}, attributed to the amorphous or disordered sp^3 network of carbon atoms. The ratio between these two bands and their positions provide information about the structural changes of CNTs induced by modifications (i.e. oxidation, doping, etc.) [14].

The graphitic structure of the prepared CNTs inside different templates and structural changes of CNTs induced by different modification processes were investigated by Raman spectroscopy (Horiba LabRAM HR Evolution Raman microprobe spectrometer). Raman spectra were obtained using a He–Ne laser of 532 nm as an excitation source.

2.8.6. X-ray Diffraction Spectroscopy (XRD)

X-ray diffraction (XRD) is a non-destructive technique that has been widely used to determine the crystallinity of the nanostructures. In XRD, a collimated beam of X-rays with a particular wavelength is directed towards the sample and then diffracted by the crystalline phases in the sample according to Bragg's law:

$$\lambda = 2\, d \sin\theta \tag{2.2}$$

where λ is the X-ray wavelength, *d* is the spacing between atomic planes in the crystalline phase, θ is the Bragg angle. This diffraction pattern is used to identify the sample's crystalline phases by comparing it with standard reference patterns since every pure substance has a unique XRD pattern (like a fingerprint) [9, 15].

The different phases of TiO_2 were determined using powder X-ray diffraction (XRD, Rigaku MiniFlex 600). XRD measurements were carried out at room temperature using X-ray diffractometer operating with diffracted beam graphite monochromators (Cu Kα with λ = 0.15406 nm) at 40 kV and 15 mA. The scan was recorded over an angular range of 20º to 80º (2θ) with a step counting at 0.02º and collection time of 2 seconds.

2.8.7. UV-Visible Spectroscopy

UV-Visible spectroscopy is one of the most commonly analytical techniques used due to its simplicity, speed and accuracy. It is used to investigate the absorption of different substances giving qualitative and quantitative information about the structure of the molecule. The principle of this technique is simply by passing a beam of light with radiation energy (hν) through a substance or a solution, the molecular orbital electrons will absorb the energy at a particular wavelength and get excited to the higher energy level. The degree of absorption at different wavelengths will be recorded giving a plot of absorbance (A) vs wavelength (λ) [16].

The amount of rhodamine B degraded by the photocatalyst (TNTs or CNTs-TNTs) was monitored by UV-Visible spectroscopy (Cary 50).

2.9. References

[1] Masuda H, Fukuda K. Ordered metal nanohole arrays made by a two-step replication of honeycomb structures of anodic alumina. *Science*. 1995;268(5216):1466-8.

[2] Masuda H, Hasegwa F, Ono S. Self-Ordering of Cell Arrangement of Anodic Porous Alumina Formed in Sulfuric Acid Solution. *Journal of the Electrochemical Society*. 1997;144(5):L127-L30.

[3] Masuda H, Yada K, Osaka A. Self-ordering of cell configuration of anodic porous alumina with large-size pores in phosphoric acid solution. *Japanese Journal of Applied Physics*. 1998;37(11A):L1340.

[4] Lillo M, Losic D. Pore opening detection for controlled dissolution of barrier oxide layer and fabrication of nanoporous alumina with through-hole morphology. *Journal of Membrane Science*. 2009;327(1–2):11-7.

[5] Losic D, Losic Jr D. Preparation of porous anodic alumina with periodically perforated pores. *Langmuir*. 2009;25(10):5426-31.

[6] Roy P, Berger S, Schmuki P. TiO2 nanotubes: synthesis and applications. *Angewandte Chemie International Edition*. 2011;50(13):2904-39.

[7] Che G, Lakshmi B, Martin C, Fisher E, Ruoff RS. Chemical vapor deposition based synthesis of carbon nanotubes and nanofibers using a template method. *Chemistry of Materials*. 1998;10(1):260-7.

[8] Unakar N, Tsui J, Harding C. Scanning electron microscopy. *Ophthalmic Research*. 1981;13(1):20-35.

[9] Cao G. Nanostructures & nanomaterials: synthesis, properties & applications: *World Scientific Publishing Company*; 2004.

[10] Egerton RF. Physical principles of electron microscopy: an introduction to TEM, SEM, and AEM: *Springer*; 2005.

[11] Goldstein J, Newbury DE, Joy DC, Lyman CE, Echlin P, Lifshin E, et al. Scanning electron microscopy and X-ray microanalysis: *Springer*; 2003.

[12] Miller SA, Young VY, Martin CR. Electroosmotic flow in template-prepared carbon nanotube membranes. *Journal of the American Chemical Society*. 2001;123(49):12335-42.

[13] Li Y, Wang P, Li F, Huang X, Wang L, Lin X. Covalent immobilization of single-walled carbon nanotubes and single-stranded deoxyribonucleic acid nanocomposites on glassy carbon electrode: Preparation, characterization, and applications. *Talanta*. 2008;77(2):833-8.

[14] Dresselhaus MS, Dresselhaus G, Saito R, Jorio A. Raman spectroscopy of carbon nanotubes. *Physics Reports*. 2005;409(2):47-99.

[15] Warren BE. X-ray Diffraction: *Dover Publications*; 1990.

[16] Skoog DA, Holler FJ, Nieman TA. *Principles of Instrumental Analysis*. 1998.

CHAPTER 3

Carbon Nanotube-Nanoporous Anodic Alumina Composite Membranes with Controllable Inner Diameters and Surface Chemistry: Influence on Molecular Transport and Chemical Selectivity

Mohammed Obid Alsawat

School of Chemical Engineering, The University of Adelaide, South Australia 5005, Australia

This chapter is based on the following peer-reviewed article:

Alsawat, M. Altalhi, T. Kumeria, T. Santos, A. and Losic, D. Carbon Nanotube-Nanoporous Anodic Alumina Composite Membranes with Controllable Inner Diameters and Surface Chemistry: Influence on Molecular Transport and Chemical Selectivity. *Carbon*, 93 (2015): 681-692.

Statement of Authorship

Title of Paper	Carbon Nanotube-Nanoporous Anodic Alumina Composite Membranes with Controllable Inner Diameters and Surface Chemistry: Influence on Molecular Transport and Chemical Selectivity
Publication Status	☑ Published ☐ Accepted for Publication ☐ Submitted for Publication ☐ Unpublished and Unsubmitted w ork w ritten in manuscript style
Publication Details	Alsawat, M. Altalhi, T. Kumeria, T. Santos, A. and Losic, D. Carbon Nanotube-Nanoporous Anodic Alumina Composite Membranes with Controllable Inner Diameters and Surface Chemistry: Influence on Molecular Transport and Chemical Selectivity. *Carbon*, 93 (2015): 681-692.

Principal Author

Name of Principal Author (Candidate)	Mohammed Alsawat		
Contribution to the Paper	Under supervision of D. Losic and A. Santos, I developed, designed, and performed the experiments, interpreted and processed the data and wrote the manuscript for submission.		
Overall percentage (%)	80		
Certification:	This paper reports on original research I conducted during the period of my Higher Degree by Research candidature and is not subject to any obligations or contractual agreements with a third party that would constrain its inclusion in this thesis. I am the primary author of this paper.		
Signature		Date	30 May 2016

Co-Author Contributions

By signing the Statement of Authorship, each author certifies that:

i. the candidate's stated contribution to the publication is accurate (as detailed above);
ii. permission is granted for the candidate in include the publication in the thesis; and
iii. the sum of all co-author contributions is equal to 100% less the candidate's stated contribution.

Name of Co-Author	Tariq Altalhi		
Contribution to the Paper	I helped the candidate with providing the technical support of chemical vapour deposition (CVD) system. I give consent for Mohammed Alsawat to present this paper for examination towards the Doctorate of philosophy.		
Signature		Date	30 May 2016

Name of Co-Author	Tushar Kumeria		
Contribution to the Paper	I helped the candidate with designing the anodization experiment of aluminium. I give consent for Mohammed Alsawat to present this paper for examination towards the Doctorate of philosophy.		
Signature		Date	30 May 2016

Name of Co-Author	Abel Santos		
Contribution to the Paper	I acted as secondary supervisor for the candidate and aided in development of the experiments and evaluation of manuscript for submission. I give consent for Mohammed Alsawat to present this paper for examination towards the Doctorate of philosophy.		
Signature		Date	30 May 2016

Name of Co-Author	Dusan Losic		
Contribution to the Paper	I acted as primary supervisor for the candidate and aided in development of the experiments and evaluation of manuscript for submission. I give consent for Mohammed Alsawat to present this paper for examination towards the Doctorate of philosophy.		
Signature		Date	30 May 2016

CHAPTER 3: Alsawat, M. Altalhi, T. Kumeria, T. Santos, A. and Losic, D. Carbon Nanotube-Nanoporous Anodic Alumina Composite Membranes with Controllable Inner Diameters and Surface Chemistry: Influence on Molecular Transport and Chemical Selectivity. *Carbon*, 93 (2015): 681-692.

CARBON 93 (2015) 681–692

Available at www.sciencedirect.com

ScienceDirect

journal homepage: www.elsevier.com/locate/carbon

Carbon nanotube-nanoporous anodic alumina composite membranes with controllable inner diameters and surface chemistry: Influence on molecular transport and chemical selectivity

Mohammed Alsawat [a], *Tariq Altalhi* [a,b], *Tushar Kumeria* [a], *Abel Santos* [a], *Dusan Losic* [a,*]

[a] *School of Chemical Engineering, The University of Adelaide, Adelaide, Australia*
[b] *Department of Chemistry, Faculty of Science, Taif University, Taif, Saudi Arabia*

ARTICLE INFO

Article history:
Received 3 February 2015
Accepted 25 May 2015
Available online 3 June 2015

ABSTRACT

This work presents the fabrication of carbon nanotube composite membranes with controllable nanotube dimensions (inner diameters and lengths) and surface chemistry and explores their influence on the transport properties and chemical based transport selectivity. These membranes were prepared by growing of vertically aligned multiwalled carbon nanotubes (MWCNTs) inside nanoporous anodic alumina membranes (NAAMs) through a catalyst-free chemical vapour deposition (CVD) approach. The deposition time during CVD process and the length of NAAMs were used to control nanotube dimensions. The thermal annealing and wet and dry oxidation processes were used to control the surface chemistry of inner walls of nanotubes from highly graphitic-hydrophobic to oxygen rich and hydrophilic. The structural features and chemical composition of the prepared membranes are characterised by scanning electron microscopy (SEM), energy dispersive X-ray spectroscopy (EDX), transmission electron microscopy (TEM), X-ray photoelectron spectroscopy (XPS) and Raman spectroscopy. The influence of the nanotube dimensions and surface chemistry on molecular transport properties of prepared membranes are assessed by analysing the transport of two models molecules with different hydrophilic–hydrophobic and charge properties. The obtained results reveal that the diffusional flux of model molecules through CNTs-NAAMs can be controlled by nanotube dimensions and surface chemistry of graphitic surface and these parameters can be used to tailor their chemical based molecular separation for specific applications.

1. Introduction

Separation processes based on membrane technology have been established for many years as a favourable strategy across many industries including chemical, food, pharmaceutical and waste and drinking water purification. Advancing membrane's performances for these applications such as energy efficiency, low operating costs, improved selectivity,

* *Corresponding author:* Fax: +61 8 8303 4373.
E-mail address: dusan.losic@adelaide.edu.au (D. Losic).
http://dx.doi.org/10.1016/j.carbon.2015.05.090

and high operational stability has attracted enormous research activities in past 50 years [1,2]. Among the plethora of available commercial membranes and membrane materials usually based on polymers and ceramics, carbon nanotubes (CNTs)-based membranes have been recently explored with great interests due to their exceptional properties, including outstanding transport properties from their smooth hydrophobic graphitic walls, ordered and vertically aligned nanotube structures with high aspect ratio, and chemical and thermal stability [3,4]. So far, several theoretical and experimental studies have successfully demonstrated outstanding transport and selective properties of CNTs membranes for a broad range of gases and molecules [3–7]. Their applications for water desalination, gas separations, nanofiltration of biological mixtures, transdermal drug delivery, ultra-sensitive sensing and energy storage suggested CNTs membranes as a new frontier in membrane separation technology.

Traditionally, vertically aligned CNTs membranes have been produced by two approaches using silicon nitride and polymer matrices. The major disadvantage of these methods is the use of expensive laboratory facilities, time consuming and low throughput fabrication processes limited to laboratory scale [3,8,9]. Another drawback of these synthesis methods is the difficulty of controlling the geometric features of CNTs structures and ability to tailor their transport and selectivity properties required for specific molecular separations. Template direct synthesis, however, makes it possible to overcome that inherent limitation by growing CNTs inside templates with precisely controlled geometry. Among various templates, nanoporous anodic alumina membranes (NAAMs), consisting of hexagonal close packed cell arrangement with nanopores, have been extensively used to prepare highly ordered nanostructures including CNTs [10,11]. Pioneering works by Kyotani et al. demonstrated that these nanoporous alumina membranes can also be used as a host material to grow CNTs by catalyst-free chemical vapour deposition method [12,13]. The resulting composite membranes (CNTs-NAAMs) present hexagonally arranged arrays of CNTs of controlled inner diameter and length. Moreover, this method not only provides a precise control over the nanotubes' geometry but also enables selective surface chemistry modification of the inner wall surface of CNTs while keeping the outer surface chemistry unaltered (i.e. asymmetric surface chemistry inner-outer surface). To establish direct correlation between the dimensional features of CNTs-NAAMs and their inner surface chemistry with the transport performance is of critical importance for advancing their properties for separation applications. Recently, our group [14] demonstrated the fabrication of CNTs-NAAMs by catalyst-free CVD approach inside NAAMs using non-degradable grocery plastic bags as a carbon source and showed their transport performance. Nevertheless, more research must be carried out in order to explore the influence of the dimensional features of CNTs and inner surface chemistry of CNTs-NAAMs on their transport and selectivity properties related for their applications for chemical based separations.

In this paper, we present a study on the transport and selectivity performance of CNTs-NAAMs as a function of the dimensional features of CNTs (i.e. inner diameters and lengths) and their internal surface chemistry. The aims of this work are: (i) to demonstrate the fabrication of CNTs membranes with controllable dimensions (i.e. pore diameters and length), (ii) to demonstrate the tailoring interfacial properties of the inner walls of CNTs by simple functionalization processes, and (iii) to explore the influence of CNTs dimensions and surface chemistry on their transport and selectivity properties. These studies will improve our understanding how to control the transport and chemical selectivity of CNTs membranes and design advanced membranes for addressing specific problems for separation of biomolecules with the same molecular size but different interfacial properties. A schematic illustration of the fabrication process of CNTs-NAAMs and subsequent surface chemistry modification is shown in Fig. 1.

CNTs-NAAMs were prepared using catalyst-free CVD approach using a mixture of toluene and ethanol. The dimensional features of CNTs-NAAMs were precisely engineered by the anodization conditions of NAAMs and the deposition time during the CVD process. The thermal annealing, hydrogen peroxide and plasma oxidation were used as simple processes to control the surface chemistry of inner walls of nanotubes from highly graphitic-hydrophobic to oxygen rich and hydrophilic. The molecular transport properties of prepared CNTs-NAAMs were explored by studying the diffusion of two model dye molecules with different hydrophobic–hydrophilic and charge properties.

2. Experimental details

2.1. Materials

High purity aluminium (Al) foils (0.32 mm, 99.999%) was obtained from Goodfellow Cambridge Ltd, UK. Copper chloride ($CuCl_2$), oxalic acid ($H_2C_2O_4$), chromium trioxide (CrO_3), phosphoric acid (H_3PO_4), hydrochloric acid (HCl), ethanol 99.7% (C_2H_6O), toluene 99.8% (C_7H_8), hydrogen peroxide (H_2O_2), hydrofluoric acid (HF), Rose Bengal ($C_{20}H_4Cl_4I_4O_5$–$(RosB)^{2-}$) and Tris(2,20-bipyridyl) dichlororuthenium(II) hexahydrate ($C_{30}H_{24}Cl_2N_6Ru{\cdot}6H_2O$–$(Ru(BPY)_3)^{2+}$) were purchased from Sigma Aldrich (Australia) and used as received. High purity deionized (DI) water (resistivity 18.2 MΩ cm) from a Milli-Q water purification system was used in all the solutions used in this study.

2.2. Fabrication of nanoporous anodic alumina membranes (NAAMs)

Al foils were cut into small pieces of 15 mm × 15 mm and used as substrates to prepare NAAMs by electrochemical anodization process as reported elsewhere [10,15,16]. Briefly, Al foils were first cleaned under sonication (10 min) in ethanol followed by water and then electro-polished in a mixture of $HClO_4$ and C_2H_6O 1:4 (v:v) at 20 V for 3 min and then dried under a nitrogen stream. NAAMs were prepared through a two-step anodization process using 0.3 M $H_2C_2O_4$ as electrolyte solution. The first anodization step was performed at 40 V and 5 °C for 20 h in a two electrode electrochemical cell, where electropolished Al foils act as anode and a platinum

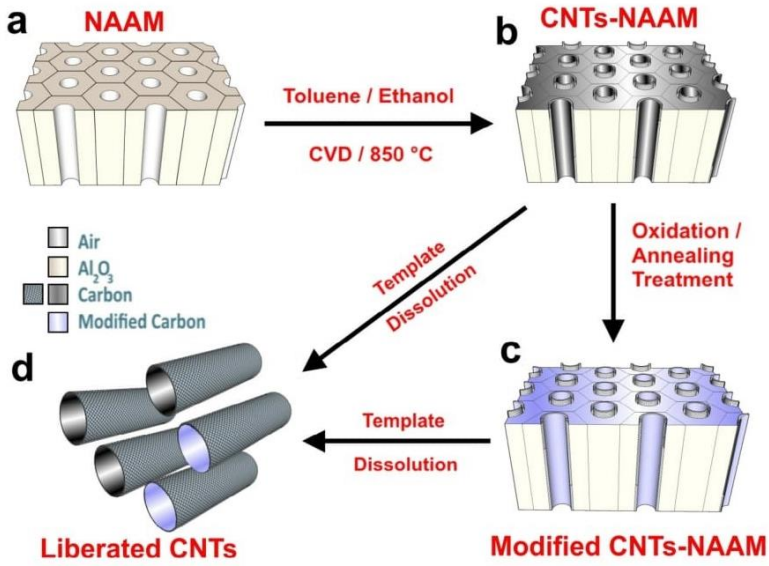

Fig. 1 – Schematic diagram of the fabrication process of CNTs-NAAMs and subsequent modifications. (a) NAAMs prepared by electrochemical anodization of Al foil; (b) prepared CNTs-NAAMs with CNTs embedded in NAAMs after the CVD process; (c) CNTs-NAAMs after oxidation or annealing treatments; (d) liberated CNTs after dissolution of NAAMs by wet chemical etching. (A colour version of this figure can be viewed online.)

wire mesh as cathode. This long first anodization step provides hexagonal ordering of pores at the bottom of the layer after the process (i.e. anodization) due to the repulsive forces and resulting mechanical stress between neighbouring pores during anodization process. The resulting layer of nanoporous alumina was removed in a mixture of H_3PO_4 (0.4 M) and H_2CrO_7 (0.2 M) at 70 °C for 3 h to obtain hexagonally organised pits on the Al surface. The second anodization step was performed using the same electrochemical setup at 40 V and 5 °C for three various anodization times of 9 h, 19 h and 28 h in order to prepare NAAMs with different pore lengths (30, 60, 90 μm), but same pore diameter (i.e. 40 ± 5 nm). NAAMs were fabricated by removing the remaining aluminium substrate from the bottom in a saturated solution of HCl and $CuCl_2$. Next, the oxide barrier layer at the bottom of NAAMs was chemically removed in 5 wt% H_3PO_4 at 35 °C. Note that this process was performed under current control in order to have a precise control over the pore opening [17,18]. The obtained NAAMs were finally rinsed with deionized water and dried under a nitrogen stream.

2.3. *Fabrication and modification of CNTs-NAAMs*

CNTs were fabricated using a catalyst-free CVD approach previously described [19]. Briefly, vertically aligned multiwalled CNTs (MWCNTs) were grown inside the pores of NAAMs by CVD process using a mixture of toluene and ethanol 1:1 (v:v) as a carbon precursor (Fig. 1). This process was carried out in a CVD system consisting of a two-stage furnace equipped with a cylindrical quartz tube (Brother Furnace Co., LTD, China). The electrochemically prepared NAAMs were placed in the deposition zone of the CVD reactor. The reactor temperature was increased at various increasing rates up to 850 °C under argon (Ar) flow, which was used as a carrier gas at flow rate of 1 dm^3 min^{-1}. Once the deposition temperature was reached, the carbon precursor was introduced in the CVD reactor by a particle generator. Different deposition times were performed in order to investigate the influence of deposition time on the wall thickness of the resulting CNTs. For this purpose, we used NAAMs with the same length (60 μm). During the CVD process, two different carbon structures with the same chemical composition are formed; (i) carbon layers on the top and bottom surface of NAAM and (ii) carbon layers on the inner wall surface of the NAAM's pores (i.e. CNTs) (Fig. 1). As-produced CNTs-NAAMs were additionally treated by oxidation and annealing treatments in order to change chemical composition of inner walls of CNTs. Oxidation treatments were carried out via wet chemical method using H_2O_2 (35 wt%) for 12 h followed by washing with deionized water and dry oxidation method using Atto Plasma System (Diener Electronic, GmbH Co. KG) operated at frequency of 40 kHz and power of 140 W and the modification time lasted for 3 min. These treatments make it possible to functionalize the inner wall surface of CNTs with oxygen-containing groups. The annealing treatment of CNTs-NAAMs was carried out to remove oxygenated functional groups by heating at 1000 °C for 3 h in the presence of Ar flowed at a constant rate.

2.4. *Structural and chemical composition characterisations*

The structural characterisation of the prepared CNTs-NAAMs was performed using a scanning electron microscope (SEM-FEG Environmental SEM, Quanta 450) equipped with energy dispersive X-ray spectroscopy (EDX). Transmission electron

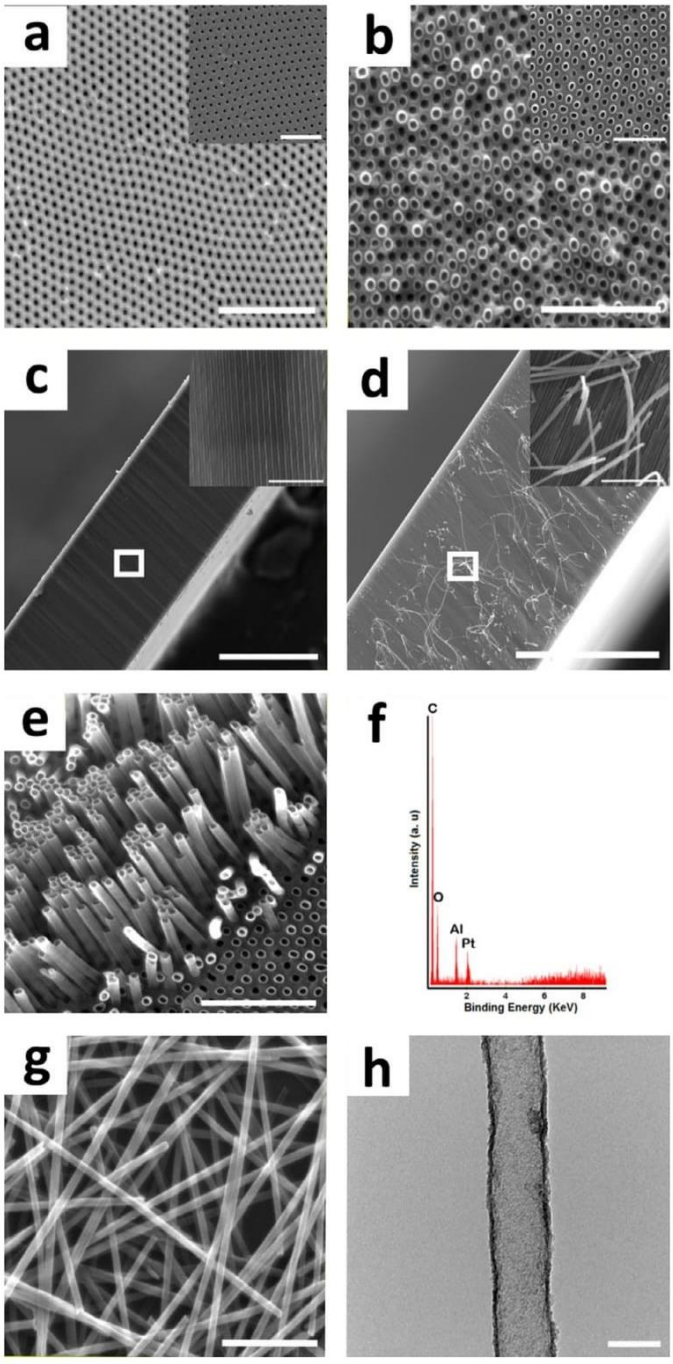

Fig. 2 – Set of SEM and TEM images and EDX spectra of prepared CNTs-NAAMs. (a) SEM image of a typical NAAMs structure produced through a two-step anodization process at 6 °C (top view, scale bar = 1 μm) (inset: bottom view, scale bar = 500 nm); (b) prepared CNTs-NAAMs with CNTs embedded in NAAMs after the CVD process for 15 min (top view, scale bar = 1 μm) (inset: bottom view, scale bar = 500 nm); (c) cross section of NAAMs (scale bar = 50 μm) (inset: magnified view of white square, scale bar = 1 μm); (d) cross section of CNTs-NAAMs (scale bar = 50 μm) (inset: magnified view of white square, scale bar = 2 μm); (e) CNTs-NAAMs after partial dissolution of NAAMs (top view, scale bar = 1 μm); (f) the EDX spectrum of CNTs-NAAMs; (g) SEM of CNTs after dissolution of NAAMs (i.e. liberated tubes); (h) TEM image of CNT produced through catalyst-free CVD for 15 min. (A colour version of this figure can be viewed online.)

microscopy (Philips CM 200 TEM) was used to assess the internal structure of CNTs. NAAMs were selectively dissolved in a 5 wt% HF solution to obtain liberated CNTs, which then were washed with deionized water and ethanol. One drop of the solution was placed on TEM copper grid and dried before characterisation. X-ray photoelectron spectroscopy (XPS Kratos Axis Ultra) was used to determine the chemical composition of as-produced and modified CNTs by using the Al Kα (1486.7 eV) monochromatic line. Raman spectroscopy (Horiba LabRAM HR Evolution Raman microprobe spectrometer) was used to characterise purity of prepared CNTs. Raman spectra were obtained using a He–Ne laser of 532 nm as an excitation source.

2.5. *The molecular transport studies*

The molecular transport studies of two dye molecules through CNTs-NAAMs were separately assessed using a H-tube permeation setup. Aqueous solutions of anionic and cationic charged dye molecules (i.e. $(RosB)^{2-}$ and $(Ru(BPY)_3)^{2+}$ with hydrophilic and hydrophobic properties, respectively) were used to study the molecular transport through CNTs-NAAMs. The set-up of the transport system consists of two half cells (i.e. feed and permeate cells) (Fig. S1 – Supporting information). The feed cell was filled with 3 mL of 10 mM of dye solution and the permeate cell was filled with the same level of water to avoid a pressure driven transportation. CNTs-NAAMs were placed between these two halves, which were sealed by two polydimethylsiloxane (PDMS) slides in order to prevent leakage, with an exposed area of 0.0314 cm^2. The diffusion of different dyes through the membrane was continuously monitored in the permeate cell using a UV–Visible fibre optic spectrophotometer (USB4000 Ocean Optics). In all transport experiments, dye's initial concentration in the feed cell was kept constant. Concentrations of $(RosB)^{2-}$ and $(Ru(BPY)_3)^{2+}$ were detected at their maximum absorbance of 552 and 452 nm, respectively, and then fitted to a calibration curve obtained by measuring absorbance of known concentrations of each dye. Transport graphs showing the dye concentration change rate in the permeate cell after flowing through membrane were generated from these data. All transport experiments were repeated three times and statistically treated.

3. Result and discussion

3.1. *Structural characterisation of prepared CNTs-NAAMs*

Fig. 2 displays a set of SEM images showing typical structure of prepared NAAMs and CNTs-NAAMs. A top surface of NAAM structure produced through a two-step anodization process at 6 °C is shown in Fig. 2a. It shows highly ordered nanopores with the hexagonal arrangement and pore diameter of 40 ± 5 nm (prepared under an anodization voltage of 40 V). CNTs grown inside the pores of NAAMs with inner diameter of 47 ± 5 nm by CVD process for 15 min is shown in Fig. 2b. The bottom views of NAAMs and CNTs-NAAMs are shown in the inset in Fig. 2a and b, respectively. Interestingly, these results indicate that an increment in the pore diameter of NAAMs takes place after CVD process. To investigate this, NAAMs samples were annealed under same temperature and ambient conditions as during CNTs fabrication. It was found that the pore diameter of the annealed NAAMs slightly increased from 40 ± 5 nm to 55 ± 5 nm. This can be related to loss of water content inside the alumina structure and reorganization of alumina to form a different crystallographic phase. It has been reported that as-produced amorphous Al_2O_3 prepared by anodization using oxalic solution transforms to γ-Al_2O_3 phase at annealing temperatures around 850 °C (the temperature used in the subsequent CVD process of CNTs growth) [20,21]. Note that, the phase change and loss of water content of alumina is thought to be the reason for bending and cracking of CNTs-NAAMs during the CVD process [22]. This can be avoided by placing NAAMs between two quartz plates and increasing the temperature from 25 °C to 850 °C at a rate of 4 °C min^{-1}. In this work we prepared CNTs-NAAMs with different lengths (30, 60 and 90 μm) and in Fig. 2c and d cross-sectional images of NAAMs and CNTs-NAAMs, respectively are presented as typical examples with the average length of 60 ± 4 μm. In Fig. 2e, aligned CNTs obtained after partial dissolution of NAAMs by HF solution. The EDX data presented in Fig. 2f provides an insight into the chemical composition and purity of CNTs-NAAMs produced by the catalyst-free CVD method used in this study. The presence of characteristic X-ray peaks for carbon (*K* = 0.277 keV), oxygen (*K* = 0.523 keV) and aluminium (*K* = 1.486 keV) not only provide fair idea about the element composition of CNTs-NAAMs but also shed light on the high level of purity of CNTs produced by our catalyst-free CVD process. Fig. 2g shows SEM image of uniform structure of CNTs liberated by selective dissolution of NAAMs used as templates, which proves the integrity of CNTs across all NAAM structure. Liberated CNTs were also characterised by high resolution TEM to determine their internal and external diameters (Fig. 2h). It also shows the poor crystallinity of prepared CNTs as a result of absence of the metal catalyst.

These results proved advantages of template-synthesized technology for the fabrication of highly aligned CNTs inside NAAMs, compared with their random orientation in CNTs membranes prepared by other methods [3,7,23,24]. In separation processes, fluids and gases are delivered through the tubular structure of CNTs and therefore these structural and chemical properties of the membranes play a key role in the separation performance [25]. Prepared CNTs-NAAMs didn't show presence of any amorphous carbon on both sides of the membrane, compared with other studies [26], which is associated with the precursor used to grow CNTs. In our work, CNTs precursor (a mixture of toluene and ethanol) was carefully chosen after our findings in several preliminary experiments. Toluene was selected as a rich source of carbon while ethanol was mixed with it in order to selectively avoid formation of amorphous carbon layer on the top and bottom surfaces of NAAMs due to its etching effect (OH radical) [27]. It has been reported that a thick amorphous carbon layer (20 μm thick) on the top of NAAMs was observed after catalyst-free CVD process using propylene as a precursor [26]. This indicates that the precursor plays a crucial role in the quality of the ultimate product (i.e. composite membrane). This feature of absence of amorphous carbon layer enables us to control

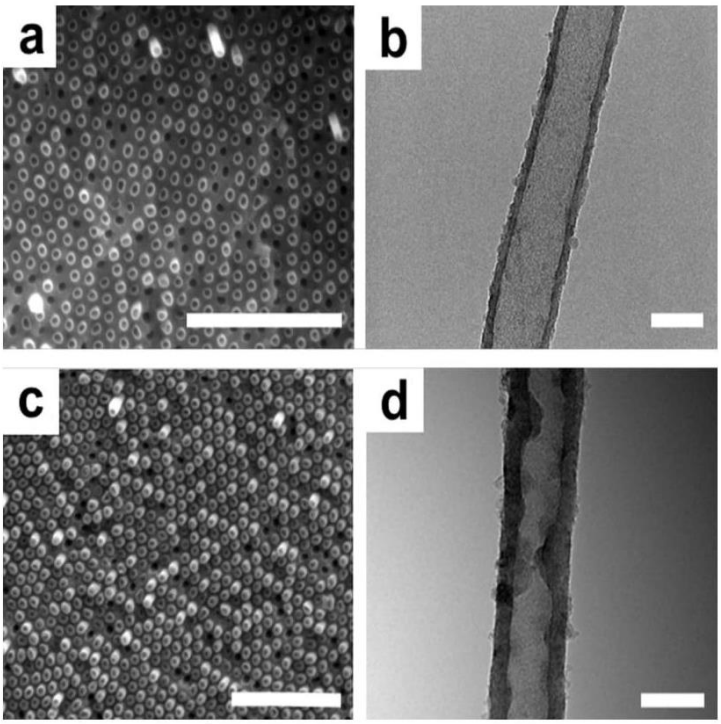

Fig. 3 – Set of comparative SEM images of CNTs-NAAMs and TEM images of liberated CNTs produced through catalyst-free CVD at different deposition times; (a and b) 30 min (scale bar = 1 μm and 50 nm, respectively); (c and d) 45 min (scale bar = 1 μm and 50 nm, respectively).

the thickness of nanotube's wall as a function of the deposition time. Moreover, the CNTs are hollow with open ends, which is not possible with catalyst based CVD process where the residual metal catalyst nanoparticles are often presented inside the nanotubes and these nanotubes are not suitable for separation applications [28,29].

3.1.1. Controlling CNTs dimensions (inner diameters and length)

As mentioned previously, the length of CNTs was controlled via the anodization time of NAAMs. NAAMs with pore lengths 30 μm, 60 μm and 90 μm were prepared and used as templates to grow CNTs. These three dimensions were selected to explore the influence of this parameter on transport properties but there is no limitation to prepare CNTs with broad range of different lengths from 1 μm to 500 μm using NAAMs with different lengths. Cross-sectional SEM images of prepared CNTs-NAAMs (Fig. S2 – Supporting information) illustrate CNTs with average nanotube lengths of 30 ± 4 μm, 60 ± 4 μm and 90 ± 4 μm, respectively. These membranes were prepared using the same deposition time (15 min) and have the same pore diameters (47 nm).

A simple approach to prepare CNTs membranes with different inner diameters of nanotubes is to use NAAMs with different pore diameters prepared by different anodization conditions. In this paper we propose to use CVD process to demonstrate that this approach can be applied for precise control of CNTs diameters. This is achieved by controlling the CVD deposition time and growth rate of graphitic layers inside NAAM's pores, which is known as the time dependent process [14]. The CVD deposition times of 15 min, 30 min and 45 min are used here to determine the influence of the CVD deposition time on CNTs growth rate and the changes of inner pore diameters. The NAAMs with 40 nm pore diameters are used to demonstrate the process with no limitations to use the NAAMs with smaller pores. SEM images of the top surface showing the prepared CNTs using different CVD deposition times are presented in Figs. 2b, 3a and c. These results confirm that the wall thickness of CNTs were significantly increased and can be controlled with the deposition time. As the deposition time increases, the more graphitic layers of carbon are formed (Figs. 2h, 3b and d). The wall thickness of CNTs prepared by deposition times of 15 min, 30 min and 45 min were 4 ± 2 nm, 7 ± 2 nm and 12 ± 2 nm respectively (Fig. 4), confirming a linear relationship with a growth rate of 0.26 nm min^{-1}. The corresponding CNTs diameters of 47 ± 5 nm, 41 ± 5 nm and 31 ± 5 nm are determined respectively. The defective walls and amorphous found in the CNTs sidewalls are a characteristic of CNTs produced by a catalyst-free CVD process [13,22]. These results show that CVD deposition time can be used for precise control of CNTs diameters in CNTs-NAAMs. The lowest inner pore diameter of CNTs presented in this work was 31 ± 5 nm, but with no limitations to make lower diameters to cc 5–10 nm by extending CVD deposition time or using NAAMs with smaller pores (eg 25 nm prepared in sulphuric acid). These

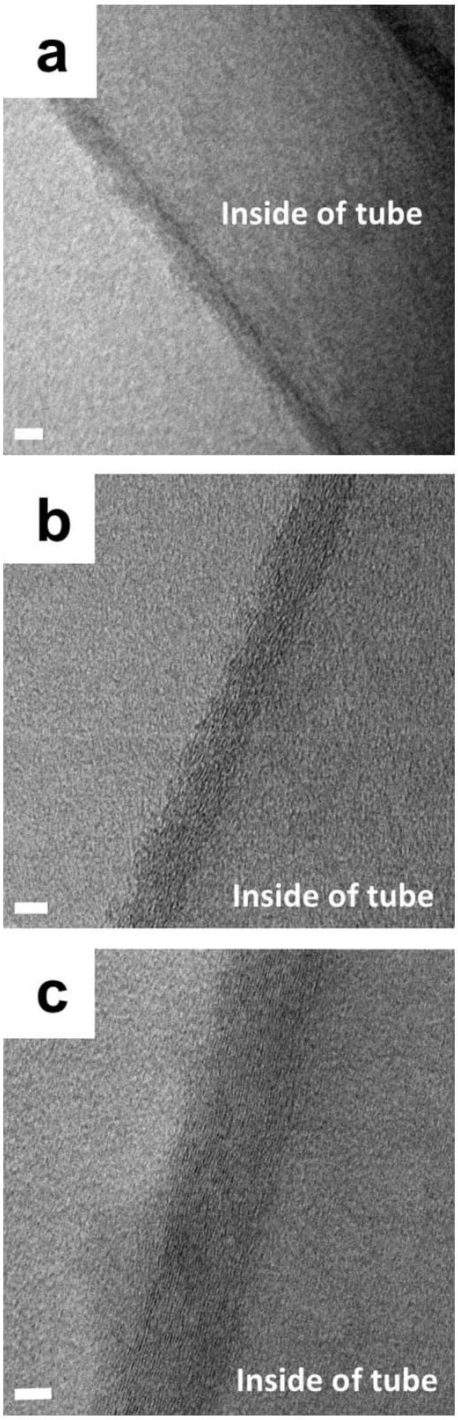

Fig. 4 – TEM magnified views of the graphitic layers structure of CNTs prepared by different deposition times. (a) 15 min (scale bar = 5 nm); (b) 30 min (scale bar = 5 nm); (c) 45 min (scale bar = 5 nm).

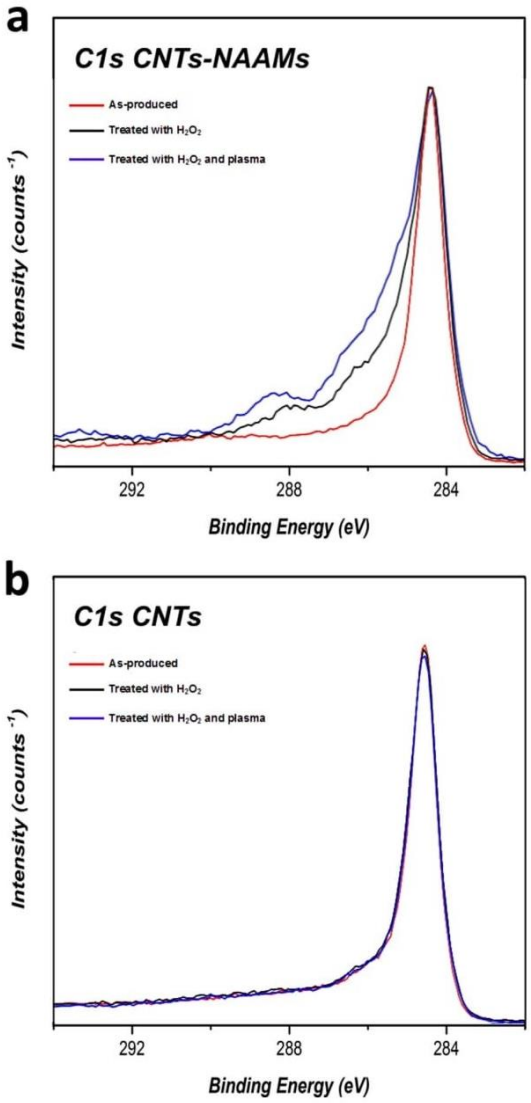

Fig. 5 – XPS analysis of CNTs-NAAMs and liberated CNTs. (a) C 1s spectra of as-produced, treated with H_2O_2 and treated with H_2O_2 and plasma CNTs-NAAMs; (b) C 1s spectra of as-produced, treated with H_2O_2 and treated with H_2O_2 and plasma liberated CNTs. (A colour version of this figure can be viewed online.)

results confirm that the CVD deposition time can be used as a simple parameter for controlling the growth of CNT's wall and the CNTs-NAAMs inner diameters. By controlling both the diameters and the length it is demonstrated that CNTs-NAAMs with desired dimensions can be designed and prepared. Our CVD process compared with other methods used for the synthesis of CNTs membranes is very simple, faster and can be scale-up. Till date, there is no detailed-established growth mechanism of CNTs prepared via free-catalyst CVD processes in NAAMs. The growth mechanism is a complicated process which is based on the catalytic role of NAAMs and the hydrocarbon thermal decomposition [22,26,30]. Nevertheless, the most general accepted growth mechanism of CNTs can be outlined as follows; (i) pyrolysis of carbon source (i.e. mixture of toluene and ethanol) into

carbon, hydrogen and oxygen species in the pyrolysis zone of the CVD reactor, (ii) transport of the carbon to the deposition zone of the CVD reactor by the carrier gas (Ar), where the NAAMs were placed, (iii) deposition of carbon on the pore walls of NAAMs. Notice that the wall thickness dependence on the deposition time indicates that this mechanism is based on thermal decomposition and subsequent deposition of carbon on the pore walls of NAAMs, which generates multiple layers of carbon as the deposition time increases.

3.2. *Controlling the surface chemistry of CNTs by oxidation and annealing processes*

The chemical modification of the wall surface inside nanopore and nanotube membranes by changing their surface chemistry or immobilization new organic molecules is well-established method to control transport properties of membranes and introduce their chemistry based separation [31]. This method is not well explored on CNTs membranes and opens new exciting opportunities to tune transport and selectivity properties for a broad range of applications. In this work we present two approaches to control the surface chemistry inside CNTs from highly hydrophobic based on thermal annealing to hydrophilic based on oxidation by introducing oxygenated groups by dry and wet oxidation process. Oxidation by strong acids and oxidants is generally known as a fundamental route for modifying CNTs external surface by generating oxygenated functional groups on the surface. Notice that, this process makes defects on graphitic structure of CNTs and results in destruction of the CNTs sidewalls and breaking CNTs [32,33]. Therefore, in this study, we utilise gentler oxidation process using hydrogen peroxide and plasma in order to functionalize the inner wall surface of CNTs and impart them with oxygen-containing functional groups (mainly hydroxyl group). The plasma modification time was 3 min to avoid any changes in the structural integrity of CNTs caused by long time modification [34]. To gain insight into the chemical composition change of CNTs after oxidation, as-produced and oxidised CNTs were characterised by XPS and Raman spectroscopy. In this sense, it should be noted that the XPS and Raman spectrum of CNTs embedded in NAAMs were obtained from the top carbon layer on NAAM's surface since this carbon layer has the same chemical structure as the inner CNTs layers [13]. The XPS survey spectra of as-produced and oxidised CNTs-NAAMs show the elements C, O and Al. As-produced CNTs-NAAMs had a 3% of oxygen, which was increased to 12% and 15% after oxidation with H_2O_2 and H_2O_2 and plasma respectively. Here we will only analyse the C1s spectra. Analysing the O1s spectra is not undertaken because it is extremely difficult, if not impossible, to distinguish between the O contribution from the aluminium oxide template and from the oxidised carbon to the O1s spectra. Fig. 5a shows the C 1s spectra of as-produced CNTs-NAAMs, treated with H_2O_2 and treated with H_2O_2 and plasma. All CNTs-NAAMs show a large peak at 284.6 ± 0.2 eV which can be attributed to the sp^2 hybridized graphite-like carbon atoms [35]. After oxidation with H_2O_2, a shoulder at 285.5–287 eV was formed which can be assigned to C–O (alcohol/ether) groups [36]. Another peak at 288 eV is attributed to C=O (keton/aldehyd) groups [37]. These results confirm that oxygenated functional groups were introduced to the carbon's surface after H_2O_2 treatment which renders CNTs-NAAMs hydrophilic [38]. Exposure to oxygen plasma treatment turns CNTs-NAAMs in superhydrophilic, which is indicated by an increase of the shoulder intensity and the presence of clear peak at 288.5 eV, which can be assigned to O=C–O (carboxyl/ester) groups [36] (Fig. 5a). Liberated CNTs were analysed by XPS to provide information on the chemical composition change of the outer surface of CNTs after oxidation. The C 1s spectra of as-produced CNTs, treated with H_2O_2 and treated with H_2O_2 and plasma are shown in Fig. 5b. It shows almost no changes in the chemical composition of the outer surface of CNTs after oxidation, which is indicated by almost the same graphitic carbon peak at 284.6 ± 0.2 eV. This clearly confirms that only the inner surface of CNTs was modified (i.e. oxidised) while the outer surface was kept intact.

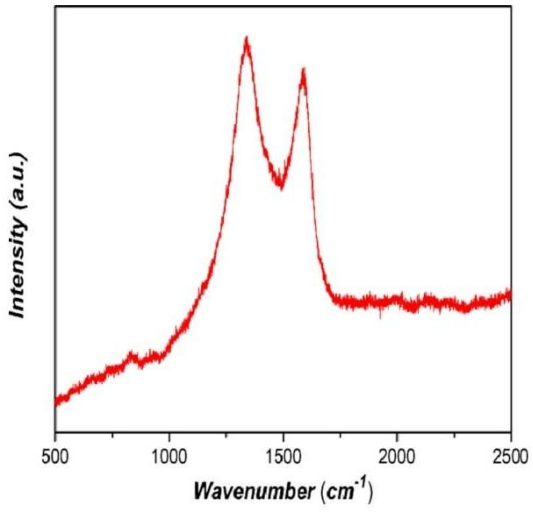

Fig. 6 – Raman spectrum of as-produced CNTs-NAAMs prepared through catalyst-free CVD approach. (A colour version of this figure can be viewed online.)

Raman spectrum of as-produced CNTs-NAAMs shows the typical profile of CNTs (i.e. D and G band peaks are not separated and partially overlapped) (Fig. 6). It shows a G-band peak (indicating highly ordered CNTs sidewalls) around 1585 cm^{-1} and a D-band peak (indicating disorder CNTs sidewalls) around 1340 cm^{-1}. The ratio between D and G bands (ID/IG) of as-produced CNTs-NAAMs was 1.05 and this high value indicates a poor graphitic feature of as-produced CNTs. This was confirmed by TEM image analysis (Fig. 4). This ID/IG ratio is comparable to the ID/IG ratio of CNTs obtained by other CVD synthesis approaches using NAAMs as templates while using ethylene and acetylene as carbon sources (ID/IG = 0.79 and 1.38 respectively) [22,39]. However, it should be taken into account that the ID/IG ratio is dependent on the excitation energy [40]. It is worth stressing that CNTs prepared through template-directed method using a catalyst-free CVD approach can be easily graphitized by further thermal treatment at temperatures as high as 2000 °C, which in turn drops the ID/IG ratio to a minimum of 0.27 [38]. Raman spectra of

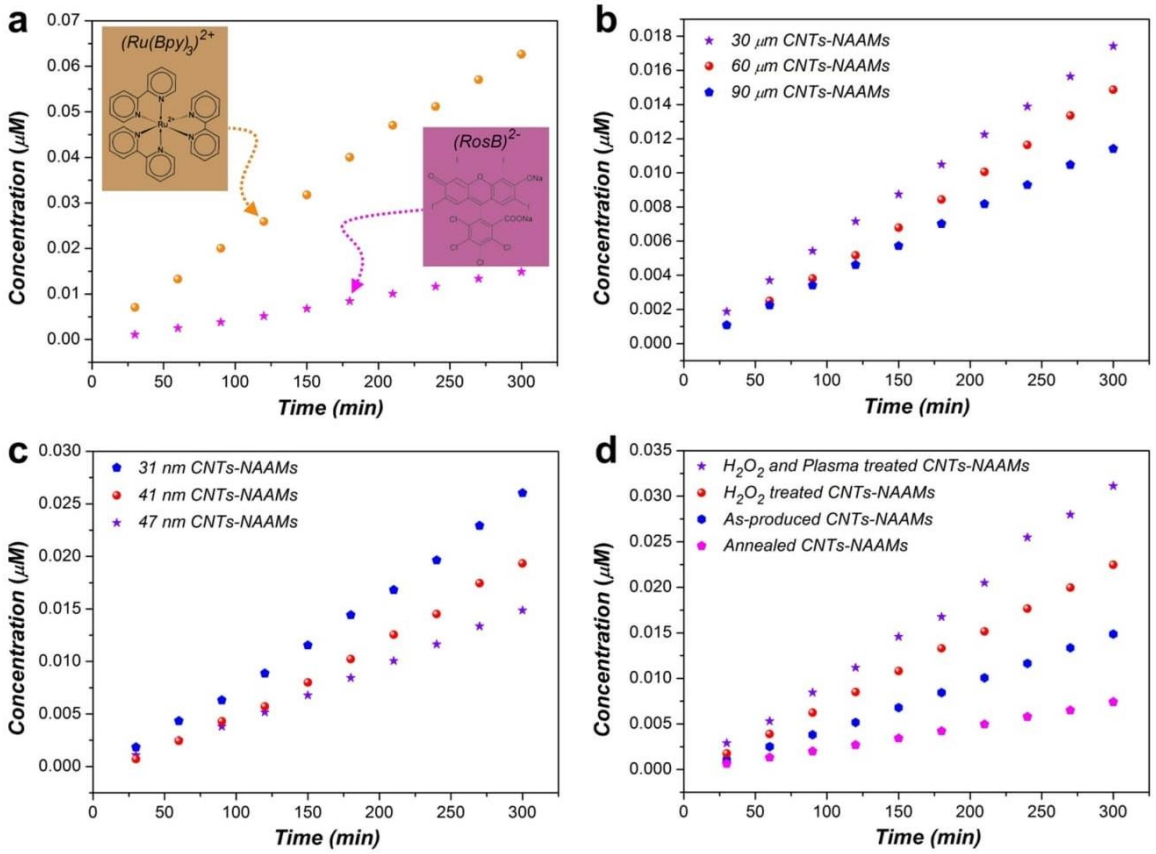

Fig. 7 – Molecular transport study through CNTs-NAAMs. (a) Diffusion of $(RosB)^{2-}$ and $(Ru(BPY)_3)^{2+}$ through CNTs-NAAMs (length was 60 μm and inner diameter was 47 nm). (b) The influence of CNTs length on diffusion of dye molecules $(RosB)^{2-}$ through 30, 60 and 90 μm long CNTs-NAAMs (inner diameter was 47 nm). (c) The influence of CNTs diameters on diffusion of dye molecules $(RosB)^{2-}$ through 47, 41and 31 nm CNTs-NAAMs (length was 60 μm). (d) Diffusion of $(RosB)^{2-}$ through as-produced, treated with H_2O_2, treated with H_2O_2 and plasma, and annealed CNTs-NAAMs (length was 60 μm and diameter was 47 nm). (Data presented here are average of three measurements, errors bars with standard deviation not presented to have clarity.) (A colour version of this figure can be viewed online.)

CNTs-NAAMs after treatments with H_2O_2 and with H_2O_2 and plasma show no shift in the position of G and D band peaks indicating no structural damage of CNTs-NAAMs after oxidation treatments. However, slight increase in the D band peak was observed after oxidation treatments (Fig. S3 – Supporting information).

These results from XPS analysis showed that the modification of the inner walls with increased amount of oxygen species was successfully accomplished. This surface chemistry is more hydrophilic compared with as-produced and annealed CNTs-NAAMs and will have significant impact on transport of molecules depends of their surface chemistry. Furthermore, these results indicate that by controlling the time of plasma and peroxide oxidation the density of oxygen groups can be tuned to required values and will allow the chemistry based separation of molecules. Prepared CNTs-NAAMs with different dimensions and amount of oxygenated functional groups were explored in the following study to assess their influence on the transport performance of these composite membranes.

3.3. *Molecular transport study of CNTs-NAAMs*

3.3.1. *Influence of graphitic CNT surface on transport of hydrophobic and hydrophilic molecules*

The transport and selectivity properties of prepared CNTs-NAAMs were explored by initial experiment using single molecule permeation experiment based on diffusion process of dyes as model molecules with different hydrophilic–hydrophobic and charge properties $(RosB)^{2-}$ and $(Ru(BPY)_3)^{2+}$. Fig. 7 and Table 1 show a summary of results of the transport graphs and diffusional fluxes of these dyes through CNTs-NAAMs with different dimensions and surface chemistry as a function of time. Fig. 7a displays transport graphs for $(RosB)^{2-}$ and $(Ru(BPY)_3)^{2+}$ showing significant difference of concentration change rates in the permeate cell of $5\times10^{-5}\pm1.3\times10^{-6}$ μM min^{-1} and $2\times10^{-4}\pm2.8\times10^{-5}$ μM min^{-1} and diffusional flux of $1.59\times10^{-3}\pm4.1\times10^{-5}$ μmol min^{-1} cm^{-2} and 6. $37\times10^{-3}\pm8.9\times10^{-4}$ μmol min^{-1} cm^{-2}, respectively. These results confirm that transport of hydrophobic (cationic) dye molecules $(Ru(BPY)_3)^{2+}$ is about 4

Table 1 – Diffusional flux and concentration change rate in the permeate cell after flowing of ionic dye molecules ($(RosB)^{2-}$ and $(Ru(BPY)_3)^{2+}$) through CNTs-NAAMs with different lengths, pore diameters and surface chemistry (0.0314 cm^2 area).

Molecular transport study	CNTs-NAAMs/dye used	Concentration change rate in the permeate cell ($\mu M\ min^{-1}$)	Diffusional flux rate ($\mu mol\ min^{-1}\ cm^{-2}$)
Transport properties of CNTs	As-produced/$(RosB)^{2-}$	$5 \times 10^{-5} \pm 1.3 \times 10^{-6}$	$1.592 \times 10^{-3} \pm 4.1 \times 10^{-5}$
	As-produced/$(Ru(BPY)_3)^{2+}$	$2 \times 10^{-4} \pm 2.8 \times 10^{-5}$	$6.369 \times 10^{-3} \pm 8.9 \times 10^{-4}$
Length influence	30 μm long/$(RosB)^{2-}$	$6 \times 10^{-5} \pm 1.7 \times 10^{-6}$	$1.911 \times 10^{-3} \pm 5.4 \times 10^{-5}$
	60 μm long/$(RosB)^{2-}$	$5 \times 10^{-5} \pm 1.3 \times 10^{-6}$	$1.592 \times 10^{-3} \pm 4.1 \times 10^{-5}$
	90 μm long/$(RosB)^{2-}$	$4 \times 10^{-5} \pm 1.6 \times 10^{-6}$	$1.274 \times 10^{-3} \pm 5.1 \times 10^{-5}$
Diameter influence	47 nm/$(RosB)^{2-}$	$5 \times 10^{-5} \pm 1.3 \times 10^{-6}$	$1.592 \times 10^{-3} \pm 4.1 \times 10^{-5}$
	41 nm/$(RosB)^{2-}$	$7 \times 10^{-5} \pm 1.1 \times 10^{-6}$	$2.229 \times 10^{-3} \pm 3.5 \times 10^{-5}$
	31 nm/$(RosB)^{2-}$	$9 \times 10^{-5} \pm 2 \times 10^{-6}$	$2.866 \times 10^{-3} \pm 6.4 \times 10^{-5}$
Modification influence	As-produced/$(RosB)^{2-}$	$5 \times 10^{-5} \pm 1.3 \times 10^{-6}$	$1.592 \times 10^{-3} \pm 4.1 \times 10^{-5}$
	Treated with H_2O_2/$(RosB)^{2-}$	$8 \times 10^{-5} \pm 1.6 \times 10^{-6}$	$2.548 \times 10^{-3} \pm 5.1 \times 10^{-5}$
	Treated with H_2O_2 and plasma/$(RosB)^{2-}$	$1 \times 10^{-4} \pm 2.3 \times 10^{-5}$	$3.185 \times 10^{-3} \pm 7.3 \times 10^{-4}$
	Annealed/$(RosB)^{2-}$	$3 \times 10^{-5} \pm 1.7 \times 10^{-6}$	$9.55 \times 10^{-4} \pm 5.4 \times 10^{-5}$

times faster than hydrophilic (anionic) dye molecules $(RosB)^{2-}$. The size of these molecules is similar (ca 1.2 nm) which leads to conclusion that their transport is influenced by chemical and interfacial properties showing potential of CNTs-NAAMs for chemical based separation. This behaviour is explained by the lowered friction between the hydrophobic graphitic walls of CNTs and the hydrophobic dye molecules $(Ru(BPY)_3)^{2+}$ which increases their transport at the interface. Considering very large pore diameters of CNTs compared with the size of permeating molecules the observed chemical selectivity effect is not significant, which is expected as only a small amount of molecules are interacting with CNTs walls compared with nanotube volume. If the pore size of CNTs is reduced to less than 5 nm the hydrophobic-hydrophobic interaction between permeating molecules at the wall interface will dominate transport and therefore significantly enhance selectivity for several order of magnitudes [31]. We are currently progressing such studies using the CNTs-NAAMs with reduced diameters to show separation of hydrophilic and hydrophobic molecules from complex model systems including oil–water emulsion and will be presented as separate publication.

3.3.2. *Influence of the CNTs dimensions (diameters and length) on molecular transport*

To study the influence of the length and diameters of CNTs-NAAMs on their transport properties, $(RosB)^{2-}$ was used as model molecules and were transported through CNTs-NAAMs with different lengths (30 μm, 60 μm and 90 μm) with the same CNTs diameter (47 nm) and different CNT diameters (31 nm, 41 nm and 47 nm) with the same CNTs length (60 μm). Fig. 7b presents $(RosB)^{2-}$ transport graphs across the CNTs-NAAMs with different lengths showing flux of $1.91 \times 10^{-3} \pm 5.4 \times 10^{-5}\ \mu mol\ min^{-1}\ cm^{-2}$ through 30 μm, $1.59 \times 10^{-3} \pm 4.1 \times 10^{-5}\ \mu mol\ min^{-1}\ cm^{-2}$ through 60 μm, and 1. $27 \times 10^{-3} \pm 5.1 \times 10^{-5}\ \mu mol\ min^{-1}\ cm^{-2}$ through 90 μm long CNTs-NAAMs. These graphs confirmed that the longer the tubes, the slower is the flux which are expected considering Fick's first law of diffusion describing the molecular transport across nanotubular structures (Details in Supporting information, Section S4). This behaviour is associated with the fact that longer nanotubes provide more contact area between CNTs wall and dye molecules and thus consuming more time than short tubes to pass through CNTs-NAAMs.

To study the influence of the inner diameters of CNTs-NAAMs on their transport properties, $(RosB)^{2-}$ molecules were transported through CNTs-NAAMs with average pore diameters of 31 nm, 41 nm, and 47 nm (Fig. 7c). The diffusional flux through CNTs with an inner diameter of 31 nm is $2.87 \times 10^{-3} \pm 6.4 \times 10^{-5}\ \mu mol\ min^{-1}\ cm^{-2}$, which is one fold higher than that obtained through CNTs with an inner diameter of 47 nm. This can be ascribed by the size influence because as the diameter gets smaller, the interactions between dye molecules and CNTs walls increase which is expected and in agreement with previous studies.

3.3.3. *Influence of the surface chemistry of CNTs on molecular transport*

CNTs-NAAMs with annealed graphitic surface and oxidised via H_2O_2 and plasma treatments were explored to investigate

the correlation between modifications and transport properties. Here we used again $(RosB)^{2-}$ as model of hydrophilic molecules to be consistent with study presented in previous sections. Fig. 7d shows $(RosB)^{2-}$ concentration change in the permeate cell after its transport across as-produced CNTs-NAAMs, treated with H_2O_2, and treated with H_2O_2 and plasma. Modification of CNTs-NAAMs with H_2O_2 led to increase the diffusional flux of hydrophilic negatively charged dye molecules $(RosB)^{2-}$. It increased from $1.59 \times 10^{-3} \pm 4.1 \times 10^{-5}$ μmol min^{-1} cm^{-2} for the unmodified CNTs-NAAMs to $2.55 \times 10^{-3} \pm 5.1 \times 10^{-5}$ μmol min^{-1} cm^{-2} for treated membrane with H_2O_2. Subsequent treatment with plasma increased the diffusional flux of $(RosB)^{2-}$ to $3.19 \times 10^{-3} \pm 7.3 \times 10^{-4}$ μmol min^{-1} cm^{-2}, which is one order of magnitude faster than unmodified membranes (Table 1). This result reveals that to create oxygenated functional groups on the inner surface of CNTs by H_2O_2 treatment led to render CNTs more hydrophilic. Hydrophilicity of CNTs-NAAMs was further enhanced by generating even more oxygenated functional groups by plasma treatment which in turn increases the diffusional flux of $(RosB)^{2-}$ which is in agreement with XPS data. These results confirm that the transport properties and chemical selectivity of CNTs-NAAMs can be tuned by simple oxidation process without of immobilization of organic molecule inside CNTs.

It is generally known that CNTs prepared via catalyst-free CVD method suffer from poor graphitic layer structures compared with catalyst based process. Annealing at temperatures higher than the one used during the CVD process (i.e. 850 °C) is proved that can enhance the graphitization of CNTs with reduction presented oxygen groups on the surface and increasing hydrophobicity [14,38]. To investigate the influence of CNTs annealing on their transport performance, CNTs-NAAMs were annealed at 1000 °C for 3 h in the presence of Ar flow. Fig. 7d shows $(RosB)^{2-}$ concentration change in the permeate cell after its transport across as-produced CNTs-NAAMs and annealed CNTs-NAAMs. Annealing treatment led to decrease the diffusional flux of hydrophilic and negatively charged dye molecules $(RosB)^{2-}$. It decreased from $1.59 \times 10^{-3} \pm 4.1 \times 10^{-5}$ μmol min^{-1} cm^{-2} for as-produced CNTs-NAAMs to $9.55 \times 10^{-4} \pm 5.4 \times 10^{-5}$ μmol min^{-1} cm^{-2} for annealed CNTs-NAAMs (Table 1). This is because annealing treatment makes CNTs more hydrophobic and in turn decreases the diffusional flux of $(RosB)^{2-}$ as it is a hydrophilic dye.

4. Conclusions

The fabrication of CNTs-NAAMs with controllable diameters and length of nanotubes is demonstrated using a catalyst-free CVD approach by a mixture of toluene and ethanol as a carbon source. The presented results show that the dimensional features of CNTs-NAAMs can be precisely engineered by controlling the anodization time on NAAMs and the deposition time during CVD process. The controlling of surface chemistry of CNTs-NAAMs from hydrophobic to hydrophilic surface by simple thermal annealing and wet and dry oxidation process (hydrogen peroxide and plasma) is demonstrated without the use of surface immobilization molecules. The changing surface chemistry is successfully confirmed by XPS analysis showing that as-produced and oxidised CNTs-NAAMs have concentrations of oxygenated functional groups that are significantly different. The performed molecular transport studies using hydrophobic and hydrophilic model molecules with the same molecular size showed that the transport and chemical selectivity properties of CNTs-NAAMs can be controlled by controlling their dimensions (diameters and length) and surface chemistry. These studies provide new knowledge and understanding how to design CNTs-NAAMs with advanced transport and chemical selectivity performance and use them for separation of complex molecular mixtures.

Acknowledgements

Authors acknowledge the financial support provided by the Australian Research Council (FT 110100711 and DE14010054). The authors acknowledge the facilities and the scientific and technical assistance of the Australian Microscopy & Microanalysis Research Facility at the Electron Microscope Unit, The University of Adelaide. Mohammed Alsawat thanks Taif University (Ministry of Education, Saudi Arabia) for funding his scholarship.

Appendix A. Supplementary data

Supplementary data associated with this article can be found, in the online version, at http://dx.doi.org/10.1016/j.carbon.2015.05.090.

REFERENCES

[1] Ho WSW, Li K. Recent advances in separations. Curr Opin Chem Eng 2012;1(2):145–7.
[2] Padaki M, Murali RS, Abdullah M, Misdan N, Moslehyani A, Kassim M, et al. Membrane technology enhancement in oil–water separation. A review. Desalination 2015;357:197–207.
[3] Majumder M, Clayton V, Ajayan AP. 1.14 carbon nanotube membranes: a new frontier in membrane science. Compr Membr Sci Eng 2010;1:291.
[4] Noy A, Park HG, Fornasiero F, Holt JK, Grigoropoulos CP, Bakajin O. Nanofluidics in carbon nanotubes. Nano Today 2007;2(6):22–9.
[5] Holt JK, Park HG, Wang Y, Stadermann M, Artyukhin AB, Grigoropoulos CP, et al. Fast mass transport through sub-2-nanometer carbon nanotubes. Science 2006;312(5776):1034–7.
[6] Ko H, Jiang C, Shulha H, Tsukruk VV. Carbon nanotube arrays encapsulated into freely suspended flexible films. Chem Mater 2005;17(10):2490–3.
[7] Majumder M, Chopra N, Andrews R, Hinds BJ. Nanoscale hydrodynamics: enhanced flow in carbon nanotubes. Nature 2005;438(7064):44.
[8] Hinds BJ, Chopra N, Rantell T, Andrews R, Gavalas V, Bachas LG. Aligned multiwalled carbon nanotube membranes. Science 2004;303(5654):62–5.
[9] Seah C-M, Chai S-P, Mohamed AR. Synthesis of aligned carbon nanotubes. Carbon 2011;49(14):4613–35.
[10] Masuda H, Fukuda K. Ordered metal nanohole arrays made by a two-step replication of honeycomb structures of anodic alumina. Science 1995;268(5216):1466–8.

[11] Md Jani AM, Losic D, Voelcker NH. Nanoporous anodic aluminium oxide: advances in surface engineering and emerging applications. Prog Mater Sci 2013;58(5):636–704.
[12] Kyotani T, Tsai L-f, Tomita A. Formation of ultrafine carbon tubes by using an anodic aluminum oxide film as a template. Chem Mater 1995;7(8):1427–8.
[13] Kyotani T, Tsai L-f, Tomita A. Preparation of ultrafine carbon tubes in nanochannels of an anodic aluminum oxide film. Chem Mater 1996;8(8):2109–13.
[14] Altalhi T, Kumeria T, Santos A, Losic D. Synthesis of well-organised carbon nanotube membranes from non-degradable plastic bags with tuneable molecular transport: towards nanotechnological recycling. Carbon 2013;63:423–33.
[15] Li A, Müller F, Birner A, Nielsch K, Gösele U. Hexagonal pore arrays with a 50–420 nm interpore distance formed by self-organization in anodic alumina. J Appl Phys 1998;84(11):6023–6.
[16] Jessensky O, Müller F, Gösele U. Self-organized formation of hexagonal pore arrays in anodic alumina. Appl Phys Lett 1998;72(10):1173–5.
[17] Lillo M, Losic D. Pore opening detection for controlled dissolution of barrier oxide layer and fabrication of nanoporous alumina with through-hole morphology. J Membr Sci 2009;327(1–2):11–7.
[18] Losic D, Losic Jr D. Preparation of porous anodic alumina with periodically perforated pores. Langmuir 2009;25(10):5426–31.
[19] Che G, Lakshmi B, Martin C, Fisher E, Ruoff RS. Chemical vapor deposition based synthesis of carbon nanotubes and nanofibers using a template method. Chem Mater 1998;10(1):260–7.
[20] Chen CC, Chen JH, Chao CG. Post-treatment method of producing ordered array of anodic aluminum oxide using general purity commercial (99.7%) aluminum. Jpn J Appl Phys 2005;44(3R):1529.
[21] Fernández-Romero L, Montero-Moreno J, Pellicer E, Peiró F, Cornet A, Morante J, et al. Assessment of the thermal stability of anodic alumina membranes at high temperatures. Mater Chem Phys 2008;111(2):542–7.
[22] Sarno M, Tamburrano A, Arurault L, Fontorbes S, Pantani R, Datas L, et al. Electrical conductivity of carbon nanotubes grown inside a mesoporous anodic aluminium oxide membrane. Carbon 2013;55:10–22.
[23] López-Lorente A, Simonet B, Valcárcel M. The potential of carbon nanotube membranes for analytical separations. Anal Chem 2010;82(13):5399–407.
[24] Miller SA, Young VY, Martin CR. Electroosmotic flow in template-prepared carbon nanotube membranes. J Am Chem Soc 2001;123(49):12335–42.
[25] Ismail A, Goh PS, Sanip S, Aziz M. Transport and separation properties of carbon nanotube-mixed matrix membrane. Sep Purif Technol 2009;70(1):12–26.
[26] Schneider JJ, Maksimova NI, Engstler J, Joshi R, Schierholz R, Feile R. Catalyst free growth of a carbon nanotube–alumina composite structure. Inorg Chim Acta 2008;361(6):1770–8.
[27] Maruyama S, Kojima R, Miyauchi Y, Chiashi S, Kohno M. Low-temperature synthesis of high-purity single-walled carbon nanotubes from alcohol. Chem Phys Lett 2002;360(3):229–34.
[28] Morjan R, Nerushev O, Sveningsson M, Rohmund F, Falk L, Campbell E. Growth of carbon nanotubes from C60. Appl Phys A 2004;78(3):253–61.
[29] Grobert N, Terrones M, Osborne A, Terrones H, Hsu W, Trasobares S, et al. Thermolysis of C60 thin films yields Ni-filled tapered nanotubes. Appl Phys A 1998;67(5):595–8.
[30] Lee JS, Gu GH, Kim H, Jeong KS, Bae J, Suh JS. Growth of carbon nanotubes on anodic aluminum oxide templates: fabrication of a tube-in-tube and linearly joined tube. Chem Mater 2001;13(7):2387–91.
[31] Jirage KB, Hulteen JC, Martin CR. Nanotubule-based molecular-filtration membranes. Science 1997;278(5338):655–8.
[32] Rosca ID, Watari F, Uo M, Akasaka T. Oxidation of multiwalled carbon nanotubes by nitric acid. Carbon 2005;43(15):3124–31.
[33] Datsyuk V, Kalyva M, Papagelis K, Parthenios J, Tasis D, Siokou A, et al. Chemical oxidation of multiwalled carbon nanotubes. Carbon 2008;46(6):833–40.
[34] Mishra P, Islam S. Surface modification of MWCNTs by O_2 plasma treatment and its exposure time dependent analysis by SEM, TEM and vibrational spectroscopy. Superlattices Microstruct 2013;64:399–407.
[35] Biniak S, Szymański G, Siedlewski J, Światkowski A. The characterization of activated carbons with oxygen and nitrogen surface groups. Carbon 1997;35(12):1799–810.
[36] Reis M, Do Rego AB, Da Silva JL, Soares M. An XPS study of the fibre-matrix interface using sized carbon fibres as a model. J Mater Sci 1995;30(1):118–26.
[37] Xie Y, Sherwood P. X-ray photoelectron-spectroscopic studies of carbon fiber surfaces. Part IX: the effect of microwave plasma treatment on carbon fiber surfaces. Appl Spectrosc 1989;43(7):1153–8.
[38] Mattia D, Rossi M, Kim B, Korneva G, Bau H, Gogotsi Y. Effect of graphitization on the wettability and electrical conductivity of CVD-carbon nanotubes and films. J Phys Chem B 2006;110(20):9850–5.
[39] Jeong S-H, Hwang H-Y, Hwang S-K, Lee K-H. Carbon nanotubes based on anodic aluminum oxide nano-template. Carbon 2004;42(10):2073–80.
[40] Soin N, Roy S, Ray S, McLaughlin J. Excitation energy dependence of Raman bands in multiwalled carbon nanotubes. J Raman Spectrosc 2010;41(10):1227–33.

Supporting Information

Carbon nanotube - nanoporous anodic alumina composite membranes with controllable inner diameters and surface chemistry: Influence on molecular transport and chemical selectivity

Mohammed Alsawat[a], Tariq Altalhi[a,b], Tushar Kumeria[a], Abel Santos[a], and Dusan Losic*[a]

[a] School of Chemical Engineering, The University of Adelaide, Adelaide, Australia.

[b] Department of Chemistry, Faculty of Science, Taif University, Taif, Saudi Arabia.

S1. Transport study set-up

The molecular transport of ionic dyes through the CNTs-NAAMs was measured using a H-tube permeation cell. **Fig S1a** shows the set-up of the transport system consists of two half of cells (i.e. feed and permeate cells) Feed cell was filled with a 3 mL of 10 mM of dye solution and the permeate cell was filled with the same level of water to avoid a pressure driven transportation. The CNTs-NAAMs were placed between these two halves, which sealed by two polydimethylsiloxane (PDMS) slides to prevent leakage, with an exposed area of 0.0314cm^2. The diffusion of two models molecules with different hydrophilic-hydrophobic and charge properties (Rose Bengal $(RosB)^{2-}$ and Tris(2,20-bipyridyl) dichlororuthenium(II) hexahydrate $(Ru(BPY)_3)^{2+}$, respectively through the membrane was monitored in the permeate cell using a UV–Visible fibre optic spectrophotometer (USB4000 Ocean Optics). **Fig. S1b and c** shows the chemical structure of hydrophilic and hydrophobic dye molecules respectively used in this study. The concentrations of $(RosB)^{2-}$ and $(Ru(BPY)_3)^{2+}$ were detected at their maximum absorbance of 552 and 452 nm, respectively.

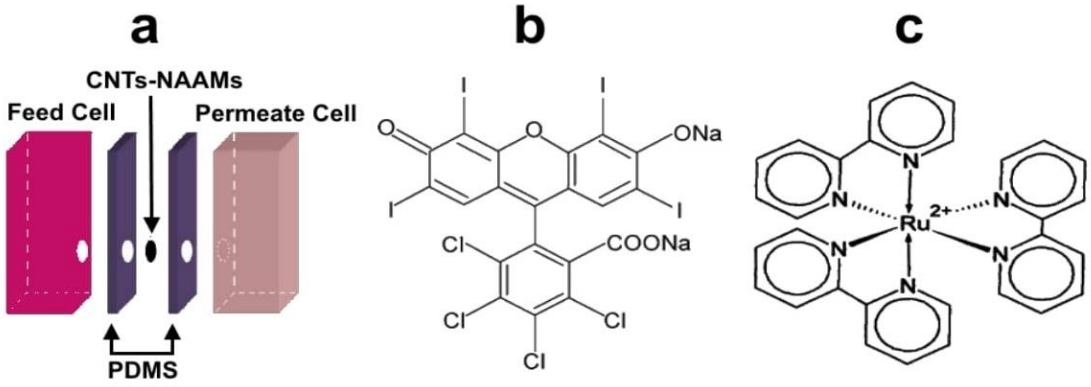

Fig. S1 Schematic diagram of the permeation cell used for transport study (a), Chemical structure of molecular dyes used in transport study; Rose Bengal $(RosB)^{2-}$ (b) and Tris(2,20-bipyridyl) dichlororuthenium(II) hexahydrate $(Ru(BPY)_3)^{2+}$ (c).

S2. Fabrication of CNTs-NAAMs

Vertically aligned multiwalled carbon nanotubes (MWCNTs) were grown by a catalyst-free chemical vapour deposition (CVD) method inside the pores of NAAMs using a mixture of toluene and ethanol 1:1 (*v:v*) as a carbon precursor. This process was carried out in a CVD system consisting of a two-stage furnace equipped with a cylindrical quartz tube. NAAMs were placed in the deposition zone of the CVD reactor. The reactor temperature was increased to 850 °C at a rate of 4 °C min^{-1} under argon (Ar) flow, which was used as a carrier gas at flow rate of 1 dm^3 min^{-1}. The CNT-NAAM's length was controlled via the anodization time of NAAMs. Different lengths of NAAMs (30, 60 and 90 µm) were prepared to grow CNTs. Cross-sectional SEM images of the CNTs-NAAMs with lengths of 30, 60 and 90 µm are shown in **Figs**. **S2a**, **b** and **c**, respectively. The inner pore diameter of CNTs was controlled via deposition time during CVD process. **Table S1** summarise the fabrication protocols for preparation of CNTs-NAAMs with different nanotubes lengths and inner pore diameters.

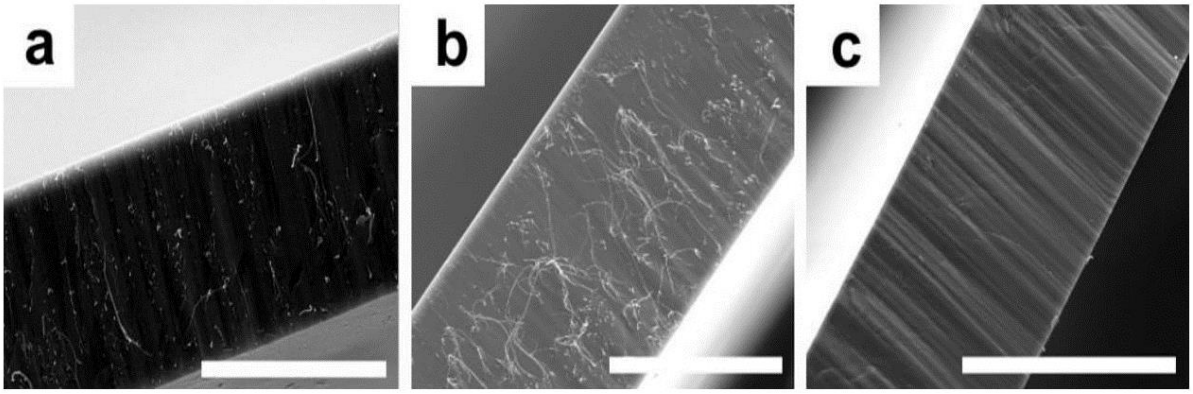

Fig. S2 Cross sectional SEM images of different lengths of CNTs-NAAMs. (a) 30 µm (scale bar = 30 µm), (b) 60 µm (scale bar = 50 µm) and (c) 90 µm (scale bar = 100 µm).

Table S1: Summary of fabrication protocols for preparation of CNTs-NAAMs with different nanotubes lengths and inner pore diameters.

Pore diameter / Length	47 nm / 60 µm	41 nm / 60 µm	31 nm / 60 µm
CVD deposition time	15 min	30 min	45 min
Pore length / Diameter	30 µm / 47 nm	60 µm / 47 nm	90 µm / 47 nm
NAAMs anodization time	9 h	19 h	28 h

S3. Chemical analysis of oxidised CNTs-NAAMs by Raman spectroscopy

Raman spectra of CNTs-NAAMs after treatment with H_2O_2 (**Fig. S3a**) and with H_2O_2 and plasma (**Fig. S3b**) show no shift in the position of G and D band peaks, however, slight increasing in the D band peak was observed after oxidation treatments.

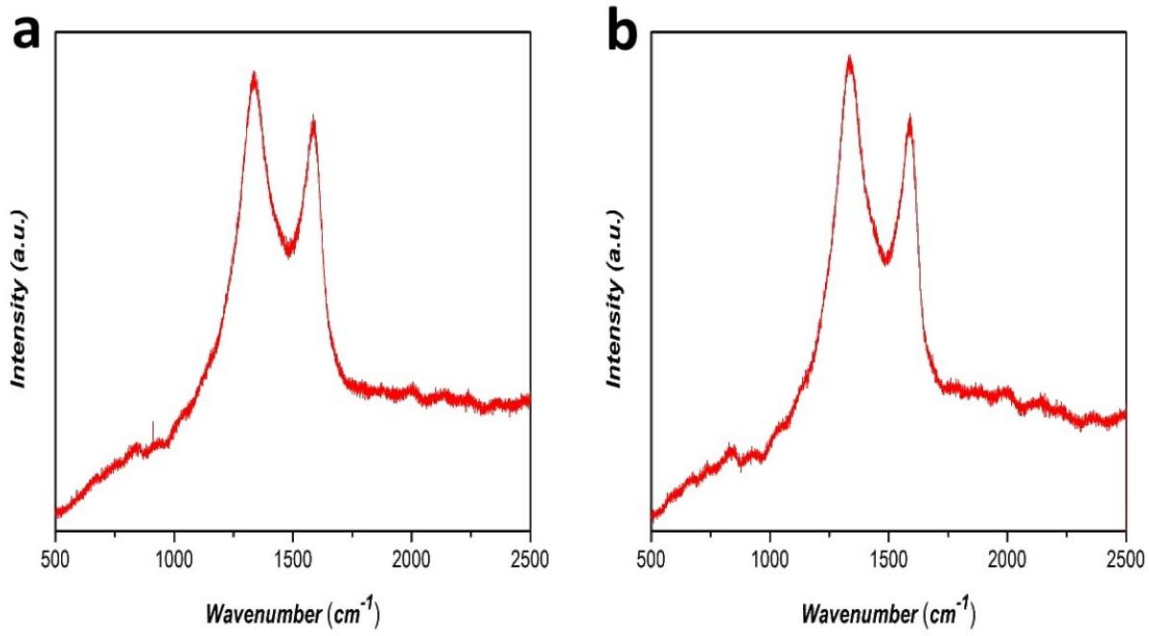

Fig. S3 Raman spectrum of CNTs-NAAMs treated with H_2O_2 (a) and treated with H_2O_2 and plasma (b).

S4. Fick's diffusion law for molecular transport across CNTs membranes

In simple terms, the diffusion through nanopores/tubes can be modelled using Fick's first law of diffusion, which is represented as:

$$J = -D\frac{dC}{dx} \quad (1)$$

Where, J is diffusion flux, D is the diffusion coefficient, dC is the change in concentration across a distance dx in one dimension (i.e. concentration gradient). According to equation (1), if the concentration on end is kept fixed and the path length is increased (which will decrease the concentration gradient) the diffusion flux will decrease. Similarly, on case of transport across our CNTs membranes, the concentration in the feed cell was kept constant in respect to the permeate cell (i.e. dC was fixed) and on increasing the thickness of the CNTs membrane the effective path length is increased (i.e. dx increased), which means a net decrease in concentration gradient across the membrane. This decrease in concentration gradient leads to slower diffusion flux.

CHAPTER 4

Carbon Nanotubes-Nanoporous Anodic Alumina Composite Membranes: Influence of Template on Structural, Chemical and Transport Properties

Mohammed Obid Alsawat

School of Chemical Engineering, The University of Adelaide, South Australia 5005, Australia

This chapter is based on the following peer-reviewed article:

Alsawat, M. Altalhi, T. Santos, A. and Losic, D. Carbon Nanotubes-Nanoporous Anodic Alumina Composite Membranes: Influence of Template on Structural, Chemical and Transport Properties. *ACS Applied Materials & Interfaces,* 2016. **(Submitted)**

Statement of Authorship

Title of Paper	Carbon Nanotubes-Nanoporous Anodic Alumina Composite Membranes: Influence of Template on Structural, Chemical and Transport Properties
Publication Status	☐ Published ☐ Accepted for Publication ☑ Submitted for Publication ☐ Unpublished and Unsubmitted w ork w ritten in manuscript style
Publication Details	Alsawat, M. Altalhi, T. Santos, A. and Losic, D. Carbon Nanotubes-Nanoporous Anodic Alumina Composite Membranes: Influence of Template on Structural, Chemical and Transport Properties. *ACS Applied Materials & Interfaces*, 2016.

Principal Author

Name of Principal Author (Candidate)	Mohammed Alsawat		
Contribution to the Paper	Under supervision of D. Losic and A. Santos, I developed, designed, and performed the experiments, interpreted and processed the data and wrote the manuscript for submission.		
Overall percentage (%)	80		
Certification:	This paper reports on original research I conducted during the period of my Higher Degree by Research candidature and is not subject to any obligations or contractual agreements with a third party that would constrain its inclusion in this thesis. I am the primary author of this paper.		
Signature		Date	30 May 2016

Co-Author Contributions

By signing the Statement of Authorship, each author certifies that:

i. the candidate's stated contribution to the publication is accurate (as detailed above);

ii. permission is granted for the candidate in include the publication in the thesis; and

iii. the sum of all co-author contributions is equal to 100% less the candidate's stated contribution.

Name of Co-Author	Tariq Altalhi		
Contribution to the Paper	I helped the candidate with providing the technical support of chemical vapour deposition (CVD) system. I give consent for Mohammed Alsawat to present this paper for examination towards the Doctorate of philosophy.		
Signature		Date	30 May 2016

Name of Co-Author	Abel Santos
Contribution to the Paper	I acted as secondary supervisor for the candidate and aided in development of the experiments and evaluation of manuscript for submission. I give consent for Mohammed Alsawat to present this paper for examination towards the Doctorate of philosophy.

Signature		Date	30 May 2016

Name of Co-Author	Dusan Losic		
Contribution to the Paper	I acted as primary supervisor for the candidate and aided in development of the experiments and evaluation of manuscript for submission. I give consent for Mohammed Alsawat to present this paper for examination towards the Doctorate of philosophy.		
Signature		Date	30 May 2016

Carbon Nanotubes-Nanoporous Anodic Alumina Composite Membranes: Influence of Template on Structural, Chemical and Transport Properties

Mohammed Alsawat[1,2], Tariq Altalhi[1,2], Abel Santos[1,3,4], and Dusan Losic*[1]*

[1] School of Chemical Engineering, The University of Adelaide, Engineering North Building, 5005 Adelaide, Australia
[2] Department of Chemistry, Faculty of Science, Taif University, Taif, Saudi Arabia
[3] Institute for Photonics and Advanced Sensing (IPAS), The University of Adelaide, 5005 Adelaide, Australia
[4] ARC Centre of Excellence for Nanoscale BioPhotonics (CNBP), The University of Adelaide, 5005 Adelaide, Australia

*E-mails: dusan.losic@adelaide.edu.au ; abel.santos@adelaide.edu.au

ABSTRACT

This work presents the synthesis of carbon nanotubes-nanoporous anodic alumina membranes (CNTs-NAAMs) composite membranes by a template-assisted catalyst-free chemical vapor deposition (CVD) approach using a mixture of toluene and ethanol as a carbon precursor. NAAMs templates were prepared by electrochemical anodization of aluminum substrates in different acid electrolytes containing sulfuric, oxalic and phosphoric acid to discern their influence on the CNTs growth. The deposition time during CVD process was modified in order to determine the formation mechanism of CNTs inside the pores of NAAMs without using metal catalysts. The structural features, chemical composition and graphitic structures of the resulting CNTs-NAAMs composites were characterized by different techniques in order to provide a comprehensive understanding of the effect of the template on the formation of these carbon-based nanostructures. CNTs-NAAMs with a range of inner pore diameters of 15-180 nm were obtained. Our results reveal that the electrolyte type used to prepare NAAMs and the deposition time during CVD process have a direct impact on the structural, chemical and graphitic structure features of CNTs-NAAMs composites. The molecular transport properties of CNTs-NAAMs composite membranes featuring different geometries and chemical compositions were evaluated via the diffusion process of Rose Bengal, dye model molecules. The obtained results show that the diffusional flux of the dye molecules was controlled by tuning the inner pore diameter of CNTs deposited inside NAAMs and the smaller the diameter of the nanotubes the faster the transport of dye molecules is. Our results provide insights into the fabrication of different CNTs composite membranes, establishing the influence of three common types of NAAMs templates on the properties of the resulting CNTs composite membranes. Our study enables the precise engineering of advanced CNTs composite membranes with controlled physical and chemical properties suitable for specific applications.

KEYWORDS: carbon nanotube, nanoporous anodic alumina membranes, electrochemical anodization, chemical vapor deposition, molecular transport

1. INTRODUCTION

For decades, carbon-based nanomaterials (e.g. carbon nanotubes, graphene, fullerene, etc.) have attracted the broad interest of the materials science community due to their extremely light nature and versatility. The properties of carbon-based nanomaterials are strongly dependent on the local bonding of the constituting carbon atoms and can be broadly modified. Therefore, nanofabrication approaches enabling the production of carbon-based nanomaterials with exquisitely controlled properties are envisaged as a means of boosting and spreading the applicability of these nanomaterials.

Among the different forms of carbon nanomaterials, carbon nanotubes (CNTs), since their discovery[1], have captured the attention of materials scientists due to their exceptional and unique transport, electrical, mechanical and thermal properties, which have spread the applicability of the different forms of CNTs across a broad range of applications and disciplines, such as solar cells, electronics, biosensing, energy storage, drug delivery, catalysis and molecular separations.[2-4] The geometric features (i.e. diameter and length) and chemical composition of CNTs are envisioned as the most determining parameters in establishing their physical and chemical properties. Therefore, to control these features of CNTs is of critical importance for advancing their properties and spreading their use towards more relevant applications. Among the different forms of CNTs, CNTs-based membranes are particularly interesting due to their potential application in water desalination, chemical separation, drug delivery, sensing and energy storage.[5-7] So far, several types of CNTs membranes have been developed and explored as advanced membranes for the above-mentioned applications.[5-8]

The formation of vertically aligned arrays of CNTs is of particular interest for achieving better performances over membranes composed of randomly distributed bundles of CNTs. Template-based synthesis approaches offer a unique route to prepare CNTs membranes with vertically aligned arrays of CNTs. Among the available templates, usually based on silicon nitride

and polymer matrices[9-10], nanoporous anodic alumina membranes (NAAMs) produced by electrochemical anodization of aluminum substrates in acid electrolytes have been demonstrated as outstanding host templates for the production of CNTs membranes due to their physical, mechanical and chemical properties.[11-15] These inorganic membranes overcome the inherent limitations of silicon nitride and polymer templates such as the dependency on the use of metal catalyst and the expensive, complex and time consuming processes. The nanopores's geometric features of NAAMs templates can be precisely engineered by means of the fabrication parameters during anodization.[16-17] Kyotani's group pioneered the use of NAAMs as host templates for the preparation CNTs membranes featuring vertically aligned cylindrical nanotubes taking advantage of a catalyst-free chemical vapor deposition (CVD) approach.[14, 18] NAAMs enable the formation of well-defined CNTs-based membranes with finely designed and engineered physical and chemical properties, which in turn makes it possible to improve and tune the performance of the resulting membranes for many applications.[19]

Furthermore, it is worthwhile noting that Kyotani's approach made it possible to overcome the limitations of traditional fabrication methods used to produce CNTs membranes by catalyst-based CVD processes using Co, Fe and Ni as metal catalysts (e.g. difficulty of controlling the geometric features of CNTs structure, incorporation of impurities into the structure of CNTs ending up with a partial or complete occlusion of the inner hollow structure of CNTs).[20-24] So far, many studies have used Kyotani's approach to produce CNTs-NAAMs composite membranes for different applications.[25-26] It is thought that the alumina template plays a critical role as a catalyst in the formation and growth of CNTs inside NAAMs templates. Nevertheless, a systematic study revealing the effect of the alumina template on the resulting properties of the CNTs produced in NAAMs is yet to come and the catalytic role of alumina in this process still remains unclear. It is generally accepted that the growth mechanism of CNTs inside NAAMs by catalyst-free CVD is divided into five stages, including i) pyrolysis of the carbon precursor in the source, ii) carbon

dissociation along the deposition zone, iii) transfer of carbon atoms from the source to the NAAM template, iv) carbon nucleation and deposition onto the inner surface of NAAM and v) formation of multi-walled CNTs. Note that NAAMs produced by electrochemical oxidation of aluminum substrates using different acid electrolyte solutions feature different chemical composition. The chemical structure of NAAMs presents an onion-like structure composed of two layers, with an outer layer close to the central pore composed of aluminium oxide (Al_2O_3) contaminated with impurities, which are incorporated into the NAA structure from the acid electrolyte during the anodization process and an inner layer far from the central nanopore, which is basically composed of pure Al_2O_3.[27-30] To discern the catalytic effect of the NAAMs in the formation of CNTs could open up new opportunities to develop CNTs with advanced chemical and physical properties, which is of critical importance for spreading the applicability of this unique carbon-based nanomaterial across different applications. Recently, we demonstrated that the transport and selectivity properties of composite membranes based on CNTs and NAAMs produced using oxalic acid electrolyte solution, can be finely tuned by engineering the dimensional features of CNTs and the surface chemistry of their inner surface by post-oxidation treatment.[19]

In this study, we discern the effect of the NAAM templates on the physical and chemical properties of CNTs grown inside NAAMs produced with different acid electrolytes by template-assisted catalyst-free CVD approach (**Figure 1**). For the first time, this study aims at: (i) demonstrating the fabrication of CNTs composite membranes with controllable dimensions (pore diameters and length) using different types of NAAMs templates, (ii) exploring the influence of the type of NAAMs templates on the structural and chemical properties of the resulting CNTs, (iii) explaining the formation mechanism of CNTs inside NAAMs of distinct chemical composition, and (iv) analyzing the effect of the NAAM template on the transport properties of the resulting composite membranes. Our study provides new insights into the fabrication of different CNTs composite membranes, establishing the influence of three common types of NAAMs templates on

the properties of the resulting CNTs composite membranes, which is of critical importance for designing CNTs-NAAMs composite membrane with precisely engineered properties for advanced applications.

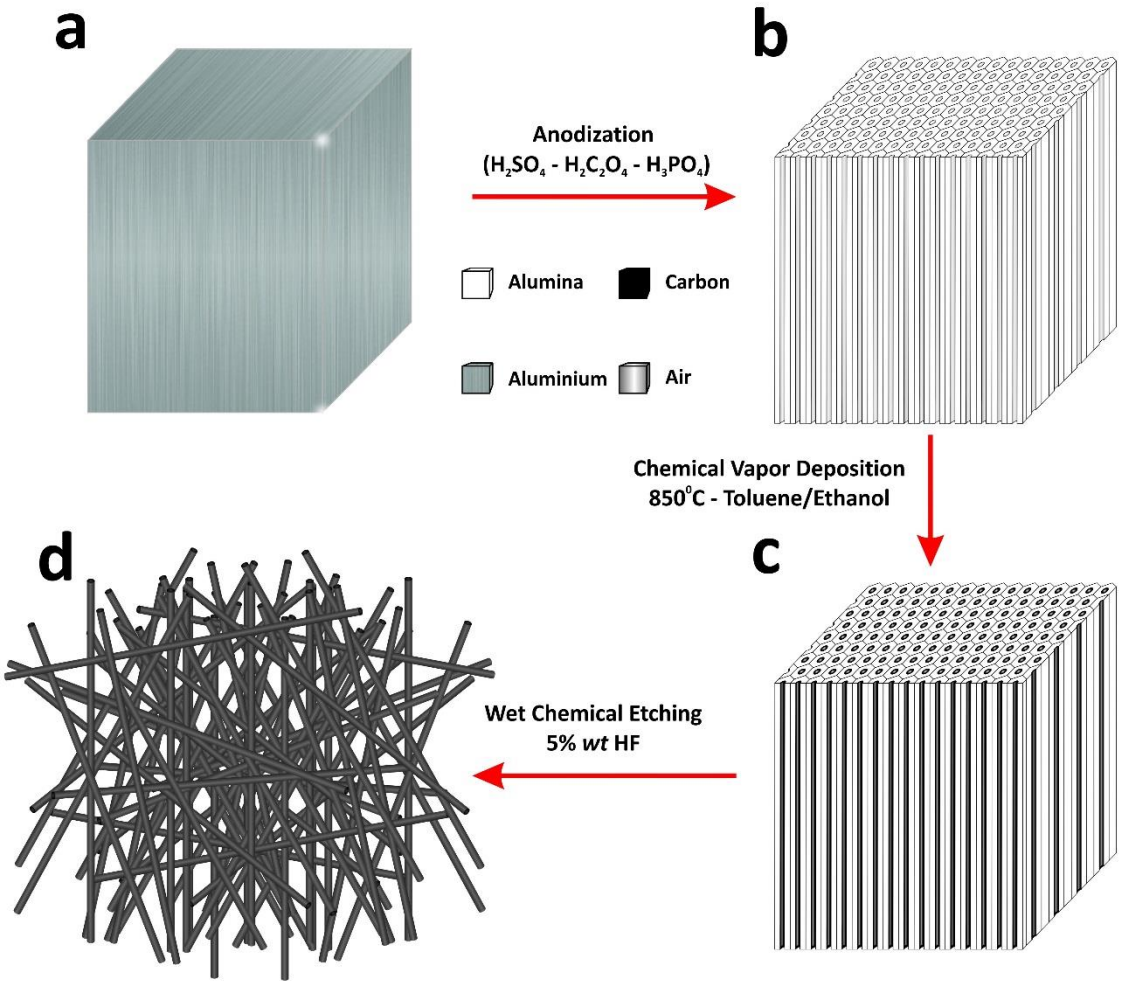

Figure 1. Schematic representation of the fabrication process of CNTs-NAAMs composite and CNTs. (a) Al foil used as substrate to prepare NAAMs; (b) NAAMs prepared by electrochemical anodization using different electrolyte solutions; (c) prepared CNTs-NAAMs composite with CNTs embedded in NAAMs after the CVD process; and (d) liberated CNTs after dissolution of NAAMs by wet chemical etching (this step is performed to characterize the CNTs structures).

2. EXPERIMENTAL SECTION

2.1. Materials

High purity aluminum (Al) foils (thickness 0.32 mm and purity 99.999%) were obtained from Goodfellow Cambridge Ltd, UK. Sulphuric acid (H_2SO_4), oxalic acid ($H_2C_2O_4$), phosphoric acid (H_3PO_4), chromium trioxide (CrO_3), copper chloride ($CuCl_2$), hydrochloric acid (HCl), ethanol 99.7% (C_2H_6O), toluene 99.8% (C_7H_8), hydrofluoric acid (HF) and Rose Bengal ($C_{20}H_4Cl_4I_4O_5$ – (RosB)) were purchased from Sigma Aldrich (Australia) and used as received. High purity deionized (DI) water (resistivity 18.2 M Ω cm) from a Milli-Q water purification system was used to prepare all the solutions used in this study.

2.2. Fabrication of NAAMs by anodization of Al substrates in different acid electrolytes

Nanoporous anodic alumina membranes (NAAMs) with hexagonal pore arrangements were prepared by two-step electrochemical anodization of aluminum substrates in different acid electrolytes containing sulfuric, oxalic and phosphoric acid following a previously reported method.[11, 31-32] Briefly, Al chips (1.5 cm in diameter) were first cleaned under sonication in ethanol and water for 10 min followed by electro-polishing in a mixture of $HClO_4$ and C_2H_6O 1:4 (*v:v*) at 20 V for 3 min and then dried under a nitrogen stream. The electro-polished Al substrates were anodized in different acid electrolytes (i.e. 0.3 M H_2SO_4, 0.3 M $H_2C_2O_4$ and 0.1 M H_3PO_4) in a two-electrode electrochemical reactor equipped with temperature controller. The corresponding anodization voltages, acid electrolyte concentrations and temperatures used to produce the different types of NAAMs used in our study are shown in **Table 1**. The first anodization step was performed for 20 h and the resulting oxide layer was selectively removed in a mixture of H_3PO_4 (0.4 M) and H_2CrO_7 (0.2 M) at 70 °C for 3 h in order to patter the surface of aluminum with hexagonally organized pits. The second anodization step was carried out for 10, 19 and 19 h for NAAMs prepared with H_2SO_4 (denoted by NAAMs-Su), $H_2C_2O_4$ (denoted by NAAMs-Ox) and

H_3PO_4 (denoted by NAAMs-Ph), respectively to specifically obtain NAAMs with pore lengths of 60 ± 2 µm, and different pore diameters (**Table 1**). After anodization, the remaining aluminum substrate was removed in a saturated solution of HCl and $CuCl_2$ followed by chemical opening of the oxide barrier layer at the bottom tips of nanopores in 5 *wt* % H_3PO_4 at 35 °C under current control to have a precise control over the pore opening and avoid undesired pore widening.[33-34]

2.3. Fabrication of CNTs-NAAMs composite membranes

CNTs were fabricated using a catalyst-free CVD approach previously described.[15, 19] Briefly, vertically aligned multi-walled CNTs (MWCNTs) were grown inside NAAMs by CVD process using a mixture of toluene and ethanol 1:1 (*v:v*) as a carbon precursor (**Figure 1**). This process was carried out in a CVD system consisting of a two-stage furnace equipped with a cylindrical quartz tube (Brother Furnace Co., LTD, China). The electrochemically prepared NAAMs were sandwiched between two quartz plates and placed in the deposition zone of the CVD reactor. The reactor temperature was increased up to 850 °C at a rate of 4 °C min^{-1} under argon (Ar) flow, which was used as a carrier inert gas at flow rate of 1 dm^3 min^{-1}. Next, the mixture of toluene and ethanol was introduced into the CVD reactor by a particle generator (i.e. nebulizer). Note that NAAMs prepared in different acid solutions were placed in the CVD reactor at the same time in order to obtain more comparable results. Different deposition times of 30, 90 and 180 min were performed in order to investigate the formation mechanism of CNTs inside NAAMs templates. For this purpose, we used NAAMs-Su featuring nanopore's diameter of 25 ± 5 nm and length of 60 ± 2 µm.

2.4. Structural and chemical composition characterizations

The structural characterization of the different CNTs-NAAMs composites and liberated CNTs was performed using a field emission gun scanning electron microscope (FEG-SEM, Quanta 450).

Transmission electron microscopy (Philips CM 200 TEM) was used to assess the internal structure of CNTs. NAAMs were selectively dissolved in a 5 wt % HF solution to obtain liberated CNTs, which were thoroughly washed with deionized water and ethanol prior to analysis. A drop of the solution containing liberated CNTs was placed on a TEM copper grid and dried before characterization. The chemical composition of the different CNTs-NAAMs composites and liberated CNTs was analyzed by X-ray photoelectron spectroscopy (XPS Kratos Axis Ultra) using the Al Kα (1486.7 eV) monochromatic line. Raman spectroscopy (Horiba LabRAM HR Evolution Raman microprobe spectrometer) was used to characterize the graphitic structure of the prepared CNTs-NAAMs composites and CNTs. Raman spectra were obtained using a He–Ne laser of 532 nm as an excitation source.

2.5. Molecular transport assessment

The transport properties of the different CNTs-NAAMs composites were assessed by analyzing the diffusion of hydrophilic dye molecule (Rose Bengal, (RosB)) through the CNTs grown in these membranes. The transport experiments were carried out in a H-tube permeation cell (consist of feed and permeate cells), in which 3 mL of 10 mM of RosB solution was added to the feed cell and the same level of water was added to the permeate cell. CNTs-NAAMs were placed between the feed and permeate cells with an exposed area of 0.0314 cm^2. The diffusion of dye molecules was continuously monitored in real-time by measuring the absorbance in the permeate cell using a UV–Visible fiber optic spectrophotometer (USB4000 Ocean Optics). Note that the concentration of RosB was detected at its maximum absorbance (i.e. λ_{abs} = 552 nm), and subsequently fitted to a calibration curve obtained by measuring absorbance of known concentrations. All transport experiments were repeated three times and statistically treated.

3. RESULTS AND DISCUSSION

3.1. Structural and chemical characterization of NAAMs template

Figure 2 displays a set of SEM images of NAAMs produced through two-step electrochemical anodization process of aluminum substrates in different acid electrolytes. **Figures 2a, 2d and 2g** show representative top view SEM images of the structure of NAAM-Su, NAAM-Ox and NAAM-Ph, respectively. These images reveal that all the NAAMs produced in this study feature a hexagonal arrangement of nanopores with diameter of 25 ± 5 nm, 40 ± 5 nm and 150 ± 5 nm, respectively, due to the self-organization conditions used during the fabrication process. A bottom view SEM images of NAAMs are shown in **Figures 2b, 2e and 2h** confirming that the pore bottom tips are opened after pore opening process, producing membranes featuring a through-hole nanoporous structure. The pore length of the different types of NAAMs used in this study was set to 60 ± 2 μm (**Figures 2c, 2f and 2i**). Note that a precise control over the pore dimensions of NAAMs can be attained by controlling the anodization conditions (i.e. anodization voltage and time and pore widening treatment). To gain insight into the structural changes occurring in the different NAAMs templates after the CVD process, NAAM-Su, NAAM-Ox and NAAM-Ph were annealed under the same temperature and ambient conditions used in the CVD process in order to mimic the conditions applied during CNTs fabrication. SEM images of the top surface of annealed NAAMs are displayed in **Figure S1 – Supporting Information**. These images reveal an increment in the pore diameter of NAAMs after annealing process. The pore diameters of the annealed NAAM-Su, NAAM-Ox and NAAM-Ph were found to be 40 ± 5 nm, 60 ± 5 nm and 190 ± 5 nm, respectively. This enlargement of pore diameter is associated with the loss of water content and reorganization of alumina in the NAAMs to form a different crystallographic phase during the CVD process (i.e. performed at 850 °C).[35-36] The chemical composition of annealed NAAMs was analyzed by energy-dispersive X-ray spectroscopy (EDX). EDX spectrum for NAAMs samples displayed typical peaks for aluminum (K = 1.486 keV) and oxygen (K = 0.523 keV), together with

the presence of sulphur (K = 2.307 keV), carbon (K = 0.277 keV) and phosphorus (K = 2.013 keV) for NAAM-Su, NAAM-Ox and NAAM-Ph, respectively **(Figure S1 – Supporting Information)**. The structural and chemical characteristics of the typical NAAMs produced by the two-step anodization process in different acid electrolytes are summarized in **Table 1**. This result demonstrates the different chemical nature of these templates, which is a result of the acid electrolyte used during the anodization process.

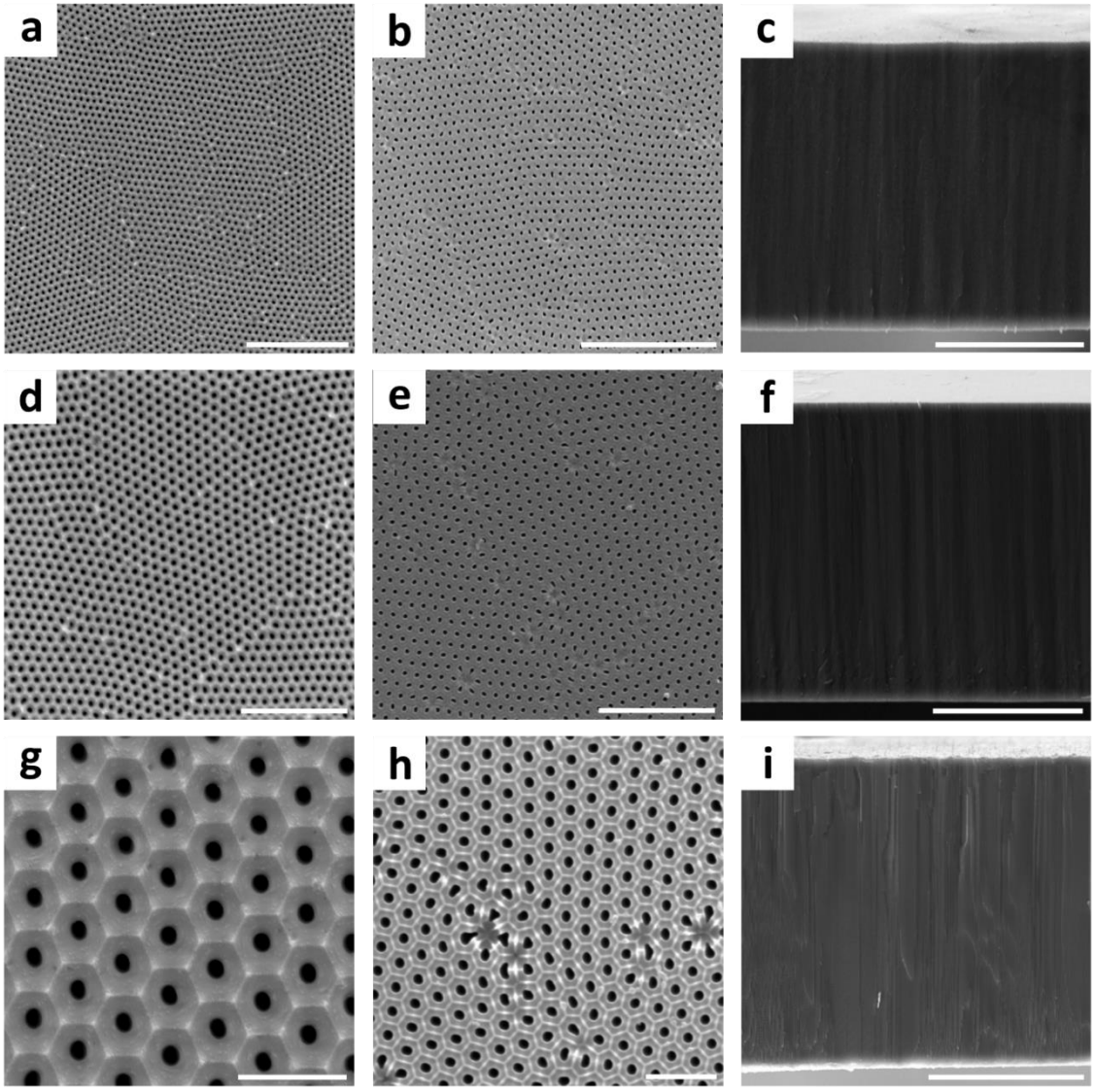

Figure 2. Set of comparative SEM images of NAAMs templates prepared in different electrolyte solutions. (a) Top view SEM image of NAAM-Su (scale bar = 1 μm); (b) its bottom view (scale bar = 1 μm); (c) its cross section (scale bar = 30 μm); (d) top view of NAAM-Ox (scale bar = 1 μm); (e) its bottom view (scale bar = 1 μm); (f) its cross section (scale bar = 30 μm); (g) top view of NAAM-Ph (scale bar = 1 μm); (h) its bottom view (scale bar = 1 μm) and (i) its cross section (scale bar = 30 μm).

Table 1. Anodization conditions for fabricating the different types of NAAMs and the structural and chemical characteristics of the resulting NAAMs.

Acid Type	Concentration (M)	Voltage (V)	Temperature (°C)	Pore Diameter (nm)	Pore Length (μm)	EDX Weight Percentage (%)				
						Al	O	S	C	P
H_2SO_4	0.3	25	5 ± 1	25 ± 5	60 ± 2	56.6	38.2	5.2	–	–
$H_2C_2O_4$	0.3	40	5 ± 1	40 ± 5	60 ± 2	65.6	33.3	–	1.1	–
H_3PO_4	0.1	195	2 ± 1	150 ± 5	60 ± 2	57.4	37.3	–	–	5.3

3.2. Structural and chemical characterization of CNTs-NAAMs composite and liberated CNTs

Figure 3 displays a set of SEM and TEM images of the CNTs-NAAMs composites and CNTs (i.e. liberated tubes). **Figures 3a, 3d and 3g** show representative top view SEM images of the CNTs grown inside the nanopores of NAAM-Su, NAAM-Ox and NAAM-Ph, respectively, by catalyst-free CVD process for 30 min of deposition using a mixture of toluene and ethanol as a carbon source. These images reveal that the CNTs were embedded inside the different NAAMs templates, replicating with precision the geometric features of the template. The length of CNTs-NAAMs was controlled *via* the anodization time of NAAMs (i.e. 2nd anodization step) and set to 60 ± 2 μm **(Figure S2 – Supporting Information)**. However, it is worthwhile to stress that there is a broad flexibility to prepare CNTs-NAAMs composite with different lengths using NAAMs featuring different nanopore lengths. CNTs were liberated by selective dissolution of the NAAMs templates **(Figure S3 – Supporting Information)** and collected for characterization by high resolution TEM images to determine their diameters (**Figures 3b, 3e and 3h**). It was found that CNTs grown inside NAAM-Su, NAAM-Ox and NAAM-Ph featured an average inner nanotube diameter of 32 ± 5

nm, 50 ± 5 nm and 180 ± 5 nm, respectively. The corresponding CNTs wall thickness were found to be 4 ± 2 nm, 5 ± 2 nm and 5 ± 2 nm, respectively. These results also reveal that the resulting composite membranes and CNTs obtained from different NAAMs have clean surface and uniform and hollow cylindrical structure, which are not attainable by other CVD synthesis approaches, in which amorphous carbon is created on the membrane surface and bamboo-like structures and metal catalyst nanoparticles residue are observed.[23, 25, 37] Such geometric and morphological defects will prevent the applicability of these membranes in a broad range of applications. In particular, applications in which their processes rely on the structural and chemical properties of the membranes (e.g. water desalination, chemical separation, drug delivery, electrodes, catalysts, etc.). A selected area electron diffraction (SAED) analysis was conducted to gain a deeper insight into the graphitic structure of the CNTs grown inside different NAAMs. The SAED pattern of CNTs grown inside the nanopores of NAAM-Su, NAAM-Ox and NAAM-Ph are presented in **Figures 3c, 3f and 3i**, respectively, revealing low graphitic features of these CNTs as a result of the absence of the metal catalyst, which is in good agreement with previous reports.[38] CNTs grown inside NAAM-Ox exhibited slightly better graphitic structure than that of others, as indicated by the presence of small arcs corresponds to the 002 diffraction, which denote some orientation of the 002 planes in the CNTs. To gain insight into the quantitative and qualitative elemental composition and surface chemistry of the inner and outer surfaces of CNTs grown inside nanopores of different NAAMs, the different CNTs-NAAMs composite membranes and liberated tubes were analyzed by XPS. The XPS survey spectra of the different CNTs-NAAMs composite membranes (shown as insets in **Figure 4**) show the presence of C, O and Al in the chemical structure of these composite membranes. The exclusive presence of these elements provides an idea about both the elemental composition and the high level of purity of these membranes produced by our catalyst-free CVD process. Here, we analyzed the C 1s spectra of the different composite membranes and liberated tubes in order to discern the chemical composition of the inner and outer surfaces of CNTs

structures. **Figures 4a, 4c and 4e** show the high resolution C 1s spectra of CNTs-NAAM-Su, CNTs-NAAM-Ox and CNTs-NAAM-Ph composite membranes, respectively. These spectra are deconvoluted into five peaks that are located at binding energies of 284.6 ± 0.2 eV, 285.7 ± 0.3 eV, 287.6 ± 0.2 eV, 289.6 ± 0.2 eV and 291.6 ± 0.3 eV, which are associated with sp^2 bonds of graphitic carbon, sp^3 network of carbon atoms, C=O (ketone/aldehyde), O=C–O (carboxyl/ester) groups, and π-π^* transition of carbon atoms, respectively.[39-40] CNTs-NAAM-Su and CNTs-NAAM-Ox showed almost the same hydrophobic surface chemistry **(Table 2)**. In contrast, CNTs-NAAM-Ph showed more hydrophilic surface chemistry, as indicated by the decline in the sp^2 carbon peak (284.6 eV) and the increase of the sp^3 hybridized structure (285.7 eV) **(Table 2)**. The intensity of the peaks in C 1s and the elemental composition of the different CNTs-NAAMs composite membranes are summarized in **Table 2.** The high resolution C 1s spectra of liberated CNTs obtained by selective dissolution of the NAAM-Su, NAAM-Ox and NAAM-Ph are presented in **Figure S4 – Supporting Information**. These spectra show almost the same chemical composition as that of the corresponding CNTs-NAAMs composites, which is indicated by the same peaks positions (i.e. 284.6 ± 0.3 eV, 285.7 ± 0.2 eV, 287.6 ± 0.2 eV, 289.6 ± 0.2 eV and 291.6 ± 0.2 eV). The intensity of the peaks in C 1s and the elemental composition of liberated CNTs are summarized in **Table S1**.

To further investigate the graphitic features of CNTs prepared by catalyst-free CVD approach inside different NAAMs templates, Raman spectroscopy analysis was conducted. **Figures 4b, 4d and 4f** present the Raman spectra of CNTs-NAAM-Su, CNTs-NAAM-Ox and CNTs-NAAM-Ph, respectively. All composite membranes showed the characteristic Raman profile of CNTs (i.e. partially overlapped D and G band peaks) with a G-band peak at 1585 cm^{-1}, which is attributed to graphitic or highly ordered CNTs sidewalls and a D-band peak at 1340 cm^{-1}, which is attributed to the amorphous or disordered sp^3 network of carbon atoms.[41] The broader D-band with higher relative intensity compared to that of G-band indicates the poor graphitic feature of CNTs in these

composite membranes, which is in good agreement with our TEM, SAED and XPS analyses. However, it is worth noting that catalyst-free CNTs can be graphitized by post-heat treatment at higher temperatures, if required.[42]

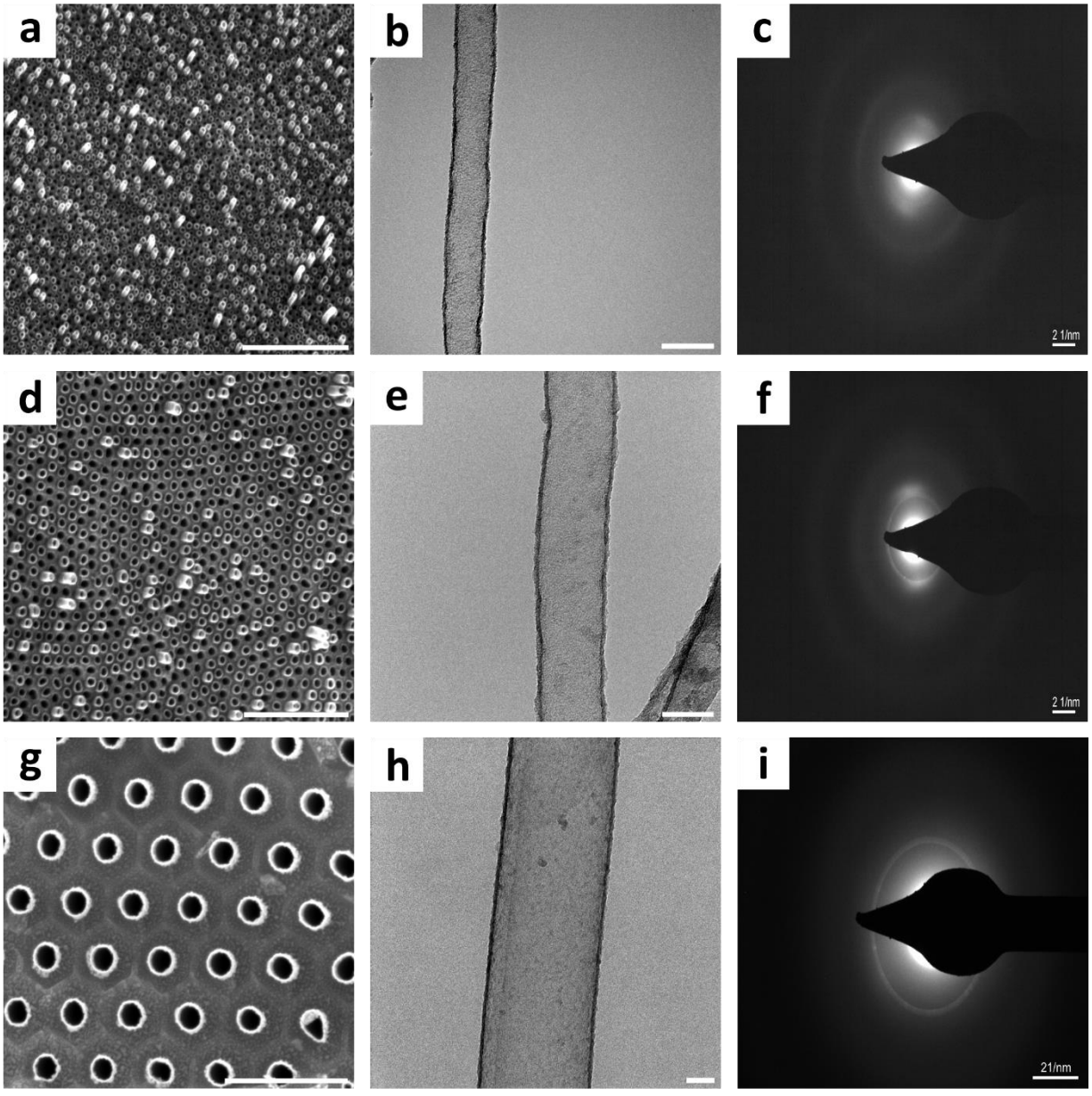

Figure 3. Set of comparative top view SEM images of prepared CNTs-NAAMs composite membranes and TEM images with SAED patterns of liberated CNTs produced through catalyst-free CVD process for 30 min using different NAAMs templates. (a, b and c) CNTs-NAAM, CNT and SAED pattern of CNT obtained from NAAM-Su (scale bar = 1 μm and 50 nm); (d, e and f) CNTs-NAAM, CNT and SAED pattern of CNT obtained from NAAM-Ox (scale bar = 1 μm and 50 nm) and (g, h and i) CNTs-NAAM, CNT and SAED pattern of CNT obtained from NAAM-Ph (scale bar = 1 μm and 50 nm).

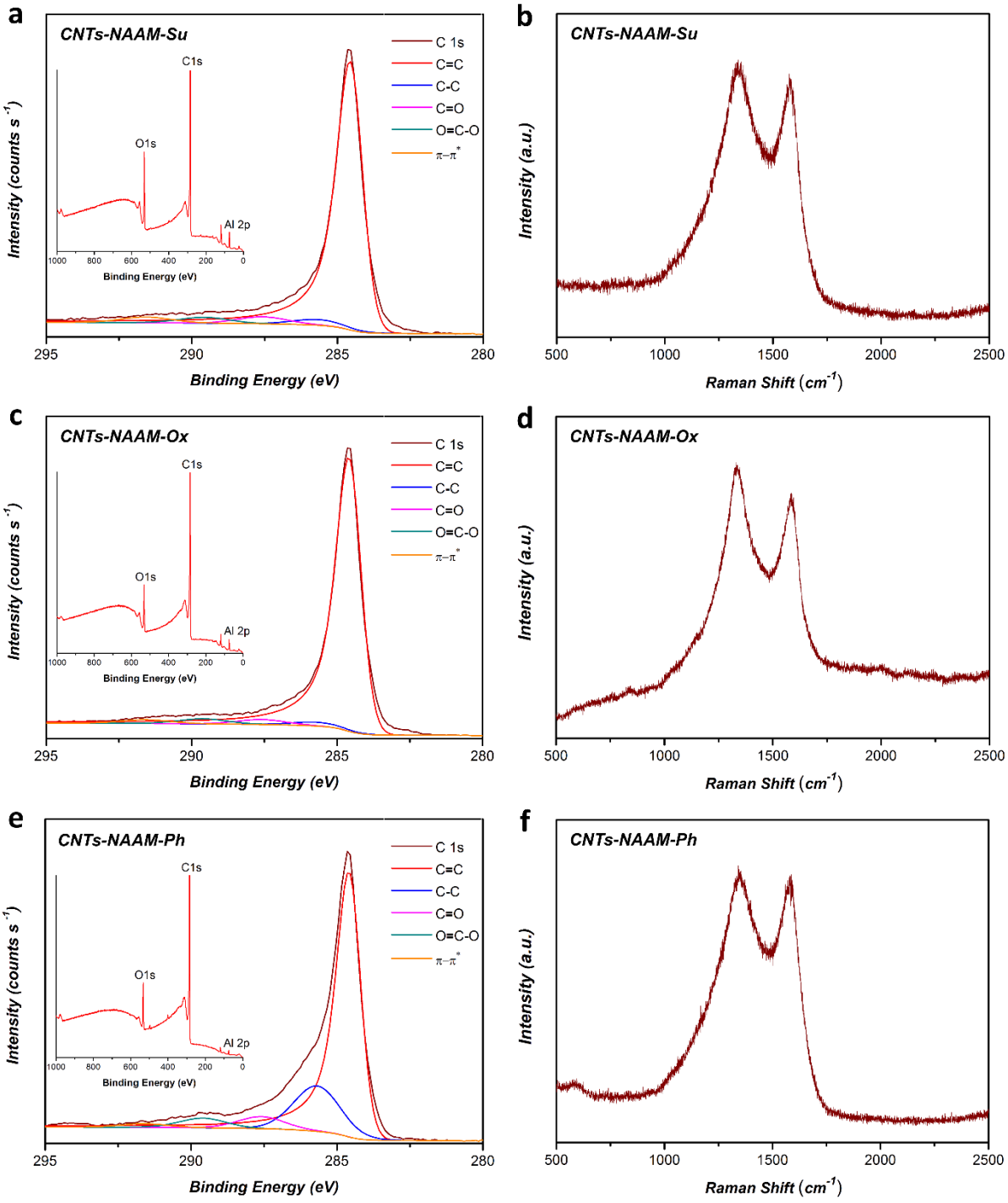

Figure 4. XPS and Raman analysis of prepared CNTs-NAAMs composite membranes produced through catalyst-free CVD process using different NAAMs templates. (a and b) XPS high resolution C 1s spectra (inset: survey spectrum) and Raman spectra of CNTs-NAAM-Su; (c and d) XPS high resolution C 1s spectra (inset: survey spectrum) and Raman spectra of CNTs-NAAM-Ox and (e and f) XPS high resolution C 1s spectra (inset: survey spectrum) and Raman spectra of CNTs-NAAM-Ph.

Table 2. Summary of elemental composition and high-resolution C 1s spectra of different CNTs-NAAMs composite membranes prepared through catalyst-free CVD process.

	Sample	**CNTs-NAAMs**	**CNTs-NAAMs**	**CNTs-NAAMs**
	Template used	NAAMs in H_2SO_4	NAAMs in $H_2C_2O_4$	NAAMs in H_3PO_4
	Peak assignment	**Intensity (%)**		
C	-	80.56	88.08	84.83
O	-	11.11	7.17	7.23
Al	-	7.30	4.51	6.81
C1s	C=C	84.64	88.50	64.98
	C–C	3.56	2.50	22.52
	C=O	4.43	3.23	5.97
	O=C–O	3.74	3.32	4.76
	π-π*	3.63	2.45	1.77

3.3. Controlling CNTs diameters and graphitic structure by CVD process

As mentioned previously, the diameter and length of CNTs were controlled by the anodization voltage and time used to produce NAAMs. Another approach that can be readily used to achieve fine control over the CNTs diameters is the deposition time during the CVD process.[19] In this study, NAAMs-Su with 25 nm pore diameters were used to reveal the catalytic role of alumina in the formation of CNTs inside NAAMs. Three deposition times (i.e. 30 min, 90 min and 180 min) were used to determine the influence of the CVD deposition time on the structural and chemical features of CNTs-NAAMs and CNTs. **Figures 3a, 5a, and 5d** show the SEM images of the top surface of CNTs-NAAMs prepared by deposition times of 30 min, 90 min and 180 min, respectively. These images reveal that the inner diameter of CNTs-NAAMs decreased significantly with the deposition time. The corresponding TEM images of liberated CNTs are

presented in **Figures 3b, 5b, and 5e**, confirming the increase in the CNTs wall thickness as a result of increasing the deposition time. The wall thickness of CNTs prepared by deposition times of 30 min, 90 min and 180 min were found to be 4 ± 2 nm, 8 ± 2 nm and 15 ± 2 nm, respectively, confirming a linear relationship with a growth rate of 0.1 nm min^{-1}. The corresponding CNTs inner diameters were found to be 32 ± 5 nm, 27 ± 5 nm and 15 ± 5 nm, respectively. It was also observed that the outer diameter of CNTs-NAAMs was slightly increased with the deposition time from 30 min to 180 min, which could be attributed to the continuous loss of water content and crystallographic structure arrangement of alumina in the NAAMs. The lowest inner pore diameter of CNTs presented in this work was 15 ± 5 nm, however, this could be extended to lower diameters to cc 5 nm by increasing the deposition time. These results are similar to those of CNTs obtained under the same experimental conditions (i.e. carbon precursor, flowing rate and temperature) using NAAMs-Ox[19], while it is different from those of CNTs obtained using TNTs as template.[43] This clearly indicates that the growth mechanism of CNTs prepared via free-catalyst CVD processes in different NAAMs is based on both the catalytic role of alumina and the hydrocarbon thermal decomposition.[25-26, 44] In this process, the catalytic role of alumina is critical at the beginning of the CVD process, in which a few layers of the carbon are deposited onto the inner walls of NAAMs. Note that, the same wall thickness of CNTs grown inside the different NAAMs (~5 nm) by fixed deposition time CVD process (i.e. 30 min) indicates that the catalytic role of alumina to grow CNTs is the same in the different NAAMs used in this study although the chemical composition of the resulting CNTs is different, as revealed by XPS analysis (**Figure 4 and Table 2**). However, the catalytic role of alumina is neutralized after the deposition of a few layers of carbon, as these block the nucleation centers for the formation of carbon. After that, the process is based on the hydrocarbon thermal decomposition and subsequent deposition of carbon, which in turn generates multiple layers of carbon as the deposition time increases. As a result, the CNTs feature a multi-walled carbon structure with concentric layers of carbon growing from the inner

surface of the nanopores to their center. It is worth noting that the growth rate of CNTs presented here using NAAMs-Su (i.e. 0.1 nm min^{-1}) is almost half of that obtained in previous studies (0.2 nm min^{-1}), where NAAMs-Ox were used as templates.[19] We infer that this phenomenon could be due to the small pore diameter of NAAMs template used in this study (i.e. 25 nm), which affects the flowing of the precursor inside the template pores and decreases the growth rate of CNTs.

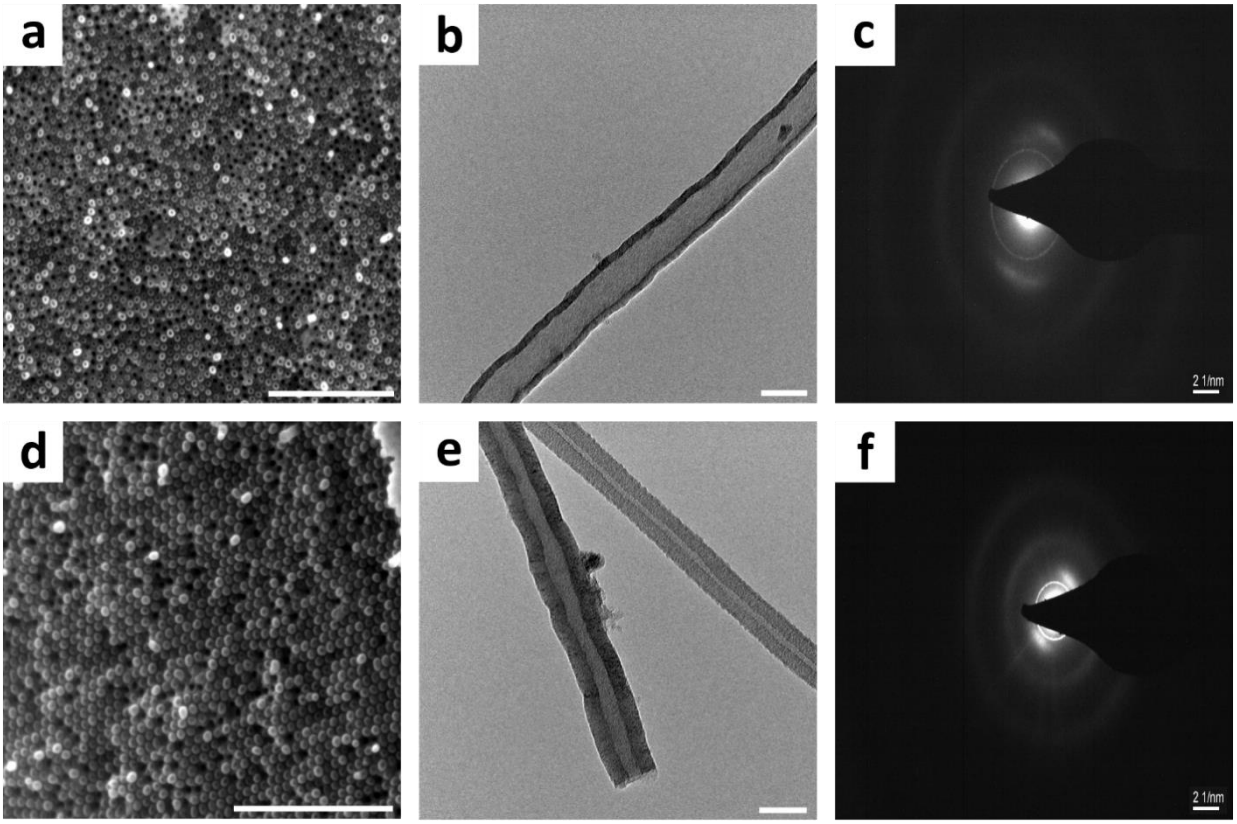

Figure 5. Set of comparative top view SEM images of prepared CNTs-NAAMs-Su composite membranes and TEM images with SAED patterns of liberated CNTs produced through different deposition time of catalyst-free CVD process. (a, b and c) CNTs-NAAM, CNT and SAED pattern of CNT prepared by deposition time of 90 min (scale bar = 1 μm and 50 nm) and (d, e and f) CNTs-NAAM, CNT and SAED pattern for CNTs prepared by deposition time of 180 min (scale bar = 1 μm and 50 nm).

Furthermore, we found that the graphitic structure of multi-layered CNTs was improved as a result of the increasing deposition time from 30 to 180 min, which is proved by selected area electron diffraction (SAED) analysis of the CNTs prepared by different deposition times **(Figures 3c, 5c,**

and 5f). As the deposition time increases, the presence of the pair of small arcs corresponding to the 002 diffraction become more pronounced, indicating an improvement of the orientation of the 002 planes in the CNTs structure. Further evidence for the aforementioned improvement could be found in the Raman spectroscopy analysis of CNTs prepared at different deposition times (i.e. 30 min, 90 min and 180 min), as shown in **Figures 6a, 6b, and 6c,** respectively. This analysis shows an increment of the G-band peak, attributed to graphitic or highly ordered CNTs sidewalls, with the deposition time. These results confirm that a precise control of CNTs diameter in CNTs-NAAMs composite can be obtained by either using NAAMs with different pore diameters prepared by different electrolyte solutions and different anodization voltages or by extending the CVD deposition time. Moreover, an increment of the CVD deposition time is shown to have a significant impact on the graphitic structure of multi-layered CNTs. Consequently, our catalyst-free CVD approach is demonstrated to be a very versatile fabrication approach to produce CNTs-NAAMs composite membranes with desired structural and chemical features, which can be precisely engineered by means of the aforementioned fabrication parameters.

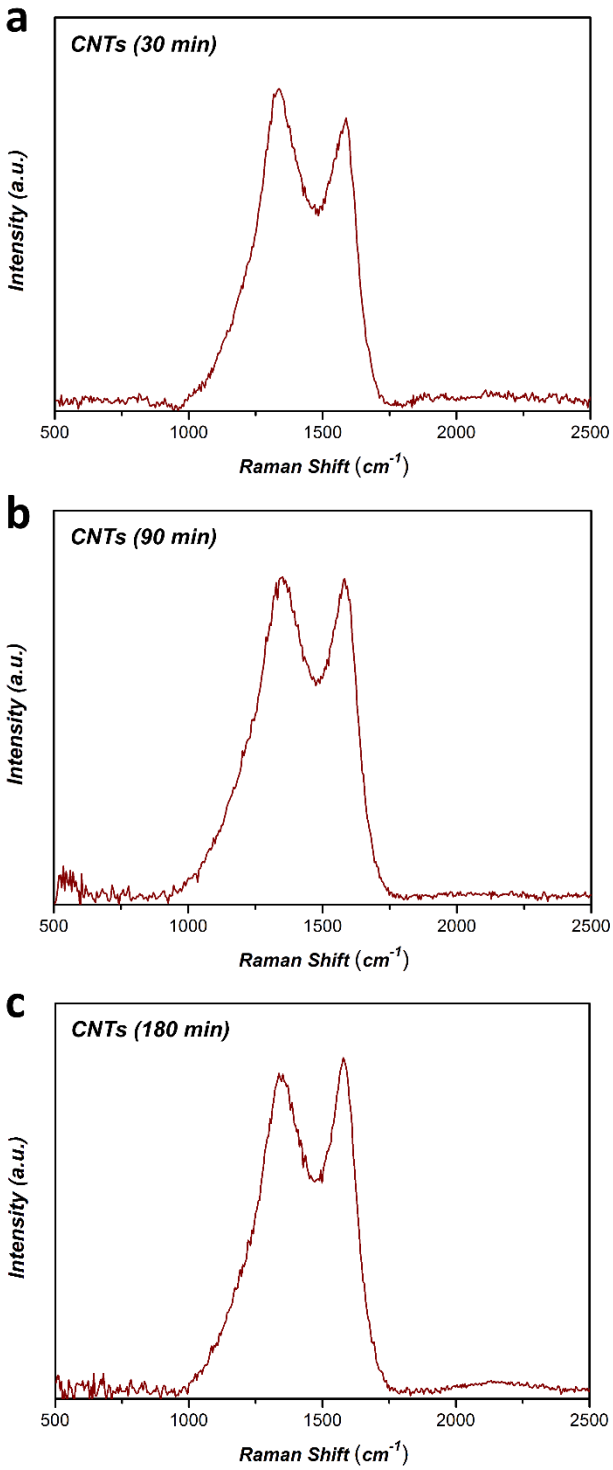

Figure 6. Raman spectra of CNTs produced through different deposition time of catalyst-free CVD process using NAAMs-Su templates. (a) Raman spectrum of CNTs prepared by deposition time of 30 min; (b) Raman spectrum of CNTs prepared by deposition time of 90 min and (c) Raman spectrum of CNTs prepared by deposition time of 180 min.

3.4. Molecular transport study of CNTs-NAAMs composite membranes

Finally, as a proof-of-concept of applicability, the transport properties of the prepared CNTs-NAAMs composites were explored by a series of permeation experiments using RosB as a model dye molecule in a H-tube permeation setup. **Figure 7a** shows representative plots of the transport of RosB across CNTs-NAAMs composite membranes prepared through our catalyst-free CVD process using different NAAMs (i.e. NAAM-Su, NAAM-Ox and NAAM-Ph). The diffusional flux of RosB molecules through these membranes was found to be 3.22 ± 0.09 nmol min^{-1} cm^{-2} for CNTs-NAAM-Su, 1.49 ± 0.13 nmol min^{-1} cm^{-2} for CNTs-NAAM-Ox, and 0.30 ± 0.06 nmol min^{-1} cm^{-2} for CNTs-NAAM-Ph. The RosB transport across the CNTs composite membranes is determined by the Fick's first law of diffusion (**Equation 1**), which is indicated by the straight line of the transport graphs displayed in **Figure 7**:

$$J = -D\frac{dC}{dx} \qquad (1)$$

where, *J* is diffusion flux, *D* is the diffusion coefficient, *dC* is the change in concentration across a distance *dx* in one dimension (i.e. concentration gradient).[45]

This result reveals that the diffusional flux rates increased by one order of magnitude (i.e. a factor of 10) for CNTs-NAAM-Su over CNTs-NAAM-Ph. The low fluxing rate of the latter composite membrane is due to their large inner pore diameter (i.e. 180 ± 5 nm, as proved by TEM result (**Figure 3h**). In contrast, the CNTs-NAAM-Su composite membrane features smaller inner pore diameter (i.e. 32 ± 5 nm), resulting in more interactions between the CNTs wall and the transported molecules. This significant result reveals that the smaller the pore diameter of CNTs in CNTs-NAAMs the faster the transport of the hydrophilic dye molecules along the nanotubes. An important aspect that distinguishes our applied synthetic method (i.e. templated-assisted catalyst-free CVD process using simple carbon precursor as toluene and ethanol) from traditional methods used to produce CNTs-based membranes is that it allows the fabrication of CNTs-NAAMs with precise structure of the pore wall and without occlusions of the inner hollow structure of the CNTs.

This results in an enhancement of the interaction between CNTs surface and the transported molecules, which is dominant at nanoscale regime. Considering that all the parameters that could play a role in the overall transport of dye molecules through CNTs-NAAMs including transported molecule's size, charge, shape, solubility and the initial concentration were kept constant, the obtained result can only be associated to the influence of the geometric features (i.e. inner pore diameter) of the composite membrane. It is worth noting that CNTs-NAAMs-Ph composite membranes have a hydrophilic character, as proved by XPS analysis (**Figure 4**), which is expected to enhance the transport of the hydrophilic dye molecules. However, the obtained results confirm that the geometric features of the membrane is the most determining parameter in establishing the performance of the resulting membranes. Motivated by these results and in order to further verify this hypothesis, we analyzed the transport of RosB molecules through CNTs-NAAMs featuring lower inner diameters of 27 and 15 nm, which were prepared by CVD deposition times of 90 and 180 min, respectively (**Figure 7b**). To decrease the inner pore diameter of CNTs-NAAMs led to a significant increment of the diffusional flux of RosB molecules. The diffusional flux through CNTs membrane with an inner diameter of 15 nm was found to be 8.80 ± 0.12 nmol min^{-1} cm^{-2}, which is two fold higher than that obtained through CNTs membrane with an inner diameter of 32 nm and three order of magnitude higher than that obtained through CNTs-NAAM-Ph with an inner diameter of 180 nm. This result reveals that to reduce the inner pore diameter of CNTs by CVD process (i.e. deposition time) is an effective way of increasing the number of interactions between transported molecules and the inner wall of CNTs in order to enhance the overall transport performance through these membranes.

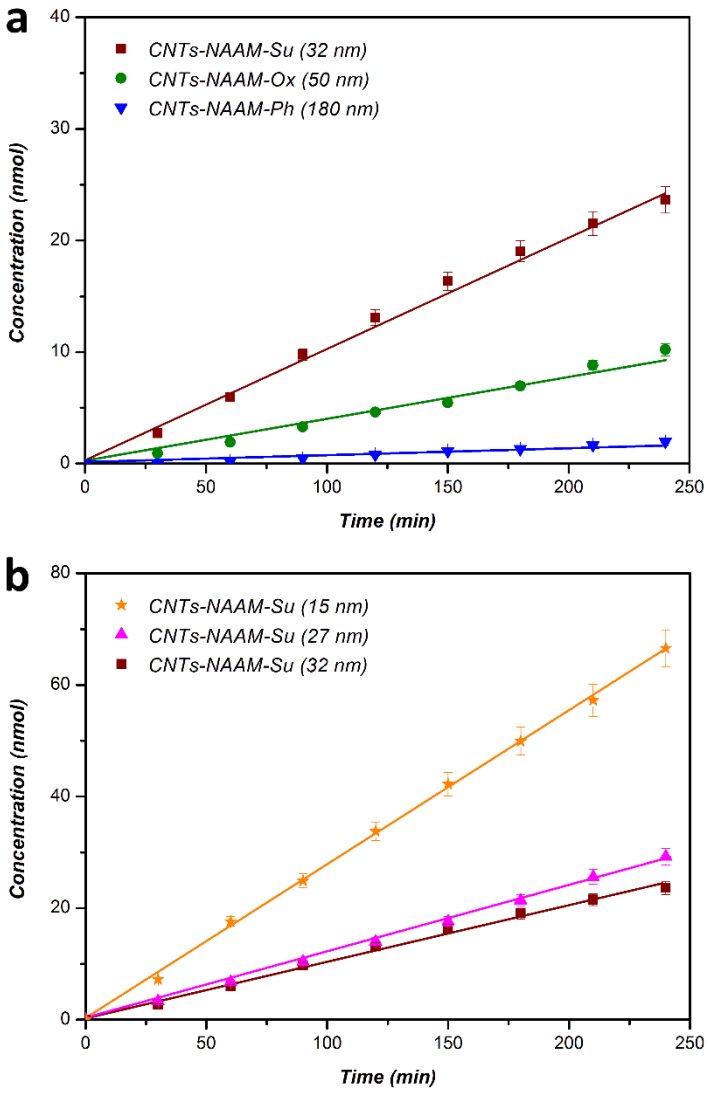

Figure 7. Molecular transport study of RosB through different CNTs-NAAMs composite membranes prepared through catalyst-free CVD process using different NAAMs templates and different deposition times. (a) Diffusion of RosB through CNTs-NAAM-Su, CNTs-NAAM-Ox and CNTs-NAAM-Ph featuring various inner pore diameters of 32, 50 and 180 nm, respectively and (b) diffusion of RosB through CNTs-NAAM-Su prepared by different deposition times featuring various inner pore diameters of 32, 27 and 15 nm.

4. CONCLUSION

To summarize, in this study we have demonstrated the fabrication of CNTs composite membranes based on NAAMs prepared using different electrolyte solution by means of a catalyst-free CVD approach, where a mixture of toluene and ethanol is used as a carbon source. The presented results

show that the structural and chemical features of the resulting CNTs-NAAMs composite membranes are influenced by the type of NAAMs used as a template. The deposition time during CVD process has been demonstrated as an effective means of controlling the inner diameter of CNTs-NAAMs, which also has a significant impact on the graphitic structure of the resulting multi-layered CNTs. XPS analysis confirmed the hydrophilic nature of CNTs-NAAMs-Ph composite membranes, over the hydrophobic character of CNTs-NAAMs-Su and CNTs-NAAMs-Ox composite membranes. The catalytic role of NAAMs in the formation of CNTs inside these nanoporous templates has been discerned and our results establish that this is directly related with the chemical composition of the host template. Furthermore, as a proof-of-concept, we have studied the influence of the geometry and chemical composition of the resulting CNTs-NAAMs composites on the transport performance for the diffusion of RosB molecules. The obtained results have demonstrated that a significant enhancement in the transport performance of the CNTs-NAAMs composite membranes can be achieved by tuning the inner diameter of the nanotubes. Our study provides new insights and understanding about how to design CNTs-NAAMs composite membranes with precisely engineered structural and chemical properties for advancing their performances in different applications.

Acknowledgements

Authors acknowledge the financial support provided by the Australian Research Council (FT 110100711 and DE140100549). The authors also acknowledge the facilities and the scientific and technical assistance of the Australian Microscopy & Microanalysis Research Facility at the Electron Microscope Unit, The University of Adelaide. Mohammed Alsawat thanks Taif University (Ministry of Education, Saudi Arabia) for funding his scholarship.

REFERENCES

1. Iijima, S., Helical microtubules of graphitic carbon. *Nature* **1991,** *354* (6348), 56-58.

2. Paradise, M.; Goswami, T., Carbon nanotubes–production and industrial applications. *Materials & Design* **2007,** *28* (5), 1477-1489.

3. Klumpp, C.; Kostarelos, K.; Prato, M.; Bianco, A., Functionalized carbon nanotubes as emerging nanovectors for the delivery of therapeutics. *Biochimica et Biophysica Acta (BBA)-Biomembranes* **2006,** *1758* (3), 404-412.

4. Holt, J. K.; Park, H. G.; Wang, Y.; Stadermann, M.; Artyukhin, A. B.; Grigoropoulos, C. P.; Noy, A.; Bakajin, O., Fast mass transport through sub-2-nanometer carbon nanotubes. *Science* **2006,** *312* (5776), 1034-1037.

5. Corry, B., Designing carbon nanotube membranes for efficient water desalination. *The Journal of Physical Chemistry B* **2008,** *112* (5), 1427-1434.

6. Majumder, M.; Stinchcomb, A.; Hinds, B. J., Towards mimicking natural protein channels with aligned carbon nanotube membranes for active drug delivery. *Life sciences* **2010,** *86* (15), 563-568.

7. Reddy, K. R.; Hassan, M.; Gomes, V. G., Hybrid nanostructures based on titanium dioxide for enhanced photocatalysis. *Applied Catalysis A: General* **2015,** *489*, 1-16.

8. Noy, A.; Park, H. G.; Fornasiero, F.; Holt, J. K.; Grigoropoulos, C. P.; Bakajin, O., Nanofluidics in carbon nanotubes. *Nano Today* **2007,** *2* (6), 22-29.

9. Hinds, B. J.; Chopra, N.; Rantell, T.; Andrews, R.; Gavalas, V.; Bachas, L. G., Aligned multiwalled carbon nanotube membranes. *Science* **2004,** *303* (5654), 62-65.

10. Holt, J. K.; Noy, A.; Huser, T.; Eaglesham, D.; Bakajin, O., Fabrication of a carbon nanotube-embedded silicon nitride membrane for studies of nanometer-scale mass transport. *Nano letters* **2004,** *4* (11), 2245-2250.

11. Masuda, H.; Fukuda, K., Ordered metal nanohole arrays made by a two-step replication of honeycomb structures of anodic alumina. *Science* **1995,** *268* (5216), 1466-1468.

12. Masuda, H.; Hasegwa, F.; Ono, S., Self-Ordering of Cell Arrangement of Anodic Porous Alumina Formed in Sulfuric Acid Solution. *Journal of the Electrochemical Society* **1997,** *144* (5), L127-L130.

13. Masuda, H.; Yada, K.; Osaka, A., Self-ordering of cell configuration of anodic porous alumina with large-size pores in phosphoric acid solution. *Japanese Journal of Applied Physics* **1998,** *37* (11A), L1340.

14. Kyotani, T.; Tsai, L.-f.; Tomita, A., Formation of ultrafine carbon tubes by using an anodic aluminum oxide film as a template. *Chemistry of Materials* **1995,** *7* (8), 1427-1428.

15. Che, G.; Lakshmi, B.; Martin, C.; Fisher, E.; Ruoff, R. S., Chemical vapor deposition based synthesis of carbon nanotubes and nanofibers using a template method. *Chemistry of Materials* **1998,** *10* (1), 260-267.

16. Lee, W.; Park, S.-J., Porous anodic aluminum oxide: anodization and templated synthesis of functional nanostructures. *Chemical Reviews* **2014,** *114* (15), 7487-7556.

17. Lee, W.; Kim, J.-C., Highly ordered porous alumina with tailor-made pore structures fabricated by pulse anodization. *Nanotechnology* **2010,** *21* (48), 485304.

18. Kyotani, T.; Tsai, L.-f.; Tomita, A., Preparation of ultrafine carbon tubes in nanochannels of an anodic aluminum oxide film. *Chemistry of Materials* **1996,** *8* (8), 2109-2113.

19. Alsawat, M.; Altalhi, T.; Kumeria, T.; Santos, A.; Losic, D., Carbon nanotube-nanoporous anodic alumina composite membranes with controllable inner diameters and surface chemistry: Influence on molecular transport and chemical selectivity. *Carbon* **2015,** *93*, 681-692.

20. Li, J.; Papadopoulos, C.; Xu, J.; Moskovits, M., Highly-ordered carbon nanotube arrays for electronics applications. *Applied Physics Letters* **1999,** *75* (3), 367-369.

21. Iwasaki, T.; Motoi, T.; Den, T., Multiwalled carbon nanotubes growth in anodic alumina nanoholes. *Applied Physics Letters* **1999,** *75* (14), 2044-2046.

22. Fan, S.; Chapline, M. G.; Franklin, N. R.; Tombler, T. W.; Cassell, A. M.; Dai, H., Self-oriented regular arrays of carbon nanotubes and their field emission properties. *Science* **1999,** *283* (5401), 512-514.

23. Morjan, R.; Nerushev, O.; Sveningsson, M.; Rohmund, F.; Falk, L.; Campbell, E., Growth of carbon nanotubes from C60. *Applied Physics A* **2004,** *78* (3), 253-261.

24. Grobert, N.; Terrones, M.; Osborne, A.; Terrones, H.; Hsu, W.; Trasobares, S.; Zhu, Y.; Hare, J.; Kroto, H.; Walton, D., Thermolysis of C60 thin films yields Ni-filled tapered nanotubes. *Applied Physics A* **1998,** *67* (5), 595-598.

25. Schneider, J. J.; Maksimova, N. I.; Engstler, J.; Joshi, R.; Schierholz, R.; Feile, R., Catalyst free growth of a carbon nanotube–alumina composite structure. *Inorganica Chimica Acta* **2008,** *361* (6), 1770-1778.

26. Sarno, M.; Tamburrano, A.; Arurault, L.; Fontorbes, S.; Pantani, R.; Datas, L.; Ciambelli, P.; Sarto, M., Electrical conductivity of carbon nanotubes grown inside a mesoporous anodic aluminium oxide membrane. *Carbon* **2013,** *55*, 10-22.

27. Yamamoto, Y.; Baba, N.; Tajima, S., Coloured materials and photoluminescence centres in anodic film on aluminium. **1981**.

28. Nielsch, K.; Choi, J.; Schwirn, K.; Wehrspohn, R. B.; Gösele, U., Self-ordering regimes of porous alumina: the 10 porosity rule. *Nano Letters* **2002,** *2* (7), 677-680.

29. Han, H.; Park, S.-J.; Jang, J. S.; Ryu, H.; Kim, K. J.; Baik, S.; Lee, W., In situ determination of the pore opening point during wet-chemical etching of the barrier layer of porous anodic aluminum oxide: nonuniform impurity distribution in anodic oxide. *ACS Applied Materials & Interfaces* **2013,** *5* (8), 3441-3448.

30. Santos, A.; Kumeria, T.; Wang, Y.; Losic, D., In situ monitored engineering of inverted nanoporous anodic alumina funnels: On the precise generation of 3D optical nanostructures. *Nanoscale* **2014,** *6* (17), 9991-9999.

31. Li, A.; Müller, F.; Birner, A.; Nielsch, K.; Gösele, U., Hexagonal pore arrays with a 50–420 nm interpore distance formed by self-organization in anodic alumina. *Journal of Applied Physics* **1998,** *84* (11), 6023-6026.

32. Jessensky, O.; Müller, F.; Gösele, U., Self-organized formation of hexagonal pore arrays in anodic alumina. *Applied Physics Letters* **1998,** *72* (10), 1173-1175.

33. Lillo, M.; Losic, D., Pore opening detection for controlled dissolution of barrier oxide layer and fabrication of nanoporous alumina with through-hole morphology. *Journal of Membrane Science* **2009,** *327* (1–2), 11-17.

34. Losic, D.; Losic Jr, D., Preparation of porous anodic alumina with periodically perforated pores. *Langmuir* **2009,** *25* (10), 5426-5431.

35. Chen, C. C.; Chen, J. H.; Chao, C. G., Post-treatment method of producing ordered array of anodic aluminum oxide using general purity commercial (99.7%) aluminum. *Japanese Journal of Applied Physics* **2005,** *44* (3R), 1529.

36. Fernández-Romero, L.; Montero-Moreno, J.; Pellicer, E.; Peiró, F.; Cornet, A.; Morante, J.; Sarret, M.; Müller, C., Assessment of the thermal stability of anodic alumina membranes at high temperatures. *Materials Chemistry and Physics* **2008,** *111* (2), 542-547.

37. Yuan, Z.-h.; Huang, H.; Liu, L.; Fan, S.-s., Controlled growth of carbon nanotubes in diameter and shape using template-synthesis method. *Chemical Physics Letters* **2001,** *345* (1), 39-43.

38. Ciambelli, P.; Arurault, L.; Sarno, M.; Fontorbes, S.; Leone, C.; Datas, L.; Sannino, D.; Lenormand, P.; Du Plouy, S. L. B., Controlled growth of CNT in mesoporous AAO through

optimized conditions for membrane preparation and CVD operation. *Nanotechnology* **2011,** *22* (26), 265613.

39. Biniak, S.; Szymański, G.; Siedlewski, J.; Światkowski, A., The characterization of activated carbons with oxygen and nitrogen surface groups. *Carbon* **1997,** *35* (12), 1799-1810.

40. Reis, M.; Do Rego, A. B.; Da Silva, J. L.; Soares, M., An XPS study of the fibre-matrix interface using sized carbon fibres as a model. *Journal of Materials Science* **1995,** *30* (1), 118-126.

41. Kim, P.; Zheng, Y.; Agnihotri, S., Adsorption equilibrium and kinetics of water vapor in carbon nanotubes and its comparison with activated carbon. *Industrial & Engineering Chemistry Research* **2008,** *47* (9), 3170-3178.

42. Mattia, D.; Rossi, M.; Kim, B.; Korneva, G.; Bau, H.; Gogotsi, Y., Effect of graphitization on the wettability and electrical conductivity of CVD-carbon nanotubes and films. *The Journal of Physical Chemistry B* **2006,** *110* (20), 9850-9855.

43. Alsawat, M.; Altalhi, T.; Gulati, K.; Santos, A.; Losic, D., Synthesis of Carbon Nanotube–Nanotubular Titania Composites by Catalyst-Free CVD Process: Insights into the Formation Mechanism and Photocatalytic Properties. *ACS Applied Materials & Interfaces* **2015,** *7* (51), 28361-28368.

44. Lee, J. S.; Gu, G. H.; Kim, H.; Jeong, K. S.; Bae, J.; Suh, J. S., Growth of carbon nanotubes on anodic aluminum oxide templates: fabrication of a tube-in-tube and linearly joined tube. *Chemistry of Materials* **2001,** *13* (7), 2387-2391.

45. Fick, A., Ueber diffusion. *Annalen der Physik* **1855,** *170* (1), 59-86.

Supporting Information

Carbon Nanotubes-Nanoporous Anodic Alumina Composite Membranes: Influence of Template on Structural, Chemical and Transport Properties

Mohammed Alsawat[1,2], Tariq Altalhi[1,2], Abel Santos[1,3,4], and Dusan Losic*[1]*

[1] School of Chemical Engineering, The University of Adelaide, Engineering North Building, 5005 Adelaide, Australia
[2] Department of Chemistry, Faculty of Science, Taif University, Taif, Saudi Arabia
[3] Institute for Photonics and Advanced Sensing (IPAS), The University of Adelaide, 5005 Adelaide, Australia
[4] ARC Centre of Excellence for Nanoscale BioPhotonics (CNBP), The University of Adelaide, 5005 Adelaide, Australia

*E-mails: *dusan.losic@adelaide.edu.au* ; *abel.santos@adelaide.edu.au*

1. Structural and chemical characterization of annealed NAAMs templates

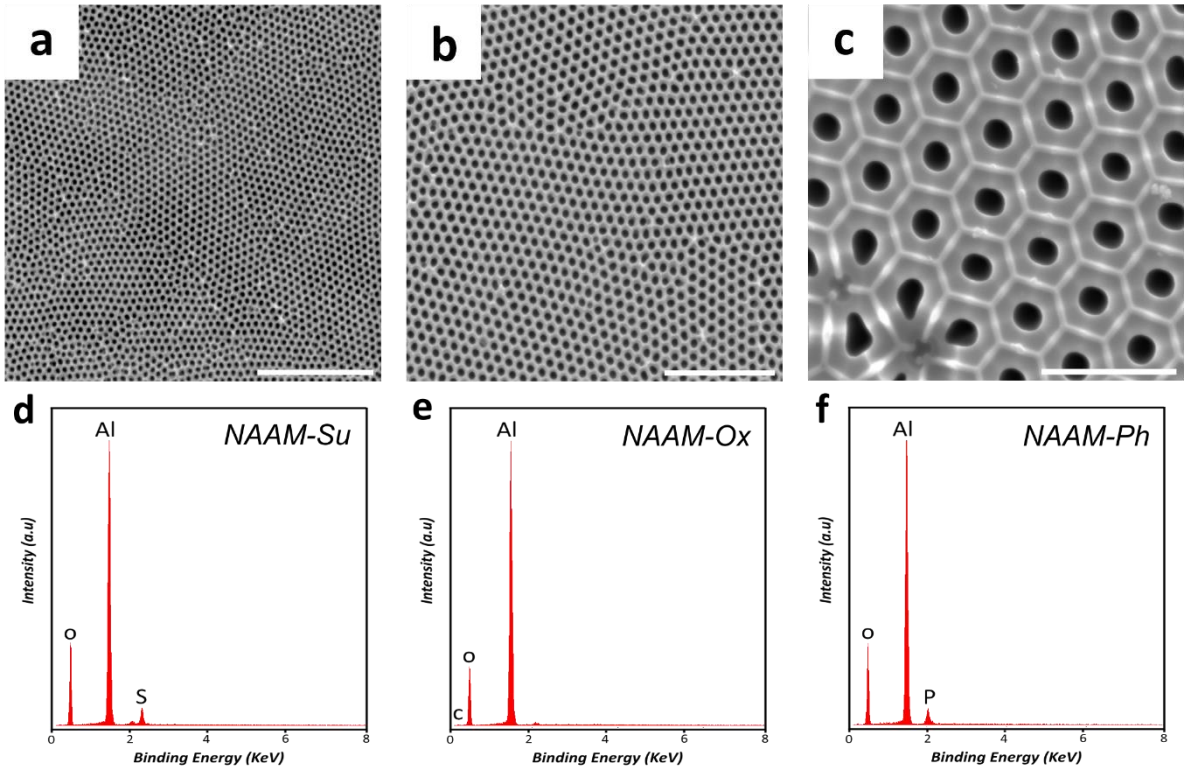

Figure S1. Top view SEM images and EDX analysis of annealed NAAMs templates prepared in different electrolyte solutions and. (a) SEM image of annealed NAAM-Su; (b) SEM image of annealed NAAM-Ox and (c) SEM image of annealed NAAM-Ph; (d) EDX spectrum of NAAM-Su; (e) EDX spectrum of NAAM-Ox; and (f) EDX spectrum of NAAM-Ph.

2. Structural and chemical characterization of CNTs-NAAMs composite and liberated CNTs

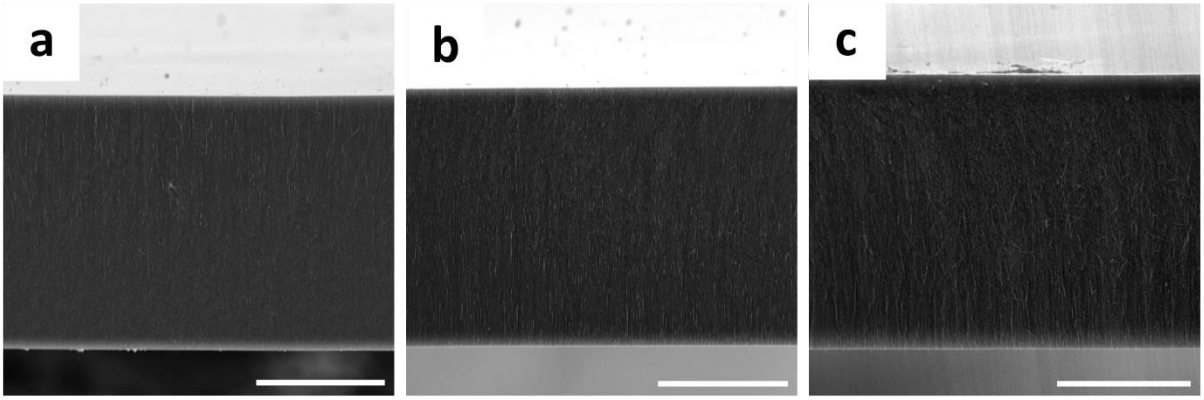

Figure S2. Cross sectional SEM images of different CNTs-NAAMs. (a) CNTs-NAAM-Su (scale bar = 30 µm), (b) CNTs-NAAM-Ox (scale bar = 30 µm) and (c) CNTs-NAAM-Ph (scale bar = 30 µm) (higher bright area is the membrane's top surface).

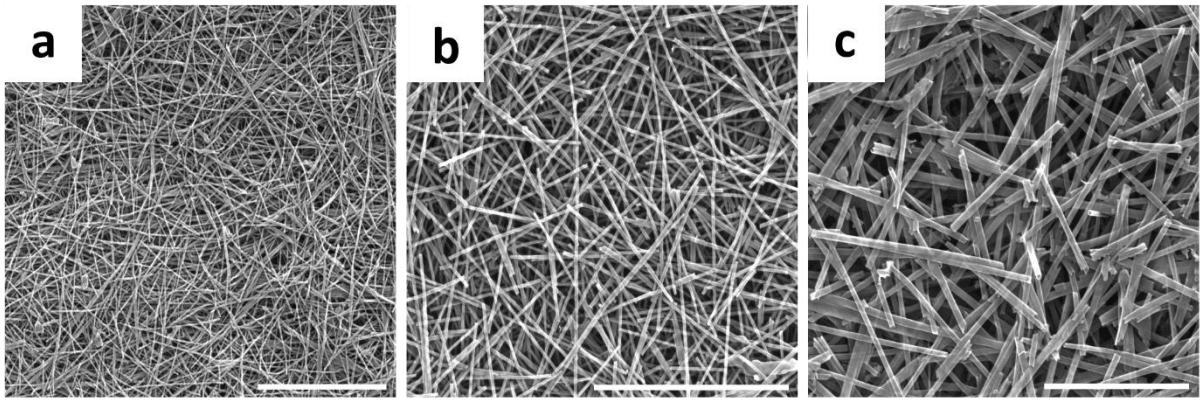

Figure S3. Top view SEM images of liberated CNTs. (a) CNTs prepared by NAAM-Su (scale bar = 2 µm), (b) CNTs prepared by NAAM-Ox (scale bar = 2 µm) and (c) CNTs prepared by NAAM-Ph (scale bar = 2µm).

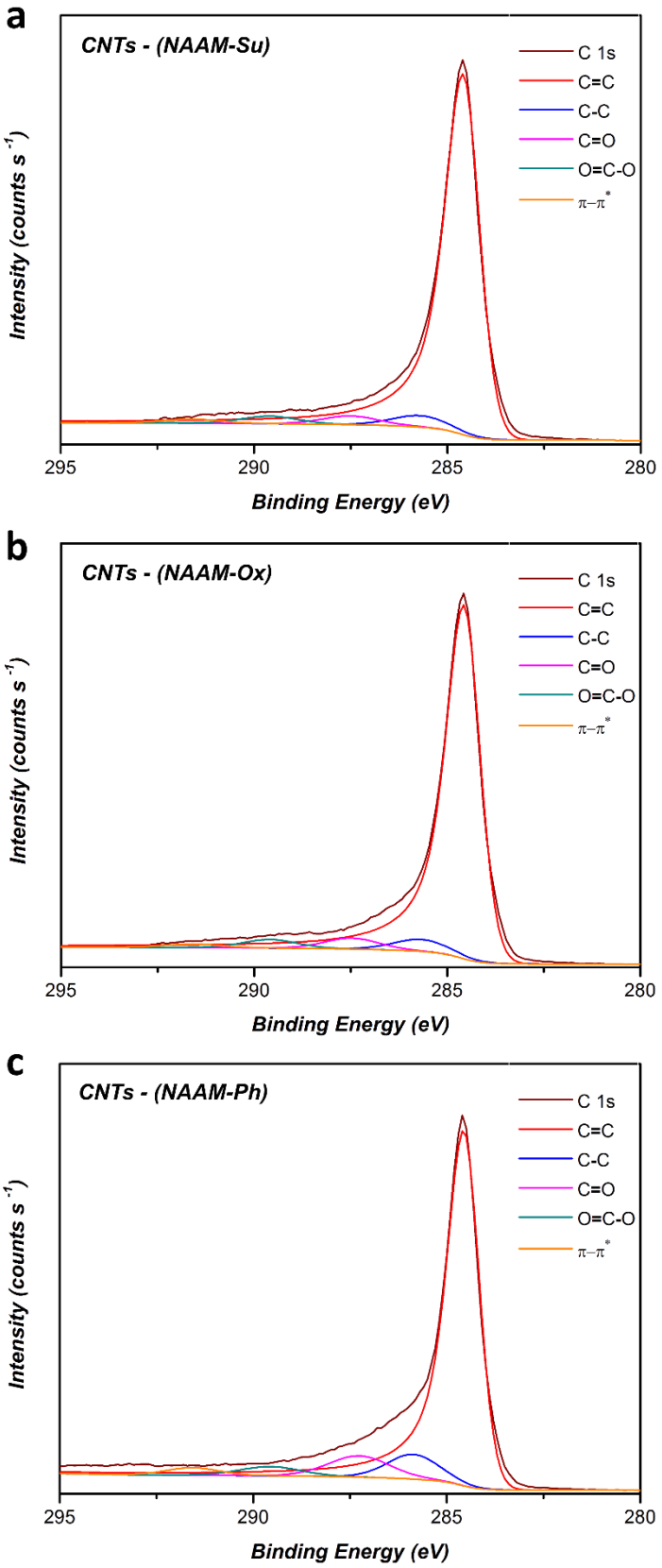

Figure S4. XPS analysis of liberated CNTs produced through catalyst-free CVD process using different NAAMs templates. (a) High resolution C 1s spectra of CNTs prepared by NAAM-Su; (b) high resolution C 1s spectra of CNTs prepared by NAAM-Ox and (c) high resolution C 1s spectra of CNTs prepared by NAAM-Ph.

Table S1. Summary of elemental composition and high-resolution C 1s spectra of different CNTs prepared through catalyst-free CVD process using different NAAMs templates.

	Sample	**CNTs**	**CNTs**	**CNTs**
	Template used	NAAMs in H_2SO_4	NAAMs in $H_2C_2O_4$	NAAMs in H_3PO_4
	Peak assignment	**Intensity (%)**		
C	-	92.49	90.98	89.58
O	-	3.81	6.40	7.01
C1s	C=C	86.88	85.43	75.22
	C–C	4.74	4.97	9.01
	C=O	3.60	4.55	9.11
	O=C–O	3.14	3.55	3.90
	π-π*	1.64	1.50	2.76

CHAPTER 5

Influence of Surface Chemistry on the Ionic Conductivity of Vertically Aligned Carbon Nanotube Composite Membranes

Mohammed Obid Alsawat

School of Chemical Engineering, The University of Adelaide, South Australia 5005, Australia

This chapter is based on the following peer-reviewed article:

Alsawat, M. Kant, K. Altalhi, T. Santos, A. and Losic, D. Influence of Surface Chemistry on the Ionic Conductivity of Vertically Aligned Carbon Nanotube Composite Membranes. *RSC Advances*, 6.50 (2016): 44288-44296.

Statement of Authorship

Title of Paper	Influence of Surface Chemistry on the Ionic Conductivity of Vertically Aligned Carbon Nanotube Composite Membranes
Publication Status	☑ Published ☐ Accepted for Publication ☐ Submitted for Publication ☐ Unpublished and Unsubmitted work written in manuscript style
Publication Details	Alsawat, M. Kant, K. Altalhi, T. Santos, A. and Losic, D. Influence of Surface Chemistry on the Ionic Conductivity of Vertically Aligned Carbon Nanotube Composite Membranes. *RSC Advances*, 6.50 (2016): 44288-44296.

Principal Author

Name of Principal Author (Candidate)	Mohammed Alsawat		
Contribution to the Paper	Under supervision of D. Losic and A. Santos, I developed, designed, and performed the experiments, interpreted and processed the data and wrote the manuscript for submission.		
Overall percentage (%)	80		
Certification:	This paper reports on original research I conducted during the period of my Higher Degree by Research candidature and is not subject to any obligations or contractual agreements with a third party that would constrain its inclusion in this thesis. I am the primary author of this paper.		
Signature		Date	30 May 2016

Co-Author Contributions

By signing the Statement of Authorship, each author certifies that:

i. the candidate's stated contribution to the publication is accurate (as detailed above);
ii. permission is granted for the candidate in include the publication in the thesis; and
iii. the sum of all co-author contributions is equal to 100% less the candidate's stated contribution.

Name of Co-Author	Tariq Altalhi		
Contribution to the Paper	I helped the candidate with providing the technical support of chemical vapour deposition (CVD) system. I give consent for Mohammed Alsawat to present this paper for examination towards the Doctorate of philosophy.		
Signature		Date	30 May 2016

Name of Co-Author	Krishna Kant
Contribution to the Paper	I helped the candidate with electrochemical impedance spectroscopy characterization. I give consent for Mohammed Alsawat to present this paper for examination towards the Doctorate of philosophy.

Signature		Date	30 May 2016

Name of Co-Author	Abel Santos
Contribution to the Paper	I acted as secondary supervisor for the candidate and aided in development of the experiments and evaluation of manuscript for submission. I give consent for Mohammed Alsawat to present this paper for examination towards the Doctorate of philosophy.

Signature		Date	30 May 2016

Name of Co-Author	Dusan Losic
Contribution to the Paper	I acted as primary supervisor for the candidate and aided in development of the experiments and evaluation of manuscript for submission. I give consent for Mohammed Alsawat to present this paper for examination towards the Doctorate of philosophy.

Signature		Date	30 May 2016

RSC Advances

PAPER

Cite this: *RSC Adv.*, 2016, **6**, 44288

Influence of surface chemistry on the ionic conductivity of vertically aligned carbon nanotube composite membranes

Mohammed Alsawat,[ab] Krishna Kant,[ac] Tariq Altalhi,[ab] Abel Santos*[a] and Dusan Losic*[a]

Received 14th March 2016
Accepted 15th April 2016

DOI: 10.1039/c6ra06701h

www.rsc.org/advances

The nano-sized solid state pores and channels that mimic nature-based systems have attracted great interest due their potential applications for molecular separation, sensing, drug delivery, and energy conversion. In this study, in order to gain more knowledge on the ion and molecular transport inside nanopores, we examined how the surface conduction and electrochemical properties of carbon nanotubes (CNTs) composite membranes produced by a template-assisted catalyst-free chemical vapour deposition (CVD) process using nanoporous anodic alumina membranes (NAAMs) as a template can be tuned readily by chemical modification of their inner surface for various applications. The inner graphitic surface of the resulting CNTs was modified chemically through wet oxidation process using hydrogen peroxide (H_2O_2) as the oxidant agent to introduce oxygen-containing groups, mainly carboxyl groups. Electrochemical impedance spectroscopy (EIS) revealed significant changes in surface conduction measured by impedance and conductance of CNTs as a result of the selective chemical modification of their inner wall surfaces. These results show that this approach makes it possible to tune the surface conductivity and interfacial properties of vertically aligned arrays of CNTs with precision, using a simple oxidation process. Therefore, this method can be used to produce CNTs composite membranes with precisely controlled electrochemical properties and conductivity related to potential applications of advanced electrically driven and bioinspired separation devices for water desalination and separation of biological molecules.

Introduction

Nano-confined structures, such as nanopores, nanotubes and nanochannels, have attracted enormous research attention in the past for their potential applications, including low-cost filtering membranes for bioseparation and desalination, filtration devices, biosensing, catalysis, and energy generation. These applications require membranes to have fast transport with high selectivity and low running costs. Since their discovery in 1991,[1] carbon nanotubes (CNTs) have attracted considerable interest due to their outstanding and unique transport, electrical, mechanical, and thermal properties. Several types of CNTs membranes have been developed and explored as advanced membranes for water desalination, gas pervaporation, nanofiltration of biological mixtures, transdermal drug delivery, and energy storage applications.[2–5] The formation of vertically aligned arrays of CNTs is of particular interest for the abovementioned applications because this configuration endows the resulting membrane systems with better performance over membranes composed of randomly distributed bundles of CNTs. Conventional fabrication techniques used to prepare CNTs membranes with vertically aligned arrays of CNTs are typically template-based synthesis approaches, where silicon nitride and polymer matrices are used as host templates.[6,7] These nanofabrication techniques, however, have some disadvantages and technical drawbacks. For example, these methods require the use of expensive laboratory facilities and long fabrication processes, limiting the production of these membranes to the laboratory scale. In addition, controlling the geometric features of CNTs structures using these techniques is difficult and challenging due to the use of a catalyst.

Thus far, several studies have shown that other cost-competitive template-assisted synthesis techniques can overcome the aforementioned disadvantages for fabricating CNTs membranes in a cost-competitive and time-effective manner on the industrial scale. Nanoporous anodic alumina membranes (NAAMs) produced by electrochemical anodization of aluminum substrates in acid electrolytes have been demonstrated as outstanding host templates for the production of CNT

[a]*School of Chemical Engineering, The University of Adelaide, Adelaide, Australia. E-mail: dusan.losic@adelaide.edu.au; abel.santos@adelaide.edu.au*
[b]*Department of Chemistry, Faculty of Science, Taif University, Taif, Saudi Arabia*
[c]*School of Chemical and Physical Sciences, Flinders University, Bedford Park, Adelaide, SA 5042, Australia*

membranes due to their physical, mechanical and chemical properties.[8–12] Electrochemical anodization of aluminum is a well-known, industrially scalable and cost-competitive process extensively used to produce highly ordered NAAMs for numerous applications.[13–15] The nanopore geometric features of the resulting templates can be precisely engineered using the fabrication parameters during anodization.[16,17] These attractive features boosted the use of NAAMs as platforms for the synthesis of one and two dimensional nanostructure materials (*i.e.* nanowires, nanorods, and nanotubes).[18–22] Kyotani's group pioneered the use of NAAMs as host templates for the preparation CNTs membranes featuring vertically aligned cylindrical nanotubes.[11,23] NAAMs enable the formation of well-defined CNTs-based membranes with precisely controlled nanotube dimensions and geometry.[24] In addition, it can be noted that CNTs-NAAMs are produced using a catalyst-free CVD approach, which overcomes the inherent drawbacks of catalyst-based CVD processes, where the use of metal catalyst particles as precursors results in CNTs with uncontrolled geometric features and incorporated impurities into the structure of CNTs, which occlude the inner hollow structure of CNTs. These factors limit and compromise the practical applicability of these membranes for a wide range of applications.[25,26] Furthermore, the surface chemistry of the inner wall surfaces of the resulting CNTs produced by this technique can be modified selectively by different approaches, opening new opportunities to develop advanced membranes with precisely engineered transport and selectivity properties. Note that the flow of ions or molecules across the CNTs membranes occurs along the graphitic surface of inner wall of the nanotubes, which results in much faster transport rates than those of common ceramic and polymeric membranes. To increase the surface activity of CNTs membranes is envisaged as a unique means of enhancing the efficiency of CNTs membranes for transport/separation/filtration applications. Although CNT membranes with tuned chemical properties are of special interest for applications, such as bioinspired and electrically driven molecular transport, this approach has not been widely explored.

In addition to their geometric features, modifying the surface chemistry of CNTs membranes for tuning their electrochemical properties and surface conductivity is of utmost importance for applications where the transport/filtration/separation processes rely on the interfacial properties and electrochemical interactions between the inner graphitic surface of the membrane and molecules. Important examples of this concept are capacitance-based desalination membranes and electrophoretic separations, which allow improved separation selectivity and cost-effective separation process. However, there is lack of understanding of the transport mechanism of ions and molecules inside the CNTs, particularly under an electrical field, wherein the role of the interfacial properties and surface charge is a performance-determining parameter.

In this study, to extend the knowledge in this field, we explore for the first time the effect of selective chemical modification of the inner surface of CNTs composite membranes produced in NAAMs by a catalyst-free CVD process on their electrochemical properties and potential impact on their transport and selectivity properties. A schematic of the fabrication process of CNTs-NAAMs and the electrochemical setup used in this study are presented in Fig. 1. The selective chemical modification of the inner surface of the CNTs was confirmed experimentally by contact angle measurements, X-ray photoelectron spectroscopy (XPS), Raman spectroscopy, and electrochemical impedance spectroscopy (EIS) characterization. The EIS technique has been employed extensively to characterise the electrical properties of the materials and the interfaces, including nanopores and nanochannels.[27] In this study, we demonstrate how the surface chemistry inside the CNTs can influence the ionic conductivity and electrochemical properties of CNTs-NAAMs composite membranes using different electrolyte concentrations. Lower electrolyte concentrations are used to cast light on how a selective chemical modification of the inner surface can be readily used as a strategy for tuning the ionic conductivity and electrochemical properties of these composite membranes, which is critical for the development of advanced membranes for electrophoretic and potential-based separation of molecules.

Experimental section

Materials

High purity aluminum (Al) foils 0.32 mm thick with 99.999% purity were obtained from Goodfellow Cambridge Ltd, UK. Copper chloride ($CuCl_2$), oxalic acid ($H_2C_2O_4$), chromium trioxide (CrO_3), phosphoric acid (H_3PO_4), hydrochloric acid (HCl), ethanol 99.7% (C_2H_6O), toluene 99.8% (C_7H_8), hydrogen peroxide (H_2O_2), hydrofluoric acid (HF) and sodium chloride (NaCl) were purchased from Sigma Aldrich (Australia) and used as received. High purity deionized (DI) water (resistivity 18.2 MΩ cm) from a Milli-Q water purification system was used in all the solutions used in this study.

Synthesis of nanoporous anodic alumina membranes

Nanoporous anodic alumina membranes (NAAMs) were prepared by a two-step electrochemical anodization process using high purity Al foils.[8,28] Briefly, circular Al foils with a diameter of 1.5 cm were first cleaned under sonication in ethanol and water for 10 min followed by electro-polishing in a mixture of $HClO_4$ and C_2H_6O 1 : 4 (v/v) at 20 V and 5 °C for 3 min and then dried under a nitrogen stream. The electro-polished Al foils were anodized in 0.3 M aqueous oxalic acid electrolyte at 40 V and 6 °C using a two electrode electrochemical cell. The first anodization step was carried out for 20 h and the resulting layer was removed by selective wet chemical etching in a mixture of H_3PO_4 (0.4 M) and H_2CrO_7 (0.2 M) at 70 °C for 3 h to obtain hexagonally organized pits on the Al surface. The second anodization step was carried out for 15 h to specifically obtain NAAMs with pore lengths of 50 ± 1 μm. The remaining aluminum substrate was removed in a saturated solution of HCl and $CuCl_2$. Finally, the oxide barrier layer at the bottom of NAAMs was chemically removed by wet chemical etching in an aqueous solution of 5 wt% H_3PO_4 at 35 °C under current control to prevent the resulting membranes from undesired pore widening.[29,30]

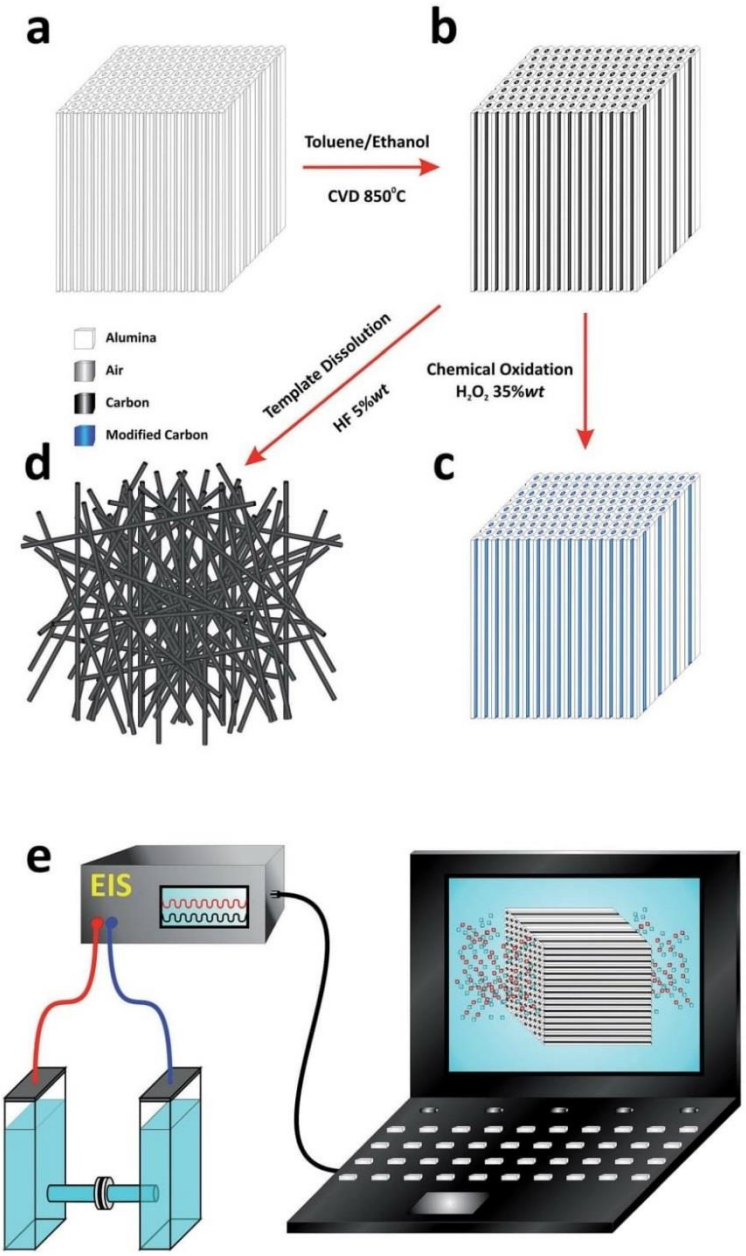

Fig. 1 Schematic of the fabrication and modification process of carbon nanotube composite membranes (CNTs-NAAMs) and the electrochemical measurements setup. (a) NAAMs prepared by electrochemical anodization of an Al foil; (b) prepared CNTs-NAAMs with CNTs embedded in NAAMs after the CVD process; (c) CNTs-NAAMs after oxidation treatments; (d) liberated CNTs after dissolution of NAAMs by wet chemical etching (this step is performed to characterize the outer surface of as-produced and oxidized CNTs structures); and (e) schematic of the electrochemical measurements setup.

Synthesis and modification of CNTs-NAAMs composite membranes

CNTs were grown inside NAAMs using a catalyst-free CVD approach previously described.[12,31] Briefly, vertically aligned multiwalled CNTs (MWCNTs) were grown inside the pores of NAAMs by CVD using a mixture of toluene and ethanol 1 : 1 (v/v) as a carbon precursor in a CVD system (Brother Furnace Co., LTD, China) (Fig. 1). The CVD process was performed at 850 °C under constant argon (Ar) flow at a rate of 1 dm^3 min^{-1} for 30 min to specifically deposit carbon in the cylindrical pores of

NAAMs. The process was adjusted to grow CNTs with a wall thickness of 7 ± 2 nm. As-produced CNTs-NAAMs were modified chemically (*i.e.* oxidized) *via* wet chemical method using H_2O_2 (35 wt%) for 16 h followed by washing with deionized water. This method made it possible to selectively and precisely functionalize the inner wall surface of CNTs with oxygen-containing groups.

Structural and chemical composition characterizations

The structural characterization of the prepared CNTs-NAAMs was performed using a scanning electron microscope (SEM-FEG Environmental SEM, Quanta 450) equipped with energy dispersive X-ray spectroscopy (EDX). X-ray photoelectron spectroscopy (XPS Kratos Axis Ultra) was used to determine the chemical composition of the as-produced and oxidized CNTs-NAAMs composite and liberated CNTs using the Al Kα (1486.7 eV) monochromatic line. Contact angle measurements (Attension Theta Optical Tensiometer, Finland) were carried out to confirm the changes in the surface properties of CNTs-NAAMs after the oxidation treatment with hydrogen peroxide. Transmission electron microscopy (Philips CM 200 TEM) was used to assess the uniformity and establish the wall thickness of CNTs. To obtain liberated CNTs from the host templates, NAAMs were first dissolved selectively in a 5 wt% HF solution and the liberated CNTs were washed thoroughly with deionised water and ethanol. Raman spectroscopy (Horiba LabRAM HR Evolution Raman microprobe spectrometer) was used to characterize the graphitic structure of the as-prepared and oxidized CNTs-NAAMs and liberated CNTs. The Raman spectra were obtained using a He–Ne laser of 532 nm as an excitation source.

Electrochemical impedance measurements

The electrochemical properties of the as-produced and oxidized CNTs-NAAMs were analysed by two electrode electrochemical impedance spectroscopy (EIS). To this end, the different membranes were placed between two halves of a H-tube permeation cell with an exposed area of 0.0314 cm^2 (Fig. 1). Both halves were filled with 3 mL of a NaCl aqueous electrolyte solution. Two gold electrodes were immersed in these halves, one in each, serving as working and counter electrode. Impedance data were obtained over a frequency range from 1 Hz to 1 MHz using various concentrations of NaCl electrolyte (*i.e.* 1, 2, 5, 10, 50, and 100 μM). The modelling of the experimental system was done using EvolCRT software (developed by Department of Chemistry, Wuhan University, China).[32]

Result and discussion

Structural characterization of the prepared CNTs composite membranes before and after oxidation

SEM images of the prepared CNTs composite membranes through different fabrications steps and before and after oxidations are summarised in Fig. 2. Fig. 2a shows the top view of a NAAM confirming the hexagonal arrangement of nanopores with an average diameter of 40 ± 5 nm. This geometry with perfectly ordered and vertically aligned nanopore structure is a result of the self-ordered anodization process.[33] The inset in Fig. 2a shows details of the bottom view of these membranes after pore opening using phosphoric acid (5 wt%) at 35 °C. The

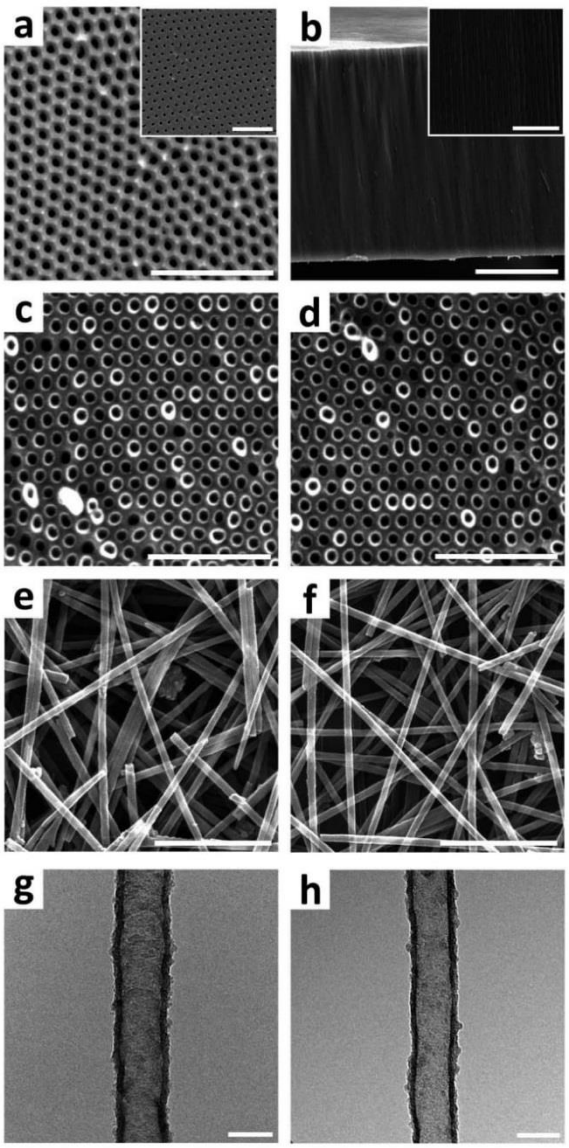

Fig. 2 Set of SEM and TEM images of NAAMs, as-produced and oxidized CNTs-NAAMs and liberated CNTs. (a) Top view SEM image of a typical NAAMs structure produced through a two-step anodization process in an oxalic acid electrolyte (scale bar = 500 nm) (inset: bottom view, scale bar = 500 nm); (b) cross-sectional view showing entire length of the NAAMs (scale bar = 20 μm) (inset: magnified view, scale bar = 500 nm); (c) top view SEM image of as-produced CNTs-NAAMs produced through catalyst-free CVD for 30 min (scale bar = 500 nm); (d) top view SEM image of oxidized CNTs-NAAMs (scale bar = 500 nm); (e) SEM image of as-produced CNTs after dissolution of NAAMs; (f) SEM image of oxidized CNTs after dissolution of NAAMs; (g) TEM image of the as-produced CNTs (scale bar = 50 nm); and (h) TEM image of oxidized CNTs (scale bar = 50 nm).

thickness of NAAMs used in this study was set to 50 μm by adjusting the anodization time during the second anodization step (Fig. 2b). The inset in Fig. 2b shows vertically aligned cylindrical nanopores from the top to bottom. Note that precise control of the dimensions of NAAMs can be achieved by controlling the anodization conditions (*i.e.* anodization voltage and time). Top view SEM images of as-produced and oxidized CNTs embedded in NAAMs are presented in Fig. 2c and d, respectively, illustrating an inner diameter of 41 ± 5 nm with no significant morphological differences between them. This result indicates a slight increase in the pore diameter of NAAMs after the CVD process. This can be explained by the loss of water from the NAAMs structure and the formation of a different crystallographic phase of alumina during the CVD process (*i.e.* 850 °C).[34,35] The hollow and uniform features of the as-produced and oxidized CNTs can be clearly seen from SEM images of liberated tubes after selective dissolution of the NAAMs host templates (Fig. 2e and f). Further evidence for the aforementioned features can be found from the transmission electron microscopy (TEM) images of the as-produced and oxidized CNTs displayed in Fig. 2g and h, respectively. TEM image analysis established an average wall thickness of 7 ± 2 nm, with CNTs presenting low graphitic features in both cases, as-produced and oxidized. However, it is worth noting that CNTs can be graphitized by post-heat treatment at higher temperatures, if required.[36]

Chemical composition characterization of prepared CNTs composite membranes before and after oxidation

The chemical composition of the as-produced and oxidized CNTs-NAAMs was analysed by energy dispersive X-ray spectroscopy (EDX), X-ray photoelectron spectroscopy (XPS) and Raman spectroscopy. The EDX spectra of the as-produced and oxidized CNTs-NAAMs are displayed in Fig. 3a and b, respectively, showing the presence of C, O and Al as major elements. This analysis provides information about both the elemental composition and the high level of purity of CNTs-NAAMs produced by our catalyst-free CVD process. The presence of Pt is related to the coating applied for SEM imaging. Note that the percentage of these elements is not included because the quantitative analysis of low atomic number elements using EDX analysis is usually overestimated. Therefore, XPS was used to gain a deeper insight into the quantitative and qualitative elemental composition and surface chemistry of the as-produced and oxidized CNTs-NAAMs and CNTs. In this sense, it should be noted that the XPS spectra of CNTs embedded in NAAMs were obtained from the top carbon layer on the NAAM's surface because this carbon layer has the same chemical structure as the inner CNTs layers.[23] It can be note that in this study, the O 1s spectra were not selected for an analysis of the composition of these CNT structures because this analysis cannot discern between the O contribution from the NAAMs template and from the oxidized CNTs to the O 1s spectra. Therefore, under such circumstances, the C 1s XPS spectrum is the best choice to discern the chemical composition of CNTs structures and the effect of the oxidation over the composition of CNTs. Fig. 3c–f show the high resolution C 1s spectra and survey spectra of the as-produced and oxidized CNTs-NAAMs and liberated CNTs. The as-produced CNTs-NAAMs had 6% oxygen, which increased to 18% after oxidation with H_2O_2. A corresponding O/C ratio of 0.07 and 0.26 was determined, respectively. Fig. 3c shows the C 1s peak of the as-produced CNTs-NAAMs, with the inset showing the survey spectrum, which is deconvoluted into five peaks located at binding energies 284.3 ± 0.2, 285.2 ± 0.3, 287.3 ± 0.2, 289.3 ± 0.2 and 291.2 ± 0.3 eV. These peaks are associated with the sp^2 bonds of graphitic carbon, disordered sp^3 network of carbon atoms, C═O (ketone/aldehyde), O═C–O (carboxyl/ester) groups, and π–π* transition of carbon atoms in graphene structures, respectively.[37,38]

After treatment with H_2O_2, the CNTs-NAAMs become more hydrophilic as the graphitic carbon peak (284.3 eV) decreased significantly and the XPS peak associated with the sp^3 network together with peaks associated with oxygen-containing functional groups (287.3, 289.3 eV) become more pronounced (Fig. 3d). Liberated CNTs were analyzed by XPS to shed light on the chemical composition change of the outer surface of the CNTs after oxidation. Although the escape depth of the photoelectrons in XPS is known to be about few nanometers, the obtained spectrum of the outer wall surface of CNTs (thickness ~7 nm) mainly provides information on the chemical composition of the outer surface of the CNTs. As-produced and oxidized CNTs had 5.5% and 6.7% of oxygen, respectively. The corresponding O/C ratio of 0.06 and 0.07 was determined, respectively. The high resolution C 1s spectra of the as-produced and oxidised CNTs are shown in Fig. 3e and f. These graphs show no change in the chemical composition of the outer surface of CNTs after oxidation, which was indicated by almost the same graphitic carbon peak and all peaks associated with oxygen-containing functional groups. The elemental composition and high-resolution C 1s spectra of as-produced and oxidized CNTs-NAAMs and liberated CNTs are summarized in Table 1. This analysis clearly confirms that only the inner surface of the CNTs was modified (*i.e.* oxidized), whereas the outer surface remained intact after the oxidation treatment. As-produced and oxidized CNTs-NAAMs were subjected to water contact angle (WCA) measurements to confirm the surface modification. WCA results are presented as insets in Fig. 3a and b, showing an average WCA of 75° and 35° for as-produced and oxidized CNTs-NAAMs, respectively. This confirms that a transition from a hydrophobic to hydrophilic surface occurred during the oxidation treatment with hydrogen peroxide. Further evidence for the selective modification of the inner wall surface of CNTs can be confirmed by Raman spectra of the as-produced and oxidized CNTs-NAAMs and liberated CNTs shown in Fig. 4a and b, respectively. All samples show the characteristic spectrum of CNTs with a G band peak around 1585 cm^{-1} and a D band peak around 1340 cm^{-1}. The slight increase in the D band peak in oxidized CNTs-NAAMs compared to the as-produced ones (Fig. 4a) and the similar peaks for oxidized and as-produced liberated CNTs (Fig. 4b) confirm the selective modification of the inner wall surface of CNTs. Moreover, this analysis also shows that the

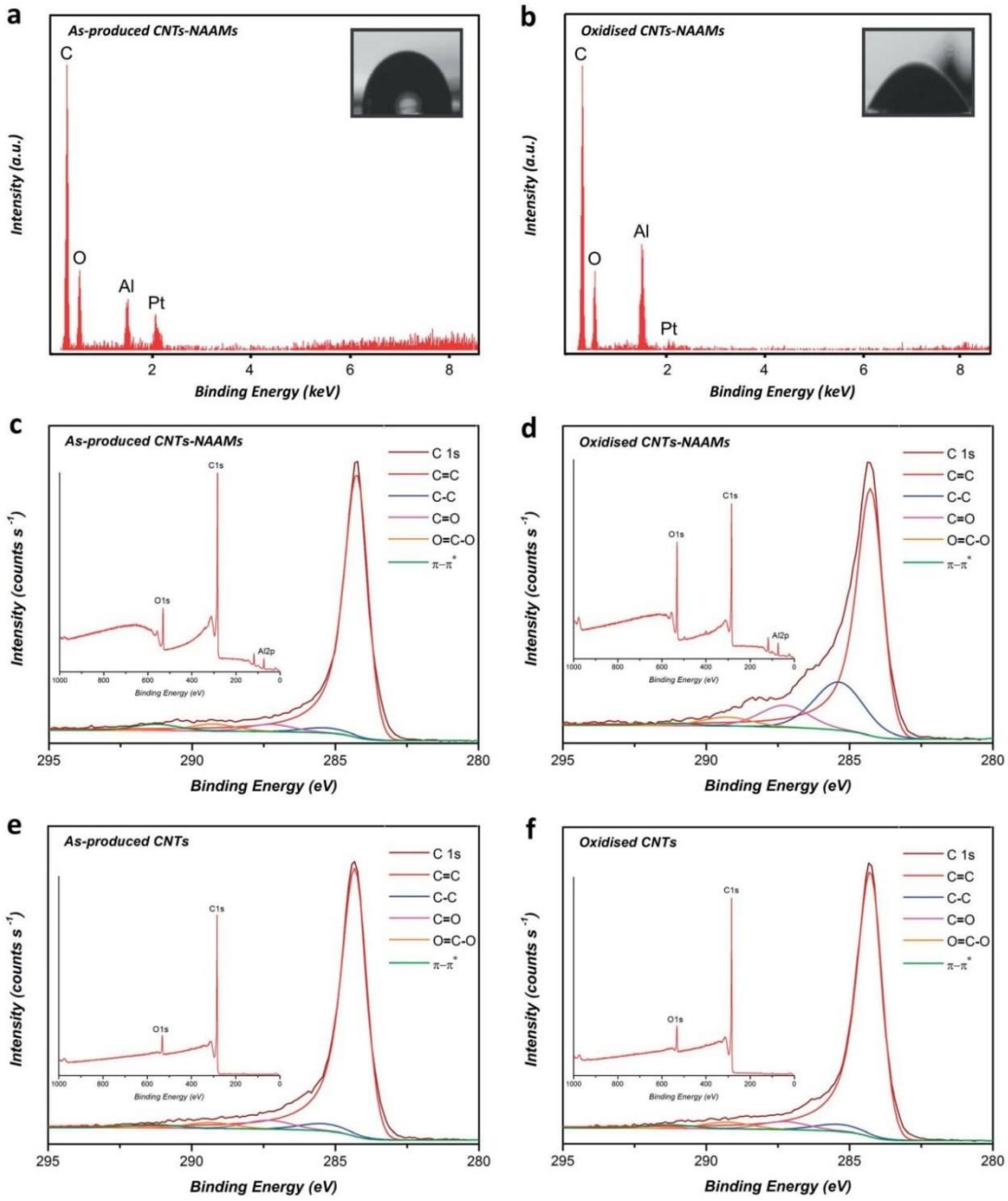

Fig. 3 EDX and XPS analysis of the as-produced and oxidized CNTs-NAAMs and liberated CNTs. (a) The EDX spectra of the as-produced CNTs-NAAMs (inset: image of a water droplet); (b) the EDX spectra of oxidized CNTs-NAAMs (inset: image of a water droplet); (c) high resolution C 1s spectra of as-produced CNTs-NAAMs (inset: survey spectrum); (d) high resolution C 1s spectra of oxidized CNTs-NAAMs (inset: survey spectrum); (e) high resolution C 1s spectra of as-produced CNTs (inset: survey spectrum); and (f) high resolution C 1s spectra of oxidized CNTs (inset: survey spectrum).

structural integrity of CNTs was not influenced by the oxidation treatment used in our study, as the D and G bands keep the same positions in the Raman spectrum. It can be concluded from the aforementioned analysis of CNTs-NAAMs and liberated tubes that the selective modification of the inner wall surface of CNTs was accomplished successfully, establishing a solid path towards the selective chemical modification of CNT structures.

Table 1 Summary of the elemental composition and high-resolution C 1s spectra of as produced and oxidized CNTs-NAAMs and liberated CNTs

	Sample		As produced CNTs-NAAMs	Oxidized CNTs-NAAMs	As produced CNTs	Oxidized CNTs
	Peak position (eV)	Peak assignment	Intensity (%)			
C	—	—	89.61	70.80	94.25	92.18
O	—	—	5.97	18.66	5.49	6.74
Al	—	—	4.42	6.90	—	—
C 1s	284.3 ± 0.2	C=C	83.4	60.0	84.0	83.9
	285.2 ± 0.2	C–C	4.3	23.7	4.5	4.4
	287.3 ± 0.3	C=O	4.6	10.8	5.5	5.1
	289.3 ± 0.2	O=C–O	3.5	4.3	3.7	4.2
	291.2 ± 0.3	π–π*	4.0	1.1	2.1	2.2

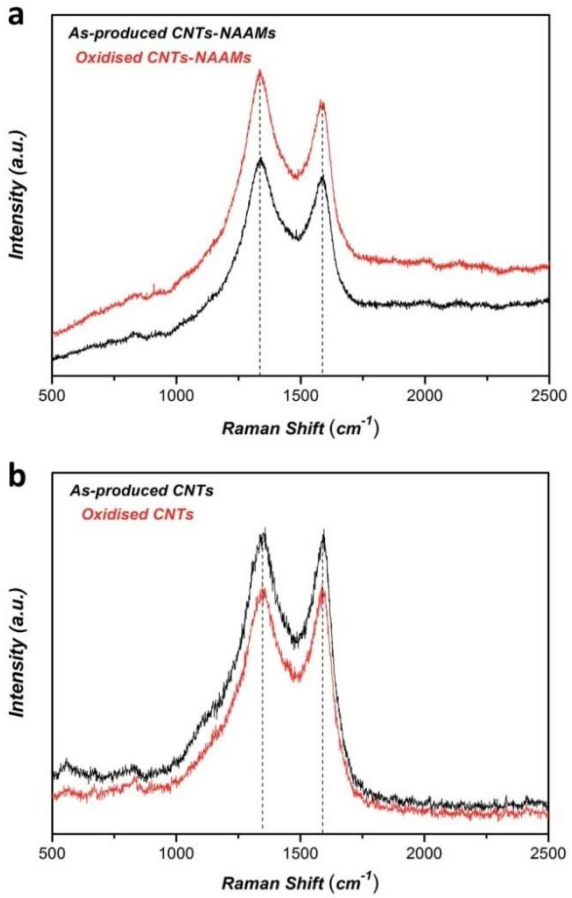

Fig. 4 Raman analysis of the as-produced and oxidized CNTs-NAAMs and liberated CNTs. (a) Raman spectra of the as-produced and oxidized CNTs-NAAMs; and (b) Raman spectra of the as-produced and oxidized CNTs.

Electrochemical characterization of CNTs composite membranes before and after oxidations

EIS measurements were performed on the as-produced CNTs-NAAMs using various concentrations of NaCl electrolyte ranging from 1 μM to 100 μM to shed light on the influence of the electrolyte concentration on the system conductivity. Fig. 5a shows that increasing the NaCl concentration from 1 μM to 100 μM decreases the conductivity of the CNTs-NAAMs. Under an electrical potential, the negatively-charged surface of the as-produced CNTs-NAAMs in contact with NaCl solution attracts positively-charged counterions and repels the co-ions to form an interfacial charge layer, the so-called electrical double layer (EDL).[39] The Debye length (k^{-1}) (*i.e.* a characteristic thickness of the EDL) varies proportionally with the electrolyte ionic strength, $k^{-1} \alpha [c]^{-1/2}$, where $[c]$ is the molar concentration of a monovalent electrolyte.[40] To maintain electric neutrality, the surface charge determines the ion conductance by controlling the ionic concentration inside the CNTs-NAAMs at low electrolyte concentrations. In contrast, ion conductance at high electrolyte concentrations is determined by the bulk conductivity and increases linearly with increasing ionic concentration.[41] However, the result indicates that the conductance decreases with increasing electrolyte ionic concentration due likely to two factors, namely, (i) the electrostatic forces between the electrolyte ions and the inner surface of CNTs composite membrane, which increases with increasing ionic concentration, resulting in a decrease in the mobility of counterions inside CNTs-NAAMs; and (ii) the entrance resistance (the so-called access resistance[42]) against ion transport, which occurs more at high ionic concentrations, resulting in a lower conductance.[43] The impedance (Z) data of bare NAAMs, as-produced and oxidized CNTs-NAAMs over a frequency range from 1 Hz to 1 MHz at constant concentration of NaCl (1 μM) were used to determine if the inner surface modification influenced the conductivity of the CNTs-NAAMs. Fig. 5b presents a Nyquist plot of the obtained impedance values. This illustrates a very low impedance of as-produced CNTs-NAAMs, indicated by a complete semicircle, over bare NAAMs. This can be attributed to the lower friction interface at the smooth inner surfaces of CNTs.[44] This analysis also shows a substantial increase in impedance of the oxidized CNTs-NAAMs compared to the as-produced CNTs-NAAMs. The surface charge of the CNTs-NAAMs composite membrane becomes more negative, as proved by XPS and Raman analyses, with the oxidation treatment used in our study. The presence of more charged oxygen species at the surface of the CNTs generates more electrostatic

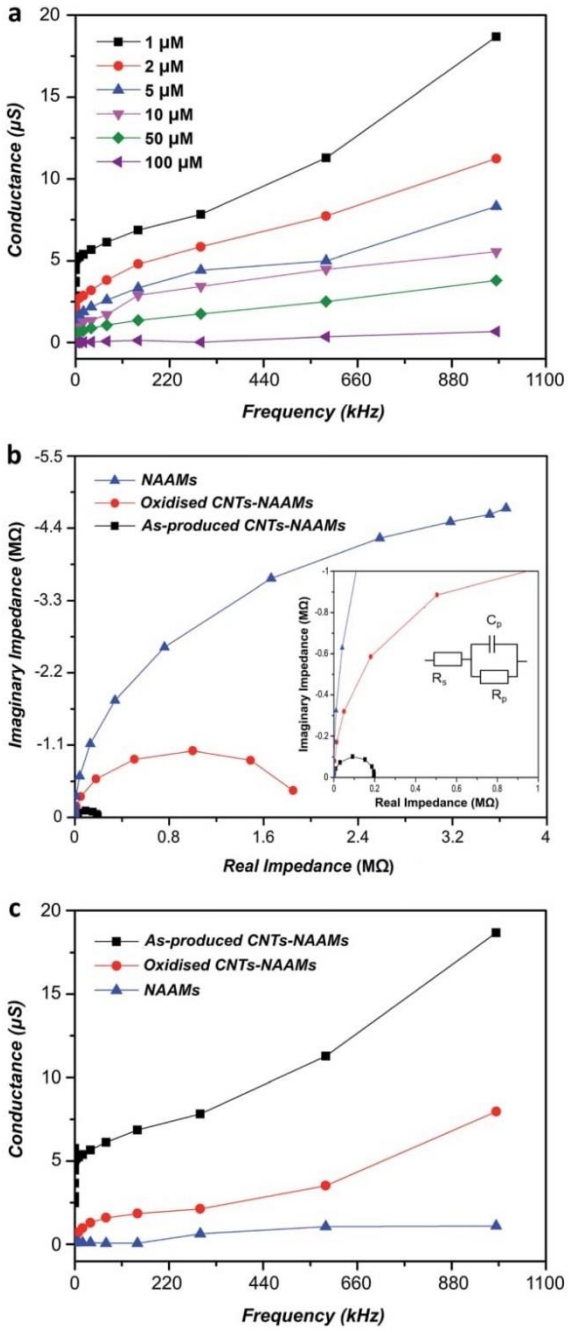

Fig. 5 EIS measurements of the as-produced and oxidized CNTs-NAAMs. (a) Conductance of as-produced CNTs-NAAMs at various NaCl concentrations; (b) Nyquist plots obtained for bare NAAMs, as-produced and oxidized CNTs-NAAMs at constant concentration of NaCl (1 μM) (inset: magnified view with full semi-circle of as-produced CNTs-NAAM and used circuit for the simulation of data points); (c) conductance change for bare NAAMs, as-produced and oxidized CNTs-NAAMs at various frequencies and constant concentration of NaCl (1 μM).

forces between the electrolyte ions and the oxygen-containing groups present along the inner wall surface of CNTs. An important aspect that distinguishes our applied synthetic method (*i.e.* templated-assisted catalyst-free CVD process using toluene and ethanol as a simple carbon precursor) from other conventional methods is that it allows the fabrication of CNTs-NAAMs with a precise cylindrical structure, smooth pore walls and without an occlusion of the inner hollow structure of CNTs. This makes the interaction between the CNTs surface and the ions of the transported electrolyte dominant at nanoscale regime. Further decrease in the pore diameter of CNTs would increase significantly the effect of such interactions, enhancing the impedance of these membranes. Considering that the chemical modification (*i.e.* oxidation) took place on the top surface of the composite membrane, the entrance resistance could play a role in the observed increase in impedance of the oxidized CNTs-NAAMs. An equivalent circuit, shown as the inset in Fig. 5b, was used to interpret the impedance data, where R_s is the solution resistance, R_p is the nanopore/nanotube resistance, and C_p is the nanopore/nanotube capacitance. A conductance *versus* frequency plot, produced by the conductance values obtained by impedance measurements is illustrated in Fig. 5c. This analysis shows that the aforementioned change in the conductivity of CNTs-NAAMs after oxidizing their inner surfaces follows a frequency-dependent mechanism. These results confirm that the surface conductivity and electrochemical properties of the CNTs-NAAMs can be precisely tuned by performing a simple H_2O_2 oxidation process. Moreover, the change in the concentration of electrolyte is shown to have a significant impact on the conductivity of the membrane due to electrostatic and access effects.

Conclusions

This study has reported on the chemical modification of the inner surface of CNTs composite membranes prepared by a catalyst-free CVD process using nanoporous anodic alumina membranes as a template and its influence on their conductivity and electrochemical properties. The selective chemical modification was confirmed by a set of characterization techniques, including contact angle measurements, X-ray photoelectron spectroscopy (XPS) and Raman spectroscopy. These analyses revealed a transition from hydrophobic to hydrophilic surface due to selective chemical functionalization of the inner surface of CNTs with oxygen-containing functional groups, which occurred by a simple oxidation treatment using hydrogen peroxide. Structural analysis of the resulting CNTs-NAAMs composite membranes revealed negligible morphological changes after chemical functionalization. The electrochemical impedance spectroscopy characterizations performed using NaCl electrolyte solutions (1–100 μM) demonstrated a substantial increase in the impedance of oxidized CNTs-NAAMs over as-produced CNTs-NAAMs, due to electrostatic and access effects. Therefore, the electrochemical properties of CNTs-NAAMs can be tuned readily by controlling their surface chemistry. These results can be used as a strategy for enhancing and tuning the electrochemical properties of CNTs composite membranes,

which is important for the development of advanced membranes for the electrophoretic and potential-based separation of molecules.

Acknowledgements

The authors acknowledge the financial support provided by the Australian Research Council (FT 110100711 and DE140100549). The authors also acknowledge the facilities and the scientific and technical assistance of the Australian Microscopy & Microanalysis Research Facility at the Electron Microscope Unit, the University of Adelaide. Mohammed Alsawat thanks Taif University (Ministry of Education, Saudi Arabia) for funding his scholarship.

References

1 S. Iijima, *Nature*, 1991, **354**, 56–58.
2 B. Corry, *J. Phys. Chem. B*, 2008, **112**, 1427–1434.
3 A. Noy, H. G. Park, F. Fornasiero, J. K. Holt, C. P. Grigoropoulos and O. Bakajin, *Nano Today*, 2007, **2**, 22–29.
4 M. Majumder, A. Stinchcomb and B. J. Hinds, *Life Sci.*, 2010, **86**, 563–568.
5 A. L. M. Reddy, S. R. Gowda, M. M. Shaijumon and P. M. Ajayan, *Adv. Mater.*, 2012, **24**, 5045–5064.
6 B. J. Hinds, N. Chopra, T. Rantell, R. Andrews, V. Gavalas and L. G. Bachas, *Science*, 2004, **303**, 62–65.
7 C.-M. Seah, S.-P. Chai and A. R. Mohamed, *Carbon*, 2011, **49**, 4613–4635.
8 H. Masuda and K. Fukuda, *Science*, 1995, **268**, 1466–1468.
9 H. Masuda, F. Hasegwa and S. Ono, *J. Electrochem. Soc.*, 1997, **144**, L127–L130.
10 H. Masuda, K. Yada and A. Osaka, *Jpn. J. Appl. Phys.*, 1998, **37**, L1340.
11 T. Kyotani, L.-f. Tsai and A. Tomita, *Chem. Mater.*, 1995, **7**, 1427–1428.
12 G. Che, B. Lakshmi, C. Martin, E. Fisher and R. S. Ruoff, *Chem. Mater.*, 1998, **10**, 260–267.
13 D. Losic, L. Velleman, K. Kant, T. Kumeria, K. Gulati, J. G. Shapter, D. A. Beattie and S. Simovic, *Aust. J. Chem.*, 2011, **64**, 294–301.
14 A. Santos, T. Kumeria and D. Losic, *TrAC, Trends Anal. Chem.*, 2013, **44**, 25–38.
15 T. Kumeria, M. M. Rahman, A. Santos, J. Ferré-Borrull, L. F. Marsal and D. Losic, *ACS Appl. Mater. Interfaces*, 2014, **6**, 12971–12978.
16 W. Lee and S.-J. Park, *Chem. Rev.*, 2014, **114**, 7487–7556.
17 W. Lee and J.-C. Kim, *Nanotechnology*, 2010, **21**, 485304.
18 K. Kant, D. Losic and R. E. Sabzi, *Int. J. Nanosci.*, 2011, **10**, 1–6.
19 H. Masuda, M. Ohya, H. Asoh, M. Nakao, M. Nohtomi and T. Tamamura, *Jpn. J. Appl. Phys.*, 1999, **38**, L1403.
20 C. R. Martin, *Science*, 1994, **266**, 1961–1966.
21 P. Hoyer, *Langmuir*, 1996, **12**, 1411–1413.
22 D. Routkevitch, T. Bigioni, M. Moskovits and J. M. Xu, *J. Phys. Chem.*, 1996, **100**, 14037–14047.
23 T. Kyotani, L.-f. Tsai and A. Tomita, *Chem. Mater.*, 1996, **8**, 2109–2113.
24 M. Alsawat, T. Altalhi, T. Kumeria, A. Santos and D. Losic, *Carbon*, 2015, **93**, 681–692.
25 R. Morjan, O. Nerushev, M. Sveningsson, F. Rohmund, L. Falk and E. Campbell, *Appl. Phys. A: Mater. Sci. Process.*, 2004, **78**, 253–261.
26 N. Grobert, M. Terrones, A. Osborne, H. Terrones, W. Hsu, S. Trasobares, Y. Zhu, J. Hare, H. Kroto and D. Walton, *Appl. Phys. A: Mater. Sci. Process.*, 1998, **67**, 595–598.
27 A. Lasia, *Electrochemical impedance spectroscopy and its applications*, Springer, 2014.
28 A. Li, F. Müller, A. Birner, K. Nielsch and U. Gösele, *J. Appl. Phys.*, 1998, **84**, 6023–6026.
29 M. Lillo and D. Losic, *J. Membr. Sci.*, 2009, **327**, 11–17.
30 D. Losic and D. Losic Jr, *Langmuir*, 2009, **25**, 5426–5431.
31 T. Altalhi, T. Kumeria, A. Santos and D. Losic, *Carbon*, 2013, **63**, 423–433.
32 J. Yu, H. Cao and Y. He, *Chemom. Intell. Lab. Syst.*, 2007, **85**, 27–39.
33 O. Jessensky, F. Müller and U. Gösele, *Appl. Phys. Lett.*, 1998, **72**, 1173–1175.
34 C. C. Chen, J. H. Chen and C. G. Chao, *Jpn. J. Appl. Phys.*, 2005, **44**, 1529.
35 L. Fernández-Romero, J. Montero-Moreno, E. Pellicer, F. Peiró, A. Cornet, J. Morante, M. Sarret and C. Müller, *Mater. Chem. Phys.*, 2008, **111**, 542–547.
36 D. Mattia, M. Rossi, B. Kim, G. Korneva, H. Bau and Y. Gogotsi, *J. Phys. Chem. B*, 2006, **110**, 9850–9855.
37 S. Biniak, G. Szymański, J. Siedlewski and A. Światkowski, *Carbon*, 1997, **35**, 1799–1810.
38 M. Reis, A. B. Do Rego, J. L. Da Silva and M. Soares, *J. Mater. Sci.*, 1995, **30**, 118–126.
39 M. Tagliazucchi and I. Szleifer, *Mater. Today*, 2015, **18**, 131–142.
40 J. N. Israelachvili, *Intermolecular and surface forces: revised third edition*, Academic press, 2011.
41 R. Karnik, K. Castelino, R. Fan, P. Yang and A. Majumdar, *Nano Lett.*, 2005, **5**, 1638–1642.
42 G. Willmott and B. Smith, *Nanotechnology*, 2012, **23**, 088001.
43 S. W. Kowalczyk, A. Y. Grosberg, Y. Rabin and C. Dekker, *Nanotechnology*, 2011, **22**, 315101.
44 M. Majumder, N. Chopra, R. Andrews and B. J. Hinds, *Nature*, 2005, **438**, 44.

CHAPTER 6

Facile and Controllable Route for Nitrogen Doping of Carbon Nanotubes Composite Membranes by Catalyst-Free Chemical Vapour Deposition

Mohammed Obid Alsawat

School of Chemical Engineering, The University of Adelaide, South Australia 5005, Australia

This chapter is based on the following peer-reviewed article:

Alsawat, M. Altalhi, T. Santos, A. and Losic, D. Facile and Controllable Route for Nitrogen Doping of Carbon Nanotubes Composite Membranes by Catalyst-Free Chemical Vapour Deposition. *Carbon*, 106 (2016): 295-305.

Statement of Authorship

Title of Paper	Facile and Controllable Route for Nitrogen Doping of Carbon Nanotubes Composite Membranes by Catalyst-Free Chemical Vapour Deposition
Publication Status	☑ Published ☐ Accepted for Publication ☐ Submitted for Publication ☐ Unpublished and Unsubmitted w ork w ritten in manuscript style
Publication Details	Alsawat, M. Altalhi, T. Santos, A. and Losic, D. Facile and Controllable Route for Nitrogen Doping of Carbon Nanotubes Composite Membranes by Catalyst-Free Chemical Vapour Deposition. *Carbon*, 106 (2016): 295-305.

Principal Author

Name of Principal Author (Candidate)	Mohammed Alsawat		
Contribution to the Paper	Under supervision of D. Losic and A. Santos, I developed, designed, and performed the experiments, interpreted and processed the data and wrote the manuscript for submission.		
Overall percentage (%)	80		
Certification:	This paper reports on original research I conducted during the period of my Higher Degree by Research candidature and is not subject to any obligations or contractual agreements with a third party that would constrain its inclusion in this thesis. I am the primary author of this paper.		
Signature		Date	30 May 2016

Co-Author Contributions

By signing the Statement of Authorship, each author certifies that:

i. the candidate's stated contribution to the publication is accurate (as detailed above);

ii. permission is granted for the candidate in include the publication in the thesis; and

iii. the sum of all co-author contributions is equal to 100% less the candidate's stated contribution.

Name of Co-Author	Tariq Altalhi		
Contribution to the Paper	I helped the candidate with providing the technical support of chemical vapour deposition (CVD) system. I give consent for Mohammed Alsawat to present this paper for examination towards the Doctorate of philosophy.		
Signature		Date	30 May 2016

Name of Co-Author	Abel Santos
Contribution to the Paper	I acted as secondary supervisor for the candidate and aided in development of the experiments and evaluation of manuscript for submission. I give consent for Mohammed Alsawat to present this paper for examination towards the Doctorate of philosophy.

Signature		Date	30 May 2016

Name of Co-Author	Dusan Losic		
Contribution to the Paper	I acted as primary supervisor for the candidate and aided in development of the experiments and evaluation of manuscript for submission. I give consent for Mohammed Alsawat to present this paper for examination towards the Doctorate of philosophy.		
Signature		Date	30 May 2016

CHAPTER 6: Alsawat, M. Altalhi, T. Santos, A. and Losic, D. Facile and Controllable Route for Nitrogen Doping of Carbon Nanotubes Composite Membranes by Catalyst-Free Chemical Vapour Deposition. *Carbon*, 106 (2016): 295-305.

Carbon 106 (2016) 295–305

Contents lists available at ScienceDirect

Carbon

journal homepage: www.elsevier.com/locate/carbon

Facile and controllable route for nitrogen doping of carbon nanotubes composite membranes by catalyst-free chemical vapour deposition

Mohammed Alsawat [a, b], Tariq Altalhi [a, b], Abel Santos [a, *], Dusan Losic [a, *]

[a] School of Chemical Engineering, The University of Adelaide, Adelaide, Australia
[b] Department of Chemistry, Faculty of Science, Taif University, Taif, Saudi Arabia

ARTICLE INFO

Article history:
Received 4 April 2016
Received in revised form
10 May 2016
Accepted 17 May 2016
Available online 18 May 2016

ABSTRACT

In this study, we present a facile approach that makes it possible to finely and selectively dope with nitrogen the structure of carbon nanotubes (CNTs) composite membranes. CNTs were grown inside nanoporous anodic alumina membranes (NAAMs) by a catalyst-free chemical vapour deposition (CVD) approach using different precursor mixtures containing carbon and nitrogen at different ratios. Different precursors were used to fabricate undoped and N-doped CNTs-NAAMs, with nitrogen content ranging from 0 to 7%. The morphology and chemical composition of the prepared composite membranes were characterized by scanning electron microscopy (SEM), transmission electron microscopy (TEM), X-ray photoelectron spectroscopy (XPS), and Raman spectroscopy. The obtained results reveal that the C/N ratio in the precursor source plays a crucial role in the doping process and incorporation of nitrogen into the structure of CNTs. It was found that a minimum threshold of 5:1 C/N ratio is required to obtain N-doped CNTs structures. This fabrication route does not compromise the morphology and graphitic structure of doped CNTs, making it an optimal process to tune the properties of these composite membranes for different applications, including catalysis, molecular separation and sensing. In this work, the molecular transport properties of N-doped CNTs-NAAMs with different level of doping were assessed by studying the diffusion of two model molecules with different hydrophilic-hydrophobic and charge properties. The obtained results show that the diffusional flux of a particular dye molecule was significantly affected by the nitrogen content of CNTs deposited inside NAAMs, confirming that the transport properties and chemical selectivity of CNTs-NAAMs composites can be controlled by nitrogen doping. This approach presents a new avenue to tune the properties of CNTs-NAAMs composites membranes, opening new opportunities for these membranes to be used in separation applications.

1. Introduction

Typical structures of carbon nanotubes (CNTs) are chemically inert as they present a chemistry based only on sp^2 carbon. However, some applications such as electronics, catalysis, sensing, transport and separation require CNTs to have specific properties (e.g. conductivity, catalytic reactivity, surface chemistry, hydrophobicity/hydrophilicity, etc.) in order to achieve optimal performances. So far, different surface modification approaches aiming to tailor the chemical properties of CNTs have been explored [1–4]. Among the various approaches, chemical oxidation, covalent immobilisation and doping with foreign atoms are the most widely employed routes to modify CNTs. The structure of CNTs can be doped with different atoms such as N, P, S, etc. which are integrated into the hexagonal sp^2 carbon structure by substitution of C atoms. Nitrogen doping of CNTs structure is particularly attractive and favourable because N has close atomic size to that of carbon (i.e. nitrogen contains one additional electron as compared to carbon) and thus nitrogen-doped CNTs structure could exhibit novel electronic and catalytic properties [5]. Nitrogen doping of CNTs has been explored for tunning and enhancing their physical, chemical and catalytic activity properties [6–8].

CNTs-based composite membranes have been recently attracting much attention due to the outstanding features of CNTs with smooth hydrophobic graphitic walls, ordered and vertically aligned structures with high aspect ratio, chemical stability, mechanical robustness and ease of chemical functionalization. These features

* Corresponding authors.
E-mail addresses: abel.santos@adelaide.edu.au (A. Santos), dusan.losic@adelaide.edu.au (D. Losic).

http://dx.doi.org/10.1016/j.carbon.2016.05.043
0008-6223/

make CNTs-based composite membranes unique candidates to mimic protein channels in biological membranes [9,10] and have spread the applicability of CNTs-based composite membranes across a broad range of applications, such as water desalination, chemical separation, catalysis, drug delivery, sensing and energy storage [11–13]. For the most of these membranes, their properties and applications are dependent on the properties and chemical composition of inner nanotube surface. In the case of membrane separation applications, fluids and gases flow through the internal tubular structure of CNTs and therefore the transport property of these membranes is of great importance for achieving optimal performances for advanced processes (e.g. detection of chemical composition of complex mixtures, separation of chemical pollutants in contaminated water, removal of ions in desalination, etc.). So far, several molecular dynamics simulations and experimental studies have successfully demonstrated the outstanding transport properties and chemical selectivity of CNTs membranes for a broad range of gases and molecules [14–18].

Structurally, two configurations of CNTs-based composite membranes have been explored for separation/transport applications: namely; i) membranes with randomly distributed bundles of CNTs and ii) membranes featuring vertically aligned arrays of CNTs grown inside different templates. The latter configuration enables an extremely fast and controllable transport of molecules through CNTs, which increases their efficiencies in separation/filtration processes as compared to the former type [14,19]. Template-assisted synthesis method is the most widespread route for preparing composite membranes featuring vertically aligned arrays of CNTs. Among the different templates, silicon nitride, polymer matrices [20,21] and nanoporous anodic alumina membranes (NAAMs) produced by electrochemical anodization of aluminium have been demonstrated as unique platforms to produce CNTs membrane with precisely controlled geometric features. These templates can be fabricated with precisely engineered nanopores, which are perfect moulds to grow CNTs with vertically aligned nanotubular structure [22–27]. Direct template synthesis of CNTs by catalyst-free chemical vapour deposition (CVD) in these templates is of particular interest since this approach overcomes the inherent drawbacks of traditional fabrication methods used to prepare CNTs.

As mentioned above, doping CNTs with nitrogen could open new opportunities to explore and understand the influence of the chemical structure of CNTs on the transport performance of CNTs composite membranes, which is of critical importance for advancing the properties of these membranes for separation applications. So far, many studies have reported on the doping of CNTs with nitrogen [28–34]. Most of these studies are based on catalyst-based CVD processes using ferrocene as metal catalyst. It is worthwhile to note that nitrogen doping of CNTs using catalyst-based CVD approach results in CNTs with periodic interlinked structures inside the nanotubes (i.e. bamboo-like structure), which are not suitable for transport and separation applications [30,31]. Moreover, significant changes in the dimensions of N-doped CNTs were observed [28,29]. Therefore, to develop a facile route to dope the structure of CNTs with dopant atoms in a selective fashion without affecting their geometric features still remains challenging. To the best of our knowledge, the nitrogen doping of CNTs membranes by a catalyst-free CVD process has not been explored yet. Recently, we demonstrated that the transport and selectivity properties of composite membranes based on CNTs and nanoporous anodic alumina membranes (NAAMs) can be finely tuned by engineering the dimensional features of CNTs and the surface chemistry of their inner surface by post-oxidation treatment [35].

Herein, we present a facile synthesis method aiming to dope the structure of CNTs composite membranes with nitrogen atoms using a catalyst-free CVD approach. CNTs composite membranes were prepared by growing vertically aligned multi-walled carbon nanotubes (MWCNTs) inside the nanopores of NAAMs, which were used as templates. The role of C/N ratio of carbon and nitrogen precursor in the formation and nitrogen content of N-doped CNTs-NAAMs was determined by using different mixtures of precursors including *N,N*-dimethylformamide (DMF), pyridine and their mixtures with toluene and ethanol. The critical C/N atomic ratio required for preparation of N-doped CNTs composite membranes was established for the first time. A schematic illustration of the CVD fabrication process of undoped and N-doped CNTs-NAAMs composite membranes and the selective doping of CNTs structure are shown in Fig. 1.

The selective nitrogen doping of the inner and outer surfaces of CNTs during the synthesis step is characterized by a set of techniques in order to establish a solid and comprehensive rationale towards understanding and tailoring the properties of CNTs for different applications. Furthermore, the transport performance and chemical selectivity of the resulting composite membranes (i.e. undoped and N-doped CNTs-NAAMs composite membranes) is assessed by a series of experiments, revealing the importance of nitrogen doping on this property of CNTs.

2. Experimental details

2.1. Materials

High purity aluminium (Al) foils (thickness 0.32 mm, purity 99.999%) were obtained from Goodfellow Cambridge Ltd, UK. Copper chloride ($CuCl_2$), oxalic acid ($H_2C_2O_4$), chromium trioxide (CrO_3), phosphoric acid (H_3PO_4), hydrochloric acid (HCl), ethanol 99.7% (C_2H_6O), toluene 99.8% (C_7H_8), *N,N*-Dimethylformamide (DMF) (C_3H_7NO), pyridine (C_5H_5N), hydrofluoric acid (HF), Rose Bengal ($C_{20}H_4Cl_4I_4O_5 - (RosB)^{2-}$) and Tris(2,20-bipyridyl) dichlororuthenium(II) hexahydrate ($C_{30}H_{24}Cl_2N_6Ru\cdot 6H_2O - (Ru(BPY)_3)^{2+}$) were purchased from Sigma Aldrich (Australia) and used as received. High purity deionized (DI) water (resistivity 18.2 M Ω cm) from a Milli-Q water purification system was used to prepare all the solutions used in this study.

2.2. Fabrication of nanoporous anodic alumina membranes (NAAMs)

Nanoporous anodic alumina membrane templates were prepared by a two-step electrochemical anodization process using high purity Al foils following a previously reported method [22,36,37]. Briefly, circular Al chips with a diameter of 1.5 cm were first cleaned under sonication in ethanol and water for 10 min followed by electro-polishing in a mixture of $HClO_4$ and C_2H_6O 1:4 (*v:v*) at 20 V and 5 °C for 3 min and then dried under nitrogen stream. The electro-polished Al foils were anodized in 0.3 M aqueous oxalic acid electrolyte at 40 V and 6 °C using a two electrode electrochemical reactor equipped with temperature controller. The first anodization step was carried out for 20 h and the resulting nanoporous layer was selectively removed in a mixture of H_3PO_4 (0.4 M) and H_2CrO_7 (0.2 M) at 70 °C for 3 h in order to obtain hexagonally organized pits on the Al surface. The second anodization step was performed for 15 h to specifically obtain NAAMs with pore lengths of 50 ± 2 μm and pore diameter 40 ± 5 nm. The remaining aluminium substrate was removed in a saturated solution of HCl and $CuCl_2$. Finally, the oxide barrier layer at the bottom of NAAMs was chemically opened in 5 *wt* % H_3PO_4 at 35 °C. This process was performed by monitoring the current over time in a U-cell in order to have a precise control over the pore opening step and prevent the membranes from undesired pore

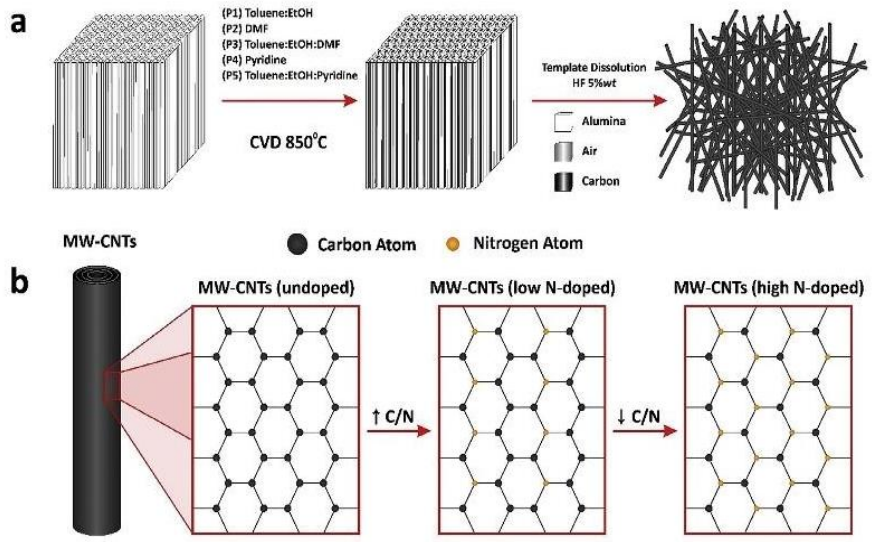

Fig. 1. Schematic representation of the fabrication process of undoped and N-doped CNTs-NAAMs and liberated CNTs. (a) Fabrication of CNTs composite membrane by catalyst free CVD process using NAAMs as host templates and liberation of CNTs by selective chemical etching of the host template and (b) schematic illustration showing how the graphitic structure of CNTs can be selectively doped with nitrogen atoms by controlling C/N ratio in the precursor mixture. (A colour version of this figure can be viewed online.)

widening [38,39]. The obtained NAAMs were finally rinsed with deionized water, dried under nitrogen stream and stored till further use.

2.3. Fabrication of undoped and N-doped CNTs-NAAMs composite membranes

CNTs were grown inside NAAMs by template synthesis using a catalyst-free CVD approach previously described [26]. This process was carried out in a CVD system consisting of a two-stage furnace equipped with a cylindrical quartz tube (Brother Furnace Co., LTD, China) (Fig. S1 – Supporting Information). Briefly, the NAAMs templates were sandwiched between two quartz plates and placed in the deposition zone of the CVD reactor. The reactor temperature was increased from 25 to 850 °C at a rate of 4 °C min^{-1} under constant argon flow at a rate of 1 dm^3 min^{-1}. Next, the carbon and nitrogen precursor was introduced into the CVD reactor by a particle generator (i.e. nebuliser) for 30 min. In this process, different precursors were explored in order to fabricate CNTs-NAAMs composites with different chemistries: namely, (i) a mixture of toluene and ethanol (1:1) (*v*:*v*) (denoted by P1) to produce undoped CNTs-NAAMs, and (ii) *N*,*N*-dimethylformamide (DMF) (denoted by P2), (iii) a mixture of toluene, ethanol and DMF (1:1:1) (*v*:*v*:*v*) (denoted by P3), (iv) pyridine (denoted by P4), and (v) a mixture of toluene, ethanol and pyridine (1:1:1) (*v*:*v*:*v*) (denoted by P5) to produce different types of N-doped CNTs-NAAMs.

2.4. Structural and chemical composition characterizations

The structural characterization of the undoped and N-doped CNTs-NAAMs was performed using a field emission gun scanning electron microscope (FEG-SEM Quanta 450). Transmission electron microscopy (Philips CM 200 TEM) was used to assess the internal structure of CNTs. For this, NAAMs were selectively dissolved in a 5 wt % HF solution to obtain liberated CNTs, which were subsequently washed with deionized water and ethanol. The chemical composition of undoped and N-doped CNTs-NAAMs and liberated CNTs was analysed by X-ray photoelectron spectroscopy (XPS Kratos Axis Ultra) using the Al Kα (1486.7 eV) monochromatic line. The graphitic structure of prepared undoped and N-doped CNTs-NAAM was assessed by Raman spectroscopy (Horiba LabRAM HR Evolution Raman microprobe spectrometer). Raman spectra were obtained using a He–Ne laser of 532 nm as an excitation source.

2.5. Transport studies of undoped and N-doped CNTs-NAAMs

The transport properties of undoped and N-doped CNTs-NAAMs were assessed by studying the transport of two model molecules with different hydrophilic-hydrophobic character and negatively and positively charge (i.e. $(RosB)^{2-}$ and $(Ru(BPY)_3)^{2+}$, respectively) using a H-tube permeation setup consisting of two half cells (i.e. feed and permeate cells) (Fig. S1 – Supporting Information). Separate permeation experiments were performed using aqueous solutions of $(RosB)^{2-}$ and $(Ru(BPY)_3)^{2+}$, in which 3 mL of 10 mM of dye solution was added to the feed cell and the same level of water was added to the permeate cell to avoid pressure driven transportation. CNTs-NAAMs were placed between these two halves and sealed by two polydimethylsiloxane (PDMS) slides in order to prevent leakage. The total exposed area of the membranes was 0.0314 cm^2. The diffusion of the dyes through the membranes was monitored in real-time in the permeate cell using a UV–Visible fibre optic spectrophotometer (USB4000 Ocean Optics). Concentrations of $(RosB)^{2-}$ and $(Ru(BPY)_3)^{2+}$ were detected at their maximum absorbance of 552 and 452 nm, respectively, and then fitted to a calibration curve obtained by measuring absorbance of known concentrations of each dye. All transport experiments were repeated three times and statistically treated calculating averages and standard deviations.

3. Result and discussion

3.1. Structural characterization of undoped and N-doped CNTs-NAAMs

Fig. 2 displays a set of SEM images of NAAMs used as a template to grow CNTs. Fig. 2a shows a representative top view SEM image of the structure of a NAAM produced through a two-step anodization process in oxalic acid electrolyte at 6 °C. This reveals that NAAMs

feature a hexagonal arrangement of nanopores with diameter of 40 ± 5 nm. A bottom view SEM image of NAAMs after pore opening process is showing in Fig. 2b, confirming that the produced membranes featured a through-hole nanoporous structure. Fig. 2c and d shows cross sectional view SEM images of NAAM showing its entire length (50 ± 2 μm) and vertically aligned cylindrical nanopores from top to bottom, respectively. It is worth stressing that the pore diameter and length of NAAMs used in this study were fixed by adjusting the anodization voltage and time, respectively (i.e. 40 V and 15 h). As demonstrated in our previous work, this fabrication process presents a broad flexibility and NAAMs can be produced with different pore dimensions [35]. Undoped and N-doped CNTs were grown inside the pores of NAAMs by the catalyst-free CVD process for 30 min using different carbon precursors are presented in Fig. 3. A SEM image of undoped CNTs-NAAM prepared by using P1 (toluene and ethanol 1:1) as a carbon precursor is shown in Fig. 3a. These CNTs presented an inner diameter of 49 ± 5 nm. SEM images of N-doped CNTs-NAAMs prepared by using P3 (toluene, ethanol and DMF 1:1:1), P4 (pyridine) and P5 (toluene, ethanol and pyridine 1:1:1) mixtures as carbon and nitrogen precursors are presented in Fig. 3c, e, and g. Note that, the increment in the pore diameter of both undoped and N-doped CNTs-NAAMs over the pore diameter of as-produced NAAMs (i.e. 49 nm and 40 nm, respectively) is thought to be associated with the loss of water content and reorganization of alumina in the NAAMs to form a different crystallographic phase during CVD process (i.e. performed at 850 °C) [40,41]. These results confirm the successful fabrication of undoped and N-doped CNTs-NAAMs using aforementioned precursors selected through initial optimization process, without observing significant morphological differences between them.

In contrast, our preliminary investigation showed no CNTs were grown inside NAAMs when P2 (*N*,*N*-Dimethylmethanamide, DMF) was used as a precursor under the same experimental conditions (i.e. flowing rate, temperature, and deposition time). Considering that the total amount of this precursor fed into the CVD reactor for 30 min deposition time was almost the same as other precursors (~10 mL) we came into conclusion that C/N ratio in precursor could play an important role. This result indicates that DMF (C_3H_7NO) is not an efficient carbon and nitrogen precursor to grow N-doped CNTs due to the high % of N in DMF with an atomic C/N ratio of 3:1 that accompanied with presence of another heteroatom (i.e. oxygen). To validate our hypothesis that C/N ratio is critical for N-doped CNTs formation, we increased the amount of carbon by adding toluene (C_7H_8) into DMF (C_3H_7NO) with different ratio. Our preliminary results showed that when the C/N ratio increased to ~5:1 the N-doped CNTs inside NAAMs started to be formed. To prove this finding that minimum atomic C/N ratio of 5:1 is critical, we selected another carbon and nitrogen precursor with this ratio; P4 (pyridine, C_5H_5N) and successfully produce N-doped CNTs (Fig. 3e and f). This finding clearly indicates the crucial role of the precursor in the formation of undoped and N-doped CNTs to produce suitable composite membranes for transport applications [42].

During the catalyst-free CVD process, carbon and N-doped carbon are deposited on the internal wall surface of the NAAM's pores and CNTs grow inside the entire length of NAAMs replicating the nanopore geometry with precision. This can be seen from cross sectional images (Fig. S2 – Supporting Information), which illustrate CNTs protruding out of NAAM pores after fracture of the

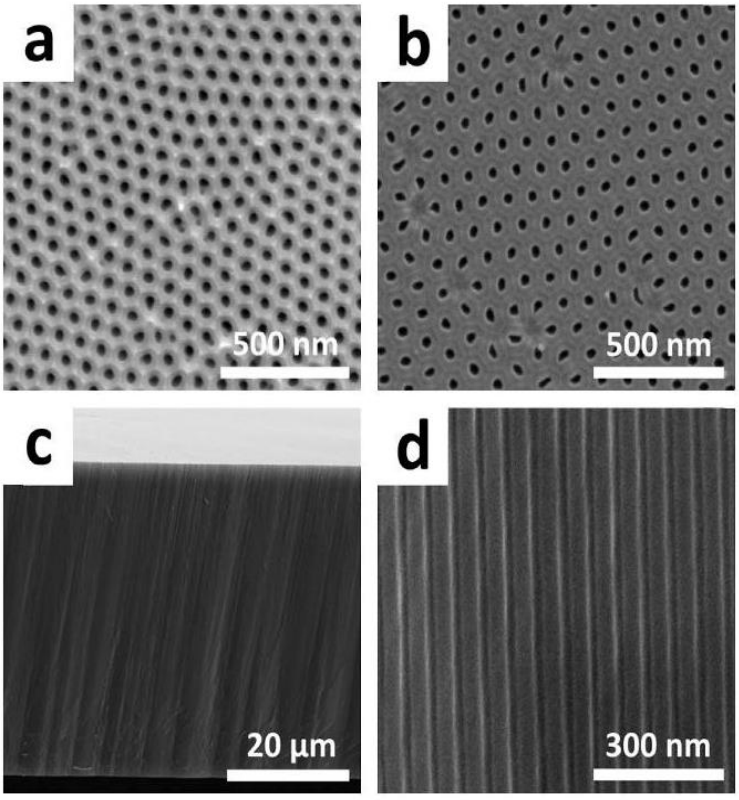

Fig. 2. Set of SEM images of NAAMs template showing top, bottom and cross-sectional structure. (a) Top view SEM image of a typical NAAM structure produced through a two-step anodization process in oxalic acid electrolyte at 6 °C; (b) bottom view of NAAM; (c) cross-sectional view (higher bright area is the membrane's top surface) showing entire length of the NAAM and (d) magnified view of (c) showing straight vertically aligned cylindrical of nanopores used to grow CNTs.

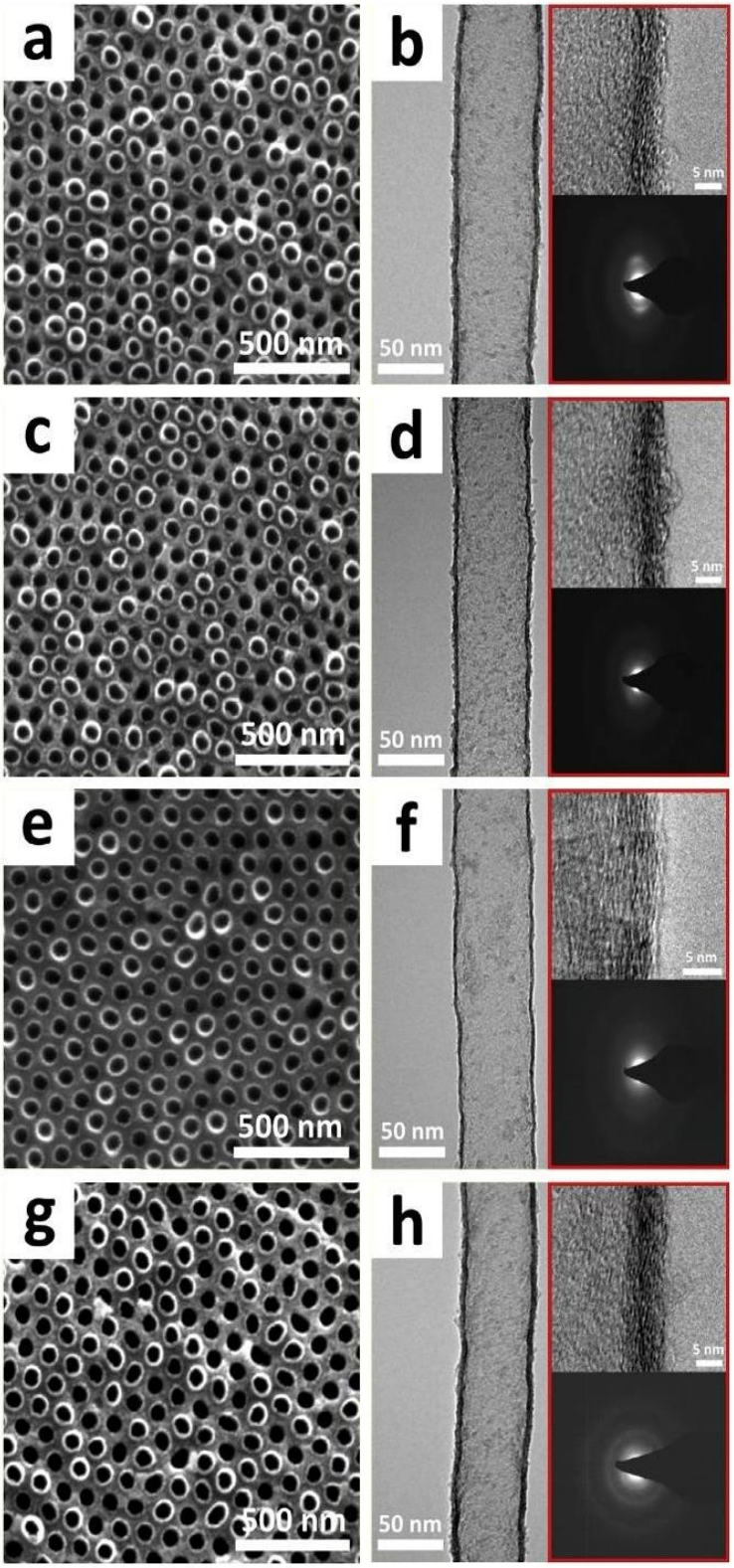

Fig. 3. Set of comparative top view SEM images of prepared CNTs-NAAMs and HRTEM images with SAED patterns of liberated CNTs produced by catalyst-free CVD process using different carbon precursors. (a and b) Undoped CNTs-NAAMs and CNT prepared by P1 (toluene and ethanol 1:1) (inset: magnified view and SAED); (c and d) N-doped CNTs-NAAMs and CNT prepared by P3 (toluene, ethanol and DMF 1:1:1), (inset: magnified view and SAED); (e and f) N-doped CNTs-NAAMs and CNT prepared by P4 (pyridine) (inset: magnified view and SAED) and (g and h) N-doped CNTs-NAAMs and CNT prepared by P5 (toluene, ethanol and pyridine 1:1:1) (inset: magnified view and SAED). For HRTEM images: the left side of the wall corresponds to the inside of the tube. (A colour version of this figure can be viewed online.)

membrane. Template-based catalyst-free CVD process enables the fabrication of vertically aligned arrays of N-doped CNTs that replicate the pore dimensions of the template with precision due to the catalytic role of alumina. In contrast, as previous studies have reported, a significant change in the dimensions of N-doped CNTs takes place when these nanostructures are prepared by catalyst-based CVD process using a mixture of toluene and benzylamine [29] or toluene and acetonitrile [28] as precursors. In our study, the integrity and uniformity of undoped and N-doped CNTs structures is not compromised, as it can be seen from SEM images of CNTs liberated by selective dissolution of NAAMs templates (Fig. S3 – Supporting Information). TEM images of undoped and N-doped liberated CNTs (Fig. 3) provide further evidence of the integrity and uniformity of these structures. The wall thickness of CNTs prepared using P1, P3, P4 and P5 as carbon precursors were found to be 5 ± 2 nm, 4 ± 2 nm, 3 ± 2 nm and 5 ± 2 nm, respectively (Fig. 3b, d, f and h). The thin wall when P4 was solely used as precursor (i.e. 3 nm) and the absence of carbon deposition for P2 to produce N-doped CNTs indicate that the C/N ratio of 5:1 is the minimum sufficient ratio to form N-doped CNTs. These images also reveal that the resulting N-doped CNTs have straight and hollow cylindrical geometric features (i.e. precise replica of the inner geometry of the nanopores in NAAMs), which are not attainable by a catalyst-based process, where bamboo-like structures are always present as a result of the interaction between the catalyst metal particles and CN species (i.e. difference in the diffusion of CN species along the catalyst particle between bulk and surface) [43–45]. This type of structures are not uniform and reproducible and will negatively influence many important properties of CNTs membranes related the molecular transport, or electronic conductivity, mechanical strength, chemical stability and so on.

The prepared undoped and N-doped CNTs was characterized by high resolution TEM analysis to determine their structures. The HRTEM image of undoped CNT's wall shows many parallel graphene layers in the direction of the nanotubes axis (inset in Fig. 3b). These layers are wrinkled to some extent indicating a poor graphitic structure of the prepared CNTs. HRTEM images of N-doped CNTs (inset in Fig. 3d, f and h) reveal no significant differences in their graphitic structure to that of undoped CNTs. It should be noted that the poor graphitic structure of prepared CNTs, which is a characteristic of CNTs produced by a catalyst-free CVD process [27,46,47], makes it difficult to reveal changes induced by incorporation of N atoms in the graphitic structure CNTs. Therefore, electron diffraction analysis over selected areas (SAED) was used to determine the graphitic structure of the undoped and N-doped CNTs. The SAED pattern of undoped CNTs (inset in Fig. 3b) shows a pair of small arcs and weak 10 and 11 diffraction rings. The pair of small arcs corresponds to the 002 diffraction, indicating some orientation of the 002 planes in the CNTs and its poor graphitic structure as a result of absence of the metal catalyst, which is in good agreement with previous reports [48]. For N-doped CNTs, the SAED patterns (inset in Fig. 3d, f and h) show only weak 10 and 11 diffraction rings indicating a decrease in the graphitic structure of CNTs as a result of incorporation of N atoms in the carbon network. In our previous work we found that graphitic structure of prepared CNTs can be significantly improved by additional annealing at higher temperature (>900 °C) but it is not performed in this work.

3.2. Chemical characterizations of undoped and N-doped CNTs-NAAMs and liberated CNTs

XPS analysis was used to obtain quantitative and qualitative information about the chemical composition of undoped and N-doped CNTs-NAAMs (i.e. inner surface) and liberated CNTs (i.e. outer surface). The XPS survey spectra of undoped and N-doped CNTs-NAAMs (insets in Fig. 4) show the presence of C, O, N and Al in the chemical structure of these composite membranes. The exclusive presence of these elements provides an idea about both the elemental composition and the high level of purity of these membranes. Undoped CNTs-NAAMs had a 0% of nitrogen, and nitrogen contents in N-doped CNTs-NAAMs determined from XPS analysis are listed in Table 1. Substitution of half of toluene and ethanol volume to the P2 and P4 (i.e. P3 and P5, respectively) yields CNTs containing 3.35% and 3.92% of nitrogen, respectively. The nitrogen content in CNTs increases to 6.92% when P4 was used as a precursor. Fig. 4 shows the high resolution C 1s and N 1s spectra of undoped and N-doped CNTs-NAAMs. Fig. 4a, b, d and f show the high resolution C 1s spectra of undoped and N-doped CNTs-NAAMs, which are deconvoluted into five peaks that are located at binding energies of 284.6 ± 0.2 eV, 285.7 ± 0.3 eV, 287.6 ± 0.2 eV, 289.6 ± 0.2 eV and 291.6 ± 0.3 eV. These peaks are associated with sp^2 bonds of graphitic carbon, sp^3 network of carbon atoms, C=O (ketone/aldehyde), O=C–O (carboxyl/ester) groups, and π-π^* transition of carbon atoms in graphene structures, respectively [49,50]. The peaks in the binding energies of 285.7 ± 0.3 eV and 287.6 ± 0.2 eV could be related to the different biding states between C and N [49,51]. N-doped CNTs-NAAMs are less hydrophobic than undoped CNTs-NAAMs, which is indicated by the decline in the sp^2 carbon peak (284.6 eV) from 88.5% of undoped CNTs-NAAMs to 78.68%, 73.22% and 82.75% for N-doped CNTs-NAAMs prepared using P3, P4 and P5 as precursors, respectively. Moreover, sp^3 hybridized structure increased significantly from 2.50% of undoped to 11.16%, 15.92% and 8.41% for the N-doped CNTs-NAAMs which again follow trend of C/N ratio in precursors.

The XPS N 1s spectra of N-doped CNTs-NAAMs showed two main peaks located at binding energies of 397.8 ± 0.5 eV and 400.1 ± 0.2 eV (Fig. 4c, e, and g). The former can be assigned to nitrogen bonded to sp^3 hybridized carbon (i.e. C–N) while the latter can be assigned to nitrogen bonded to sp^2 hybridized carbon (i.e. C=N) [51,52]. The intensity of the peaks in C 1s and N 1s spectra of undoped and N-doped CNTs-NAAMs are summarized in Table 1.

Liberated CNTs were analysed by XPS to shed light on the chemical composition of the outer surface of CNTs after incorporation of nitrogen. The XPS survey spectra of undoped and N-doped CNTs (insets in Fig. S4 – Supporting Information) show the presence of C, O, and N. The nitrogen contents in N-doped CNTs were 1.75, 6.26 and 2.64% for CNTs prepared using P3, P4 and P5 as precursors, respectively. This clearly confirms that, in addition to the inner surface, the outer surface of CNTs was doped with nitrogen in this process. The high resolution C 1s and N 1s spectra of undoped and N-doped CNTs are shown in Fig. S4 – Supporting Information. The intensity of the peaks in C 1s and N 1s spectra and the elemental composition of undoped and N-doped CNTs are summarized in Table S1. An important feature of the template-directed catalyst-free CVD process is that it allows the fabrication of CNTs with controlled surface chemistry for both inner and outer surfaces through one step (i.e. synthetic step).

The graphitic features of undoped and N-doped CNTs-NAAMs were also characterized by Raman spectroscopy. All these membranes showed the characteristic Raman profile of CNTs (i.e. partially overlapped D and G band peaks) (Fig. 5) with a G band peak (graphitic or highly ordered CNTs sidewalls) around 1585 cm^{-1} and a D band peak (disordered CNTs sidewalls) around 1340 cm^{-1}. However, the overlap between G and D band peaks become more pronounced for N-doped CNTs-NAAMs. This was accompanied with a slight increment in the line width of the peak, indicating a poor graphitic feature of CNTs prepared through template-directed method using a catalyst-free CVD approach. These results indicate a certain degree of structural disorder in N-doped CNTs-NAAMs as compared to those composite membranes

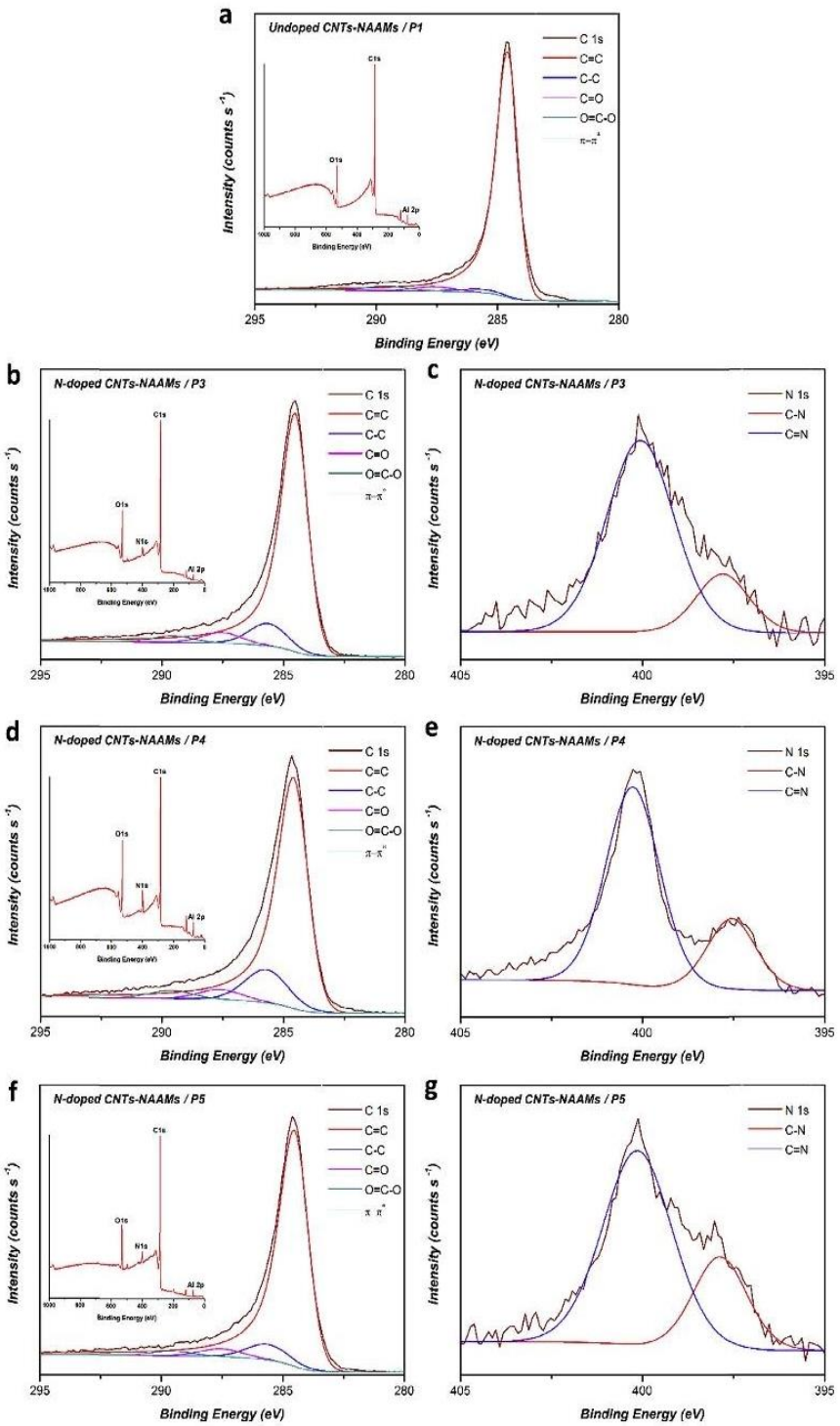

Fig. 4. C 1s and N 1s core-level spectra of undoped and N-doped CNTs-NAAMs. (a) C 1s of undoped CNTs-NAAMs prepared by P1 (toluene and ethanol 1:1) (inset: survey spectrum); (b) C 1s of N-doped CNTs-NAAMs prepared by P3 (toluene, ethanol and DMF 1:1:1) (inset: survey spectrum); (c) N 1s of N-doped CNTs-NAAMs; (d) C 1s of N-doped CNTs-NAAMs prepared by P4 (pyridine) (inset: survey spectrum); (e) N 1s of N-doped CNTs-NAAMs; (f) C 1s of N-doped CNTs-NAAMs prepared by P5 (toluene, ethanol and pyridine 1:1:1) (inset: survey spectrum) and (g) N 1s of N-doped CNTs-NAAMs. (A colour version of this figure can be viewed online.)

prepared with a pure carbon source, which is in good agreement with the results obtained from SAED and XPS analysis. However, it is worth stressing that we did not observe neither the change in peaks positions nor the presence of I band peak (around 1220 cm^{-1}) ascribed to the disruptions in the sp^2 carbon framework and to the impurities in the graphite lattice reported in

Table 1
Summary of elemental composition and high-resolution C 1s and N 1s spectra of undoped and N-doped CNTs-NAAMs prepared through catalyst-free CVD process using different precursors.

	Sample	Undoped CNTs-NAAMs	N-doped CNTs-NAAMs	N-doped CNTs-NAAMs	N-doped CNTs-NAAMs
	Precursor	Toluene:EtOH P1	Toluene:EtOH:DMF P3 (C/N = 12/1)	Pyridine P4 (C/N = 5/1)	Toluene:EtOH:Pyridine P5 (C/N = 14/1)
	Peak assignment	Intensity (%)			
C	–	88.08	82.85	75.33	82.06
O	–	7.17	9.98	11.18	8.87
N	–	_	3.35	6.92	3.92
Al	–	4.51	3.40	6.41	3.77
C1s	C=C	88.50	78.68	73.22	82.75
	C–C/C–N	2.50	11.16	15.92	8.41
	C=O/C–N	3.23	5.33	4.84	4.33
	O=C–O	3.32	3.24	3.87	2.49
	π-π^*	2.45	1.59	2.15	2.02
N1s	C–N	_	19.40	24.53	26.93
	C=N	_	80.60	75.47	73.07

Refs. [28,53]. It can be concluded from XPS and Raman analysis of undoped and N-doped CNTs-NAAMs and liberated tubes that N atoms were incorporated into the bulk structure of CNTs, as denoted by the presence of nitrogen in both inner and outer surfaces, resulting in more hydrophilic surface chemistry and less graphitised structure as compared to undoped CNTs-NAAMs. Nevertheless, N doping did not alter the graphitic structure of CNTs in a significant manner, as revealed by the Raman analysis. Additionally, the nitrogen content in CNTs-NAAMs can be finely tuned by controlling the concentration of nitrogen in the precursor mixture. This is of great importance for expanding and spreading the applicability of CNTs towards relevant applications such as electronics, separation and medicine [54].

3.3. Molecular transport study using undoped and N-doped CNTs-NAAMs

There are many possible applications of N-doped CNTs-NAAMs composite membrane and in this work we selected to explore their transport and selectivity properties with aim to demonstrate how these properties can be tailored by doping process. For that purpose, undoped and N-doped CNTs-NAAMs were explored by performing separate permeation experiments of two model molecules with different hydrophilic-hydrophobic character and charge properties (i.e. $(RosB)^{2-}$ and $(Ru(BPY)_3)^{2+}$, respectively) using a H-tube permeation setup. Fig. 6 shows representative plots of the transport of $(RosB)^{2-}$ and $(Ru(BPY)_3)^{2+}$ through undoped and N-doped CNTs-NAAMs prepared through catalyst-free CVD process using different carbon and nitrogen precursors as a function of time. The diffusional flux and concentration change rate in the permeate cell data for $(RosB)^{2-}$ and $(Ru(BPY)_3)^{2+}$ transport through undoped and N-doped CNTs-NAAMs are summarized in Table 2. The transport of $(RosB)^{2-}$ and $(Ru(BPY)_3)^{2+}$ were found to be linear as denoted by the straight lines shown in Fig. 6. This indicates a steady state transport, which can be described by the Fick's first law diffusion across the CNTs composite membrane [55] represented as:

$$J = -D\frac{dC}{dx} \quad (1)$$

where, J is diffusion flux, D is the diffusion coefficient, dC is the change in concentration across a distance dx in one dimension (i.e. concentration gradient). Several parameters could play a role in the overall transport of dye molecules through CNTs-NAAMs such as; the geometric features, the chemical character of CNTs-NAAMs and the diffusion coefficient of the transported dye molecule. The latter is attributed to factors such as the molecule's size, charge, shape and solubility. In the present study, the geometric features of CNTs and the initial concentration of dye molecules in the feed cell were kept constant. Moreover, the transported molecules have similar sizes (ca 1.2 nm) but different chemical composition, charge and interfacial properties. Hence, the flux of a particular dye through a given CNTs-NAAMs system is expected to be influenced mainly by the chemical character of the membrane and the dye charge properties. To this end, we wanted demonstrate the differences in transport of two dyes molecules with different hydrophilic-hydrophobic and charge properties (i.e. $(RosB)^{2-}$ and $(Ru(BPY)_3)^{2+}$) when flowing through membranes with different chemical characters (i.e. undoped and N-doped CNTs-NAAMs).

Fig. 6 represent molecular transport of two model molecules $(RosB)^{2-}$ and $(Ru(BPY)_3)^{2+}$ over time through undoped CNTs-NAAMs (Fig. 6a). The diffusional flux of the positively hydrophobic molecule ($(Ru(BPY)_3)^{2+}$) was found to be ca 3.1 times higher than that of the negatively hydrophilic molecule ($(RosB)^{2-}$) (Table 2). This could be ascribed to the repulsion interaction or

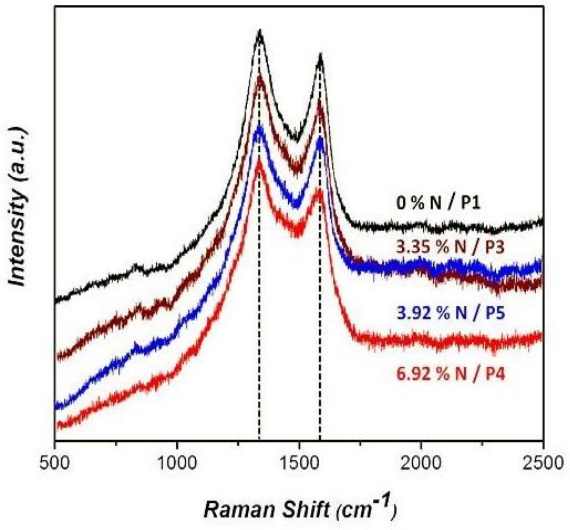

Fig. 5. Raman spectra of undoped and N-doped CNTs-NAAMs with nitrogen content of 0%, 3.35%, 3.92% and 6.92% prepared by P1 (toluene and ethanol 1:1), P3 (toluene, ethanol and DMF 1:1:1), P5 (toluene, ethanol and pyridine 1:1:1) and P4 (pyridine), respectively. (A colour version of this figure can be viewed online.)

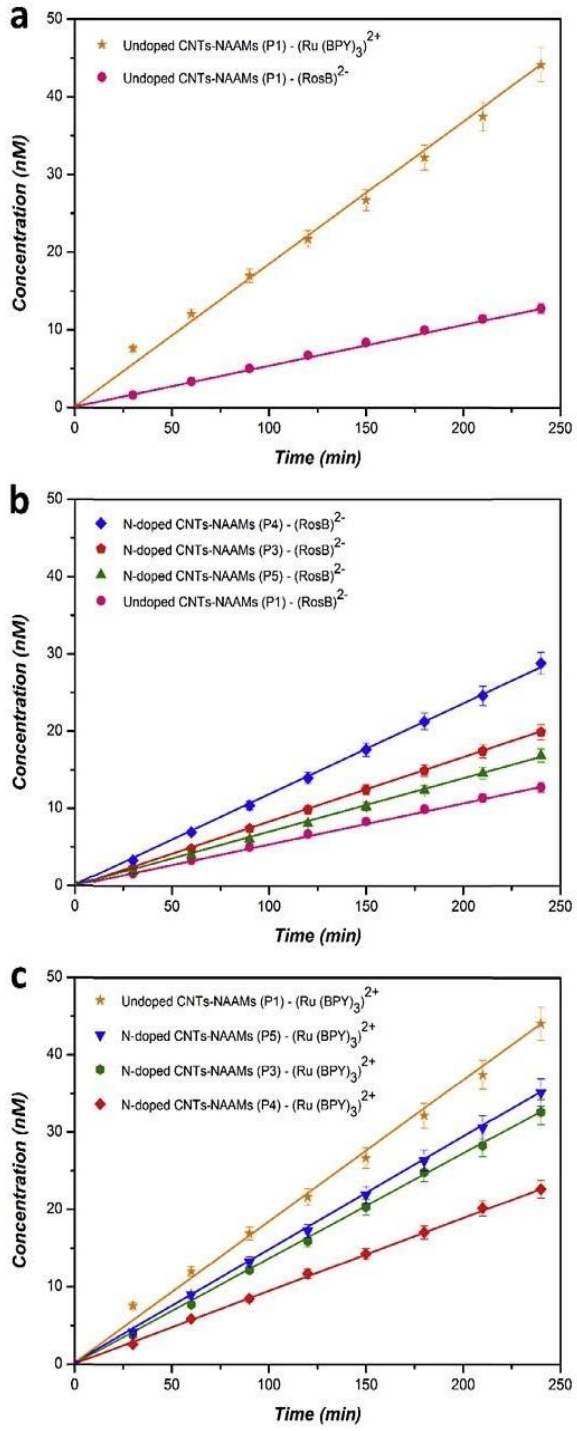

Fig. 6. Molecular transport study of $(RosB)^{2-}$ and $(Ru(BPY)_3)^{2+}$ through undoped and N-doped CNTs-NAAMs. (a) Diffusion of $(RosB)^{2-}$ and $(Ru(BPY)_3)^{2+}$ through undoped CNTs-NAAMs; (b) diffusion of $(RosB)^{2-}$ through undoped CNTs-NAAMs prepared by P1 and N-doped CNTs-NAAMs prepared by P3, P4 and P5 and (c) diffusion of $(Ru(BPY)_3)^{2+}$ through undoped CNTs-NAAMs prepared by P1 and N-doped CNTs-NAAMs prepared by P3, P4 and P5. (A colour version of this figure can be viewed online.)

lower friction between the hydrophobic graphitic walls of CNTs and the hydrophobic dye $(Ru(BPY)_3)^{2+}$. These results are in agreement with previous studies and our work [35] revealing the selective transport properties of undoped CNTs-NAAMs. The precise structure of the pore wall of CNTs prepared by templated-assisted catalyst-free CVD process makes the interaction between the inner surface of CNTs and the molecules of transported dye dominant at such nanoscale regime. Further decrement in the pore diameter of CNTs would significantly increase the effect of such interaction, enhancing the selectivity and transport properties of these membranes. The transport data obtained from the undoped CNTs-NAAMs are further compared to the transport data of N-doped CNTs-NAAMs to determine whether changing the membrane surface's chemical character resulting from doping CNTs with different content of nitrogen influenced the chemical selectivity of CNTs-NAAMs. Fig. 6b displays a representative plot of the transport of $(RosB)^{2-}$ through undoped and series of N-doped CNTs-NAAMs with different N doping levels as a function of time. These results show that the transport rate of hydrophilic $(RosB)^{2-}$ through N-doped CNTs-NAAMs is considerably higher compared with undoped CNTs-NAAMs with noticeable impact of level of N doping. Table 2 shows concentration change rates in the permeate cell of $5.48 \pm 0.13 \times 10^{-2}$ nM min^{-1} for undoped CNTs-NAAMs and $8.35 \pm 0.11 \times 10^{-2}$ nM min^{-1}, $1.18 \pm 0.17 \times 10^{-1}$ nM min^{-1} and $6.94 \pm 0.13 \times 10^{-2}$ nM min^{-1} for N-doped CNTs-NAAMs prepared from P3, P4 and P5, respectively, after flowing $(RosB)^{2-}$. It was found the correlation between level of hydrophilicity and the diffusional fluxes for $(RosB)^{2-}$ in the N-doped CNTs-NAAMs showing the fastest flux for N-doped CNTs membranes with the most hydrophilic properties having higher % of N prepared using precursor P4 (pyridine) (Table 2). Fig. 6c presents a comparative plot of the transport of hydrophobic $(Ru(BPY)_3)^{2+}$ through undoped and series of N-doped CNTs-NAAMs with different N doping levels as a function of time. Transport graphs show that the transport of hydrophobic molecules through the N-doped CNTs-NAAMs is reduced in comparison to the transport through the undoped CNTs-NAAMs. Table 2 shows that the concentration change rates in the permeate cell after flowing $(Ru(BPY)_3)^{2+}$ across different membranes have decreased from $1.72 \pm 0.21 \times 10^{-1}$ nM min^{-1} for undoped CNTs-NAAMs to $1.36 \pm 0.13 \times 10^{-1}$ nM min^{-1}, $9.61 \pm 0.11 \times 10^{-2}$ nM min^{-1}, and $1.46 \pm 0.16 \times 10^{-1}$ nM min^{-1} for N-doped CNTs-NAAMs prepared from P3, P4 and P5, respectively. The corresponding transport fluxes of 5.48 ± 0.13 nmol min^{-1} cm^{-2}, 4.33 ± 0.12 nmol min^{-1} cm^{-2}, 3.06 ± 0.10 nmol min^{-1} cm^{-2}, and 4.65 ± 0.23 nmol min^{-1} cm^{-2} were determined, respectively. The correlation with level of hydrophilicity is again observed showing the largest impact on transport for N-doped CNTs membranes with most hydrophilic properties having higher % of N prepared using precursor P4 (pyridine). The N-doped CNTs-NAAMs exhibits more hydrophilic properties than those of undoped CNTs-NAAMs, as confirmed by XPS analysis, and hence facilitate the transport of hydrophilic dye molecules and decrease transport of hydrophobic ones.

These results confirm that the chemical character of CNTs-NAAMs, in particular the inner wall surface of nanotubes where the influence of molecular flow is the most significant, plays a crucial role on the behaviour of molecules transported and their transport performance. Results demonstrate that the chemical character of CNTs-NAAMs tuned by the level of nitrogen doping can control transport properties of membranes and used as a strategy to tailor their separation performances based on chemical selectivity. An important feature of presented templated-assisted catalyst-free CVD method is that it allows the fabrication of N-doped CNTs membrane with tuneable chemical character without occlusion of their inner hollow structure or compromising their geometric features and morphology which is main obstacle in previously reported methods. It is worth noting that the chemical

Table 2
Diffusional flux and concentration change rate in the permeate cell data for ionic dye molecules ($(RosB)^{2-}$ and $(Ru(BPY)_3)^{2+}$) transport through undoped and N-doped CNTs-NAAMs prepared through catalyst-free CVD process using different precursors (0.0314 cm^2 area).

Membrane/precursor used	Concentration change rate in the permeate cell ($nM\ min^{-1}$)		Diffusional flux rate ($nmol\ min^{-1}\ cm^{-2}$)	
	$(RosB)^{2-}$	$(Ru(BPY)_3)^{2+}$	$(RosB)^{2-}$	$(Ru(BPY)_3)^{2+}$
Undoped CNTs-NAAMs/P1	$5.48 \pm 0.13 \times 10^{-2}$	$1.72 \pm 0.21 \times 10^{-1}$	1.75 ± 0.09	5.48 ± 0.13
N-doped CNTs-NAAMs/P3	$8.35 \pm 0.11 \times 10^{-2}$	$1.36 \pm 0.13 \times 10^{-1}$	2.66 ± 0.11	4.33 ± 0.12
N-doped CNTs-NAAMs/P4	$1.18 \pm 0.17 \times 10^{-1}$	$9.61 \pm 0.11 \times 10^{-2}$	3.76 ± 0.17	3.06 ± 0.10
N-doped CNTs-NAAMs/P5	$6.94 \pm 0.13 \times 10^{-2}$	$1.46 \pm 0.16 \times 10^{-1}$	2.21 ± 0.13	4.65 ± 0.23

character of the outer surface of CNTs can be tuned by this method as well, as proved by XPS analysis of liberated CNTs, providing the capability of this approach for making N-doped MWCNTs for a broad applications. Consider that internal chemistry of these N-doped CNTs can be changed by simple surface modifications process before liberation allowing easy preparation of CNTs with different internal and external chemistry that is very challenging synthetic problem.

4. Conclusion

We have reported a facile approach aiming to fabricate CNTs composite membranes doped with different level of nitrogen using catalyst-free CVD process and NAAMs as templates. N-doping of the inner and outer surfaces of CNTs was demonstrated for the first time using specific selection of carbon and nitrogen precursors. Our results reveal that the C/N ratio of carbon and nitrogen precursor plays a crucial role in the formation of N-doped CNTs-NAAMs. It was found out that a minimum 5:1 C/N ratio is required to achieve the formation of N-doped CNTs inside pore structure of NAAMs template. By the use of different carbon/nitrogen precursors with different C/N ratios, a selective nitrogen doping of CNTs membranes with different nitrogen content (3.35–6.92%) was demonstrated. Structural and chemical characterizations of the N-doped CNTs-NAAMs composite membranes have revealed that N-doped CNTs formed inside NAAMs templates replicate the geometric features of the nanopores in the template with precision, without the presence of periodic interlinked structures in their inner hollow structure. XPS analysis confirmed the hydrophilic nature of N-doped CNTs-NAAMs, over the hydrophobic character of undoped CNTs-NAAMs. Molecular transport studies of hydrophobic and hydrophilic dye molecules through series of N-doped CNTs-NAAMs compared with undoped CNTs-NAAMs (control) have revealed the tunability and enhancement in the transport performance and chemical selectivity properties of CNTs-NAAMs after nitrogen doping. These results provide a new knowledge and technological advances in synthesis of doped CNTs-based composite membranes with tailorable transport and chemical selectivity performances, opening new opportunities to spread the applicability of these membranes across a broad range of fields and applications. Furthermore, the presented synthesis method could pave the way towards extending the applications of these membranes based on their unique electronic, catalytic, electrochemical, charge transport and chemical properties.

Acknowledgement

Authors acknowledge the financial support provided by the Australian Research Council (FT 110100711 and DE140100549). The authors acknowledge the facilities and the scientific and technical assistance of the Australian Microscopy & Microanalysis Research Facility at the Electron Microscope Unit, The University of Adelaide. Mohammed Alsawat thanks Taif University (Ministry of Education, Saudi Arabia) for funding his scholarship.

Appendix A. Supplementary data

Supplementary data related to this article can be found at http://dx.doi.org/10.1016/j.carbon.2016.05.043.

References

[1] Á. Kukovecz, T. Kanyó, Z. Kónya, I. Kiricsi, Long-time low-impact ball milling of multi-wall carbon nanotubes, Carbon 43 (5) (2005) 994–1000.
[2] B. Ni, S.B. Sinnott, Chemical functionalization of carbon nanotubes through energetic radical collisions, Phys. Rev. B 61 (24) (2000) R16343.
[3] K. Balasubramanian, M. Burghard, Chemically functionalized carbon nanotubes, Small 1 (2) (2005) 180–192.
[4] A. Star, Y. Liu, K. Grant, L. Ridvan, J.F. Stoddart, D.W. Steuerman, et al., Noncovalent side-wall functionalization of single-walled carbon nanotubes, Macromolecules 36 (3) (2003) 553–560.
[5] M. Terrones, A. Jorio, M. Endo, A. Rao, Y. Kim, T. Hayashi, et al., New direction in nanotube science, Mater. Today 7 (10) (2004) 30–45.
[6] K.-Y. Chun, H.S. Lee, C.J. Lee, Nitrogen doping effects on the structure behavior and the field emission performance of double-walled carbon nanotubes, Carbon 47 (1) (2009) 169–177.
[7] S.-W. Bian, Z. Ma, W.-G. Song, Preparation and characterization of carbon nitride nanotubes and their applications as catalyst supporter, J. Phys. Chem. C 113 (20) (2009) 8668–8672.
[8] K. Gong, F. Du, Z. Xia, M. Durstock, L. Dai, Nitrogen-doped carbon nanotube arrays with high electrocatalytic activity for oxygen reduction, Science 323 (5915) (2009) 760–764.
[9] A. Noy, H.G. Park, F. Fornasiero, J.K. Holt, C.P. Grigoropoulos, O. Bakajin, Nanofluidics in carbon nanotubes, Nano Today 2 (6) (2007) 22–29.
[10] M. Majumder, V. Clayton, A.P. Ajayan, 1.14 carbon nanotube membranes: a new Frontier in membrane science, Compr. Membr. Sci. Eng. 1 (2010) 291–310.
[11] B. Corry, Designing carbon nanotube membranes for efficient water desalination, J. Phys. Chem. B 112 (5) (2008) 1427–1434.
[12] M. Majumder, A. Stinchcomb, B.J. Hinds, Towards mimicking natural protein channels with aligned carbon nanotube membranes for active drug delivery, Life Sci. 86 (15) (2010) 563–568.
[13] A.L.M. Reddy, S.R. Gowda, M.M. Shaijumon, P.M. Ajayan, Hybrid nanostructures for energy storage applications, Adv. Mater. 24 (37) (2012) 5045–5064.
[14] J.K. Holt, H.G. Park, Y. Wang, M. Stadermann, A.B. Artyukhin, C.P. Grigoropoulos, et al., Fast mass transport through sub-2-nanometer carbon nanotubes, Science 312 (5776) (2006) 1034–1037.
[15] M. Majumder, N. Chopra, R. Andrews, B.J. Hinds, Nanoscale hydrodynamics: enhanced flow in carbon nanotubes, Nature 438 (7064) (2005) 44.
[16] A.I. Skoulidas, D.M. Ackerman, J.K. Johnson, D.S. Sholl, Rapid transport of gases in carbon nanotubes, Phys. Rev. Lett. 89 (18) (2002) 185901.
[17] V.P. Sokhan, D. Nicholson, N. Quirke, Fluid flow in nanopores: accurate boundary conditions for carbon nanotubes, J. Chem. Phys. 117 (18) (2002) 8531–8539.
[18] Z. Mao, S.B. Sinnott, Separation of organic molecular mixtures in carbon nanotubes and bundles: molecular dynamics simulations, J. Phys. Chem. B 105 (29) (2001) 6916–6924.
[19] M. Endo, H. Muramatsu, T. Hayashi, Y. Kim, M. Terrones, M. Dresselhaus, Nanotechnology:'Buckypaper'from coaxial nanotubes, Nature 433 (7025) (2005) 476.
[20] B.J. Hinds, N. Chopra, T. Rantell, R. Andrews, V. Gavalas, L.G. Bachas, Aligned multiwalled carbon nanotube membranes, Science 303 (5654) (2004) 62–65.
[21] C.-M. Seah, S.-P. Chai, A.R. Mohamed, Synthesis of aligned carbon nanotubes, Carbon 49 (14) (2011) 4613–4635.
[22] H. Masuda, K. Fukuda, Ordered metal nanohole arrays made by a two-step replication of honeycomb structures of anodic alumina, Science 268 (5216) (1995) 1466–1468.
[23] H. Masuda, F. Hasegwa, S. Ono, Self-Ordering of cell arrangement of anodic porous alumina formed in sulfuric acid solution, J. Electrochem. Soc. 144 (5)

(1997) L127–L130.
[24] H. Masuda, K. Yada, A. Osaka, Self-ordering of cell configuration of anodic porous alumina with large-size pores in phosphoric acid solution, Jpn. J. Appl. Phys. 37 (11A) (1998) L1340.
[25] T. Kyotani, L.-f. Tsai, A. Tomita, Formation of ultrafine carbon tubes by using an anodic aluminum oxide film as a template, Chem. Mater. 7 (8) (1995) 1427–1428.
[26] G. Che, B. Lakshmi, C. Martin, E. Fisher, R.S. Ruoff, Chemical vapor deposition based synthesis of carbon nanotubes and nanofibers using a template method, Chem. Mater. 10 (1) (1998) 260–267.
[27] T. Kyotani, L.-f. Tsai, A. Tomita, Preparation of ultrafine carbon tubes in nanochannels of an anodic aluminum oxide film, Chem. Mater. 8 (8) (1996) 2109–2113.
[28] L. Bulusheva, A. Okotrub, A. Kurenya, H. Zhang, H. Zhang, X. Chen, et al., Electrochemical properties of nitrogen-doped carbon nanotube anode in Li-ion batteries, Carbon 49 (12) (2011) 4013–4023.
[29] A.A. Koós, M. Dowling, K. Jurkschat, A. Crossley, N. Grobert, Effect of the experimental parameters on the structure of nitrogen-doped carbon nanotubes produced by aerosol chemical vapour deposition, Carbon 47 (1) (2009) 30–37.
[30] H. Liu, Y. Zhang, R. Li, X. Sun, S. Désilets, H. Abou-Rachid, et al., Structural and morphological control of aligned nitrogen-doped carbon nanotubes, Carbon 48 (5) (2010) 1498–1507.
[31] T. Sharifi, F. Nitze, H.R. Barzegar, C.-W. Tai, M. Mazurkiewicz, A. Malolepszy, et al., Nitrogen doped multi walled carbon nanotubes produced by CVD-correlating XPS and Raman spectroscopy for the study of nitrogen inclusion, Carbon 50 (10) (2012) 3535–3541.
[32] S. Maldonado, S. Morin, K.J. Stevenson, Structure, composition, and chemical reactivity of carbon nanotubes by selective nitrogen doping, Carbon 44 (8) (2006) 1429–1437.
[33] W. Xu, T. Kyotani, B.K. Pradhan, T. Nakajima, A. Tomita, Synthesis of aligned carbon nanotubes with double coaxial structure of nitrogen-doped and undoped multiwalls, Adv. Mater. 15 (13) (2003) 1087–1090.
[34] Q. Yang, W. Xu, A. Tomita, T. Kyotani, Double coaxial structure and dual physicochemical properties of carbon nanotubes composed of stacked nitrogen-doped and undoped multiwalls, Chem. Mater. 17 (11) (2005) 2940–2945.
[35] M. Alsawat, T. Altalhi, T. Kumeria, A. Santos, D. Losic, Carbon nanotube-nanoporous anodic alumina composite membranes with controllable inner diameters and surface chemistry: influence on molecular transport and chemical selectivity, Carbon 93 (2015) 681–692.
[36] A. Li, F. Müller, A. Birner, K. Nielsch, U. Gösele, Hexagonal pore arrays with a 50–420 nm interpore distance formed by self-organization in anodic alumina, J. Appl. Phys. 84 (11) (1998) 6023–6026.
[37] O. Jessensky, F. Müller, U. Gösele, Self-organized formation of hexagonal pore arrays in anodic alumina, Appl. Phys. Lett. 72 (10) (1998) 1173–1175.
[38] M. Lillo, D. Losic, Pore opening detection for controlled dissolution of barrier oxide layer and fabrication of nanoporous alumina with through-hole morphology, J. Membr. Sci. 327 (1–2) (2009) 11–17.
[39] D. Losic, D. Losic Jr., Preparation of porous anodic alumina with periodically perforated pores, Langmuir 25 (10) (2009) 5426–5431.
[40] C.C. Chen, J.H. Chen, C.G. Chao, Post-treatment method of producing ordered array of anodic aluminum oxide using general purity commercial (99.7%) aluminum, Jpn. J. Appl. Phys. 44 (3R) (2005) 1529.
[41] L. Fernández-Romero, J. Montero-Moreno, E. Pellicer, F. Peiró, A. Cornet, J. Morante, et al., Assessment of the thermal stability of anodic alumina membranes at high temperatures, Mater. Chem. Phys. 111 (2) (2008) 542–547.
[42] J.J. Schneider, N.I. Maksimova, J. Engstler, R. Joshi, R. Schierholz, R. Feile, Catalyst free growth of a carbon nanotube–alumina composite structure, Inorg. Chim. Acta 361 (6) (2008) 1770–1778.
[43] M. Reyes-Reyes, N. Grobert, R. Kamalakaran, T. Seeger, D. Golberg, M. Rühle, et al., Efficient encapsulation of gaseous nitrogen inside carbon nanotubes with bamboo-like structure using aerosol thermolysis, Chem. Phys. Lett. 396 (1) (2004) 167–173.
[44] B.G. Sumpter, V. Meunier, J.M. Romo-Herrera, E. Cruz-Silva, D.A. Cullen, H. Terrones, et al., Nitrogen-mediated carbon nanotube growth: diameter reduction, metallicity, bundle dispersability, and bamboo-like structure formation, ACS Nano 1 (4) (2007) 369–375.
[45] Y. Wang, G. Tang, F. Koeck, B. Brown, J. Garguilo, R. Nemanich, Experimental studies of the formation process and morphologies of carbon nanotubes with bamboo mode structures, Diam. Relat. Mater. 13 (4) (2004) 1287–1291.
[46] A. Burian, J.C. Dore, T. Kyotani, V. Honkimaki, Structural studies of oriented carbon nanotubes in alumina channels using high energy X-ray diffraction, Carbon 43 (13) (2005) 2723–2729.
[47] S. Kumar, I. Levchenko, K.K. Ostrikov, J.A. McLaughlin, Plasma-enabled, catalyst-free growth of carbon nanotubes on mechanically-written Si features with arbitrary shape, Carbon 50 (1) (2012) 325–329.
[48] P. Ciambelli, L. Arurault, M. Sarno, S. Fontorbes, C. Leone, L. Datas, et al., Controlled growth of CNT in mesoporous AAO through optimized conditions for membrane preparation and CVD operation, Nanotechnology 22 (26) (2011) 265613.
[49] S. Biniak, G. Szymański, J. Siedlewski, A. Światkowski, The characterization of activated carbons with oxygen and nitrogen surface groups, Carbon 35 (12) (1997) 1799–1810.
[50] M. Reis, A.B. Do Rego, J.L. Da Silva, M. Soares, An XPS study of the fibre-matrix interface using sized carbon fibres as a model, J. Mater. Sci. 30 (1) (1995) 118–126.
[51] M. Tabbal, P. Mérel, S. Moisa, M. Chaker, A. Ricard, M. Moisan, X-ray photoelectron spectroscopy of carbon nitride films deposited by graphite laser ablation in a nitrogen postdischarge, Appl. Phys. Lett. 69 (12) (1996) 1698–1700.
[52] N. Hellgren, M.P. Johansson, E. Broitman, L. Hultman, J.-E. Sundgren, Role of nitrogen in the formation of hard and elastic CN x thin films by reactive magnetron sputtering, Phys. Rev. B 59 (7) (1999) 5162.
[53] A. Cuesta, P. Dhamelincourt, J. Laureyns, A. Martinez-Alonso, J.D. Tascón, Raman microprobe studies on carbon materials, Carbon 32 (8) (1994) 1523–1532.
[54] P. Ayala, R. Arenal, M. Rümmeli, A. Rubio, T. Pichler, The doping of carbon nanotubes with nitrogen and their potential applications, Carbon 48 (3) (2010) 575–586.
[55] A. Fick, Ueber diffusion, Ann. Phys. 170 (1) (1855) 59–86.

Supporting Information

Facile and Controllable Route for Nitrogen Doping of Carbon Nanotubes Composite Membranes by Catalyst-Free Chemical Vapour Deposition

Mohammed Alsawat[a,b], Tariq Altalhi[a,b], Abel Santos*[a], and Dusan Losic*[a]

[a] School of Chemical Engineering, The University of Adelaide, Adelaide, Australia.

[b] Department of Chemistry, Faculty of Science, Taif University, Taif, Saudi Arabia.

1. Structural Characterization of Undoped and N-doped CNTs-NAAMs using SEM

CNTs were grown inside NAAMs by template synthesis using a catalyst-free CVD approach in a CVD system consisting of a two-stage furnace equipped with a cylindrical quartz tube. A schematic illustration of the CVD setup used in our study is shown in **Fig. S1a.** The transport performance and chemical selectivity of the undoped and N-doped CNTs-NAAMs composite membranes are assessed by studying the transport of two model molecules with different hydrophilic-hydrophobic character using a H-tube permeation setup consisting of two half cells (i.e. feed and permeate cells). A schematic illustration of the molecular transport setup used in our study is shown in **Fig. S1b**. The length of undoped and N-doped CNTs-NAAMs were fixed to 50 **± 2** μm by adjusting the anodization time of NAAMs. Cross-sectional SEM images of the undoped and N-doped CNTs-NAAMs prepared by using precursors of P1, P3, P4 and P5 are presented in **Figs. S2a, S2b, S2c and S2d,** respectively. It shows CNTs protruding out of NAAM pores across all NAAM structure confirming that undoped and N-doped CNTs were grown inside the entire length of NAAMs. **Fig. S3** shows SEM images of undoped and N-doped CNTs liberated by selective dissolution of NAAMs templates revealing the integrity and uniformity of these tubes.

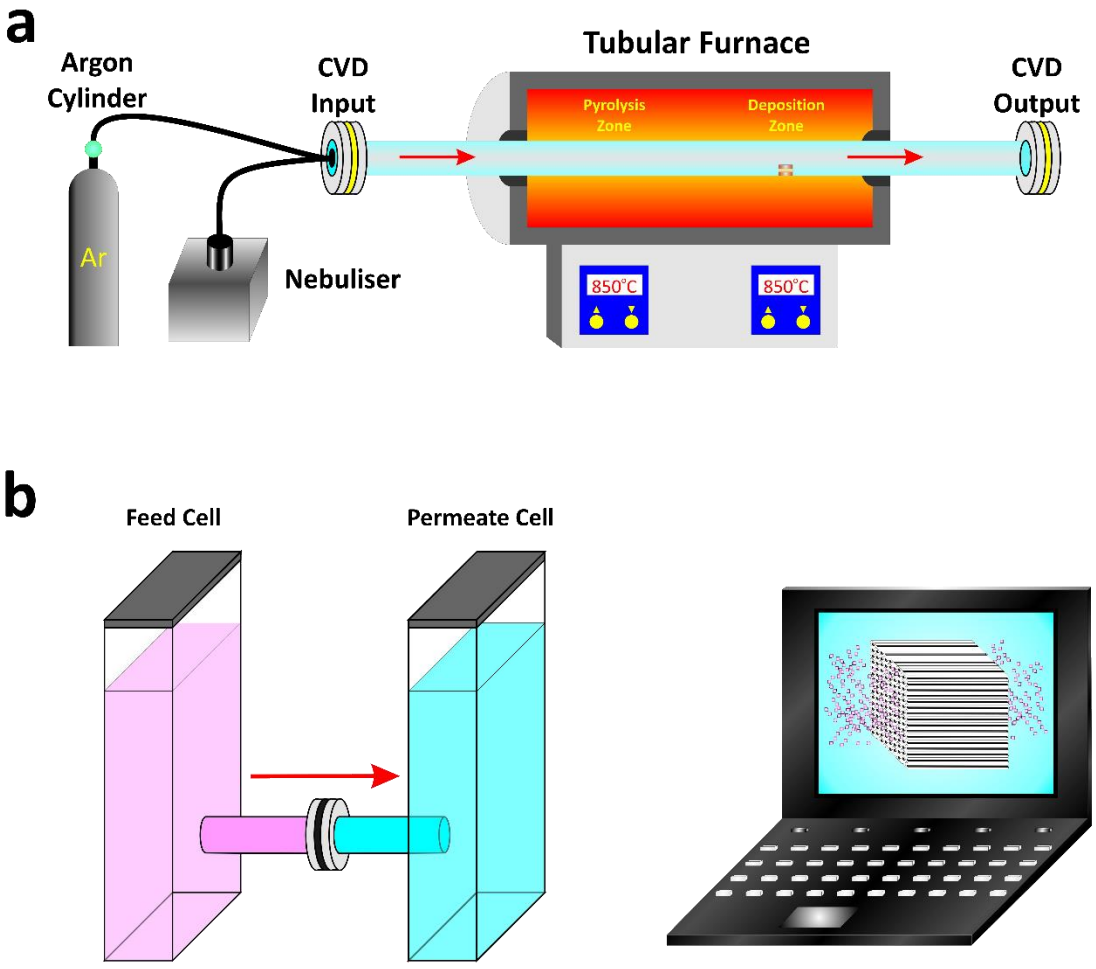

Fig. S1 Schematic representation of the CVD and the molecular transport setups. (a) Scheme illustrating the different parts of the CVD setup used to fabricate CNTs; and (b) scheme illustrating the molecular transport setup.

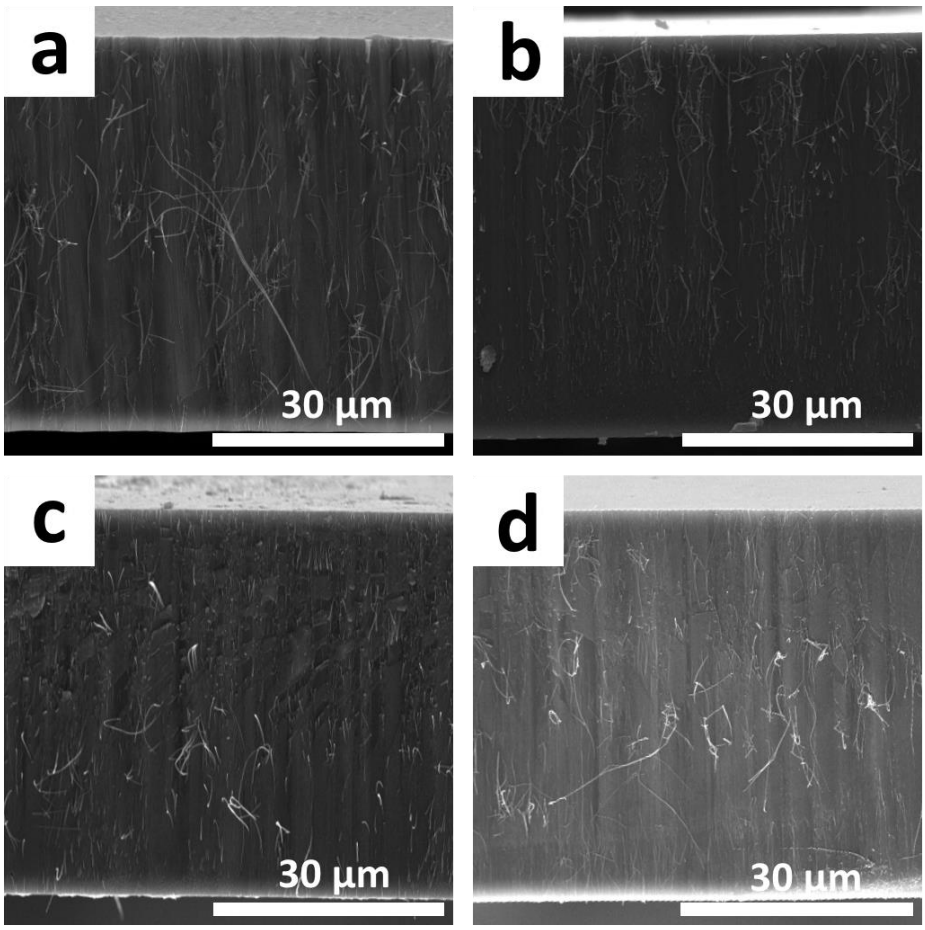

Fig. S2 Cross sectional SEM images of different CNTs-NAAMs. (a) Undoped CNTs-NAAMs, (b) N-doped CNTs-NAAMs prepared by P3, (c) N-doped CNTs-NAAMs prepared by P4 and (d) N-doped CNTs-NAAMs prepared by P5 (higher bright area is the membrane's top surface).

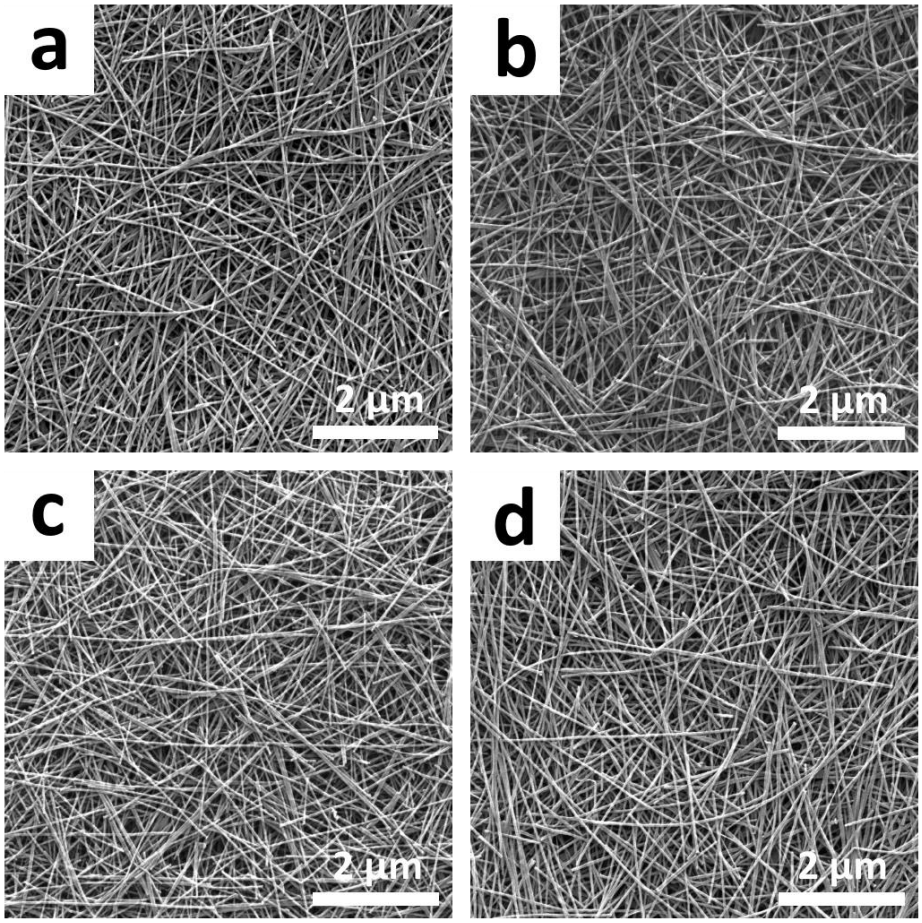

Fig. S3 Top view SEM images of liberated CNTs. (a) Undoped CNTs, (b) N-doped CNTs prepared by P3, (c) N-doped CNTs prepared by P4 and (d) N-doped CNTs prepared by P5.

2. Chemical Characterization of Undoped and N-doped CNTs using XPS

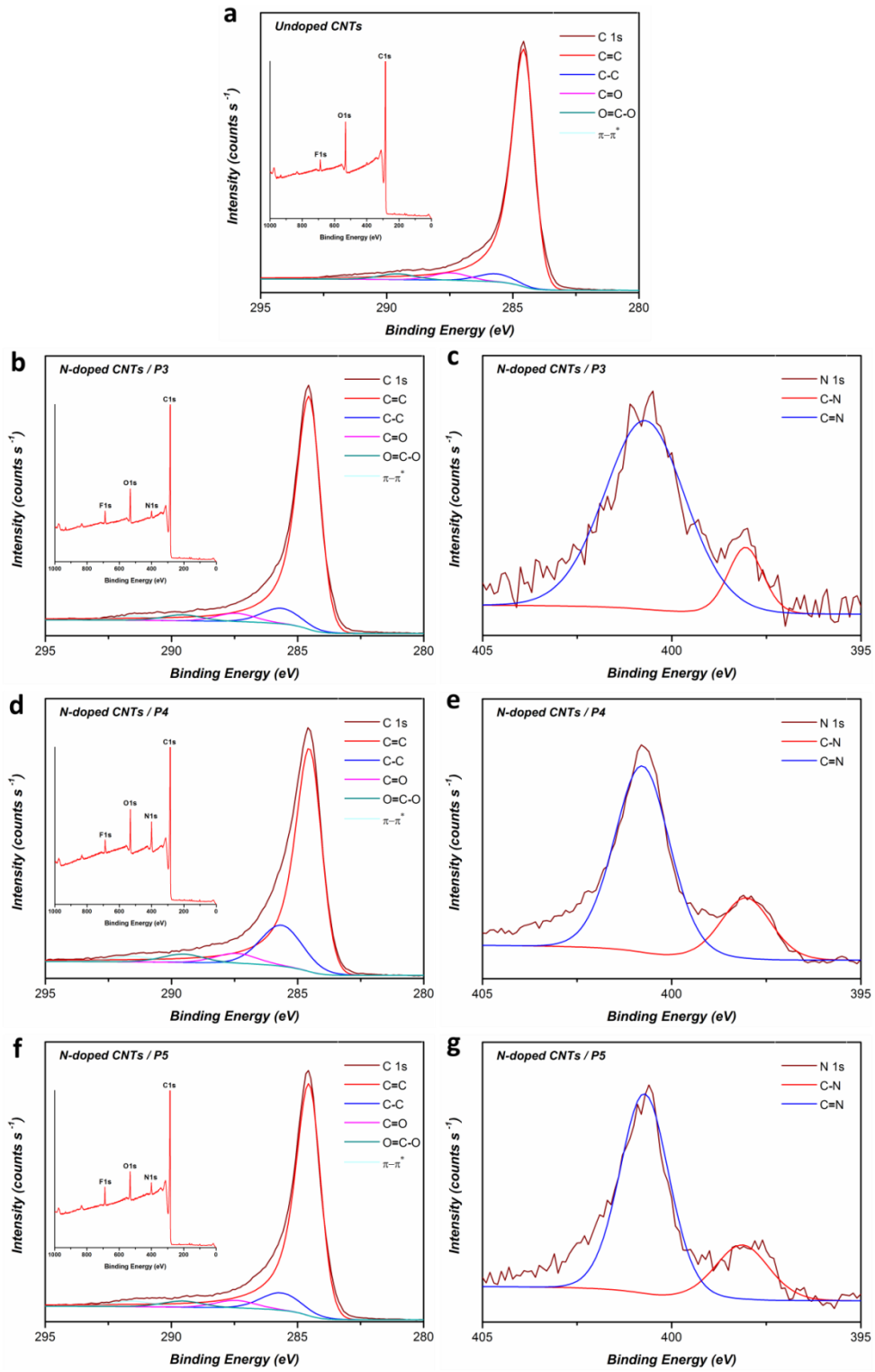

Fig. S4 C 1s and N 1s core-level spectra of undoped and N-doped CNTs. (a) C 1s of undoped CNTs (inset: survey spectrum); (b) C 1s of N-doped CNTs prepared by P3 (inset: survey spectrum); (c) N 1s of N-doped CNTs; (d) C 1s of N-doped CNTs prepared by P4 (inset: survey spectrum); (e) N 1s of N-doped CNTs; (f) C 1s of N-doped CNTs prepared by P5 (inset: survey spectrum) and (g) N 1s of N-doped CNTs.

Table S1. Summary of elemental composition and high-resolution C 1s and N 1s spectra of undoped and N-doped CNTs prepared through catalyst-free CVD process using different precursors.

	Sample	**Undoped CNTs**	**N-doped CNTs**	**N-doped CNTs**	**N-doped CNTs**
	Precursor	**Toluene:EtOH**	**Toluene:EtOH:DMF**	**Pyridine**	**Toluene:EtOH:Pyridine**
		P1	**P3**	**P4**	**P5**
	Peak assignment	**Intensity (%)**			
C	-	90.98	90.07	86.80	91.10
O	-	6.40	5.52	4.92	3.95
N	-	_	1.75	6.26	2.64
C 1s	C=C	85.43	79.96	66.79	78.60
	C–C / C-N	4.97	9.11	21.04	10.11
	C=O / C-N	4.55	4.94	5.15	4.48
	O=C–O	3.55	3.51	4.22	3.62
	π-π*	1.50	2.48	2.80	3.19
N1s	C-N	_	13.05	22.86	22.71
	C=N	_	86.95	77.14	77.29

CHAPTER 7

Synthesis of Carbon Nanotube–Nanotubular Titania Composites by Catalyst-Free CVD Process: Insights into the Formation Mechanism and Photocatalytic Properties

Mohammed Obid Alsawat

School of Chemical Engineering, The University of Adelaide, South Australia 5005, Australia

This chapter is based on the following peer-reviewed article:

Alsawat, M. Altalhi, T. Gulati, K. Santos, A. and Losic, D. Synthesis of Carbon Nanotubes-Nanotubular Titania Composites by Catalyst-Free CVD Process: Insights into the Formation Mechanism and Photocatalytic Properties. *ACS Applied Materials & Interfaces*,7.51 (2015): 28361-28368.

Statement of Authorship

Title of Paper	Synthesis of Carbon Nanotubes-Nanotubular Titania Composites by Catalyst-Free CVD Process: Insights into the Formation Mechanism and Photocatalytic Properties
Publication Status	☑ Published ☐ Accepted for Publication ☐ Submitted for Publication ☐ Unpublished and Unsubmitted w ork w ritten in manuscript style
Publication Details	Alsawat, M. Altalhi, T. Gulati, K. Santos, A. and Losic, D. Synthesis of Carbon Nanotubes-Nanotubular Titania Composites by Catalyst-Free CVD Process: Insights into the Formation Mechanism and Photocatalytic Properties. *ACS Applied Materials & Interfaces*,7.51 (2015): 28361-28368.

Principal Author

Name of Principal Author (Candidate)	Mohammed Alsawat		
Contribution to the Paper	Under supervision of D. Losic and A. Santos, I developed, designed, and performed the experiments, interpreted and processed the data and wrote the manuscript for submission.		
Overall percentage (%)	80		
Certification:	This paper reports on original research I conducted during the period of my Higher Degree by Research candidature and is not subject to any obligations or contractual agreements with a third party that would constrain its inclusion in this thesis. I am the primary author of this paper.		
Signature		Date	30 May 2016

Co-Author Contributions

By signing the Statement of Authorship, each author certifies that:

i. the candidate's stated contribution to the publication is accurate (as detailed above);
ii. permission is granted for the candidate in include the publication in the thesis; and
iii. the sum of all co-author contributions is equal to 100% less the candidate's stated contribution.

Name of Co-Author	Tariq Altalhi		
Contribution to the Paper	I helped the candidate with providing the technical support of chemical vapour deposition (CVD) system. I give consent for Mohammed Alsawat to present this paper for examination towards the Doctorate of philosophy.		
Signature		Date	30 May 2016

Name of Co-Author	Karan Gulati
Contribution to the Paper	I helped the candidate with designing and performing the anodization experiment of titanium. I give consent for Mohammed Alsawat to present this paper for examination towards the Doctorate of philosophy.

Signature		Date	30 May 2016

Name of Co-Author	Abel Santos
Contribution to the Paper	I acted as secondary supervisor for the candidate and aided in development of the experiments and evaluation of manuscript for submission. I give consent for Mohammed Alsawat to present this paper for examination towards the Doctorate of philosophy.

Signature		Date	30 May 2016

Name of Co-Author	Dusan Losic
Contribution to the Paper	I acted as primary supervisor for the candidate and aided in development of the experiments and evaluation of manuscript for submission. I give consent for Mohammed Alsawat to present this paper for examination towards the Doctorate of philosophy.

Signature		Date	30 May 2016

CHAPTER 7: Alsawat, M. Altalhi, T. Gulati, K. Santos, A. and Losic, D. Synthesis of Carbon Nanotubes-Nanotubular Titania Composites by Catalyst-Free CVD Process: Insights into the Formation Mechanism and Photocatalytic Properties. *ACS Applied Materials & Interfaces*,7.51 (2015): 28361-28368.

ACS APPLIED MATERIALS & INTERFACES

Research Article

www.acsami.org

Synthesis of Carbon Nanotube–Nanotubular Titania Composites by Catalyst-Free CVD Process: Insights into the Formation Mechanism and Photocatalytic Properties

Mohammed Alsawat,[†,‡] Tariq Altalhi,[†,‡] Karan Gulati,[†] Abel Santos,[*,†] and Dusan Losic[*,†]

[†]School of Chemical Engineering, The University of Adelaide, Adelaide, South Australia 5005, Australia

[‡]Department of Chemistry, Faculty of Science, Taif University, Taif, Saudi Arabia

ABSTRACT: This work presents the synthesis of carbon nanotubes (CNTs) inside titania nanotube (TNTs) templates by a catalyst-free chemical vapor deposition (CVD) approach as composite platforms for photocatalytic applications. The nanotubular structure of TNTs prepared by electrochemical anodization provides a unique platform to grow CNTs with precisely controlled geometric features. The formation mechanism of carbon nanotubes inside nanotubular titania without using metal catalysts is explored and explained. The structural features, crystalline structures, and chemical composition of the resulting CNTs–TNTs composites were systematically characterized using scanning electron microscopy (SEM), transmission electron microscopy (TEM), X-ray diffraction (XRD), X-ray photoelectron spectroscopy (XPS), and Raman spectroscopy. The deposition time during CVD process was used to determine the formation mechanism of CNTs inside TNTs template. The photocatalytic properties of CNTs–TNTs composites were evaluated via the degradation of rhodamine B, an organic model molecule, in aqueous solution under mercury–xenon Hg (Xe) lamp irradiation monitored by UV–visible spectroscopy. The obtained results reveal that CNTs induces a synergestic effect on the photocatalytic activity of TNTs for rhodamine B degradation, opening new opportunities to develop advanced photocatalysts for environmental and energy applications.

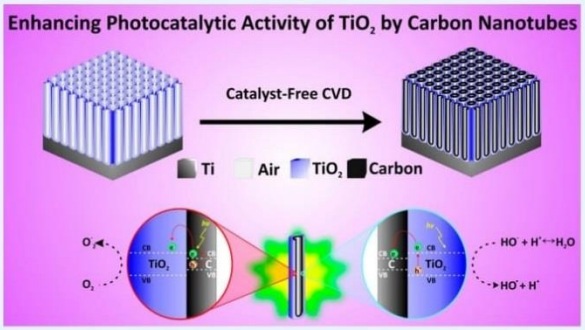

KEYWORDS: *carbon nanotube, titania nanotubes, electrochemical anodization, chemical vapor deposition, photodegradation*

1. INTRODUCTION

In recent years, nanosized titanium dioxide (TiO_2 or titania) has received considerable attention due to its exceptional properties, including cost-competitive fabrication process, large specific surface area, chemical stability, nontoxicity, and high photocatalytic activity. These features have spread the applicability of the different forms of titania across a broad range of applications, such as dye-sensitized solar cells, water splitting, and environmental applications (e.g., adsorption and degradation of pollutants in air and water).[1−4] However, the large energy separation (~3.2 eV) between valence and conduction bands of TiO_2 has diminished its practical applications as only the irradiation in the near UV range of light (λ < 387 nm) can be effectively used for catalysis applications (less than 5% of the total solar irradiation).

To address these limitations, different approaches have been employed to increase the efficiency of TiO_2 to absorb solar energy including; doping TiO_2 with nonmetal elements (nitrogen, sulfur, and carbon)[5−8] and chemically modified n-TiO_2.[9,10] Another approach explored to enhance the photocatalytic efficiency of TiO_2 is to fabricate nanocomposites combining TiO_2 with other materials, such as Ag,[11] Pt,[12] SiO_2, ZrO_2,[13] Cu_2O,[14] and C.[15,16]Among the aforementioned composites, carbon nanotube (CNTs)-based composites have recently been attracting much attention because of their exceptional properties, including electrical properties, high aspect ratio, high adsorption capacity, and chemical and thermal stability.[15,16] So far, several studies have demonstrated that CNTs–TiO_2 composites prepared through a sol–gel approach can be a means of enhancing the photocatalytic efficiency of TiO_2.[17−20] However, this approach suffers from some intrinsic limitations such as the difficulty of preparing a uniform composites, which has limited the positive impact of coupling these two materials. Another limitation is that most of TiO_2-based composites explored were based in powder forms of TiO_2, which posses less photocatalytic activity than that of nanotubular structures of TiO_2.[21,22] Therefore, the development of CNTs–TNTs composite materials with precisely designed and engineered physical and chemical features is of critical importance for improving the photocatalytic properties of TiO_2.

Received: September 22, 2015
Accepted: November 20, 2015
Published: November 20, 2015

DOI: 10.1021/acsami.5b08956
ACS Appl. Mater. Interfaces 2015, 7, 28361−28368

Titania nanostructures can be synthesized by different approaches, which include template method,[23] sol−gel method,[24] hydrothermal treatment,[25] and electrochemical anodization approach. Among the different forms of titania, TNTs produced by electrochemical anodization of titanium substrates has gained a lot of interest as this method makes it possible to produce TNTs with precisely engineered geometric features by a simple, inexpensive and scalable process. The resulting arrays of TNTs feature vertically aligned and highly ordered nanotubular or nanoporous structures.[26,27] Recently, Qu X et al. reported on a preparation method to produce a uniform composite structure of CNTs−TNTs using anodic aluminum oxide (AAO) membranes as templates to grow TNTs.[28] Although this method results in arrays of CNTs−TNTs with controlled geometry, the preparation of highly ordered AAO templates by a two-step anodization process is time-consuming. In that respect, the direct utilization of TNTs grown by anodizing titanium substrates is considered a more facile approach in order to synthesize CNTs−TNTs composite structures with controlled geometry, taking advantage of a catalyst-free CVD approach.

Up to now, very limited reports about fabricating CNTs in TNTs templates are available.[29−32] Most of these studies were based on catalyst-based CVD processes using ferrocene[29] and cobalt[30] as metal catalysts. Nonetheless, it is worth noting that the catalyst CVD process for CNTs preparation has several disadvantages: namely; (i) uncontrolled geometric features of CNTs structure, (ii) heterogeneous composition due to the formation of other phases and composite materials, (iii) occlusion of the inner hollow structure of CNTs by tortuosity effect, and (iv) cross-contamination and incorporation of impurities into the structure of CNTs from the catalysts and precursors, which exist even after purification treatments, making the resulting CNTs potentially toxic for humans and the environment.[33] These inherent drawbacks diminish the advantages of using a nanotubular geometry for photocatalysis, which is desired for providing short carrier diffusion path in the nanotube's wall and straight diffusion path for reactants.[21,34]

In this paper, we present for the first time a facile synthesis approach aiming to produce composite CNTs−TNTs by a catalyst-free CVD approach using TNTs produced by anodization of titanium substrates as templates. The aims of this work are 2-fold: first, to demonstrate the catalyst-free synthetic process of CNTs−TNTs composites explaining the formation mechanism of CNTs inside arrays of TNTs; second, to evaluate the photocatalytic properties of prepared CNTs−TNTs composites. Our study provides new insights into the fabrication of this type of composite materials aiming to enhance the photocatalytic properties of TNTs for engineering advanced CNTs−TNTs electrodes for photocatalytic applications. A schematic illustration of the fabrication process of CNTs−TNTs composite used in our study is shown in Figure 1. Titana nanotubes (TNTs) with precisely engineered dimensions were prepared using a two-step anodization process. Vertically aligned multiwalled carbon nanotubes (MWCNTs) were grown inside TNTs through a catalyst-free chemical vapor deposition (CVD) approach using a mixture of toluene and ethanol as a carbon source. The photocatalytic properties of TNTs and CNTs−TNTs were evaluated via the degradation of rhodamine B, an organic model molecule, in aqueous solution under mercury−xenon Hg (Xe) lamp irradiation monitored by UV−visible spectroscopy.

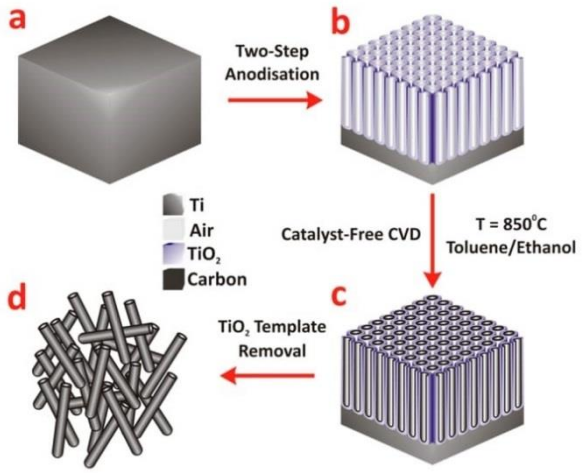

Figure 1. Schematic representation of the fabrication process of TNTs and CNTs−TNTs composite. (a) Ti foil used as substrate to grow TNTs; (b) TNTs prepared by electrochemical anodization; (c) prepared CNTs−TNTs composite with CNTs embedded in TNTs after the CVD process; (d) liberated CNTs after dissolution of TNTs by wet chemical etching (this step is performed to characterize the CNTs structures).

2. EXPERIMENTAL SECTION

2.1. Materials. High-purity titanium (Ti) foils (0.25 mm, 99.7%), ethylene glycol ($C_2H_6O_2$), ammonium fluoride (NH_4F), ethanol 99.7% (C_2H_6O), toluene 99.8% (C_7H_8), hydrofluoric acid (HF), and rhodamine B ($C_{28}H_{31}ClN_2O_3$, RhoB) were purchased from Sigma-Aldrich (Australia) and used as received. High-purity deionized (DI) water (resistivity 18.2 M Ω cm) from a Milli-Q water purification system was used in all the solutions prepared in this study.

2.2. Fabrication of TNTs by Anodization of Ti Substrates. Ti foils were cut into small pieces of 15 × 15 mm and used as substrates to prepare TNTs by electrochemical anodization process as reported elsewhere.[35] Briefly, Ti foils were first mechanically polished using abrasive paper, and then cleaned by sonicating in acetone and ethanol followed by rinsing with deionized water and drying with nitrogen. TNTs were prepared through a two-step anodization process at 25 °C using ethylene glycol electrolyte with 0.3% (*w*/*v*) NH_4F and 3% (*v*/*v*) water (Figure 1). The first anodization step was performed at 80 V for 2 h in a two-electrode electrochemical cell, where electropolished Ti foils act as anode and a platinum wire serves as cathode, permitting anodization in a circular area of diameter 1 cm. The resulting layer of TNTs was removed mechanically by sonicating in methanol. The second anodization step was performed at 80 V for 1 h using the above-mentioned electrolyte.

2.3. Fabrication of CNTs−TNTs Composites. CNTs were fabricated using a catalyst-free CVD approach previously described.[36] Briefly, vertically aligned multiwalled CNTs (MWCNTs) were grown inside TNTs by CVD process using a mixture of toluene and ethanol 1:1 (*v*:*v*) as a carbon precursor (Figure 1). This process was carried out in a CVD system consisting of a two-stage furnace equipped with a cylindrical quartz tube (Brother Furnace Co., LTD, China). The electrochemically prepared TNTs were placed in the deposition zone of the CVD reactor. The reactor temperature was increased up to 850 °C under argon (Ar) flow, which was used as a carrier gas at flow rate of 1 dm^3 min^{-1}. Once the deposition temperature was reached, the carbon precursor was introduced in the CVD reactor by a particle generator (i.e., nebulizer). Different deposition times (15 and 45 min) were performed in order to investigate the formation mechanism of CNTs inside TNTs template. For this purpose, we used TNTs with the same nanotube length (50 μm) in both experiments.

2.4. Structural Characterizations. The structural characterization of the prepared CNTs−TNTs was performed using a scanning

DOI: 10.1021/acsami.5b08956
ACS Appl. Mater. Interfaces 2015, 7, 28361−28368

electron microscope (SEM-FEG Environmental SEM, Quanta 450). Transmission electron microscopy (Philips CM 200 TEM) was used to assess the internal structure of CNTs. TNTs were selectively dissolved in a 5 wt % HF solution to obtain liberated CNTs, which were washed with deionized water and ethanol. One drop of the solution was placed on a TEM copper grid and dried before characterization. Powder X-ray diffraction (XRD) method was used for crystal phase identification. XRD measurements were carried out at room temperature using a Rigaku MiniFlex 600 X-ray diffractometer operating with diffracted beam graphite monochromators (Cu Kα with λ = 0.15406 nm) at 40 kV and 15 mA. The phase composition of TNTs (i.e., anatase and rutile phases) was estimated based on the most intense peaks using the following equations

$$WA = [1 + 1.26(IR/IA)] - 1 \quad (1)$$

$$WR = [1 + 0.8(IA/IR)] - 1 \quad (2)$$

where IA and IR are the X-ray integrated intensities of reflection of anatase and rutile, respectively.[37] X-ray photoelectron spectroscopy (XPS Kratos Axis Ultra) was used to determine the chemical composition of as-produced CNTs−TNTs composite and liberated CNTs by using the Al Kα (1486.7 eV) monochromatic line. Raman spectroscopy (Horiba LabRAM HR Evolution Raman microprobe spectrometer) was used to characterize the graphitic structure of the prepared CNTs. Raman spectra were obtained using a He−Ne laser of 532 nm as an excitation source.

2.5. Photodegradation Assessment. The photocatalytic activity of TNTs and CNTs−TNTs composites were assessed via the photodegradation of rhodamine B molecules in aqueous solution. The photodegradation experiments were carried out in a photoreactor using a 1000 W mercury−xenon Hg (Xe) lamp, which distributes a continuous spectrum from the ultraviolet to infrared range. In these experiments, TNTs or CNTs−TNTs samples of 1 cm in diameter (8−10 mg) ware placed in 10 mL of rhodamine B aqueous solution with an initial concentration (C_0) of 1.6 mg/L and continuously stirred in dark for 1 h in order to reach adsorption/desorption equilibrium. Next, the reaction solution was irradiated vertically from the top with a distance of 6 cm. Note that the solution was kept under stirrer throughout the reaction using a magnetic stirrer. The concentration of rhodamine B was analyzed after irradiation time intervals of 30 min by measuring the absorbance of the solution at its maximum (i.e., λ_{abs} = 554 nm) with UV−vis spectroscopy. The degradation efficiency was calculated through the equation

$$\text{degradation efficiency } (\%) = [(C_0 - C_t)/C_0]100 \quad (3)$$

where C_0 is the initial concentration of rhodamine B and C_t is the rhodamine B concentration at time t (min).

3. RESULTS AND DISCUSSION

3.1. Structural Characterization of Prepared CNTs−TNTs Composites. Figure 2 displays a set of SEM and TEM images of TNTs template and the resulting CNTs−TNTs composite after our catalyst-free CVD approach. A typical structure of TNTs platform produced through a two-step anodization process at 25 °C is shown in Figure 2a−c. The SEM images confirmed the formation of verticaly aligned TNTs structure with closed ends grown on Ti by electrochemical process. The average nanotube diameters of 100 ± 10 nm were determined from high-resolution SEM image (Figure 2a). The nanotube length of TNTs used for this study was set to 50 μm (Figure 2c). Note that, a precise control of the dimensions and the intertube distance of TNTs can be achieved by controlling the anodization conditions (i.e., anodization voltage and time) and the electrolyte water content, respectively.[34] A representative SEM image of CNTs grown inside the pores of TNTs by our catalyst-free CVD process for 15 min is shown in Figure 2d. It is seen that the CNTs were

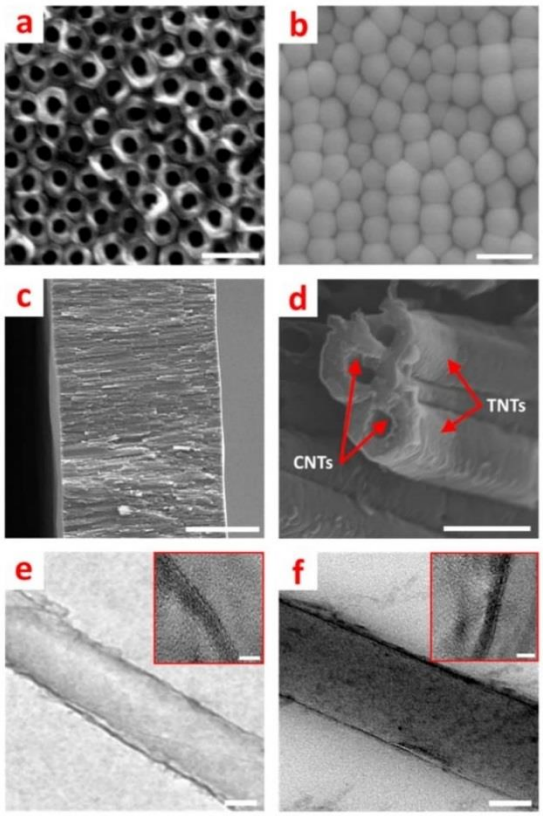

Figure 2. Set of SEM and TEM images of prepared CNTs−TNTs composite. (a) Top-view SEM image of a typical TNTs structure produced through a two-step anodization process (scale bar = 400 nm); (b) bottom view of TNTs (scale bar = 400 nm); (c) cross-section of TNTs (scale bar =20 μm); (d) prepared CNTs−TNTs with CNTs embedded in TNTs after the CVD process for 15 min (scale bar = 400 nm); (e) TEM image of CNTs produced through catalyst-free CVD for 15 min (scale bar = 50 nm) (inset, magnified view; scale bar = 5 nm); (f) TEM image of CNTs produced through catalyst-free CVD for 45 min (scale bar = 50 nm) (inset: magnified view, scale bar = 5 nm).

embedded inside the TNTs template, replicating with precision the geometric features of the template. The length of CNTs−TNTs was controlled via the anodization time of TNTs (i.e., second anodization step). However, it is worthwhile to stress that there is no limitation to prepare CNTs−TNTs composite with different lengths using TNTs featuring different nanotube lengths. CNTs were liberated by selective dissolution of the TNTs templates and collected for characterization by high resolution TEM to determine their diameters (Figure 2e, f). It was found that CNTs featured an average internal nanotube diameter of 100 ± 10 nm, indicating a slight increment in the pore diameter of TNTs after CVD process. This can be explained by the loss of water content of TNTs structure during the CVD process, performed at 850 °C, and the formation of a different crystallographic phase of titania. These results also reveal that the resulting CNTs have straight and hollow cylindrical features, geometric features that are not attainable by a catalyst-based CVD process, where overgrowth of CNTs on the template surface and residual metal catalyst nanoparticles occur.[29,30] Such features will influence the overall

DOI: 10.1021/acsami.5b08956
ACS Appl. Mater. Interfaces 2015, 7, 28361−28368

photocatalytic activity of the resulting composite (i.e., diffusion of dye molecules and light). The formation of CNTs on the TNT's inner wall without using metal catalysts indicates the catalytic role of TNTs templates in the growth of CNTs.

3.2. Formation Mechanism of CNTs inside TNTs Template. As mentioned previously, the diameter and length of CNTs were controlled by the anodization voltage and time of TNTs. To gain insight into the formation mechanism of CNTs inside TNTs templates, two CVD deposition times of 15 and 45 min were used here to determine the influence of the CVD deposition time on the CNTs growth rate and the changes in inner pore diameters. TNTs templates with ~100 nm pore diameters were used to discern the catalytic role of TNTs in the deposition process. TEM images of the liberated CNTs prepared at 15 and 45 min CVD deposition times are presented in Figure 2e, f, respectively. The wall thickness of CNTs prepared by deposition times of 15 and 45 min was determined from HRTEM images (insets in Figure 2e, f) and were found to be almost the same (4 ± 2 nm), (with internal CNTs diameters of 100 ± 10 nm) indicating a time independent process. These results are different from those of CNTs obtained under the same experimental conditions (i.e., carbon precursor, flowing rate, temperature, and deposition times) while using AAO membranes as templates.[38] In contrast to TNTs, a significant increase of the wall thickness of CNTs grown is observed when AAO membranes are used as a template as a result of increasing deposition time from 15 to 45 min (nearly three times, from 4 to 12 nm). This phenomenon indicates that the deposition of the carbon atoms onto the inner walls of TNTs template is due to Lewis acid sites of these inner surfaces.[32] Consequently, the formation mechanism of CNTs inside TNTs template can be outlined as follows; (i) pyrolysis of carbon precursor (i.e., mixture of toluene and ethanol) into carbon, hydrogen and oxygen species in the pyrolysis zone of the CVD reactor, (ii) transfer of the carbon atoms to the deposition zone of the CVD reactor by the carrier gas (Ar), (iii) deposition of a few layers of the carbon onto the inner walls of TNTs catalyzed by the Lewis acid sites of these tubes, (iv) after the formation of several graphitic layers, these sites get blocked by carbon atoms, leading to deactivation and hence stopping the deposition of carbon. These results confirm that a precise control of CNTs diameter in CNTs–TNTs composite can be only obtained by using TNTs with different pore diameters prepared by different anodization voltages.

3.3. XRD Analysis. To gain insight into the crystallographic phase change of TNTs after the CVD process, as-produced TNTs template and CNTs–TNTs composite were characterized by XRD. The XRD patterns of as-produced TNTs template and CNTs–TNTs composite are displayed in Figure 3. The as-produced TNTs showed a broad peak indicating the amorphous phase of titania before CVD process (Figure 3a). The XRD pattern of CNTs–TNTs composite shows a peak at $2\theta = 26.5°$, which can be associated with the 002 reflection of graphite (Figure 3b). The observed peaks at $2\theta = 25.2$, 38.8, 55, 63.3, and 68.6° correspond to the reflections 101, 112, 201, 204, and 116 of the anatase crystallographic phase of TiO_2, respectively, whereas the diffraction peaks at $2\theta = 27.5$, 36, 41.1, 43.6, and 54.3° correspond to the reflections 110, 101, 111, 210, and 211 of the rutile type TiO_2, respectively.[39] This demonstrates that the amorphous phase of TNTs template is crystallized to anatase–rutile mixtures (i.e., 24.6% anatase and 75.4% rutile, using eqs 1 and 2 in the experimental details section) after CVD process (i.e., heating at 850 °C).

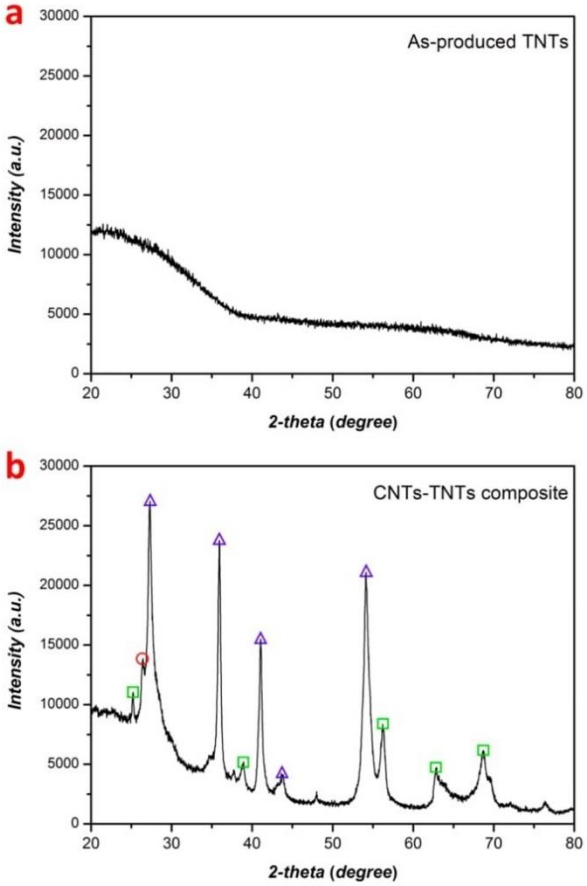

Figure 3. XRD patterns of (a) TNTs template and (b) CNTs–TNTs composite. (○) Graphite, (□) anatase, and (Δ) rutile peaks.

3.4. Chemical Characterization of CNTs–TNTs Composites and Liberated CNTs. The CNTs–TNTs composite and liberated CNTs were analyzed by XPS to provide information on the chemical composition of the prepared composite and the outer surface of CNTs (i.e., liberated CNTs), respectively. The XPS survey spectrum of CNTs–TNTs composite shows the elements C, O, and Ti (inset in Figure 4a). The presence of these elements provides an idea about both the elemental composition of CNTs–TNTs composite and the high level of purity of CNTs produced by our catalyst-free CVD process. Figure 4a shows the high-resolution C 1s spectrum of CNTs–TNTs composite, which is deconvoluted into four peaks located at binding energies of 284.7 ± 0.2, 285.7 ± 0.2, 286.7 ± 0.2, and 291.7 ± 0.3 eV. These peaks are associated with sp^2 bonds of graphitic carbon, disordered sp^3 network of carbon atoms, C–O (alcohol/ether) groups, and π–π^* transition of carbon atoms in graphene structures, respectively.[40,41] The XPS spectra of Ti 2p region shows peaks at 458.8 ± 0.2 eV and 464.5 ± 0.2 eV (Figure 4b), which can be attributed to Ti $2p_{3/2}$ and Ti $2p_{1/2}$, respectively.[42] The separation energy of 5.7 eV between these two peaks confirms the presence of the Ti^{4+}.[43] The XPS survey spectrum of liberated CNTs shows C and O as major elements with percentage weight of 81% and 13%, respectively (inset in

DOI: 10.1021/acsami.5b08956
ACS Appl. Mater. Interfaces 2015, 7, 28361−28368

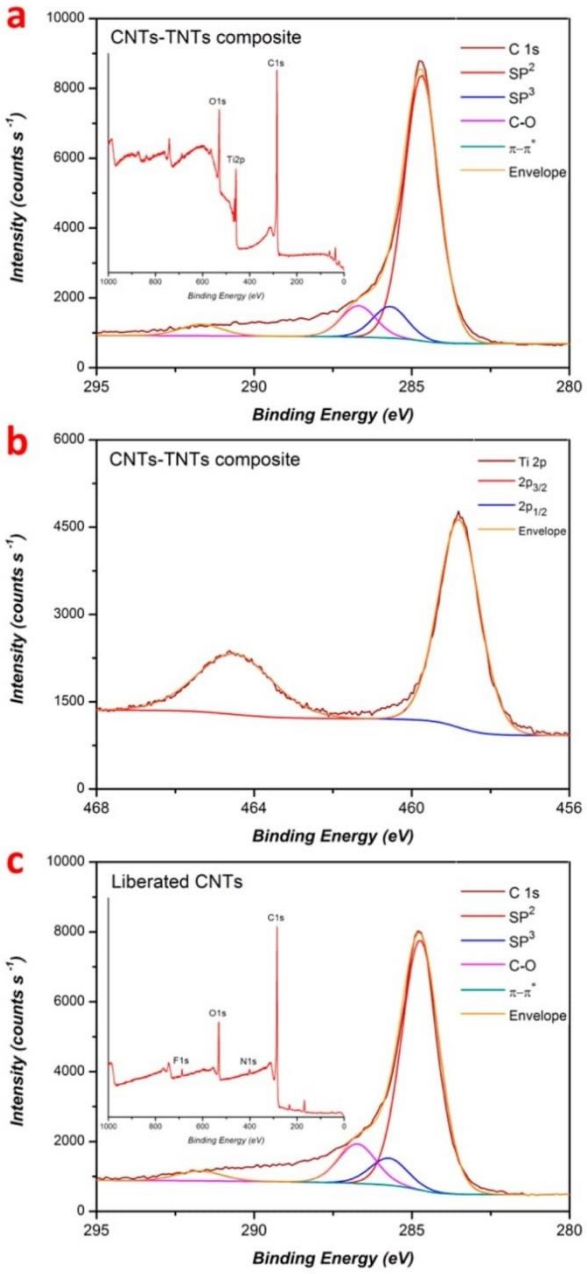

Figure 4. XPS analysis of CNTs–TNTs composites and liberated CNTs. (a) High-resolution C 1s spectra of CNTs–TNTs composite (inset, survey spectrum); (b) Ti 2p region of CNTs–TNTs composite; and (c) high-resolution C 1s spectra of liberated CNTs (inset, survey spectrum).

Figure 4c). Nitrogen and fluorine were present with percentage weights of 3% and 2%, respectively, and their presence is related to the chemical dissolution process of the template using HF and subsequent washing process. The high-resolution C 1s spectrum of liberated CNTs is presented in Figure 4c. It shows almost the same chemical composition as that of CNTs–TNTs composite, which is indicated by the same peaks positions (i.e., 284.7 ± 0.2, 285.7 ± 0.2, 286.7 ± 0.2, and 291.7 ± 0.2 eV). The slight increment in the C–O peak intensity is due to the washing treatment process.

To investigate the graphitic features of CNTs prepared by catalyst-free CVD approach inside TNTs templates, Raman spectroscopy analysis was conducted. Figure 5 presents Raman

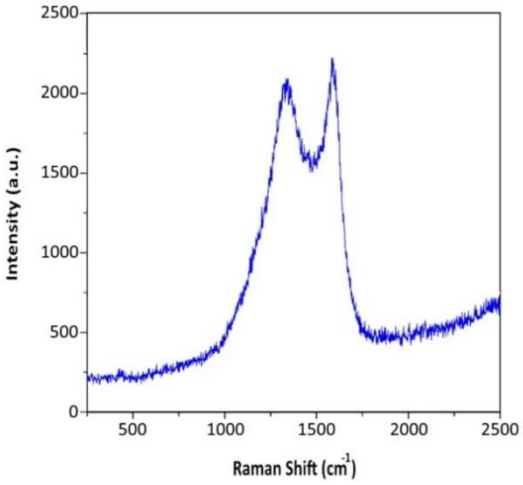

Figure 5. Raman spectrum of CNTs prepared through catalyst-free CVD approach showing characteristic D and G band.

spectrum of CNTs. It shows G-band peak at 1590 cm^{-1}, which is attributed to single-crystal graphite peak (E_{2g} symmetry of interlayers) and D-band peak at 1338 cm^{-1} indicating the presence of amorphous or disordered sp^3 network of carbon atoms.[44] The ratio between D and G bands (I_D/I_G) was estimated to be 0.94, indicating a poor graphitic feature and structural disorder of the carbon network of CNTs. This was confirmed by TEM image and XPS analysis. This ratio is comparable to that of CNTs obtained by CVD synthesis approaches using the same carbon sources while using AAO membranes as templates (I_D/I_G = 1.05).[38]

3.5. Photodegradation Study of CNTs–TNTs Composite. The photocatalytic activity of the prepared CNTs–TNTs composites was explored by the degradation of rhodamine B in aqueous solution under mercury–xenon lamp irradiation. More than 95% of the initial concentration of rhodamine B was decomposed within 90 min of irradiation in the presence of CNTs–TNTs composite (Figure 6a), whereas only 29% of the initial dye concentration was decomposed in the presence of bare TNTs for the same time of irradiation. Figure 6b shows the semilog graph of the photocatalytic degradation of rhodamine B using TNTs and CNTs–TNTs composite. Rhodamine B degradation followed a pseudo-first-order reaction, which is indicated by the straight line of the semilog graph in both samples. The kinetic rate constant was calculated using the eq 4

$$\ln(C_0/C) = kt \quad (4)$$

where k is the rate constant, t is the irradiation time, C is the concentration, and C_0 is the concentration at t = 0.[45] The rhodamine B degradation reaction using TNTs and CNTs–TNTs composite had rate constants (k) of 3.3 × 10^{-3} min^{-1} (R^2 = 0.97) and 3.3 × 10^{-2} min^{-1} (R^2 = 0.98), respectively. This result confirms that the kinetic rate constant is increased by 1 order of magnitude (i.e., a factor of 10) when CNTs–

DOI: 10.1021/acsami.5b08956
ACS Appl. Mater. Interfaces 2015, 7, 28361–28368

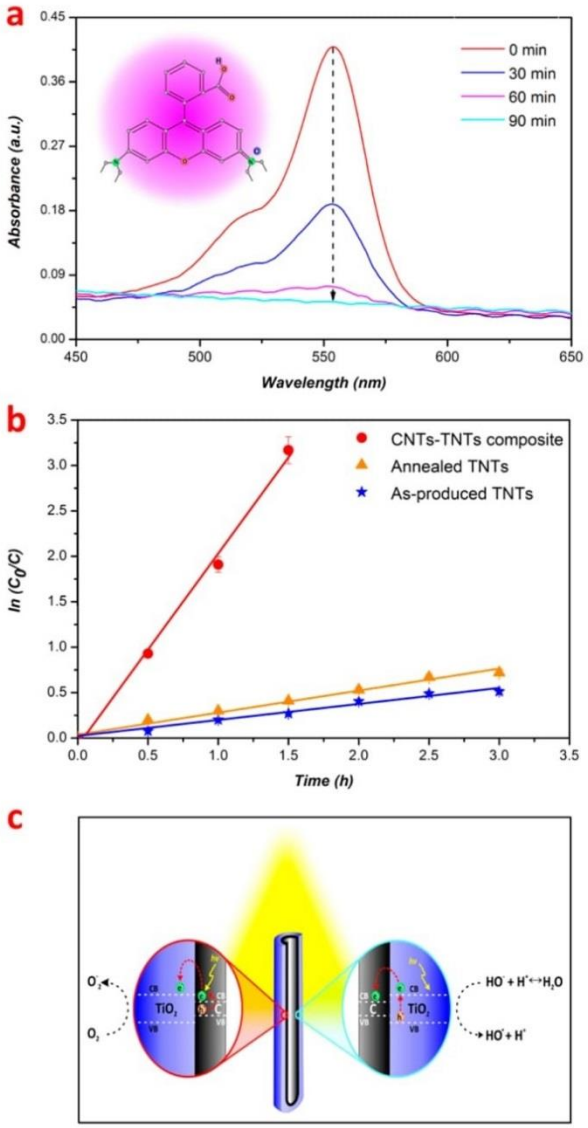

Figure 6. Photocatalytic performance of CNTs−TNTs composite and TNTs template for degradation of rhodamine B. (a) Absorption spectra for the degradation of rhodamine B aqueous solution in the presence of CNTs−TNTs composites under Hg (Xe) light irradiation (inset, chemical structure of rhodamine B dye molecule); (b) semilog graph of the degradation of rhodamine B using as-produced TNTs, annealed TNTs, and CNTs−TNT composites; and (c) schematic representation of electron transfer in CNTs−TNT composites under irradiation.

TNTs composites were used. The low degradation rate of bare TNTs is due to their amorphous structure, as proved by XRD result (Figure 3a). It is generally known that crystalline structure of TiO_2 is preferred in photocatalytic applications as it eliminates surface defects characteristic of the amorphous phase of titania. These defects act as recombination centers of the photogenerated electron−hole pairs, which in turn influence the catalytic properties negatively.[46,47] For CNTs−TNTs composite, several parameters could play a role in their high photocatalytic efficiency such as surface area, band gap energy and absorption capacity. Furthermore, the amorphous phase of TNTs template crystallized during CNTs−TNTs preparation process to an anatase−rutile mixture (24.6% anatase and 75.4% rutile) (Figure 3b) enhances the catalytic properties of the resulting composite. To investigate the influence of this conversion in the composite activity, we annealed TNTs samples under the same temperature and ambient conditions as during CNTs fabrication and used them to catalyze rhodamine b degradation. It was found that about 33.8% of the initial concentration of rhodamine B was decomposed within 90 min of irradiation with rate constant of 4×10^{-3} min^{-1} ($R^2 = 0.98$) (Figure 6b). Hence, these results reveal that although the crystallographic phase of TNTs enhances the photocatalytic activity of the composite CNTs−TNTs, the conversion of crystal structure of TNTs in the composite had a minimized influence on the CNTs−TNTs activity. Consequently, the better photocatalytic performance of CNTs−TNTs could be explained as follows; when the photocatalyst (CNTs−TNTs composite) was irradiated under mercury−xenon lamp, electrons transited from the valence band (VB) to the conduction band (CB) of TiO_2, creating a hole with a positive charge in its valence band. This step is followed by the formation of hydroxyl radicals (•HO) that are responsible for the degradation of rhodamine B molecules.[48] Electron−hole pair can rapidly recombine on the TiO_2 surface before redox reactions take place, decreasing the efficiency of the CNTs−TNTs catalyst. However, CNTs have large electron storage capacity,[49] which could play a role in minimizing or eliminating that rapid recombination by accepting the photoinduced electrons at the TiO_2 interface, leading to a high enhancement of quantum efficiency.[50,51]

Moreover, considering that CNTs are electrically conductive, they might be excited under visible light irradiation and inject electrons to the conduction band of TiO_2 generating hydroxyl and superoxide radicals.[51−54] An important feature of our method is the catalyst-free CVD process with the growth of CNTs using simple carbon precursors as toluene and ethanol. This process allows the fabrication of CNTs without catalyst impurities, as confirmed by XPS analysis (Figure 4). The purity of CNTs is expected to influence their properties, particularly their conductivity, which is a critical factor for charge carrier separation process. Schematic representation of the proposed electron transfer processes in CNTs−TNTs composite under irradiation is presented in Figure 6c. On the other hand, after coupling TNTs with CNTs, the prepared composite can absorb more light in the visible region to generate more electrons and holes.[51−53,55] It is worth stressing that the prepared CNTs−TNTs composite has oxygen containing groups in the CNTs surface (as proved by XPS, Figure 4) and these groups could play a role in the electronic transfer process between CNTs and TNTs.[56]

4. CONCLUSION

We have successfully developed a synthetic approach to produce CNTs−TNTs composites using a catalyst-free CVD approach, where a mixture of toluene and ethanol is used as a carbon source. Structural characterizations of the resulting composite material have shown that CNTs formed inside TNTs templates replicate the inner geometry of TNTs. The mechanism of the formation of CNTs inside TNTs structures was found to be a time independent process as results of specific properties of titania surface. Furthermore, we have studied the photocatalytic performance of prepared composites

DOI: 10.1021/acsami.5b08956
ACS Appl. Mater. Interfaces 2015, 7, 28361−28368

for degradation of rhodamine B. The obtained results have demonstrated the substantial improvement in the photocatalytic performance of the CNTs−TNTs composite over that of bare TNTs. Therefore, coupling TNTs with CNTs improves charge carrier separation and extend the spectral response to the visible−light region, making the catalytic activity of this composite material 1 order of magnitude better than that of bare TNTs. These studies provide new insights, knowledge, and understanding about how to design CNTs−TNTs composites with advanced photocatalytic performances. Our results could result in advanced electrodes with cutting-edge properties and performances for a broad range of catalytic applications.

■ AUTHOR INFORMATION

Corresponding Authors

*E-mail: abel.santos@adelaide.edu.au. Phone: +61 8 8313 1535. Fax: +61 8 8303 4373. Web page: http://www.adelaide.edu.au/directory/abel.santos.

*E-mail: dusan.losic@adelaide.edu.au. Phone: +61 8 8313 4648. Fax: +61 8 8303 4373. Web page: http://www.adelaide.edu.au/directory/dusan.losic.

Notes

The authors declare no competing financial interest.

■ ACKNOWLEDGMENTS

The authors acknowledge the financial support provided by the Australian Research Council (FT 110100711 and DE140100549). The authors also acknowledge the facilities and the scientific and technical assistance of the Australian Microscopy & Microanalysis Research Facility at the Electron Microscope Unit, The University of Adelaide. M.A. thanks Taif University (Ministry of Education, Saudi Arabia) for funding his scholarship.

■ REFERENCES

(1) Nakata, K.; Fujishima, A. TiO 2 Photocatalysis: Design and Applications. *J. Photochem. Photobiol., C* **2012**, *13* (3), 169−189.

(2) Reddy, K. R.; Hassan, M.; Gomes, V. G. Hybrid Nanostructures Based on Titanium Dioxide for Enhanced Photocatalysis. *Appl. Catal., A* **2015**, *489*, 1−16.

(3) Ochiai, T.; Fujishima, A. Photoelectrochemical Properties of TiO 2 Photocatalyst and Its Applications for Environmental Purification. *J. Photochem. Photobiol., C* **2012**, *13* (4), 247−262.

(4) Roy, P.; Berger, S.; Schmuki, P. TiO2 Nanotubes: Synthesis and Applications. *Angew. Chem., Int. Ed.* **2011**, *50* (13), 2904−2939.

(5) Asahi, R.; Morikawa, T.; Ohwaki, T.; Aoki, K.; Taga, Y. Visible-Light Photocatalysis in Nitrogen-Ddoped Titanium Oxides. *Science* **2001**, *293* (5528), 269−271.

(6) Ohno, T.; Akiyoshi, M.; Umebayashi, T.; Asai, K.; Mitsui, T.; Matsumura, M. Preparation of S-Doped TiO 2 Photocatalysts and Their Photocatalytic Activities Under Visible Light. *Appl. Catal., A* **2004**, *265* (1), 115−121.

(7) Ren, W.; Ai, Z.; Jia, F.; Zhang, L.; Fan, X.; Zou, Z. Low Temperature Preparation and Visible Light Photocatalytic Activity of Mesoporous Carbon-Doped Crystalline TiO 2. *Appl. Catal., B* **2007**, *69* (3), 138−144.

(8) Hamal, D. B.; Klabunde, K. J. Synthesis, Characterization, and Visible Light Activity of New Nanoparticle Photocatalysts Based on Silver, Carbon, and Sulfur-Doped TiO 2. *J. Colloid Interface Sci.* **2007**, *311* (2), 514−522.

(9) Nagaveni, K.; Hegde, M.; Ravishankar, N.; Subbanna, G.; Madras, G. Synthesis and Structure of Nanocrystalline TiO2 with Lower Band Gap Showing High Photocatalytic Activity. *Langmuir* **2004**, *20* (7), 2900−2907.

(10) Khan, S. U.; Al-Shahry, M.; Ingler, W. B. Efficient Photochemical Water Splitting by A Chemically Modified n-TiO2. *Science* **2002**, *297* (5590), 2243−2245.

(11) Akhavan, O. Lasting Antibacterial Activities of Ag−TiO 2/Ag/a-TiO 2 Nanocomposite Thin Film Photocatalysts Under Solar Light Irradiation. *J. Colloid Interface Sci.* **2009**, *336* (1), 117−124.

(12) Chen, Y.; Crittenden, J. C.; Hackney, S.; Sutter, L.; Hand, D. W. Preparation of A Novel TiO2-Based pn Junction Nanotube Photocatalyst. *Environ. Sci. Technol.* **2005**, *39* (5), 1201−1208.

(13) Fu, X.; Clark, L. A.; Yang, Q.; Anderson, M. A. Enhanced Photocatalytic Performance of Titania-Based Binary Metal Oxides: TiO2/SiO2 and TiO2/ZrO2. *Environ. Sci. Technol.* **1996**, *30* (2), 647−653.

(14) Siripala, W.; Ivanovskaya, A.; Jaramillo, T. F.; Baeck, S.-H.; McFarland, E. W. A Cu 2 O/TiO 2 Heterojunction Thin Film Cathode for Photoelectrocatalysis. *Sol. Energy Mater. Sol. Cells* **2003**, *77* (3), 229−237.

(15) Liu, H.; Zuo, K.; Vecitis, C. D. Titanium Dioxide-Coated Carbon Nanotube Network Filter for Rapid and Effective Arsenic Sorption. *Environ. Sci. Technol.* **2014**, *48* (23), 13871−13879.

(16) Majumder, M.; Clayton, V.; Ajayan, A. P. 1.14 Carbon Nanotube Membranes: A New Frontier in Membrane Science. *Compr. Membr. Sci. Eng.* **2010**, *1*, 291−310.

(17) Wang, W.; Serp, P.; Kalck, P.; Faria, J. L. Photocatalytic Degradation of Phenol on MWNT and Titania Composite Catalysts Prepared by A Modified Sol−Gel Method. *Appl. Catal., B* **2005**, *56* (4), 305−312.

(18) Yu, Y.; Yu, J. C.; Chan, C.-Y.; Che, Y.-K.; Zhao, J.-C.; Ding, L.; Ge, W.-K.; Wong, P.-K. Enhancement of Adsorption and Photocatalytic Activity of TiO 2 by Using Carbon Nanotubes for the Treatment of Azo Dye. *Appl. Catal., B* **2005**, *61* (1), 1−11.

(19) Xia, X.-H.; Jia, Z.-J.; Yu, Y.; Liang, Y.; Wang, Z.; Ma, L.-L. Preparation of Multi-Walled Carbon Nanotube Supported TiO 2 and Its Photocatalytic Activity in the Reduction of CO 2 with H 2 O. *Carbon* **2007**, *45* (4), 717−721.

(20) Gao, B.; Chen, G. Z.; Puma, G. L. Carbon Nanotubes/Titanium Dioxide (CNTs/TiO 2) Nanocomposites Prepared by Conventional and Novel Surfactant Wrapping Sol−Gel Methods Exhibiting Enhanced Photocatalytic Activity. *Appl. Catal., B* **2009**, *89* (3), 503−509.

(21) Macak, J. M.; Zlamal, M.; Krysa, J.; Schmuki, P. Self-Organized TiO2 Nanotube Layers as Highly Efficient Photocatalysts. *Small* **2007**, *3* (2), 300−304.

(22) Jennings, J. R.; Ghicov, A.; Peter, L. M.; Schmuki, P.; Walker, A. B. Dye-Sensitized Solar Cells Based on Oriented TiO2 Nanotube Arrays: Transport, Trapping, and Transfer of Electrons. *J. Am. Chem. Soc.* **2008**, *130* (40), 13364−13372.

(23) Lee, J.-H.; Leu, I.-C.; Hsu, M.-C.; Chung, Y.-W.; Hon, M.-H. Fabrication of Aligned TiO2 One-Dimensional Nanostructured Arrays Using A One-Step Templating Solution Approach. *J. Phys. Chem. B* **2005**, *109* (27), 13056−13059.

(24) Kasuga, T.; Hiramatsu, M.; Hoson, A.; Sekino, T.; Niihara, K. Formation of Titanium Oxide Nanotube. *Langmuir* **1998**, *14* (12), 3160−3163.

(25) Ou, H.-H.; Lo, S.-L. Review of Titania Nanotubes Synthesized via the Hydrothermal Treatment: Fabrication, Modification, and Application. *Sep. Purif. Technol.* **2007**, *58* (1), 179−191.

(26) Ghicov, A.; Schmuki, P. Self-Ordering Electrochemistry: A Review on Growth and Functionality of TiO 2 Nanotubes and Other Self-Aligned MO x Structures. *Chem. Commun.* **2009**, *20*, 2791−2808.

(27) Gulati, K.; Ramakrishnan, S.; Aw, M. S.; Atkins, G. J.; Findlay, D. M.; Losic, D. Biocompatible Polymer Coating of Titania Nanotube Arrays for Improved Drug Elution and Osteoblast Adhesion. *Acta Biomater.* **2012**, *8* (1), 449−456.

(28) Qu, X.; Cao, L.; Du, F. Fabrication of Ordered Arrays of CNT/TiO 2 Nanotubes and Their Photocatalytic Properties. *RSC Adv.* **2015**, *5* (27), 20976−20980.

(29) Hesabi, Z. R.; Allam, N. K.; Dahmen, K.; Garmestani, H.; El-Sayed, M. A. Self-Standing Crystalline TiO2 Nanotubes/CNTs

DOI: 10.1021/acsami.5b08956
ACS Appl. Mater. Interfaces 2015, 7, 28361−28368

Heterojunction Membrane: Synthesis and Characterization. *ACS Appl. Mater. Interfaces* **2011**, *3* (4), 952−955.
(30) Mishra, A.; Banerjee, S.; Mohapatra, S. K.; Graeve, O. A.; Misra, M. Synthesis of Carbon Nanotube−TiO2 Nanotubular Material for Reversible Hydrogen Storage. *Nanotechnology* **2008**, *19* (44), 445607.
(31) Eswaramoorthi, I.; Hwang, L.-P. Synthesis and Characterisation of Larger Diameter Multi-Walled Carbon Nanotubes Over Anodic Titanium Oxide Template. *Carbon* **2006**, *44* (11), 2341−2344.
(32) Eswaramoorthi, I.; Hwang, L.-P. Anodic Titanium Oxide: A New Template for the Synthesis of Larger Diameter Multi-Walled Carbon Nanotubes. *Diamond Relat. Mater.* **2007**, *16* (8), 1571−1578.
(33) Tejral, G.; Panyala, N. R.; Havel, J. Carbon Nanotubes: Toxicological Impact on Human Health and Environment. *Carbon* **2009**, *7* (1), 1−13.
(34) Alsawat, M.; Altalhi, T.; Shapter, J. G.; Losic, D. Influence of Dimensions, Inter-Distance and Crystallinity of Titania Nanotubes (TNTs) on Their Photocatalytic Activity. *Catal. Sci. Technol.* **2014**, *4* (7), 2091−2098.
(35) Kant, K.; Losic, D. A Simple Approach for Synthesis of TiO2 Nanotubes with Through-Hole Morphology. *Phys. Status Solidi RRL* **2009**, *3* (5), 139−141.
(36) Che, G.; Lakshmi, B.; Martin, C.; Fisher, E.; Ruoff, R. S. Chemical Vapor Deposition Based Synthesis of Carbon Nanotubes and Nanofibers Using A Template Method. *Chem. Mater.* **1998**, *10* (1), 260−267.
(37) Spurr, R. A.; Myers, H. Quantitative Analysis of Anatase-Rutile Mixtures with An X-ray Diffractometer. *Anal. Chem.* **1957**, *29* (5), 760−762.
(38) Alsawat, M.; Altalhi, T.; Kumeria, T.; Santos, A.; Losic, D. Carbon Nanotube-Nanoporous Anodic Alumina Composite Membranes with Controllable Inner Diameters and Surface Chemistry: Influence on Molecular Transport and Chemical Selectivity. *Carbon* **2015**, *93*, 681−692.
(39) Lee, K.; Kim, D.; Roy, P.; Paramasivam, I.; Birajdar, B. I.; Spiecker, E.; Schmuki, P. Anodic Formation of Thick Anatase TiO2Mesosponge Layers for High-Efficiency Photocatalysis. *J. Am. Chem. Soc.* **2010**, *132* (5), 1478−1479.
(40) Biniak, S.; Szymański, G.; Siedlewski, J.; Światkowski, A The Characterization of Activated Carbons with Oxygen and Nitrogen Surface Groups. *Carbon* **1997**, *35* (12), 1799−1810.
(41) Reis, M.; Do Rego, A. B.; Da Silva, J. L.; Soares, M. An XPS Study of the Fibre-Matrix Interface Using Sized Carbon Fibres as A Model. *J. Mater. Sci.* **1995**, *30* (1), 118−126.
(42) Liu, D.; Zhang, Y.; Xiao, P.; Garcia, B. B.; Zhang, Q.; Zhou, X.; Jeong, Y.-H.; Cao, G. TiO 2 Nanotube Arrays Annealed in CO Exhibiting High Performance for Lithium Ion Intercalation. *Electrochim. Acta* **2009**, *54* (27), 6816−6820.
(43) Song, Z.; Hrbek, J.; Osgood, R. Formation of TiO2 Nanoparticles by Reactive-Layer-Assisted Deposition and Characterization by XPS and STM. *Nano Lett.* **2005**, *5* (7), 1327−1332.
(44) Kim, P.; Zheng, Y.; Agnihotri, S. Adsorption Equilibrium and Kinetics of Water Vapor in Carbon Nanotubes and its Comparison with Activated Carbon. *Ind. Eng. Chem. Res.* **2008**, *47* (9), 3170−3178.
(45) Konstantinou, I. K.; Albanis, T. A. TiO 2-Assisted Photocatalytic Degradation of Azo Dyes in Aqueous Solution: Kinetic and Mechanistic Investigations: A Review. *Appl. Catal., B* **2004**, *49* (1), 1−14.
(46) Vaenas, N.; Bidikoudi, M.; Stergiopoulos, T.; Likodimos, V.; Kontos, A. G.; Falaras, P. Annealing Effects on Self-Assembled TiO 2 Nanotubes and Their Behavior as Photoelectrodes in Dye-Sensitized Solar Cells. *Chem. Eng. J.* **2013**, *224*, 121−127.
(47) Beranek, R.; Tsuchiya, H.; Sugishima, T.; Macak, J.; Taveira, L.; Fujimoto, S.; Kisch, H.; Schmuki, P. Enhancement and Limits of the Photoelectrochemical Response From Anodic TiO∼ 2 Nanotubes. *Appl. Phys. Lett.* **2005**, *87* (24), 243114.
(48) Gaya, U. I.; Abdullah, A. H. Heterogeneous Photocatalytic Degradation of Organic Contaminants over Titanium Dioxide: A Review of Fundamentals, Progress and Problems. *J. Photochem. Photobiol., C* **2008**, *9* (1), 1−12.
(49) Martínez, C.; Fernández, M.; Santaballa, J.; Faria, J. Kinetics and Mechanism of Aqueous Degradation of Carbamazepine by Heterogeneous Photocatalysis using Nanocrystalline TiO 2, ZnO and Multi-Walled Carbon Nanotubes−Anatase Composites. *Appl. Catal., B* **2011**, *102* (3), 563−571.
(50) Hoffmann, M. R.; Martin, S. T.; Choi, W.; Bahnemann, D. W. Environmental Applications of Semiconductor Photocatalysis. *Chem. Rev.* **1995**, *95* (1), 69−96.
(51) An, G.; Ma, W.; Sun, Z.; Liu, Z.; Han, B.; Miao, S.; Miao, Z.; Ding, K. Preparation of Titania/Carbon Nanotube Composites using Supercritical Ethanol and Their Photocatalytic Activity for Phenol Degradation under Visible Light Irradiation. *Carbon* **2007**, *45* (9), 1795−1801.
(52) Lettmann, C.; Hildenbrand, K.; Kisch, H.; Macyk, W.; Maier, W. F. Visible Light Photodegradation of 4-Chlorophenol with A Coke-Containing Titanium Dioxide Photocatalyst. *Appl. Catal., B* **2001**, *32* (4), 215−227.
(53) Wang, W.; Serp, P.; Kalck, P.; Faria, J. L. Visible Light Photodegradation of Phenol on MWNT-TiO 2 Composite Catalysts Prepared by A Modified Sol−Gel Method. *J. Mol. Catal. A: Chem.* **2005**, *235* (1), 194−199.
(54) Wang, W.; Serp, P.; Kalck, P.; Silva, C. G.; Faria, J. L. Preparation and Characterization of Nanostructured MWCNT-TiO 2 Composite Materials for Photocatalytic Water Treatment Applications. *Mater. Res. Bull.* **2008**, *43* (4), 958−967.
(55) Palanivelu, K.; Im, J.-S.; Lee, Y.-S. Carbon Doping of TiO 2 for Visible Light Photo Catalysis-A Review. *Carbon letters* **2007**, *8* (3), 214−224.
(56) da Silva, C. G.; Faria, J. L. Photochemical and Photocatalytic Degradation of an Azo Dye in Aqueous Solution by UV Irradiation. *J. Photochem. Photobiol., A* **2003**, *155* (1), 133−143.

DOI: 10.1021/acsami.5b08956
ACS Appl. Mater. Interfaces 2015, 7, 28361−28368

CHAPTER 8

CONCLUSIONS AND FUTURE WORK

Mohammed Obid Alsawat

School of Chemical Engineering, The University of Adelaide, South Australia 5005, Australia

CHAPTER 8: Conclusions and Future Work

8.1. Conclusions

This thesis advances the knowledge and understanding about the fabrication of CNTs-based composites with precisely engineered dimensions and properties by means of a template-assisted catalyst-free CVD approach. Two types of templates (NAAMs and TNTs) were used to develop CNTs-based composites and different carbon precursors and deposition conditions were explored as precise means of controlling the physical and chemical properties of these systems. The knowledge generated from this thesis will make it possible to design advanced membranes composed of vertically aligned arrays of CNTs grown inside the pores of NAAMs with a range of inner pore diameters of 15-180 nm and lengths of 30-90 μm. Moreover, this thesis demonstrates that the molecular transport and chemical selectivity of these composite membranes can be precisely engineered by manipulating the physical and chemical properties of CVD-grown CNTs using different approaches. The third major contribution of this thesis is the development of advanced photocatalysts, composed of vertically aligned arrays of CNTs grown inside the nanotubular structure of TNTs, which can find broad applicability for environmental and energy applications. The following subsections summarise the conclusions drawn from the different studies and investigations carried out in the course of this PhD thesis, which have been described in detail throughout the previous sections.

8.1.1. Carbon Nanotube-Nanoporous Anodic Alumina Composite Membranes with Controllable Inner Diameters and Surface Chemistry: Influence on Molecular Transport and Chemical Selectivity

This chapter reported the fabrication of CNTs-NAAMs composite membranes with controllable nanotube dimensions and surface chemistry and explores their influence on the transport properties

and chemical-based transport selectivity. The following points summarise the conclusions drawn from this study:

1. By means of a catalyst-free CVD approach using a mixture of toluene and ethanol as a carbon source, vertically aligned MWCNTs were grown inside the pores of NAAMs prepared through a two-step electrochemical anodisation process. By controlling the anodisation time on NAAMs and the deposition time during CVD process, the dimensions of CNTs-NAAMs can be precisely engineered.
2. The morphological and structural investigations revealed that the resulting composite membranes and CNTs have clean surface and straight, uniform and hollow cylindrical structure, which are not attainable by other CVD synthesis approaches.
3. The thermal annealing and wet and dry oxidation processes (hydrogen peroxide and plasma treatments) were used to control the surface chemistry of inner walls of CNTs. The modification of the surface chemistry of CNTs-NAAMs from hydrophobic to hydrophilic surface was successfully confirmed by XPS analysis showing that as-produced and oxidised CNTs-NAAMs have concentrations of oxygen-containing functional groups that are significantly different.
4. The performed molecular transport studies using two model molecules with different hydrophilic-hydrophobic and charge properties ($(RosB)^{2-}$ and $(Ru(BPY)_3)^{2+}$, respectively) with the same molecular size showed that the transport and chemical selectivity properties of CNTs-NAAMs can be controlled by controlling their dimensions (diameters and length) and surface chemistry.

8.1.2. Carbon Nanotubes-Nanoporous Anodic Alumina Composite Membranes: Influence of Template on Structural, Chemical and Transport Properties

This chapter highlighted the fabrication of CNTs composite membranes based on NAAMs prepared using different electrolyte solutions by means of a catalyst-free CVD approach aiming to discern their influence on the CNTs growth. It also reports and explains the formation mechanism of CNTs inside the pores of NAAMs and their transport properties. The following points summarise the conclusions drawn from this study:

1. By means of a catalyst-free CVD approach using a mixture of toluene and ethanol as a carbon source, vertically aligned MWCNTs were grown inside the pores of different NAAMs, prepared through electrochemical anodisation of aluminium substrates in different acid electrolytes containing sulfuric, oxalic and phosphoric acid, resulting in a composite membranes with a range of inner pore diameters of 15-180 nm.
2. The deposition time during CVD process was modified in order to determine the formation mechanism of CNTs inside the pores of NAAMs without using metal catalysts, indicating a time dependent process as results of both the catalytic role of alumina and the hydrocarbon thermal decomposition.
3. The structural and chemical investigations revealed that the electrolyte type used to prepare NAAMs and the deposition time during CVD process have a direct impact on the structural, chemical and graphitic structure features of CNTs-NAAMs composites.
4. Furthermore, the influence of the geometry and chemical composition of the resulting CNTs-NAAMs composites on the transport performance for the diffusion of RosB molecules was demonstrated.
5. The results revealed that a significant enhancement in the transport performance of the CNTs-NAAMs composite membranes can be achieved by tuning the inner diameter of the nanotubes.

8.1.3. Influence of Surface Chemistry on the Ionic Conductivity of Vertically Aligned Carbon Nanotube Composite Membranes

To gain more knowledge on the influence of ion and molecular transport inside nanopores related to their potential applications for molecular separations, sensing, drug delivery and energy conversion, this chapter aimed at exploring the chemical modification of the inner surface of CNTs composite membranes prepared by a catalyst-free CVD process using NAAMs as templates and its influence on their conductivity and electrochemical properties. The following points summarise the conclusions drawn from this study:

1. The selective chemical modification of the inner surface of CNTs with oxygen-containing functional groups was performed by simple oxidation treatment using hydrogen peroxide.
2. Contact angle measurements, XPS and Raman analyses of CNTs-NAAMs composite membranes and liberated CNTs before and after oxidation treatment revealed a transition from hydrophobic to hydrophilic surface of CNTs-NAAMs and selective modification of the inner surface of CNTs, while maintaining the nanotube's morphology.
3. The performed electrochemical impedance spectroscopy characterisations using NaCl electrolyte solutions (1-100 μM) have demonstrated the substantial increase in impedance of oxidised CNTs-NAAMs over as-produced CNTs-NAAMs, revealing that the surface conduction and electrochemical properties of CNTs-NAAMs can be readily tuned by chemical modification of their inner surfaces.
4. The analysis of the conductance of the CNTs-NAAMs composite membranes as a function of frequency revealed that the change in their conductivity after oxidising their inner surfaces follows a frequency-dependent mechanism. Moreover, the change in the concentration of electrolyte is shown to have a significant impact on the conductivity of the membrane.

8.1.4. Facile and Controllable Route for Nitrogen Doping of Carbon Nanotubes Composite Membranes by Catalyst-Free Chemical Vapour Deposition

A facile approach to fabricate CNTs composite membranes doped with different level of nitrogen was established using catalyst-free CVD process and NAAMs as templates. N-doping of the inner and outer surfaces of CNTs was demonstrated, using specific selection of carbon and nitrogen precursors, which makes it possible to tailor their transport and chemical selectivity properties. The following points summarise the conclusions drawn from this study:

1. By means of a catalyst-free CVD approach using different precursor mixtures containing carbon and nitrogen at different ratios, vertically aligned MWCNTs were grown inside the pores of NAAMs with different nitrogen content (3.35 to 6.92 %).
2. The role of the C/N ratio in the precursor mixture during the formation of N-doped CNTs-NAAMs has been explored revealing that a minimum 5:1 C/N ratio is required to obtain N-doped CNTs structures.
3. XPS and Raman analysis of undoped and N-doped CNTs-NAAMs composite membranes and liberated tubes revealed that N atoms were incorporated into the bulk structure of CNTs, without compromising their morphology, resulting in more hydrophilic surface chemistry and less graphitised structure as compared to undoped CNTs-NAAMs composite membranes.
4. Finally, the molecular transport properties of N-doped CNTs-NAAMs with different level of doping were assessed by studying the diffusion of two model molecules with different hydrophilic-hydrophobic and charge properties ($(RosB)^{2-}$ and $(Ru(BPY)_3)^{2+}$, respectively). The results revealed that the diffusional flux of a particular dye molecule was significantly affected by the nitrogen content of CNTs deposited inside NAAMs, confirming that the transport properties and chemical selectivity of CNTs-NAAMs composites can be controlled by nitrogen doping.

8.1.5. Synthesis of Carbon Nanotubes-Nanotubular Titania Composites by Catalyst-Free CVD Process: Insights into the Formation Mechanism and Photocatalytic Properties

This chapter reported the fabrication of CNTs-TNTs composites using a catalyst-free CVD approach, where a mixture of toluene and ethanol is used as a carbon source. It also reports and explains the formation mechanism of CNTs inside TNTs structures and their photocatalytic properties. The following points summarise the conclusions drawn from this study:

1. By means of a catalyst-free CVD approach using a mixture of toluene and ethanol as a carbon source, vertically aligned MWCNTs were grown inside the nanotubular structure of TNTs prepared through a two-step electrochemical anodisation process. A precise control of the dimensions and the inter-tube distance of TNTs could be achieved by controlling the anodisation conditions (i.e. anodisation voltage and time) and the electrolyte water content, respectively.
2. The formation mechanism of CNTs inside TNTs structures, explored and explained by means of the deposition time during CVD process, was found to be a time independent process as a results of the specific properties of titania surface.
3. The photocatalytic properties of CNTs-TNTs composite were evaluated via the degradation of rhodamine B, an organic model molecule, in aqueous solution under mercury-xenon Hg (Xe) lamp irradiation monitored by UV–visible spectroscopy.
4. The results demonstrated the substantial improvement in the photocatalytic performance of the CNTs-TNTs composite (one order of magnitude) over that of bare TNTs, due to coupling TNTs with CNTs improves charge carrier separation and extend the spectral response to the visible light region.

5. This study is a significant contribution to understand and develop advanced photocatalysts based on coupling TNTs with CNTs, which could result in advanced electrodes with cutting-edge properties and performances for a broad range of catalytic applications.

8.2. Future work

The results and investigations presented in this thesis advance the knowledge in designing CNTs-based composites with different physical and chemical properties in a precise manner for transport and photocatalysis applications. These results are envisaged as starting points towards advancing the existing knowledge in the field of CNTs composite membrane and materials and boosting the applicability of these systems across multiple disciplines and industrial applications. The following points outline possible future directions:

1. Further investigations have to be directed towards optimisation of the mechanical properties of CNTs-NAAMs composite membranes to increase their strength and hence spread their applicability for pressure driven molecular separations.
2. Designing novel CNTs composite membranes featuring asymmetric surface chemistry of their inner and outer wall surfaces by using different carbon precursors containing different heteroatoms (e.g. N, P, S, etc.) during the CVD process. This will result in incorporation of two different types of heteroatoms into the inner and outer wall surfaces of CNTs. This could spread the applicability of these tubes and composite membranes across a broad range of fields and applications (e.g. microelectronics, biomedical, etc.).
3. Designing sophisticated separation nanodevices based on CNTs membranes to ascertain their capability for separation applications using micro-chip technology (e.g. all-in-one lab-on-a-chip devices).
4. Further improvements of developed photocatalyst (CNTs-TNTs composite) could be obtained by designing a membrane structure of CNTs-TNTs. Such structure could advance the photocatalyst efficiency by allowing direct and flow-through photocatalytic experiments.